PolyPublie
Polytechnique Montréal

POLYTECHNIQUE MONTRÉAL
UNIVERSITÉ D'INGÉNIERIE

Titre: Title:	Conducting Polymer Based Flexible Epidermal Patch Electrodes for Human Healthcare
Auteur: Author:	Xin Zhou
Date:	2023
Type:	Mémoire ou thèse / Dissertation or Thesis
Référence: Citation:	Zhou, X. (2023). Conducting Polymer Based Flexible Epidermal Patch Electrodes for Human Healthcare [Thèse de doctorat, Polytechnique Montréal]. PolyPublie. https://publications.polymtl.ca/54130/

Document en libre accès dans PolyPublie
Open Access document in PolyPublie

URL de PolyPublie: PolyPublie URL:	https://publications.polymtl.ca/54130/
Directeurs de recherche: Advisors:	Fabio Cicoira, & Gregory Lodygensky
Programme: Program:	Génie chimique

Ce fichier a été téléchargé à partir de PolyPublie, le dépôt institutionnel de Polytechnique Montréal
This file has been downloaded from PolyPublie, the institutional repository of Polytechnique Montréal

https://publications.polymtl.ca

POLYTECHNIQUE MONTRÉAL

affiliée à l'Université de Montréal

Conducting Polymer Based Flexible Epidermal Patch Electrodes for Human Healthcare

XIN ZHOU

Département de génie chimique

Thèse présentée en vue de l'obtention du diplôme de *Philosophiæ Doctor*

Génie chimique

Juin 2023

© Xin Zhou, 2023.

POLYTECHNIQUE MONTRÉAL

affiliée à l'Université de Montréal

Cette thèse intitulée :

Conducting Polymer Based Flexible Epidermal Patch Electrodes for Human Healthcare

présentée par **Xin ZHOU**

en vue de l'obtention du diplôme de *Philosophiae Doctor*

a été dûment acceptée par le jury d'examen constitué de :

Géraldine MERLE, présidente
Fabio CICOIRA, membre et directeur de recherche
Gregory LODYGENSKY, membre et codirecteur de recherche
Marco BONIZZATO, membre
Jadranka TAVAS SEJDIC, membre externe

DEDICATION

To nature and science.

ACKNOWLEDGEMENTS

First of all, I would like to express my deepest gratitude to my research director, Prof. Fabio Cicoira, for giving me the opportunity to study in the field of epidermal bioelectronics and for his guidance, support, and encouragement throughout my Ph. D. program at Polytechnique Montreal. Thanks a lot for letting me decide my projects. I am very grateful for your patience and constructive guidance when we discuss the projects. I am inspired by your passion for scientific research and your skills and knowledge on paper writing. Thank you for your support after the end of my CSC scholarship.

I wish to extend my gratitude to my co-supervisor, Dr. Gregory A. Lodygensky, for his expert and valuable advice throughout my Ph. D. I am inspired by his work involving premature babies. You have provided me with valuable suggestions on soft and adhesive electrodes for premature babies.

I would like to express my immense gratitude to the jury members, Prof. Géraldine Merle, Prof. Marco Bonizzato, and Prof. Jadranka Tavas Sejdic for their time and valuable suggestions on my work.

I would like to acknowledge the financial support from China Scholarship Council (CSC) over 4 years and the endless support during the pandemic. I am grateful to the Natural Science and Engineering Council Canada (NSERC) for supporting this research.

I am beyond grateful to my friends and colleagues for their supports and help during my Ph. D. Thanks a lot to Dr. Yang Li for the fruitful discussions on PEDOT-based epidermal electronics and giving me valuable suggestions on PVA-borax hydrogel system, as well as the cooperation of writing the review: “Recent Progress on Self-Healable Conducting Polymers”. Many thanks to Dr. Arunprabaharan Subramanian for his help during my Ph. D. Thanks to Jo’Elen for her help during my Ph. D. I would like to immensely thank my colleague Pierre for his help, cooperation, fruitful discussions, and valuable suggestions on soft epidermal electrodes. I also would like to thank my other colleagues Mona, Jiaxin, Noémy, Jinsil, Chi-hyeong, Floriane, Meijing, Sara, Jeeyeon, Gayaneh, Kathel, Kate, and Remi.

I would like to give thanks to Eric Quenneville (Biomomentum) for fruitful discussions on the mechanical measurements. I am grateful to Prof. Marc Lavertu for the permission to use his laboratory for cell culture. Many thanks to Chi Yuan Chang and Sylvie Taillon for the cell culture

training, discussions, and valuable advice. Thanks to Matthieu Gauthier for the TGA, rheology training and valuable advice.

Lastly, I am grateful to my girlfriend Xinxin Pi and family for their endless support. Thank you Xinxin for your support, care, and encouragement, especially during my illness.

RÉSUMÉ

La demande en dispositifs portables et bioélectroniques suscite un besoin en matériaux étirables, flexibles et conducteurs. Les matériaux souples, adhésifs et auto-cicatrisants ayant un module de Young correspondant aux tissus biologiques (module de Young allant de 0,5 à 500 kPa) sont devenus un point névralgique de la recherche, grâce à leur interface de contact améliorée entre l'électronique et les tissus biologiques. À ce jour, divers matériaux conducteurs, sous forme de films, d'adhésifs bio-inspirés, de textiles et d'hydrogels, ont été utilisés pour l'électronique sur la peau. Les polymères conducteurs, en raison de leur flexibilité inhérente, leur biocompatibilité, leur facilité de traitement et de leur conductivité électronique et ionique mixte, sont considérés comme des candidats idéaux pour l'électronique portable et la bioélectronique. Cependant, des problèmes demeurent dont l'adhérence, les propriétés mécaniques, la conductivité, la capacité d'auto-cicatrisation et une compréhension incomplète des types de cicatrisation et de leurs capabilités. Ainsi, un besoin existe pour la poursuite de recherches pour améliorer l'utilisation des polymères conducteurs en bioélectronique et en électronique portable.

Cette thèse est dévouée à la préparation de matériaux conductifs et mous, et la fabrication d'électrodes épidermiques pour la surveillance de signaux électrophysiologiques. Par conséquent, cette thèse utilise un polymère conducteur, le poly(3,4-éthylènedioxythiophène):poly(styrène sulfonate) (PEDOT:PSS), pour préparer différents hydrogels, films et organohydrogels. Nous étudions les propriétés mécaniques, la capacité d'auto-cicatrisation, la conductivité, l'adhérence, le comportement de gonflement, les capacités antigel et de rétention d'eau, et la biocompatibilité de ces matériaux. De plus, des électrodes épidermiques fabriquées à partir de ces matériaux ont été utilisées pour enregistrer des biosignaux, y compris l'électromyographie (EMG), l'électrocardiographie (ECG) et l'interface homme-machine.

En raison de leur biocompatibilité, leurs propriétés électriques et mécaniques ajustables, et leur forte teneur en eau, les hydrogels conducteurs sont très prometteurs dans le domaine de l'électronique épidermique. La première partie de cette thèse démontre une approche simple pour fabriquer des hydrogels hautement adhésifs, étirables et auto-cicatrisants en mélangeant de l'alcool polyvinylique (APV), du borax et une pâte de sérigraphie commerciale (Clevios™ SV3 STAB) contenant du PEDOT:PSS, du diéthylène glycol et du propylène glycol. L'ajout de la pâte au réseau APV-borax a conduit à des hydrogels avec une souplesse et une extensibilité plastique améliorée,

des temps d'auto-cicatrisation plus courts et une adhérence améliorée sur la peau. Les hydrogels résultants démontrent une adhérence élevée de 1,96 N/cm^2 à la peau porcine, une extensibilité plastique exceptionnelle (> 10000 %), un faible module de compression (entre 0,3 et 3,7 kPa) et une performance d'auto-cicatrisation remarquable. Les électrodes épidermiques fabriquées avec les hydrogels sont d'une haute qualité pour l'enregistrement d'ECG et d'EMG. Ces résultats ont été publiés dans la revue Acta Biomaterialia.

Les films adhésifs et auto-cicatrisants se distinguent par leur potentiel prometteur pour les électrodes épidermiques en raison de leur capacité à former des contacts conformes à la peau sans l'usage de rubans adhésifs et à récupérer leurs fonctions après avoir subi des dommages. Dans la deuxième partie de cette thèse, nous avons préparé des films étirables, auto-cicatrisants et adhésifs avec un module de Young faible (~ 450 kPa) en mélangeant du PEDOT:PSS, de l'éthylène glycol (EG) et de l'acide tannique (AT). Nous avons étudié l'impact de l'AT sur les propriétés mécaniques, électriques, d'auto-cicatrisation et d'adhérence des films. L'augmentation de la concentration d'AT a réduit le module de Young des films et augmenté l'allongement à la rupture. La présence de structures cycliques aromatiques de catéchol et de pyrogallol dans l'AT a donné les films ayant la plus forte adhérence de 6 N/cm sur le verre et de 0,7 N/cm sur la peau de porc lorsque la concentration d'AT a été augmentée à environ 10 % de la masse totale. Par ailleurs, les films PEDOT/EG/AT ont montré des propriétés d'auto-cicatrisation autonome et induite par adhérence exceptionnelles en raison de leur souplesse et de leur viscoélasticité, ainsi que de la grande quantité de liaisons hydrogène. Nous avons évalué la biocompatibilité des films en cultivant des cellules musculaires C2C12 sur la surface des films. La viabilité cellulaire sur les films était de 88%, ce qui est supérieur au critère de non cytotoxicité (70% du groupe contrôle) selon l'ISO 10993-5. Les résultats indiquent que nos films pourraient fournir un environnement viable pour la croissance cellulaire, assurant ainsi leur utilisation en bioélectronique. Enfin, nous avons fabriqué des patchs d'électrodes épidermiques à base de films adhésifs. Ces électrodes ont montré une faible impédance à l'interface entre l'électrode et la peau à basse fréquence et une excellente qualité d'enregistrement des signaux d'ECG et d'EMG par rapport aux électrodes à gel d'Ag/AgCl commerciales. Un article présentant ces résultats a été soumis à la revue Nano-Micro Letters.

Les hydrogels conventionnels contiennent généralement une teneur élevée en eau (70 à 99%), ce qui peut ne pas convenir à une utilisation à long terme dans des environnements secs et froids en raison de l'évaporation ou du gel de l'eau, ce qui entraînerait des modifications des propriétés

mécaniques et électriques. Par conséquent, dans la troisième partie de la thèse, nous avons développé des organohydrogels antigel et à rétention d'eau pour de longue durée en utilisant une suspension concentrée de PEDOT: PSS, d'EG et d'AT.

La formation du gel est attribuée à la formation d'un réseau physique entre les chaînes polymères du PEDOT, qui est facilitée par l'ajout de l'AT. Les gels de PEDOT/EG/AT ont présenté des propriétés antigel, tolérant une congélation jusqu'à -24°C, et ce, en raison de la formation d'amas moléculaires entre les molécules d'AT et d'H_2O, entraînant une réduction du point de congélation et de la pression de vapeur d'eau. En outre, les gels ont démontré des capacités de rétention d'eau durables en raison de la formation de liaisons hydrogène entre l'eau et l'EG, tout en présentant également un faible module de Young en compression (~ 20 kPa) et une conductivité élevée (15 S/cm). De plus, nous avons étudié le comportement de gonflement du gel. Enfin, nous avons utilisé les gels pour fabriquer des électrodes épidermiques, qui présentaient une faible impédance à l'interface entre l'électrode et la peau, et des enregistrements d'ECG et d'EMG d'excellente qualité par rapport aux électrodes à gel d'Ag/AgCl commerciales. De surcroît, le gel déshydraté a également affiché une excellente qualité d'enregistrement d'ECG. Nous avons soumis ces résultats à la revue Advanced Sensor Research.

La fabrication d'électrodes épidermiques ayant une multitude d'attributs comme la conductivité électrique, l'auto-cicatrisation, l'extensibilité, l'adhésion et la souplesse, est devenue un point important de la recherche et reste un défi dans l'électronique portable et la bioélectronique. Cette recherche ouvre la voie à la conception et à la préparation de différentes formes de matériaux mous (hydrogels, films et organohydrogels) dont le module de Young correspond aux tissus biologiques. Par ailleurs, cette recherche démontre la fabrication d'électrodes épidermiques de haute performance, ce qui contribue au marché croissant de la bioélectronique pour des systèmes de santé personnels.

ABSTRACT

The demand for wearable electronics and bioelectronics has sparked a need for stretchable, flexible, and conductive materials. Soft, adhesive, and self-healable materials with moduli similar to human tissues (Young's modulus ranging from 0.5 to 500 kPa) have become a research hotspot, owing to their improved contact interface between electronics and biological tissues. To date, various conductive materials, in form of films, bio-inspired adhesives, fabrics, and hydrogels, have been utilized for on-skin electronics. Conducting polymers, owing to their inherent flexibility, biocompatible property, easy processability, and combination of electronic and ionic conductivity, are considered ideal candidates for wearable electronics and bioelectronics. However, issues such as adhesion, mechanical properties, conductivity, self-healing performance, and insufficient understanding of self-healing types and their capabilities still remain. Thus, there is a need for further investigation to enhance the use of conducting polymers in bioelectronics and wearable electronics.

This thesis is devoted to the preparation conductive and soft materials and fabrication soft epidermal patch electrodes for electrophysiological signals monitoring. Therefore, this thesis utilizes a conductive polymer, poly(3,4 -ethylene dioxythiophene):poly(styrenesulfonate) (PEDOT:PSS), to prepare hydrogels, films, and organohydrogels. We investigate the mechanical properties, self-healing ability, conductivity, adhesion, swelling behavior, anti-freezing and water retention ability, and biocompatibility of these materials. Furthermore, epidermal electrodes fabricated from these materials were used to record bio-signals, including electromyography (EMG), electrocardiography (ECG), and human-machine interface.

Due to their biocompatibility, tunable electrical and mechanical properties, and high-water content, conductive hydrogels are highly promising in the field of epidermal electronics. The first part of this thesis demonstrates an approach to fabricate highly adhesive, stretchable, and self-healable hydrogels by blending polyvinyl alcohol (PVA), borax, and a commercial screen-printing paste (Clevios^{TM} S V3 STAB) containing PEDOT:PSS, diethylene glycol and propylene glycol. The addition of the paste to the PVA/borax network led to hydrogels with improved softness and plastic stretchability, shorter self-healing times, and enhanced adhesion. The resulting hydrogels demonstrate a high adhesion of 1.96 N/cm^2 on porcine skin, remarkable plastic stretchability (>10000% strain), low compressive modulus (range from 0.3 to 3.7 kPa), and outstanding self-

healing performance. Epidermal electrodes fabricated from the hydrogels exhibited high ECG and EMG recording quality. These results were published in the journal of Acta Biomaterialia.

Adhesive and self-healable films have emerged with promising potential for use in epidermal electrodes owing to their ability to form conformal contacts to the skin without adhesive tapes and recover their functionality after damage. In the second part of this thesis, we prepared stretchable, self-healable, and adhesive films with a low Young's modulus (~ 450 kPa) by mixing PEDOT:PSS, ethylene glycol (EG), and tannic acid (TA). We investigated the impact of TA on the mechanical, electrical, self-healing and adhesion properties of the films. Increasing TA concentration decreased the Young's modulus of the films and increased the elongation at break. The presence of catechol and pyrogallol aromatic ring structures in TA imparted to the films high adhesion, with a value of ~ 6 N/cm on glass and 0.7 N/cm on porcine skin, when the TA concentration was increased to ~ 10 wt%. Additionally, the PEDOT/EG/TA films showed outstanding autonomic and cut-stick healing properties because of their softness and large amount of hydrogen bonds. We evaluated the biocompatibility of the films by culturing C2C12 muscle cells on their surface. The cell viability on the films was 88%, which is higher than the non-cytotoxic criterion (70% of the control group), according to ISO 10993-5. The results indicate our films could endow a safe medium for cellular proliferation, which ensures their use towards bioelectronics. Lastly, we fabricated the adhesive film-based skin patch electrodes. These electrodes showed low skin-electrode impedance at low frequency and high-quality signals for ECG and EMG recording compared to Ag/AgCl gel electrodes. We have submitted an article presenting these results to the Nano-Micro Letters journal.

Conventional hydrogels typically contain high water content (70 - 99%), which may not be suitable for long-term use in dry and cold environments due to water evaporation or freezing, resulting in changes in both mechanical and electrical performance. Therefore, in the third part of the thesis, we developed anti-freezing and long-lasting water-retaining organohydrogels using a concentrated PEDOT:PSS suspension, EG, and TA. The formation of the gel is due to the physical network formed between PEDOT polymer chains, which is facilitated by the addition of TA. The PEDOT/EG/TA gels exhibited anti-freezing properties, remaining unfrozen down to -24°C, due to the formation of molecular clusters between EG and H_2O molecules, leading to a reduced freezing point and water vapor pressure. Additionally, the gels demonstrated long-lasting water retention capabilities because of the formation of hydrogen bonds between water and EG, while also exhibiting a low compressive Young's modulus (~20 kPa) and a high conductivity (15 S/cm).

Furthermore, we investigated the volumetric swelling behavior of the gel and the dehydrated gel showed a volumetric swelling of ~135 % of its initial value. Finally, we utilized the gels to fabricate epidermal electrodes, which exhibited low skin-electrode impedance and high-quality for ECG and EMG recordings compared to commercial Ag/AgCl gel electrodes. Moreover, the dehydrated gel also displayed excellent ECG recording quality. We submitted these results to the Advanced Sensor Research journal.

The fabrication of epidermal electrodes that contain a plethora of attributes, such as being conductive, self-healing, stretchable, adhesive, and soft has become a research hotspot and remains a challenge in the field of wearable electronics and bioelectronics. This research paves the way to the design and preparation of many different forms of soft materials (hydrogels, films, and organohydrogels) with Young's modulus matching biological tissues. In addition, this study also provides some fundamental guidelines to the healing behavior of conductive polymers-based hydrogels and adhesive films. Furthermore, this research demonstrates the fabrication of high-performance epidermal electrodes, which contributes to the growing market of bioelectronics for personal healthcare systems.

TABLE OF CONTENTS

DEDICATION iii

ACKNOWLEDGEMENTS iv

RÉSUMÉ vi

ABSTRACT ix

TABLE OF CONTENTS xii

LIST OF TABLES xvii

LIST OF FIGURES xviii

LISTE OF SYMBOLS AND ABBREVIATIONS xxvi

LIST OF APPENDICES xxx

CHAPTER 1 INTRODUCTION 1

1.1 Epidermal patch electronics 1

1.2 Motivations 2

1.3 Hypothesis and objectives 3

1.4 Organization of the work 5

CHAPTER 2 LITERATURE REVIEW 6

2.1 Human skin 6

2.2 Conventional medical epidermal electrodes for healthcare 8

2.3 Bio-inspired adhesives and adhesive electrodes 10

2.4 Film electrodes 15

2.5 PEDOT or PEDOT:PSS based epidermal electronics for healthcare 17

2.5.1 PEDOT:PSS and its properties 17

2.5.2 Electrical and mechanical properties of PEDOT:PSS 19

2.6 Applications of PEDOT:PSS in epidermal electronics for healthcare 21

2.6.1 PEDOT or PEDOT:PSS based film for healthcare 21

2.6.2 PEDOT based textiles 28

2.6.3 PEDOT or PEDOT:PSS based hydrogels 30

CHAPTER 3 METHODOLOGY 35
3.1 Preparation of PEDOT:PSS-based hydrogels, films, and organohydrogels 35
3.2 Fabrication of the SV3/PVA hydrogels, PEDOT/EG/TA films, and PEDOT/EG/TA organohydrogels epidermal patch electrodes 35
3.3 Electrical conductivity test 35
3.4 Mechanical characterization 36
3.4.1 Electromechanical tests 36
3.4.2 Compressive test 37
3.4.3 Creep-recover test 37
3.5 Rheology measurements 37
3.6 Adhesion strength measurements 37
3.7 Self-healing test 38
3.8 Composition characterization 39
3.8.1 FTIR 39
3.8.2 Zeta potential 39
3.9 Biocompatibility test 39
3.10 Characteristic of epidermal patch electrodes 40
3.10.1 The skin-electrode impedance 40
3.10.2 ECG & EMG measurements 40
CHAPTER 4 ARTICLE 1 : SELF-HEALING, STRETCHABLE, AND HIGHLY ADHESIVE HYDROGELS FOR EPIDERMAL PATCH ELECTRODES 42
4.1 Abstract 42
4.2 Introduction 43
4.3 Materials and methods 45
4.3.1 Materials 45
4.3.2 PEDOT:PSS/PVA hydrogel preparation 45
4.3.3 SV3/PVA strain sensor fabrication and strain sensitivity 45
4.3.4 SV3/PVA electrodes preparation 46
4.3.5 Characterization 46
4.3.6 Mechanical characterization 47
4.3.7 Electrical conductivity 47

4.3.8 Self-healing 48
4.3.9 Electrochemical impedance spectroscopy 48
4.3.10 Electrophysiological signals recording 48
4.3.11 Statistical analysis 49
4.4 Results and Discussion 50
4.4.1 Modelling and compliance properties of SV3/PVA hydrogels 50
4.4.2 Rheological and Fourier-transform infrared (FTIR) spectroscopy properties 51
4.4.3 Adhesion and compressive mechanical properties 52
4.4.4 Mechanical and electrical self-healing properties 55
4.4.5 Strain sensitivity of SV3/PVA hydrogels 58
4.4.6 Impedance properties on skin 59
4.4.7 Epidermal electrodes for ECG and EMG recording 60
4.5 Conclusions and perspectives 62
4.6 Acknowledgments 62
CHAPTER 5 ARTICLE 2 : STRETCHABLE, SOFT, HIGHLY ADHESIVE, AND SELF-HEALING CONDUCTIVE POLYMER FILMS FOR HEALTHCARE MONITORING 63
5.1 Abstract 63
5.2 Introduction 64
5.3 Experimental Section 65
5.3.1 Materials 65
5.3.2 Film preparation 66
5.3.3 Conductivity Measurement 66
5.3.4 Mechanical characterization 67
5.3.5 Fourier-transform infrared (FT-IR) spectroscopy 68
5.3.6 Self-healing 68
5.3.7 Preparation of electrodes 69
5.3.8 Characterization of epidermal electrodes 69
5.3.9 Biocompatibility essays 70
5.4 Results and Discussion 70
5.4.1 Mechanical and electrical tensile properties 70
5.4.2 Adhesion properties of PEDOT/EG/TA films 73
5.4.3 Self-healing properties of films 74
5.4.4 Skin-electrode impedance and ECG & EMG recording properties 76
5.4.5 Biocompatibility essay 78

5.5 Conclusions and perspectives....79
5.6 Acknowledgments....80
CHAPTER 6 ARTICLE 3 : SOFT, CONDUCTIVE AND ANTI-FREEZING CONDUCTING POLYMER ORGANOHYDROGELS....81
6.1 Abstract:....82
6.2 Introduction....82
6.3 Materials and methods....84
6.3.1 Materials....84
6.3.2 PEDOT/EG/TA organohydrogel preparation....84
6.3.3 Preparation of gel electrodes....85
6.3.4 Conductivity Measurement....86
6.3.5 Mechanical characterization....86
6.3.6 Fourier-transform infrared (FTIR) spectroscopy....86
6.3.7 Zeta potential measurements....87
6.3.8 Water retention measurements....87
6.3.9 Anti-freezing measurements....87
6.3.10 Swelling properties....88
6.3.11 Characterization of epidermal electrodes....88
6.4 Results and Discussion....89
6.4.1 Fabrication and characterization....89
6.4.2 Mechanical properties....90
6.4.3 Electrical characterization....91
6.4.4 Water retention and anti-freezing properties....91
6.4.5 Swelling ability of PEDOT/EG/TA gels....94
6.4.6 Skin-electrode impedance, ECG & EMG measurements....95
6.5 Conclusions and perspectives....97
6.6 Acknowledgments....98
CHAPTER 7 GENERAL DISSCUSSION....99
CHAPTER 8 CONCLUSION AND RECOMMANDATIONS....102
8.1 Conclusion....102
8.2 Recommandations....103

REFERENCES.....105

APPENDICES.....121

LIST OF TABLES

Table 2.1 Summary of various types of bioinspired skin patches. 10

Table 2.2 Summary of PEDOT:PSS based films for epidermal electronics. 22

Table 2.3 Summary of PEDOT/PEDOT:PSS based skin patch on various substrates with different techniques. 27

Table 2.4 Summary of PEDOT:PSS based textile for health care. 29

Table 2.5 Summary of PEDOT or PEDOT:PSS based hydrogels for healthcare. 32

Table 4.1 Perpendicular adhesion on pig skin and compressive Young's modulus in the 0-20% strain range of SV3/PVA and PVA hydrogels. Data for adhesion force (n = 6) and compressive Young's modulus (n = 3) are reported as mean ± standard deviation. 54

Table 5.1 PEDOT/EG/TA film samples used in this study. 66

Table 5.2 Thickness, tensile Young's modulus in the 0 -10% strain range, elongation at break, 90° peeling-off adhesion on glass and porcine skin, and conductivity of the films. The thicknesses ranged between ~65 μm and ~130 μm, depending on the amount of TA. Data for the adhesion force (n = 3), tensile Young's modulus (n = 3), elongation at break (n = 3), and conductivity (n = 5) are reported as the mean ± standard deviation 73

Table 6.1 Summary of PEDOT/EG/TA gel samples used in this work. 85

Table 6.2 Compressive Young's moduli and gel conductivities in the 0-10% strain range. Data for the compressive Young's moduli (n = 3) and conductivities (n = 5) are reported as the mean ± standard deviation. 91

Table 6.3 Comparison of the conductivities of PEDOT/EG/TA and PEDOT/TA gels before and after seven days. Data for the conductivities of the PEDOT/EG/TA gel (n = 5) and PEDOT/TA gel (n = 3) are reported as mean ± standard deviation. 93

LIST OF FIGURES

Figure 2.1 Illustration of human skin as a diagnostic platform. Reproduced with permission from [14]. Copyright 2017, American Chemical Society. 6

Figure 2.2 Elastic moduli for various representative materials including metals, polymers, conductors, and biological tissues. Reproduced with permission from [14]. Copyright 2017, American Chemical Society. 7

Figure 2.3 Medical epidermal electrodes. (a) Suction-based electrode, (b) Cup electrode, (c) Dry electrode, and (d) Disposable Ag/AgCl gel electrode. 9

Figure 2.4 Gecko-inspired epidermal adhesive patches with diagnostic functions. (a) Illustration of the microstructure adhesive as biomedical bandage; (b) SEM images of the micropillars with a constant pillar diameter of 5 μm and an aspect ratio of 3; (c) Adhesion force on the skin with different aspect ratios; (d) Utilization of the adhesive as a fixation unit for ECG recording. (a-d) are reprinted with permission [23]. (e) A micropillars adhesive patch with low modulus PDMS as the tips and high modulus PDMS as the stem; (f) Adhesion force on skin with different amounts of PDMS curing agent; (g) Adhesion force versus repeating cycles; (h) The use of the patch to attach a metal electrode on the skin for ECG recording. (e-h) are reproduced with permission [24]. 11

Figure 2.5 Gecko-inspired mushroom-like epidermal patches with diagnostic functions. (a) Cross-sectional SEM image showing an adhesive patch with micropillar structure; (b) Digital photo of the adhesive patch attaching to forearm skin; (c) Force versus displacement plots of a micropatterned adhesive film. The figure displays enhanced adhesive force compared to unstructured patches; (d) The use of the patch as a strain sensor. (a-d) are reproduced with permission [25]. (e) An adhesive and conductive patch made of silver microparticles and Ecoflex 00-30; (f) Adhesion force versus different polymer electrodes (porous structure electrodes and microstructures electrodes with small AgSMP and large AgLMP microparticles); The application of the patch electrodes for ECG (g) and EEG (h) recording. (e-h) are reproduced with permission [27]. (i) An adhesive and conductive patch comprised of graphene/CNTs/PDMS. (j) Adhesion force on the skin replica versus pillar height (the insert is the top view of SEM image of the skin replica. AR represents aspect ratio); (k) The

use of the patch for ECG monitoring under movements. (i-k) are reproduced with permission from [26]. Copyright 2016, American Chemical Society. 12

Figure 2.6 Bioinspired adhesive patches. (a) Digital photo of an octopus-inspired architecture patch; (b) SEM image of microcavities array with protuberance-like dome-shaped structures; (d) Adhesion strength on pigskin as a function of preload for OIA patches. (a-c) are reproduced with permission [29]. (d) Photograph of a cephalopod tentacle (left) and 3D laser scanning image of a suction cup (right). (e) SEM images of the side view (bottom) and top view (top) of mSCs; (f) Adhesion force on the skin with different surface-structured patches (flat, m-pillars, and mSCs with different moduli); (g) Illustration of multiple functions of the patch including ECG recording, respiration monitoring, body temperature monitoring, and drug-delivery. (d-g) are reproduced with permission [28]. 14

Figure 2.7 Ultrathin and ultra-conformable skin patch with diagnostic functions. (a) The layout of the EES includes bar, disk, and FS mesh-type designs; (b) An ultra-conformable EES for EMG recording. The colorized SEM images illustrate the degree of conformal contact between the skin surface made of silicon (gray color) and elastomer membranes with various thicknesses (blue color); EMG recording while blinking eyes (c) and bending the forefinger (d). (a-d) are reproduced with permission [7]. (e) A self-adhesive ultrathin and ultra-conformable film electrode with a sandwich structure for ECG measurement; (f) ECG recording with the use of ultrathin film and wet Ag/AgCl electrodes. (e-f) are reproduced with permission [35]. 15

Figure 2.8 Tattoo-based ultrathin and ultra-conformable skin patch electronics with diagnostic functions. (a) Image illustration of the EES with multiple electronic components (FS mesh sensors, LEDs, wireless coils, RF communications, etc.) and with various diagnostic functions including ECG, EMG, EEG, and temperature measurements. The skin patch can be transferred to the skin and showed good compressible (b) and stretchable (c) properties. (a-c) are reproduced with permission [36]. 16

Figure 2.9 The chemical and core-shell structure of PEDOT:PSS. The orange color represents while the blue color indicates short PEDOT chains [40]. Reproduced with permission. 18

Figure 2.10 Applications for PEDOT:PSS in the fields of energy, electronics, and biology [47]. Reproduced with permission. 19

Figure 2.11 (a) A representative schematic diagram of the morphology of PEDOT:PSS films with STEC enhancer; (b) Stress-strain curves of free-standing PEDOT/STEC films. (a-b) are reproduced with permission [45]. (c) Stress versus strain plots of pristine PEDOT:PSS films and polymer films obtained by blending PEDOT:PSS with soft polymers (PEG, PEO, and PVA); (d) Conductivity of thick free-standing PEDOT:PSS/polymer films as a function of soft polymer weight fraction. Reproduced with permission from [46]. Copyright 2015, American Chemical Society. 20

Figure 2.12 PEDOT:PSS-based ultrathin tattoo skin patch electrode for ECG and EMG recording. (a) Layers schematic 3D view of the tattoo electrodes; (b) Circular tattoo electrode on the arm; (c) Continuous ECG recording (top) and a single beat (bottom), achieved by tattoo (red) and standard (blue) electrodes; (d) Rectified EMG recording with using tattoo (red) and Ag/AgCl gel electrodes (blue). (a-d) are reproduced with permission [48]. 23

Figure 2.13 PWS adhesive films. (a) Chemical structures of PEDOT:PSS, WPU, and D-sorbitol. (b) Schematic illustration for the preparation of PWS films. (c) Characteristics of the films. Stress-strain plots (upper) with various PEDOT:PSS loadings, Young's modulus and elongation at break (middle), and Adhesion (bottom) of PWS films. (a-c) are reproduced with permission [18]. 24

Figure 2.14 (a) current as a function of time for PEDOT:PSS film shows a cut-healing effect with a stainless-steel blade cut and a drop of water healing on the damaged area, 0.2 voltage was applied. SEM images display the damaged area of a PEDOT:PSS film before (b) and after (c) water healing. (a-c) are reproduced with permission [43]. (d) Time-lapse current plot for a PEDOT:PSS/Triton X-100 film during several "cut-heal" cycles. Digital photos of the self-healing process of a PEDOT:PSS/Triton X-100 film with a LED bulb lit off (cut, e) and lit on (healed, f). (d-f) are reproduced with permission [60]. (g) Current versus time measurements during the cut and healing process for four different films obtained from mixtures comprising PEDOT:PSS and 4% PEG-400. SEM images of the cut (h) and healed (i) area of a PEDOT:PSS/PEG film. (g-i) are reproduced with permission [55]. 25

Figure 2.15 Schematic illustration (a) and optical image (b) of the concentric ring electrode; (c) Illustration of the adhesive electrode on the skin. The use of the electrode for EEG (d), ECG (e), and EMG (f) measurements. (a-f) are reproduced with permission [63]. 28

Figure 2.16 (a) Illustration of RT-PEDOT:PSS hydrogel preparation; (b) Injectable properties of RT-PEDOT:PSS hydrogels; (c) Illustration of self-healing of RT-PEDOT:PSS hydrogel by cut-stick process. (a-c) are reproduced with permission [89]. (d) Schematic illustration of pure PEDOT:PSS hydrogel preparation; (e) Chemical structures of PEDOT, PSS, and DMSO; (f) Free-standing pure PEDOT:PSS hydrogel pattern. (d-f) are reproduced with permission [90]. 30

Figure 2.17 (a) Schematic diagram of PSGO-PEDOT nanosheet and its incorporation in hydrogel; (b) Adhesive properties of PSGO-PEDOT hydrogels; (c) EEG, EMG, and ECG recording. (a-c) are reproduced with permission [97]..... 33

Figure 2.18 (a) Schematic illustration of the preparation PEDOT:PSS/PVA/EG organohydrogels; (b) Tensile (left) and compressive (right) stress–strain plot of the anti-freezing conductive organohydrogels with different mass ratios of H_2O and EG; (c) Digital photos of compressive and bending measurements at -40 °C for the anti-freezing organohydrogels (up) and at -10 °C for pure conductive hydrogel (without EG, down). (a-c) are reproduced with permission [106]. 34

Figure 3.1 Adhesion tests schema. (a) Perpendicular adhesion strength and (b) 90° peel adhesion force measurements..... 38

Figure 4.1 (a) Scheme of the processing of the hydrogels and 3D rendering of the hydrogel network. (b) Scheme of the chemical bonds which can be formed in the hydrogel: PVA-borax (b_1), PEDOT:PSS-borax (b_2), PG-water and borax-PG (b_3), DEG-water and borax-DEG (b_4). (c) Digital pictures of SV3/PVA-1-3 hydrogel modelled into various shapes: letters (c_1), cube (c_2) and sphere (c_3). (d) Digital pictures of SV3/PVA-1-3 hydrogel on the finger skin: top view (d_1), side view (d_2), side view during finger bending (d_3)..... 50

Figure 4.2 (a) Storage modulus (G′) and loss modulus (G″) as a function of angular frequency for PVA hydrogel and SV3/PVA hydrogels. (b) FTIR spectrum of SV3/PVA hydrogels and PVA hydrogel..... 52

Figure 4.3 Adhesion and compressive stress-strain measurements of SV3/PVA-1-3, SV3/PVA-1-2, SV3/PVA-1-1, and PVA hydrogels. (a) Perpendicular adhesion force on pig skin versus displacement, (b) average perpendicular adhesion force on pig skin, (c) compressive stress versus strain, and (d) average compressive Young's modulus at 20% strain. Data for adhesion

force (n = 6) and compressive Young's modulus (n = 3) are reported as mean ± standard deviation. 54

Figure 4.4 (a) Storage modulus (G′) and loss modulus (G″) versus strain% for PVA and SV3/PVA hydrogels (ω = 6.28 rad/s). (b) G′ and G″ versus time in continuous step strain sweep with an alternating small strain (1%, ω = 6.28 rad/s) and large strain (100% for PVA hydrogel, SV3/PVA-1-3, SV3/PVA-1-2, and SV3/PVA-1-1 and 400% for SV3/PVA-2-1, ω = 6.28 rad/s) oscillation force. 55

Figure 4.5 Electrical self-healing of SV3/PVA-1-3 hydrogel. (a) Circuit comprises the self-healing SV3/PVA-1-3 hydrogel in series with a battery and a LED indicator: (a_1) original (closed), (a_2) cut (open), and (a_3) healed (closed). (b) Current versus time measurements under a constant voltage of 0.6 V upon various cutting-healing cycles. (c) A magnification of b showing the time evolution of the electrical healing process after the first cut. 58

Figure 4.6 Characterization of the skin-electrode impedance without skin preparation and attachment pressure. (a) Impedance measurement configuration. (b) Skin-electrode impedance versus frequency for a SV3/PVA-1-3 hydrogel electrode and a commercial Natus® Ag/AgCl gel electrode. The diameter of the electrodes was 18 mm. The inset shows a magnification for measurements from 10 Hz to 100 Hz. Data for skin-electrode impedance are reported as mean ± standard deviation (*n = 3*). Note: WE: working electrodes, RE: reference electrodes, and CE: counter electrodes. 59

Figure 4.7 (a) ECG electrodes placed on the forearms of a volunteer. The ground (GE) and the positive (PE) electrodes are placed on the left forearm; the negative electrode (NE) is placed on the right forearm. ECG biopotentials (voltage versus time) recorded with SV3/PVA-1-3 hydrogel electrodes (b and c), commercial Natus®(d), SkinTact®(e), Ambu®(f), and 3M® (g) Ag/AgCl gel electrodes. The plot in (b) shows a magnification of the ECG signal between 0.5 - 1.3 s from the plot in (c). 60

Figure 4.8 EMG signals recording for different electrode types. (a) EMG electrodes placed on the forearm of a volunteer. EMG biopotentials between the electrodes were recorded with ground electrode (GE), positive electrode (PE), and negative electrode (NE) on the right forearm. EMG monitoring with using (b) SV3/PVA-1-3 hydrogel electrodes, commercial (c) Natus®, (d) SkinTact®, (e) Ambu®, and (f) 3M® Ag/AgCl gel electrodes under relax and clenching

phases. (g) Computed SNR values over the 24 s recording period for SV3/PVA-1-3 electrodes and 4 different commercial Ag/AgCl gel electrodes. SNR data are reported as mean ± standard deviation (n = 3). 61

Figure 5.1 (a) Chemical structures of PEDOT:PSS (a_1), EG (a_2), and TA (a_3). Schematic of the film preparation (b). Digital pictures of free standing PEDOT/EG/TA-3 films on the finger skin: top view (c_1), side view (c_2), and side view during finger bending (c_3)..... 71

Figure 5.2 Mechanical and electrical tensile properties of PEDOT/EG/TA films. (a) Tensile stress versus strain. (b) Average tensile Young's modulus at 10% strain and elongation at break of films with different TA content. (c) Electrical resistance versus tensile strain of PEDOT/EG/TA films obtained during stress-strain measurements, as shown in Fig. 2a. (d) Creep deformation (strain vs time) and (e) strain recovery time plots of the PEDOT/EG/TA-0 and PEDOT/EG/TA-3 films. A constant creep stress of 150 kPa was applied for 5 min, and the strain was allowed to recover for 10 min after the stress removal. Tensile Young's modulus (n = 3) and elongation at break (n = 3) of films are reported as the mean ± standard deviation. 72

Figure 5.3 Adhesion force versus displacement for PEDOT/EG/TA-2 (~7% TA) and PEDOT/EG/TA-3 (~10% TA) films on glass (a) and porcine skin (b). A 90° peeling-off geometry is used. The fluctuations during the peeling process were likely caused by high adhesion on the glass, which led to damage during peeling (Figure SB6). The adhesion force dropped to noise level for TA contents below 3.5 wt% (Figure SB7). 74

Figure 5.4 Electrical and mechanical autonomous (a-d) and cut-stick (e-k) healing properties of PEDOT/EG/TA-3 films. Autonomous healing process: a) Current versus time measurements under a constant voltage of 0.2 V upon various cutting-healing cycles, optical microscopy images of the self-healing process b) before cutting, c) after cutting, and d) after healing. Electrical cut-stick healing process: e) Current versus time measurements under a constant voltage of 9 V upon repeated cut-stick healing cycles; f-h) Visualization of the healing effect with an LED indicator: f) original (closed), g) cut (open), and h) healed (closed). Mechanical cut-stick healing process: i) tensile stress-strain plots of original and cut-stick healing films. Images of the film mounted on the tensile tester g) before stretching (the overlap area of film was 10 mm × 3 mm) and k) during stretching. 76

Figure 5.5 ECG and EMG signal recordings for the PEDOT/EG/TA film electrodes. a) Configuration of ECG measurements in a volunteer. Positive (PE) and ground (GE) electrodes were placed on the left forearm and the negative electrode (NE) was placed on the right forearm. b) ECG biopotentials (voltage versus time) recorded using PEDOT/EG/TA-3 film electrodes. c) Configuration of EMG measurements in a volunteer. EMG biopotentials between the electrodes were recorded with a PE and NE on the right forearm and a GE on the elbow. d) EMG monitoring with using PEDOT/EG/TA film electrodes. 77

Figure 5.6 (a) Representative images of the live/dead assay of mouse muscle cells (C2C12) cultured on uncoated (positive control) and PEDOT/EG/TA-3 film-coated PS substrates for one and three days. (b) Quantitative analysis of cell viability. As a negative control, cell viability was approximately 0. Error bars represent standard deviation (n = 3). 78

Figure 6.1 (a) Chemical structures of PEDOT:PSS (a_1), EG (a_2), and TA (a_3). (b) Schematic illustration of PEDOT/EG/TA gel preparation and 3D rendering of the gel network including PEDOT crosslink, hydrogen bonding, π–π stacking, and hydrophobic attractions. (c) PEDOT/EG/TA gel modelled into round disk (c_1), printed into curves, nozzle size:0.5 uL (c_2), and injected into a heart shape (c_3). 89

Figure 6.2 Compressive stress-strain and Young's modulus of gels. (a) Compressive stress versus strain (inset shows the magnification of compressive stress versus strain) and (b) average compressive Young's modulus at 10% strain of PEDOT/EG/TA and PEDOT/TA gels. Data for Young's modulus (n = 3) is reported as the mean ± standard deviation. 90

Figure 6.3 (a) Digital images of the fresh PEDOT/EG/TA and PEDOT/TA gels. (b) Digital images of PEDOT/EG/TA and PEDOT/TA gels stored at ambient temperature for seven days. (c) Mass change of PEDOT/EG/TA and PEDOT/TA gels over seven days. (d) Compressive stress versus strain of PEDOT/EG/TA and PEDOT/TA gels stored at ambient temperature for seven days. Data for mass change (n = 3) are reported as mean ± standard deviation. 92

Figure 6.4 Swelling properties of PEDOT/EG/TA gels. (a) Digital images showing the volumetric shrinkage of the gel (cylindrical geometry) dehydrated at 140 °C for a_1) 0, a_2) 2, a_3) 4, and a_4) 6 h. (b) Volumetric shrinkage ratio versus time plots of PEDOT/EG/TA gel dehydrated at 140 °C for 6 h. (c) Digital images showing the volumetric swelling of the dried gel rehydrated at ambient temperature for c_1) 0, c_2) 3, c_3) 6, and c_4) 24 h. (d) Volumetric swelling ratio versus

time plots of the dried gel rehydrated at ambient temperature for 48 h. V denotes the volume of the gel at a given baking or soaking time. V_0 is the initial volume of the gel before baking and V_i represents the volume of the gel after baking for 6 h (shown in Figure a_4)..... 95

Figure 6.5 ECG and EMG signal recordings of PEDOT/EG/TA gel electrodes. (a) Configuration of ECG measurement in a volunteer. Positive (PE) and ground (GE) electrodes were attached to the left forearm, and a negative electrode (NE) was placed on the right forearm. ECG biopotentials (voltage versus time) were recorded using the PEDOT/EG/TA gel electrodes. (c) Configuration of EMG measurements on a volunteer. The EMG biopotentials between the electrodes were recorded using PE and NE on the right forearm and GE on the elbow. (d) EMG monitoring using PEDOT/EG/TA gel electrodes: EMG signals (PEDOT/EG/TA gel electrodes) were used to control the motion of the robotic hand, that is, closed (e) and open (f) hand. 96

LISTE OF SYMBOLS AND ABBREVIATIONS

AC	Alternating current
ACS	American Chemical Society
Ag	Silver
Ag/AgCl	Silver/Silver chloride
ASTM	American Society for Testing and Materials
CE	Counter electrode
CNT	Carbon nanotubes
CVDs	Cardiovascular diseases
DBSA	Dodecylbenzenesulfonic acid
DEG	Diethylene glycol
DI	Deionized
DMEM	Dulbecco’s modified Eagle’s medium
DMSO	Dimethyl sulfoxide
DPBS	Dulbecco’s phosphate-buffered saline
ECG	Electrocardiography
EDOT	3,4-ethylenedioxythiophene
EEG	Electroencephalography
EES	Epidermal electronic system
EG	Ethylene glycol

EGaIn	Gallium-Indium eutectic
EMG	Electromyography
EMI	Electromagnetic interference shielding
EOG	Electrooculography
f-BNNS	Functionalized boron nitrogen sheets
FBS	Fetal bovine serum
FS	Filamentary serpentine
FSWCNT	Functionalized single-wall carbon nanotubes
FTIR	Fourier-transform infrared
IPA	Isopropyl alcohol
ISO	International Organization for Standardization
GE	Ground electrode
GF	Gauge factor
LED	Light-emitting diode
LVER	Linear viscoelastic regions
mSC	Miniaturized suction cups
OECT	Organic electrochemical transistor
OIAs	Octopus-inspired architectures
OTf	Trifluoromethanesulfonate

PAA	Poly (acrylic acid)
PAAM	Poly(acrylamide)
PANI	Polyaniline
PBS	Phosphate-buffered saline
PC	Proanthocyanins
PDA	Polydopamine
PDMS	Polydimethylsiloxane
PEDOT	Poly(3,4-ethylenedioxythiophene)
PEDOT:PSS	Poly(3,4-ethylenedioxythiophene):polystyrene sulfonate
PEG	Polyethylene glycol
PEN	Polyethylene naphthalate
PEO	Polyethylene oxide
PET	Polyethylene Terephthalate
PG	Propylene glycol
PI	Polyimide
PNIPAM	Poly(N-isopropylacrylamide)
PPEGMEA	Poly(poly(ethylene glycol) methyl ether acrylate)
PPy	Polypyrrole
PSS	Polystyrene sulfonate

PU	Polyurethane
PUA	Poly(urethane acrylate)
PVA	Polyvinyl alcohol
PWS	PEDOT :PSS/Waterborne polyurethane/D-sorbitol
RE	Reference electrode
RF	Radio frequency
rGO	Reduced graphene oxide
RMS	Root mean square
SA	Sulfosuccinic acid
SEBS	Styrene ethylene butylene styrene
SEM	Scanning electron microscopy
SNR	Signal-to-noise ratio
SRT	Squid ring teeth
STEC	Stretchability and electrical conductivity
TA	Tannic acid
Tos	Para-toluene sulfonate
Triton X-100	Polyethylene glycol tert-octylphenyl ether
WPU	Waterborne polyurethane

LIST OF APPENDICES

APPENDIX A SUPPLEMENTARY INFORMATION FOR ARTICLE 1 : Self-healing, stretchable, and highly adhesive hydrogels for epidermal patch electrodes 121

APPENDIX B SUPPLEMENTARY INFORMATION FOR ARTICLE 2 : Stretchable, Soft, Highly Adhesive, and Self-healing Conductive Polymer Films for Healthcare Monitoring 130

APPENDIX C SUPPLEMENTARY INFORMATION FOR ARTICLE 3 : Soft, conductive and anti-freezing conducting polymer organohydrogels 137

APPENDIX D LIST OF PUBLICATIONS AT POLYTECHNIQUE MONTREAL NOT INCLUDED IN THE THESIS 147

APPENDIX E PARTICIPATION TO CONFERENCES 148

CHAPTER 1 INTRODUCTION

1.1 Epidermal patch electronics

Human health has been an increasingly prevalent topic discussed in our daily life. In 2016, cardiovascular diseases (CVDs) caused an estimated 17.9 million deaths worldwide, representing 31% of all global deaths, as reported by the World Health Organization [1]. The introduction of a non-invasive system to the human body is an effective strategy to monitor the heart's electrical activity and reduce deaths resulting from CVDs. Epidermal patch electronics, commonly referred to as "electronic skin", are non-invasive devices that are mounted directly onto the skin. They are widely explored for applications in human healthcare, including monitoring of vital signs, blood pressure, body temperature, the analysis of biomarkers in bodily fluids, as well as for human-machine interfaces [2-9]. Monitoring vital signs, such as electrocardiography (ECG), electromyography (EMG), and electroencephalography (EEG), is critical for point-of-care diagnostics.

Generally, epidermal patch electronics consist of an adhesive patch of thin flexible substrates (e. g. polydimethylsiloxane (PDMS), (styrene ethylene butylene styrene) SEBS, polyethylene Terephthalate (PET), and Ecoflex), which functions to create skin attachment, and multiple functional sensors composed of conductive materials (e. g. silver Nano particles (NPs), Au NPs, carbon nanotubes (CNTs), graphene, and conductive polymers).

Metal electrodes with various shapes such as bar, ground strap, and cup, and Ag/AgCl gel electrodes are currently used to acquire vital signs (ECG, EMG, and EEG) [10, 11]. However, metal electrodes can cause skin damage and irritation as a result of the mechanical mismatch between the metal electrodes and skin. Similarly, Ag/AgCl gel electrodes can lead to skin irritation because of their strong adhesion [4, 10, 12]. Furthermore, an electrolyte gel is required to improve the conformability and conductivity between the rigid metal and the skin. Such rigid electrodes are unable to endure bending and stretching and, as a result, they are not suitable for long-term recording of bio-signals due to poor conformability and skin irritation occurring after the drying of the electrolyte gel [4, 13].

Poly(3,4-ethylenedioxythiophene):polystyrene sulfonate (PEDOT:PSS) is a conductive polymer widely used in numerous applications including wearable electronics, bioelectronics, energy

storage (e.g., supercapacitors and organic solar cells), and optical devices (e.g., transparent electrodes and diodes). PEDOT:PSS-based flexible hybrid electronics possess several advantages over conventional medical electrodes, including flexibility, stretchability, electrochemical inertness, good film formation, self-healing, and biocompatibility. These properties make it an ideal material for bioelectronics, such as implantable and epidermal electronics. Despite the widespread use of PEDOT:PSS-based patch electrodes on various substrates, including PDMS, PET and fabric, there are still existing limitations, particularly in the case of PEDOT:PSS-based textile electrodes, including motion artifacts and the stability and quality of bio-signal recording. Although ultrathin PEDOT:PSS-based skin patches (e.g., nanoscale tattoo electrodes) could reduce motion artifacts and achieve high-quality signal recording, they are difficult to handle and are mechanically less durable, leading to limited reusability. However, conductive, adhesive, and soft PEDOT:PSS based patches have shown promise in monitoring human health. Therefore, developing a cost-effective and straightforward approach for producing robust, biocompatible and functional skin adhesive patch electrodes is an important area of research, making epidermal electronics for personal healthcare systems one of the most exciting current applications of PEDOT:PSS.

1.2 Motivations

Human skin is naturally soft, consisting of the epidermis, dermis, hypodermis, and muscle layers, and its surface is a microrelief structure with multiscale roughness with folds, wrinkles, and hairs. In contrast, conventional metal-based epidermal electrodes are rigid and have a high Young's modulus. One challenge of epidermal electronics for health monitoring is to achieve a conformable contact to skin and to withstand strain caused by movement while retaining consistent electrical performance. Several materials have been reported to achieve the objective, in form of films, bio-inspired adhesives, conductive fabrics and gels. The use of thin films can decrease the effective modulus of the materials, thus improving the contact with the skin. Adhesive film electrodes are another attractive option for the application of epidermal electronics due to their ability to adhere to the skin and achieve conformal contact without the requirement of an adhesive tape. Owing to their biocompatibility, tunable electrical and mechanical properties, and high-water content, conductive gels are highly promising in the field of epidermal electronics. However, issues, such as adhesion, mechanical properties, conductivity, anti-freezing, long-water retention, self-healing

performance, and insufficient understanding of self-healing types and their respective ability, require further investigation to enhance their use in bioelectronics and wearable electronics.

Self-healing is a desirable feature in materials utilized for bioelectronic devices, as it enables them to recover their functionalities after damage. This feature prolongs the lifetime of the electronics, increasing their durability and reliability. Conducting polymer-based self-healable bioelectronics are still a relatively underexplored area of research, with only a limited number of reports available. Furthermore, the healing mechanism of such electronics, particularly in self-adhesive films, is not yet well understood.

To meet the high requirement for next-generation bioelectronics, extensive research efforts are being focused on the design and fabrication of stretchable, adhesive, biocompatible, and self-healable epidermal electrodes.

1.3 Hypothesis and objectives

In the PVA-borax hydrogel system, other materials (e. g. polydopamine, graphene, silver nanowires, and agarose) are often incorporated to enhance its self-healing, mechanical, and electrical performance. PEDOT:PSS ink (Clevios SV3), a commercially available screen-printing paste, is composed of PEDOT:PSS and high amounts of diethylene glycol (DEG, 10-30%) and propylene glycol (PG, 60-80%). We hypothesize that this formulation can reduce the amount of dynamic borate ester bonds by promoting the formation of hydrogen bonds between PEDOT:PSS, PG, DEG and PVA, as well as enable the rearrangement of the PVA chains. These interactions can enable the development of hydrogels with enhanced plastic stretchability, self-healing performance, compliance, and adhesion.

Pure PEDOT:PSS films are fragile and non-adhesive. PEDOT:PSS films also show limited stretchability. Ethylene glycol (EG), acting as a conductivity and softness enhancer, is introduced to the PEDOT:PSS system to increase the electrical and mechanical properties of PEDOT:PSS films. Tannic acid (TA), a natural polyphenol, has been widely used to prepare skin adhesives, especially in hydrogels. Here, our hypothesis is that the addition of EG and TA into PEDOT:PSS films can enhance the stretchability and adhesion. In addition, we also hypothesize that TA can result in the gelation of PEDOT:PSS at high PEDOT:PSS concentration and high processing temperature. Furthermore, EG is also known to yield hydrogels with long-water retention and anti-

freezing properties. We further hypothesize that the long-water retention and anti-freezing properties can be improved by adding EG into the hydrogel system.

Thereby, the primary specific objectives of this thesis are as follows:

1) To improve the mechanical (softness and stretchability) and self-healing properties of PVA-borax hydrogel and fabricate soft and adhesive epidermal hydrogel electrodes.

To achieve this objective, we introduced PEDOT:PSS ink into a PVA-borax hydrogel system. We investigated different ratios of PEDOT:PSS ink and PVA solution (10%) on the adhesion, conductivity, mechanical behaviors, rheological properties, and self-healing ability of the SV3/PVA hydrogels. We illustrated the adhesion ability of the hydrogels on various materials (e. g., plastic, ceramic, glass, and stainless steel). We used the optimized sample to fabricate the epidermal patch electrodes and evaluated their performance by the skin-impedance measurements. Last, we recorded ECG & EMG bio-potential and compared their performance with different types of commercial Ag/AgCl gel electrodes.

2) To prepare soft, stretchable and adhesive film and to acquire a more comprehensive understanding of the self-healing mechanism of the adhesive film (autonomic and cut-stick healing).

Conductive, soft, stretchable, and adhesive films are of great interest for the wearable electronics and bioelectronics. To prepare such films, we incorporated TA (functioned as skin adhesive) and EG (acted as conductivity and softness enhancer) into PEDOT:PSS suspension and dried the mixture in a mold. We explored the effect of different amounts of TA on the adhesion, mechanical properties, and self-healing ability of the PEDOT/EG/TA films. We investigated the biocompatibility (cell viability) of the films by culturing C2C12 mouse muscle cells. Epidermal patch electrodes based on the optimized sample were prepared. The skin-electrodes impedance, ECG & EMG tests were performed to evaluate the electrodes.

3) To fabricate soft and highly conductive gels with anti-freezing and long-water retention properties and use them for long-term ECG recording.

To accomplish this objective, we used TA which can lead to the gelation of PEDOT:PSS, and EG (acted as the anti-freezing agent) to prepare PEDOT/EG/TA gels. First, we investigated the effect of TA on the gelation by heating PH1000 and concentrated PEDOT:PSS suspension (3%) and

explained the mechanism of the gelation. We investigated the effect of EG on the mechanical, anti-freezing, and water retention properties of the gels. We fabricated the gels-based epidermal patch electrodes with Tegaderm tape and assessed their performance by the skin-electrode impedance measurements. The gel electrodes were used to record ECG and EMG bio-signals and used for human-machine interface to control a robotic hand in real-time. Last, we investigated the long-term use of the gels by dehydrating them at ambient condition for one week. We measured the conductivity and the skin-electrode impedance and recorded ECG big-potential with the dehydrated gels epidermal patch electrodes.

1.4 Organization of the work

This thesis comprises the following chapters and three articles: one already published and two submitted to scientific journals.

Chapter 2 presents a comprehensive literature review on epidermal electronics used for healthcare, including the introduction of human skin, conventional epidermal electrodes, bio-inspired adhesives, film electrodes, fabrics, and PEDOT:PSS based epidermal electrodes.

Chapter 3 describes the material processing and synthesis, along with a brief overview of the research methodology utilized throughout the study.

Chapters 4 to 6 consist of three articles, of which I was the first author, that have been reprinted for this thesis.

In Chapter 7, a brief discussion is presented on the main results.

Chapter 8 summarizes the conclusions and presents future prospects.

CHAPTER 2 LITERATURE REVIEW

Unlike implantable electronics that are positioned inside or on organs, epidermal devices placed on the skin offer a non-invasive approach to human healthcare, enabling the monitoring of physical activities, vital signs, and molecular changes in sweat, saliva, wound exudate, and exhaled breath. Here, we focus on the use of epidermal patch electrodes to monitor vital signs such as ECG, EMG, and EEG.

2.1 Human skin

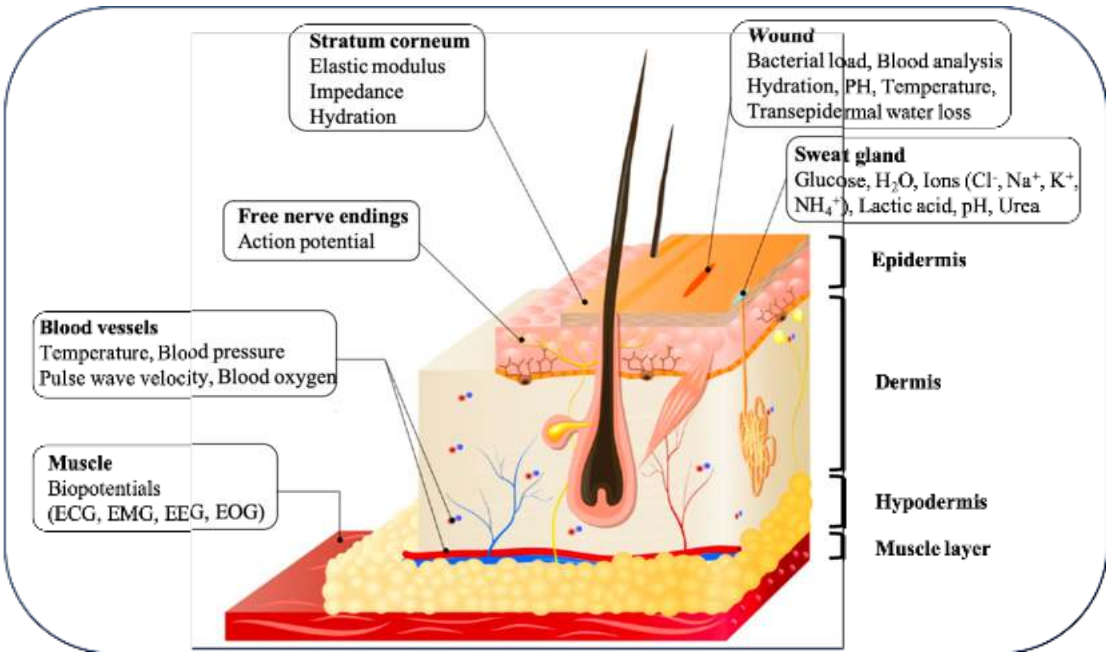

Figure 2.1 Illustration of human skin as a diagnostic platform. Reproduced with permission from [14]. Copyright 2017, American Chemical Society.

Human skin is the largest organ of the body, which acts as the outermost barrier against the invasion of external organisms. It consists of the epidermis, dermis, hypodermis, and muscle layers, where the surface is a complex microrelief structure with folds, wrinkles, and hairs at multiple scales of roughness (Figure 2.1) [15]. The stratum corneum in the epidermis is composed of stacked layers of cells (live basal cells and dead corneocytes), and acts as a water-retaining layer, providing a basis for hydration assessments. In addition, the epidermis also acts as an outlet for sweat, which contains various biomarkers including mineral ions, glucose, lactic acid, and urea.

Human skin provides a diagnostic interface that epidermal devices can mount on and measure physiological statuses such as electrophysiology, temperature, hydration, blood pressure, blood oxygen level, pH, and biomarkers in sweat. For example, electrophysiological signals, including ECG, EMG, EEG, and electrooculography (EOG), can be easily monitored with an epidermal device.

The Young's modulus of human skin (Figure 2.2) varies from 2-80 kPa in the dermis to 140-600 kPa in the epidermis, depending on factors including age, skin type, hydration levels, and overall health [16, 17]. Human skin is known for its soft and flexible nature, with a typical elastic stretchability of 30% strain [18]. Therefore, epidermal electrodes should be able to bend and conform to the skin's surface and also capable of stretching and adapting to the movements of the body.

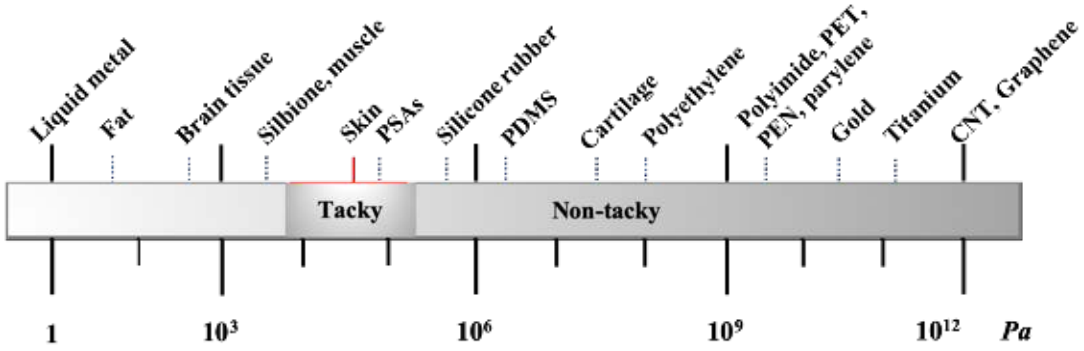

Figure 2.2 Elastic moduli for various representative materials including metals, polymers, conductors, and biological tissues. Reproduced with permission from [14]. Copyright 2017, American Chemical Society.

Bio-signals produced by muscles are transmitted by converting ion current at the human tissues into electron current, to be delivered via electrical wires to measuring devices. Skin-electrode impedance, which refers to the resistance to the flow of electrical current between the skin and the electrode mounted on it, is an important factor for bio-signals recording. The quality of signal detection and monitoring is significantly influenced by the contact conditions, which could be affected by various factors including contacting area, skin hydration, skin type, temperature, and the presence of skin oils. For instance, the skin-electrode impedance can range from 10^7 Ω under dry conditions to 10^3 Ω under wet conditions. In addition, poor contact between the electrode and

the skin can easily result in high impedance and lead to high noise. Thus, the choice of material for epidermal electrodes and conformal contacts is significant for high-quality biopotential recording.

2.2 Conventional medical epidermal electrodes for healthcare

Generally, conventional patch electrode consists of adhesive supports that promote skin attachment, and conductive materials, i.e. metals and Ag/AgCl gel.

Horace Day reported the first pressure-sensitive tape that was used as a skin adhesive in 1845 [19, 20]. He demonstrated an adhesive surgical cloth coated with a natural rubber, which was used in practice. The first commercial medical bandage (Band-Aid) was introduced by the company Johnson & Johnson in 1920 [4].

Skin adhesives have evolved significantly for medical applications, such as medical device fixation, minor wound management, self-adhesive electrodes, and athletic taping [4]. Acrylic-based pressure-sensitive adhesives are widely used for clinical practice due to their stability and strong bonding ability to the skin [4, 21, 22]. However, such adhesives have some drawbacks. For instance, they can cause skin irritation and damage upon removal, such as skin stripping, blistering, and skin tear [4]. In addition, their adhesion can degrade because of exposure to water and sweat during physical activity [4]. Additionally, these adhesives have limited reusability because the adhesive surface quickly becomes contaminated [4].

The acquisition of bio-signals is typically achieved with metal (ground strap, bar, or cup type) and Ag/AgCl gel electrodes (Figure 2.3). For instance, electrodes made of a suction cup and an attached bulb are commonly used to measure ECG due to their ease of attachment and relocation (Figure 2.3a) [11]. Similarly, metal cup electrodes consisting of a cup-shaped electrode with an open-top hole, through which electrolyte gel is added to enhance conductivity, are widely used to measure EEG (Figure 2.3b). In contrast, dry electrodes are made of conductive materials, silicone elastomer, and a lead wire, and do not require a conductive gel (Figure 2.3c). Another type of electrode commonly used for recording ECG, EEG, and EMG is the Ag/AgCl gel electrode, comprising an Ag/AgCl sensing layer and conductive gel (Figure 2.3d).

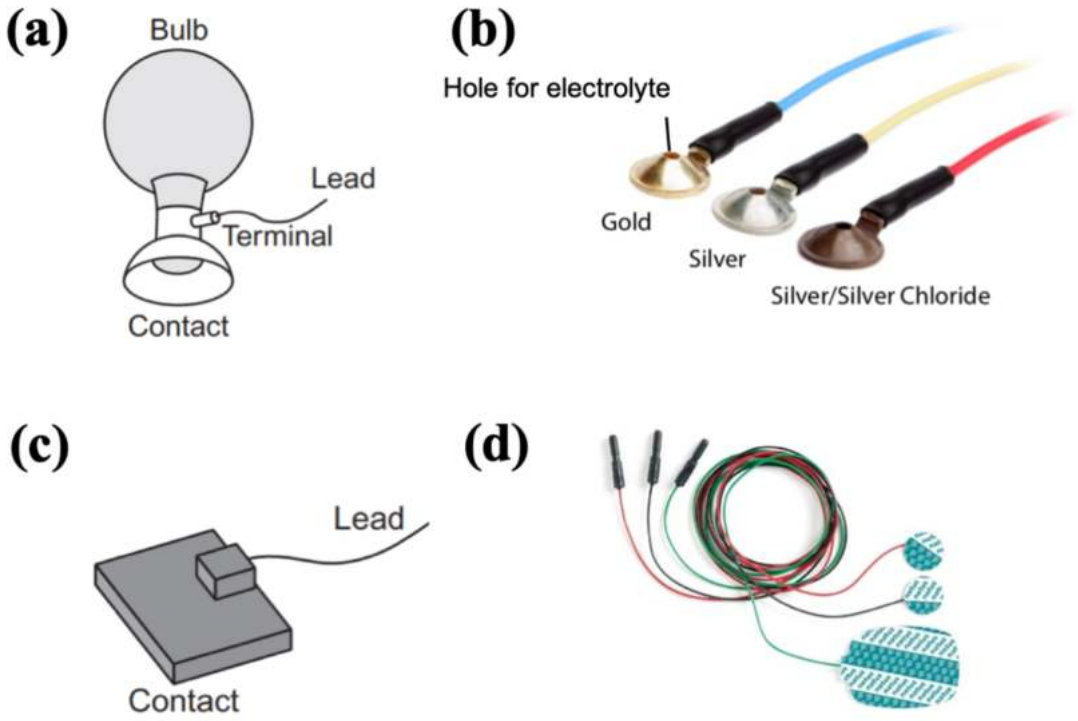

Figure 2.3 Medical epidermal electrodes. (a) Suction-based electrode, (b) Cup electrode, (c) Dry electrode, and (d) Disposable Ag/AgCl gel electrode.

Metal-based electrodes are associated with several limitations. One of the main concerns is that skin irritation and injury (e. g., skin stripping and blistering) are caused by the mechanical mismatch between the electrode surface and skin. This can make metal electrodes unsuitable for use on sensitive and fragile skin, particularly in neonates, where they can cause iatrogenic injuries and scarring [8]. Additionally, the use of an electrolyte gel is necessary to improve conformability and conductivity between the rigid metal and the skin. Metal electrodes are not suitable for long-term bio-signal recording due to the risk of skin irritation and poor conformability after the electrolyte gel dries out [4].

Currently, medical disposable Ag/AgCl gel electrodes are commonly utilized to measure patient biopotentials due to their ability to achieve high-quality recording [10]. However, the extended use of such electrodes can result in skin irritation caused by the adhesives and the electrolyte evaporation. Additionally, skin preparation procedures like shaving and cleaning are often necessary before the measurements [10].

2.3 Bio-inspired adhesives and adhesive electrodes

To address the limitations of conventional epidermal electrodes, researchers have developed bioinspired electrodes with innovative adhesion patches. These patches incorporate mushroom-like, suction cup-shaped, and micro- or nanopillar array structures to enhance their adhesive properties (summarized in Table 2.1).

Table 2.1 Summary of various types of bioinspired skin patches.

Types	Components	Engaged Substrates	Adhesion strength (N/cm^2)	Features	Applications	Ref.
Mushroom-shaped structure	PDMS	Dry human skin	1.3	Biphasic composite micropillar, fixation function	ECG recording	[23]
	High modulus PDMS base and low modulus tips	Dry human skin	1.8	Biphasic composite micropillar, fixation function	ECG monitoring	[24]
	PDMS and vinylsiloxane tips	Dry and wet human skin	1.8	Biphasic composite micropillar, stain sensor	Respiratory and heartrate monitoring	[25]
	PDMS, CNT, and graphene nanopowder	Dry skin replica	1.3	Conductive self-adhesive composite	ECG recording	[26]
	Ecoflex 00-30 and silver micropaticles	Dry human skin	0.1	Conductive self-adhesive composite	ECG and EEG monitoring	[27]
Suction cup	PDMS	PUA skin replica	0.15	Gradual miniaturized suction cup structure	ECG, pulse, respiration monitoring, body temperature measurement, and drug-delivery	[28]
	PDMS or soft PUA	Dry and wet skin	1.33 (dry)	Protuberance inspired dome structure	Transport a large silicon wafer in air and under water	[29]
	PDMS	Dry and wet pig skin	1.5 (dry) 1.8 (wet)	Meniscus-controlled unfoldable tip	-- --	[30]
	PDMS and reduced graphene oxide (rGO)	Dry and wet skin	Peeling force	hexagonal convex cup architectures	ECG monitoring	[31]
Micro- or nano-pillar	poly(glycerol-co-sebacate acrylate) coating with oxidized dextran	Porcine intestinal tissue	$4.8x10^4$ N/m^2 (shear force)	Nanoscale pillar arrays structure	-- --	[32]
	PDMS with PS nanotips	Ni metal	Pull-off force	Hexagonal arrays of cylindrical PS nanopillars	-- --	[33]

Bioinspired by the gecko, a mushroom-like micropillar array patch made of PDMS by a two-step photolithography and etching process was developed (Figure 2.4a and b) [23]. The resulting

adhesive patch was utilized for ECG recording (Figure 2.4d) and possessed several advantages over the traditional pressure-sensitive tape, such as painless detachment, improved biocompatibility, reduced inflammation, and self-cleaning capability. However, the adhesion of these patches (~1.3 N/cm^2, Figure 2.4c) was lower than that of commercial acrylic adhesives (~3.0 N/cm^2). Similar gecko-inspired micropillar structured patches were obtained to improve adhesive strength by utilizing a soft PDMS top layer (Young's modulus: ~0.8 MPa) to enhance conformability, and a high modulus PDMS stem (~8.2 MPa) to increase structural stability (Figure 2.4e) [24]. The patches showed enhanced adhesion (1.8 N/cm^2, Figure 2.4f) and proved to be highly durable, withstanding ~30 cycles (Figure 2.4g). Acting as an adhesive, the patch is capable of recording ECG signals in real-time (Figure 2.4h).

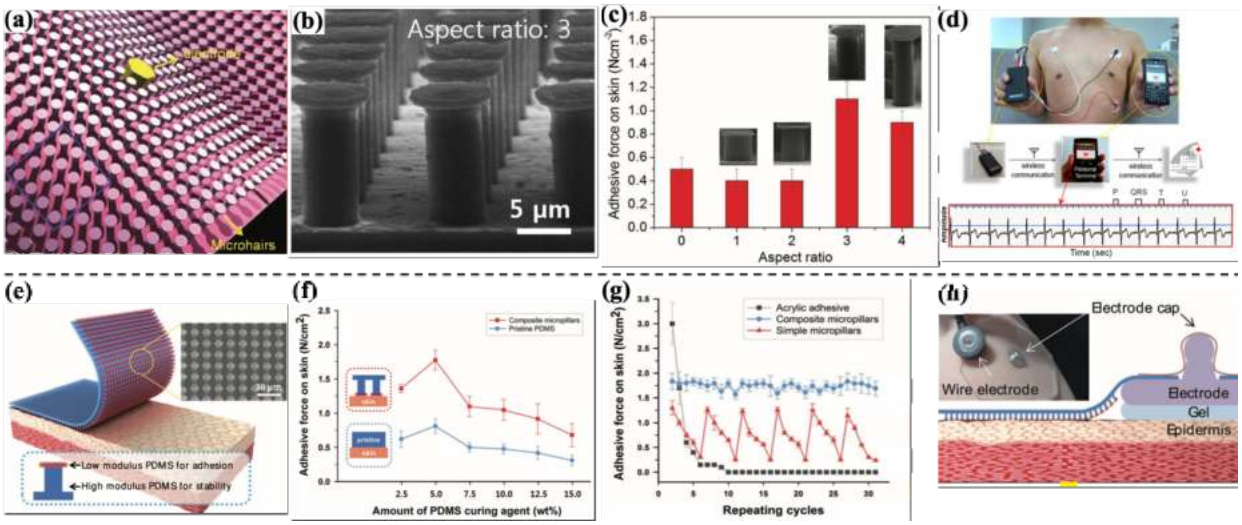

Figure 2.4 Gecko-inspired epidermal adhesive patches with diagnostic functions. (a) Illustration of the microstructure adhesive as biomedical bandage; (b) SEM images of the micropillars with a constant pillar diameter of 5 μm and an aspect ratio of 3; (c) Adhesion force on the skin with different aspect ratios; (d) Utilization of the adhesive as a fixation unit for ECG recording. (a-d) are reprinted with permission [23]. (e) A micropillars adhesive patch with low modulus PDMS as the tips and high modulus PDMS as the stem; (f) Adhesion force on skin with different amounts of PDMS curing agent; (g) Adhesion force versus repeating cycles; (h) The use of the patch to attach a metal electrode on the skin for ECG recording. (e-h) are reproduced with permission [24].

Similarly, a patch inspired by geckos was fabricated, which featured a PDMS micropillar structure decorated with mushroom-shaped vinylsiloxane (VS) tips (shown in Figures 2.5a) [25]. This patch could conform well to the skin and exhibited an adhesive strength of 1.8 N/cm^2 (Figure 2.5 b and

c). The patch was employed as a skin-adhesive strain sensor (Figure 2.5d) to monitor heart rate and respiration, resulting in an impressive signal-to-noise ratio (SNR) of ~60. Conductive adhesive patches with mushroom-shaped tips were prepared by mixing Ag microparticles with Ecoflex 00-30 (Figure 2.5e) [27]. The conductive patch, despite having a low adhesion of 0.1 N/cm^2 (Figure 2.5f), demonstrated lower electrode skin impedance in comparison to medical Ag/AgCl gel electrodes. They could be utilized in healthcare for monitoring ECG (Figure 2.5g) and EMG (Figure 2.5h) signals without causing skin irritation, even during activities like swimming. Also inspired by the gecko, Seokwoo et al. proposed conductive and adhesive patches with mushroom-like structures obtained by incorporating CNT, carbon fillers (including carbon black, Nano-graphite, and graphene nanopowder) into PDMS (Figure 2.5i) [26]. This resulting skin patch exhibits both high adhesive strength (1.3 N/cm^2, Figure 2.5j) and electrical conductivity (100 Ω cm), possessing high-quality ECG signal detection, even during physical activity (Figure 2.5k).

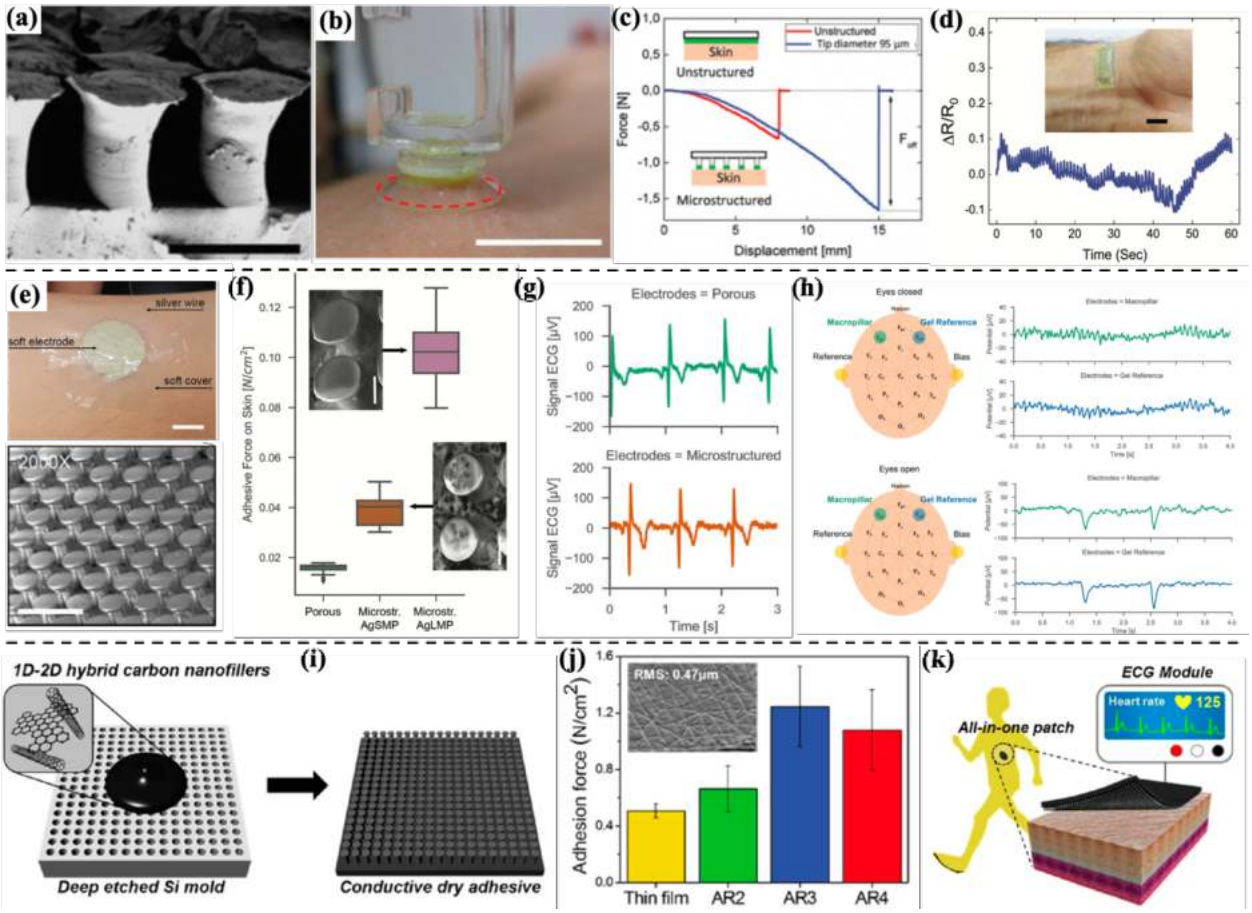

Figure 2.5 Gecko-inspired mushroom-like epidermal patches with diagnostic functions. (a) Cross-sectional SEM image showing an adhesive patch with micropillar structure; (b) Digital photo of

the adhesive patch attaching to forearm skin; (c) Force versus displacement plots of a micropatterned adhesive film. The figure displays enhanced adhesive force compared to unstructured patches; (d) The use of the patch as a strain sensor. (a-d) are reproduced with permission [25]. (e) An adhesive and conductive patch made of silver microparticles and Ecoflex 00-30; (f) Adhesion force versus different polymer electrodes (porous structure electrodes and microstructures electrodes with small AgSMP and large AgLMP microparticles); The application of the patch electrodes for ECG (g) and EEG (h) recording. (e-h) are reproduced with permission [27]. (i) An adhesive and conductive patch comprised of graphene/CNTs/PDMS. (j) Adhesion force on the skin replica versus pillar height (the insert is the top view of SEM image of the skin replica. AR represents aspect ratio); (k) The use of the patch for ECG monitoring under movements. (i-k) are reproduced with permission from [26]. Copyright 2016, American Chemical Society.

In recent years, there have been reports of adhesives inspired by cephalopods with microscale suction cup structures[28-31]. For instance, an adhesive patch with octopus-inspired architectures (OIAs) obtained from PDMS or a soft polyurethane-acrylate-based polymer (Figure 2.6a and b) [29], exhibited robust adhesion (3.0 N with a patch area of 1.5×1.5 cm^2) to pig skin when loaded with phosphate-buffered saline (PBS) (Figure 2.6c). Additionally, Kim et al. demonstrated cephalopod-inspired patches with miniaturized suction cups (mSC) made up of 2D micro-hole arrays (Figure 2.6d and e) [28]. The intaglio mSC mold was coated with gradual modulus PDMS (ranging from ~1.6 MPa to ~500 kPa), with the high modulus layer forming the mSC structure and the low modulus layer providing conformal contact to the skin. With the mSC structure, the skin patches achieved an adhesion strength of 0.15 N/cm^2 to dry poly(urethane acrylate) (PUA) skin (Figure 2.6f). The patches exhibit a broad range of biological applications such as ECG recording, respiration monitoring, body temperature measurement, and drug delivery (Figure 2.6g).

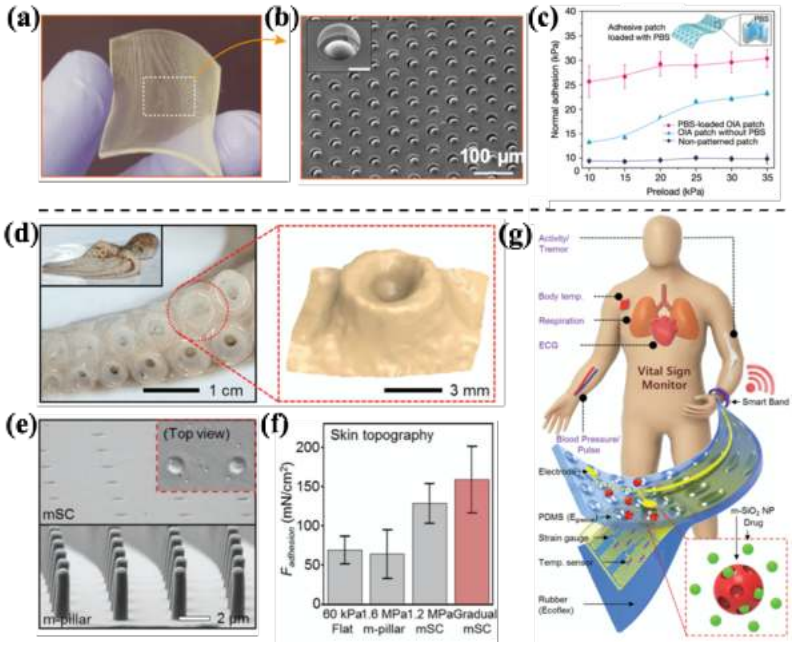

Figure 2.6 Bioinspired adhesive patches. (a) Digital photo of an octopus-inspired architecture patch; (b) SEM image of microcavities array with protuberance-like dome-shaped structures; (d) Adhesion strength on pigskin as a function of preload for OIA patches. (a-c) are reproduced with permission [29]. (d) Photograph of a cephalopod tentacle (left) and 3D laser scanning image of a suction cup (right). (e) SEM images of the side view (bottom) and top view (top) of mSCs; (f) Adhesion force on the skin with different surface-structured patches (flat, m-pillars, and mSCs with different moduli); (g) Illustration of multiple functions of the patch including ECG recording, respiration monitoring, body temperature monitoring, and drug-delivery. (d-g) are reproduced with permission [28].

Bioinspired skin patches show several advantages over conventional medical electrodes, including biocompatibility, skin-friendliness, and the ability to be removed and re-adhered repeatedly. However, they also have some limitations. The primary challenge is the enhancement of their adhesion to the skin, as most bioinspired adhesives have a low adhesive force (less than 1.4 N/cm^2), which is not comparable to commercial skin adhesives (3 N/cm^2) [23, 26, 27]. Although some researchers have used softer and tackier materials to improve skin adhesion, micro or nanostructures used to achieve this tend to collapse, reducing their adhesive abilities [4]. Additionally, the manufacturing process for bioinspired adhesives is time-consuming and expensive [34]. The photolithographic technique is currently the most common approach for fabricating bioinspired adhesive patches, but it significantly increases production costs and time

compared to traditional medical patches. Therefore, developing a simple and cost-effective approach is essential for practical use.

2.4 Film electrodes

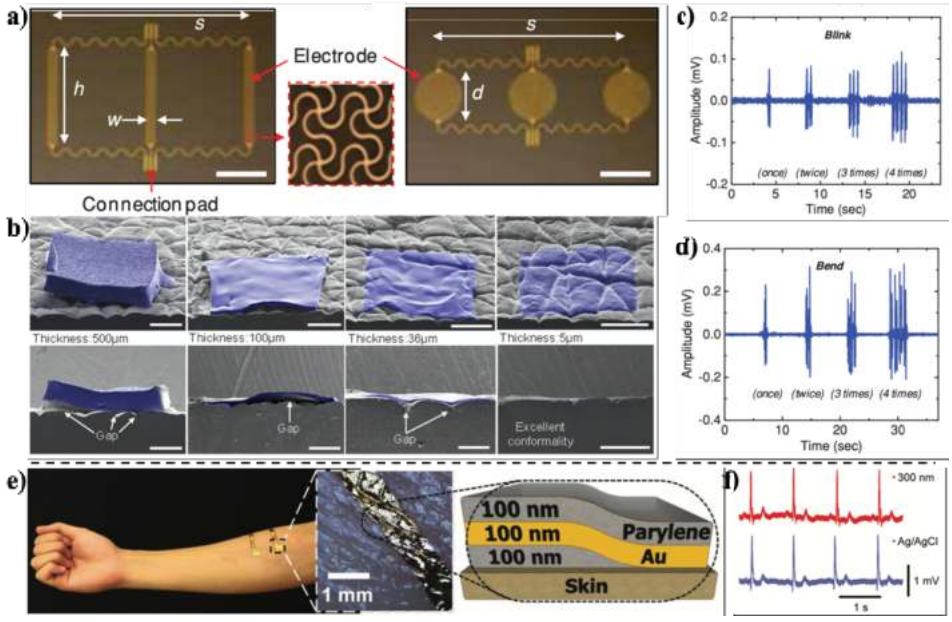

Figure 2.7 Ultrathin and ultra-conformable skin patch with diagnostic functions. (a) The layout of the EES includes bar, disk, and FS mesh-type designs; (b) An ultra-conformable EES for EMG recording. The colorized SEM images illustrate the degree of conformal contact between the skin surface made of silicon (gray color) and elastomer membranes with various thicknesses (blue color); EMG recording while blinking eyes (c) and bending the forefinger (d). (a-d) are reproduced with permission [7]. (e) A self-adhesive ultrathin and ultra-conformable film electrode with a sandwich structure for ECG measurement; (f) ECG recording with the use of ultrathin film and wet Ag/AgCl electrodes. (e-f) are reproduced with permission [35].

The utilization of thin films can reduce the effective modulus of materials and result in conformal contact with the skin [4, 7]. In addition, the integration of sensors, wireless systems, and circuits onto thin polymeric substrates, such as PDMS, silicone rubber, silbione, Tegaderm film, PET, polyethylene naphthalate (PEN), and polyimide (PI), presents an effective approach for the preparation of epidermal electrodes. As a result, these ultra-thin and ultra-conformable patch electrodes provide a range of advantages, including accurate measurement, excellent stability for long-term bio-signal recording, and freedom from interface failure and skin irritation [4, 7].

Rogers' group has developed an ultra-conformable epidermal electronic system (EES) incorporating gold filamentary serpentine (FS) meshes as an active layer (200 nm), presented in Figure 2.7a [7]. They investigated the correlation between membrane thickness and its ability to conform to the skin, revealing that a thin film (5 μm) enabled robust contact with a silicone replica of human skin, while a thicker membrane (>25 μm) resulted in nonconformal attachment to the skin-replicated surface (Figure 2.7b). The ultra-conformable device was utilized to record EEG and EMG signals (Figure 2.7c and d). In a similar case, Robert et al. fabricated a sandwich-structured, self-adhesive, ultrathin, and ultra-conformable patch electrode with a gold layer (100 nm) deposited on the middle layers, shown in Figure 2.7e [35]. The thin film sensor exhibited exceptional signal quality for ECG recording and was able to monitor biopotentials without motion artifacts due to its ultra-conformability (Figure 2.7f).

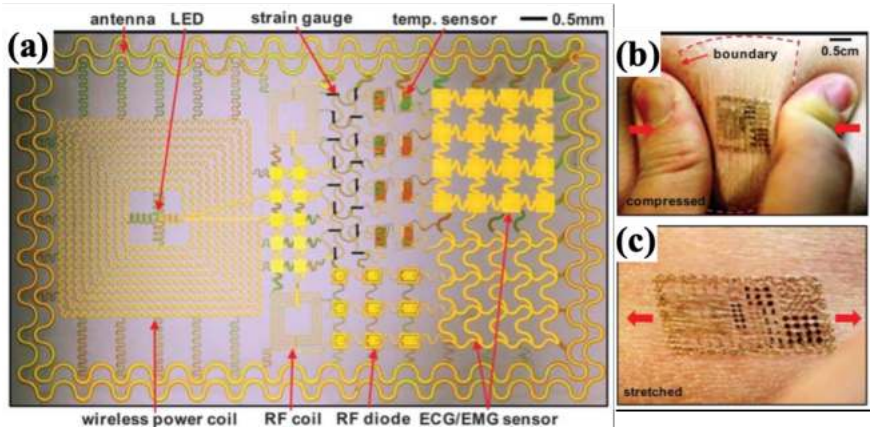

Figure 2.8 Tattoo-based ultrathin and ultra-conformable skin patch electronics with diagnostic functions. (a) Image illustration of the EES with multiple electronic components (FS mesh sensors, LEDs, wireless coils, RF communications, etc.) and with various diagnostic functions including ECG, EMG, EEG, and temperature measurements. The skin patch can be transferred to the skin and showed good compressible (b) and stretchable (c) properties. (a-c) are reproduced with permission [36].

Also, in Rogers' group, a tattoo-based EES was designed with multiple electronic components (e. g., FS sensors (<7μm), wireless power coil, light-emitting diodes (LEDs), and radio frequency (RF) communications) and multiple diagnostic functions such as ECG, EMG, EEG, and temperature measurements, presented in (Figure 2.8 a) [36]. The thin patch electronics can then be transferred to skin and resist compression and stretching (Figure 2.8 b and c).

Despite the ability of ultrathin electrodes to establish an intimate attachment to the skin, these types of electrodes have some drawbacks including challenges related to handling and poor mechanical durability, as well as the need for a carrier substrate (often a sacrificial layer, such as PVA or soluble papers) to transfer the patch to the skin [4]. Moreover, once transferred and printed onto the skin, the ultrathin skin patch is challenging to reuse.

2.5 PEDOT or PEDOT:PSS based epidermal electronics for healthcare

Conductive polymers are distinct from inorganic materials, as they can combine electronic and ionic conductivity, as well as the capability of ionic-electronic coupling [37]. This unique combination of properties makes them ideal candidates for bioelectronics. Conducting polymers offer several advantages over inorganic electronic materials. Firstly, their flexibility and stretchability are major advantages, as they can be bent, stretched, or twisted, which makes them ideal for use in wearable electronics. Secondly, their electrical conductivity can be tailored using additives and electrochemical synthesis techniques [38]. Thirdly, conducting polymers can be easily processed via solution-based techniques, including inkjet printing and spin coating, which allows for large-scale fabrication and low-cost electronics [39].

2.5.1 PEDOT:PSS and its properties

Poly(3,4-ethylene dioxythiophene):poly(styrene sulfonate) (PEDOT:PSS) is a commercially available conductive polymer that consists of two components: conjugated PEDOT (positive charges) and saturated PSS (negative charges). PEDOT has a repeating unit of $(C_8H_6O_2S)_n$ and consists of a thiophene ring with two ethylenedioxy groups attached to it. The ethylenedioxy groups provide solubility in water and organic solvents, while the thiophene ring provides the electrical conductivity (Figure 2.9a). PSS is a sulfonated polystyrene polymer. The structure of PSS is a linear chain of styrene monomers with sulfonate groups attached to the side chains (Figure 2.9 left). The sulfonate groups provide water solubility and act as a counterion to the positively charged PEDOT chain. When PEDOT and PSS are blended, the negatively charged sulfonate groups of PSS electrostatically bind to the positively charged PEDOT chains, forming a stable, conductive polymer blend. Short PEDOT chains are bound to long PSS chains via Coulombic forces [40], and a coiled structure of the PSS segment with PEDOT inside is formed due to the repulsion of PSS chains (Figure 2.9b). In addition, PSS is a water-soluble polymer that acts as a stabilizer for PEDOT, which enables PEDOT:PSS to be stable in water and easily processed. Moreover,

PEDOT:PSS acts as a mixed conductor, where cations are transported through PSS segments, while electrons move within the regions rich in PEDOT. The network structure of PEDOT:PSS can be influenced by several factors, including the concentration of PEDOT and PSS, the processing conditions, the pH value of the solution, and the presence of other additives or impurities.

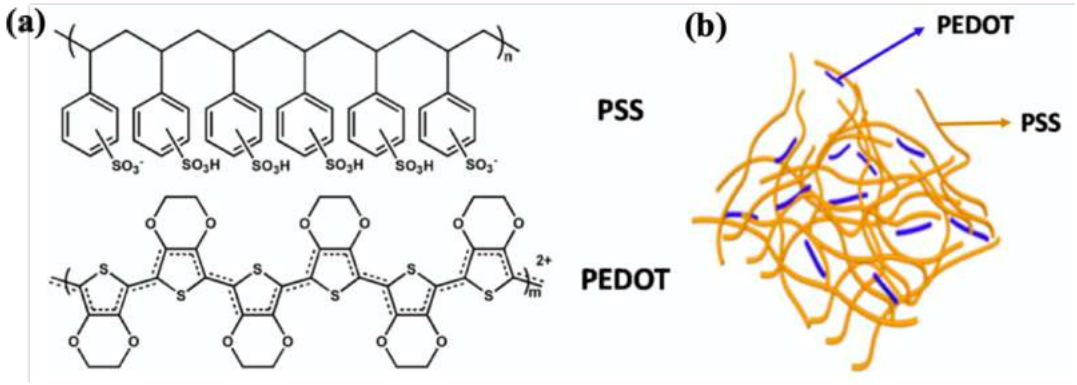

Figure 2.9 The chemical and core-shell structure of PEDOT:PSS. The orange color represents while the blue color indicates short PEDOT chains [40]. Reproduced with permission.

PEDOT:PSS suspensions are currently available under the trade name Clevios™ by Heraeus. These PEDOT:PSS aqueous solutions are categorized into several products based on different parameters such as solid content, viscosity, particle size, and conductivity, which are summarized in the reference [40]. Also, commercial PEDOT:PSS ink, such as Clevios™ S V3 STAB ink from Heraeus, is developed for screen printing applications.

PEDOT:PSS possesses several outstanding properties, including adjustable conductivity (10^{-5} - 10^{3} S/cm), high transmittance, outstanding thermal stability, biocompatibility, self-healing, and good film-forming ability [40-47], which enables it to be widely used in energy, electronics, and biology (Figure 2.10).

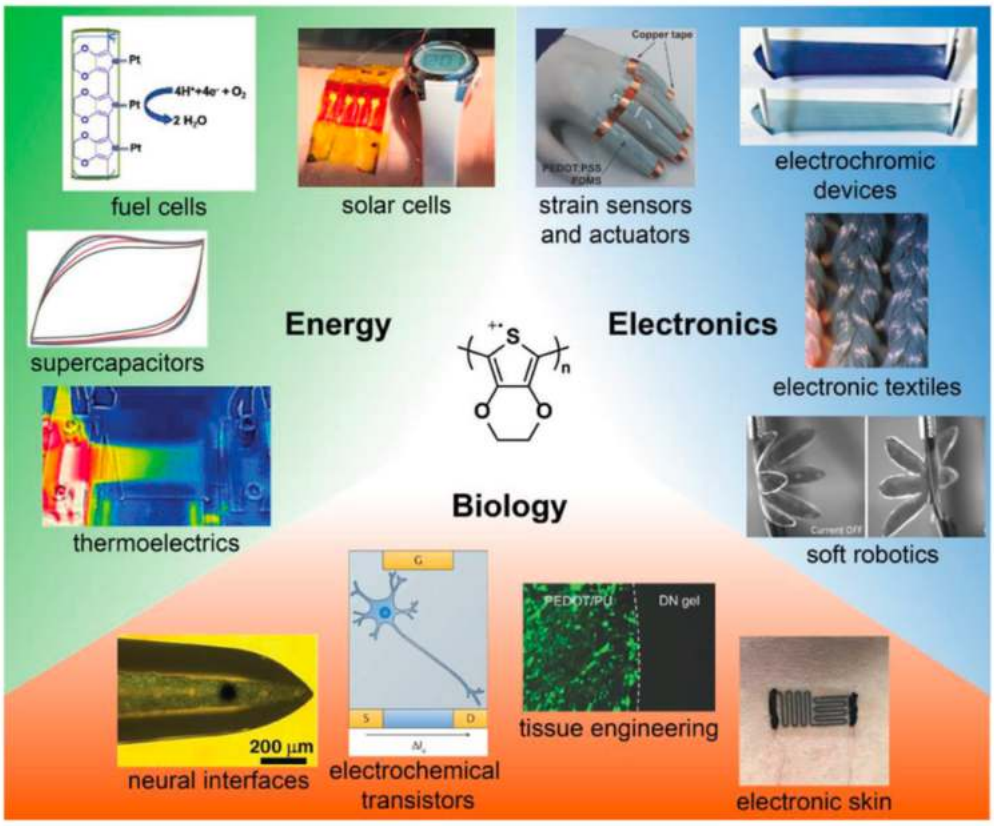

Figure 2.10 Applications for PEDOT:PSS in the fields of energy, electronics, and biology [47]. Reproduced with permission.

Biological applications are of significant interest in healthcare for disease diagnosis and therapy. In comparison to rigid materials like silicon and metal oxides, PEDOT:PSS is a more appealing option for use in flexible electronics, such as epidermal and implantable electrodes.

2.5.2 Electrical and mechanical properties of PEDOT:PSS

Pristine PEDOT:PSS films have limited electrical conductivity and mechanical properties, which limits their applications in wearable devices and bioelectronics. For instance, pristine PEDOT:PSS films obtained from commercial PEDOT:PSS PH1000 solution exhibit a conductivity range between 10^{-4} and 1 S/cm [44]. Also, pristine films typically show a limited stretchability (< 5% strain). Therefore, the electrical and mechanical properties of PEDOT:PSS need to be improved for their practical applications.

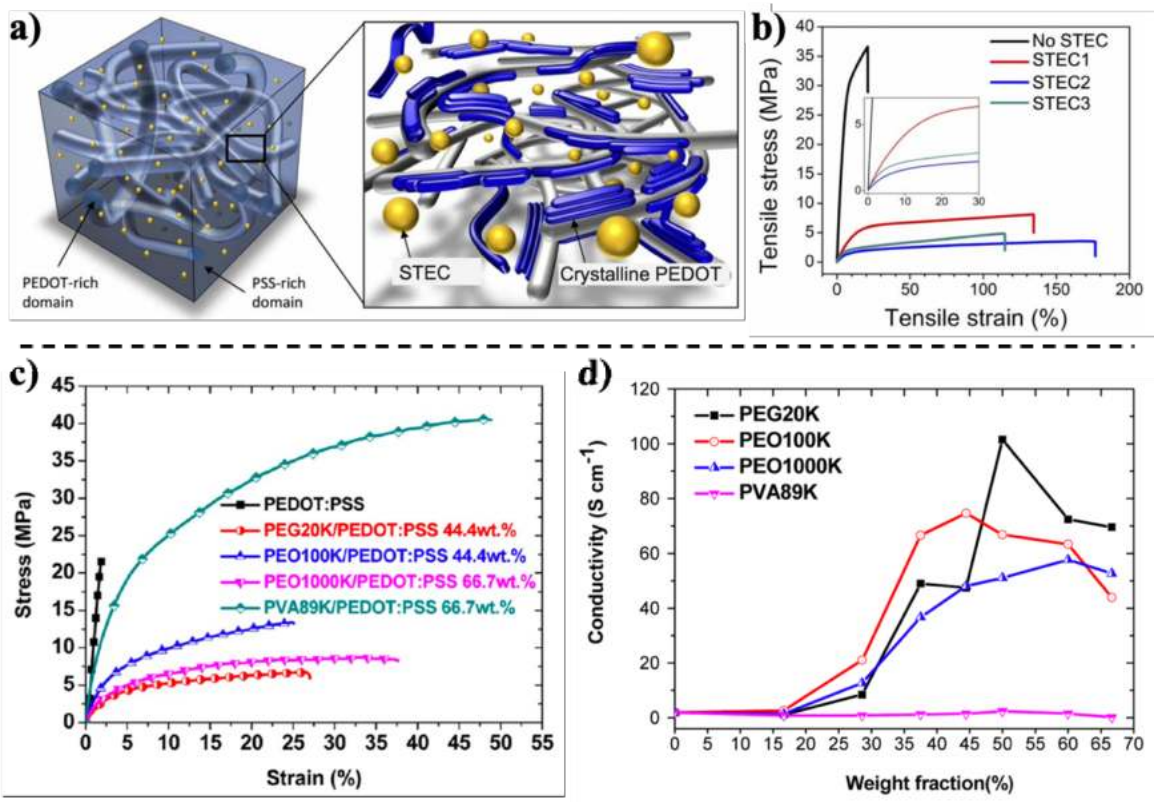

Figure 2.11 (a) A representative schematic diagram of the morphology of PEDOT:PSS films with STEC enhancer; (b) Stress-strain curves of free-standing PEDOT/STEC films. (a-b) are reproduced with permission [45]. (c) Stress versus strain plots of pristine PEDOT:PSS films and polymer films obtained by blending PEDOT:PSS with soft polymers (PEG, PEO, and PVA); (d) Conductivity of thick free-standing PEDOT:PSS/polymer films as a function of soft polymer weight fraction. Reproduced with permission from [46]. Copyright 2015, American Chemical Society.

There are several methods to enhance the electrical conductivity of PEDOT:PSS, including doping, post-treatment, and adding additives. Doping PEDOT with dopants (e. g., protonic acids and polyanions) is an effective way to increase their electrical conductivity [38, 40]. The dopant ions are incorporated into the PEDOT chains, resulting in an increase in charge carrier density and conductivity. Post-treatments (e. g., thermal annealing and exposure to solvents), which can help to increase the crystallinity and alignment of the PEDOT chains, are another method to improve the conductivity of PEDOT:PSS [38, 40]. Numerous additives (e. g., surfactants, polar solvents, small-molecule plasticizers, and polymers) can be added to the PEDOT:PSS suspension to enhance their electrical conductivity [38, 40]. These additives can help to improve the dispersion of the PEDOT and PSS chains, which leads to a more homogeneous polymer network [38, 40].

Similarly, adding additives can improve the mechanical properties of PEDOT:PSS. For instance, the introduction of small-molecule plasticizers (e. g., ionic liquids, xylitol, EG, glycerol, etc.) into PEDOT:PSS can enhance their conductivity and stretchability [47]. Adding sugar alcohols and subsequent heating can also increase the stretchability of PEDOT:PSS films [42]. Bao and coworkers introduced ionic additives (stretchability and electrical conductivity enhancers, STEC) into PEDOT:PSS, resulting in the increased conductivity of PEDOT:PSS films (Figure 2.11a). The conductivity could reach 600 S/cm for free-standing films and 3100 S/cm when supported on SEBS (Figure 2.12a) [45, 47]. The free-standing PEDOT:PSS/STEC films demonstrated high stretchability compared to pristine PEDOT:PSS films (Figure 2.12b). Mixing PEDOT:PSS with water-soluble polymers such as PEO and PEG [46], can improve the conductivity and stretchability of the resulting films (shown in Figures 2.12c and d).

2.6 Applications of PEDOT:PSS in epidermal electronics for healthcare

Various types of PEDOT or PEDOT:PSS composites have been widely used for wearable and bioelectronics, typically in form of films, fabrics, and hydrogels.

2.6.1 PEDOT or PEDOT:PSS based film for healthcare

Several fabrication methods, including drop cast, spin coating, and electro-polymerization, have been employed to prepare PEDOT or PEDOT:PSS-based films. In addition, various additives (e. g., dimethyl sulfoxide (DMSO), EG, PEG, TA, protein, waterborne polyurethane (WPU), etc) have been introduced into PEDOT systems, which endows the films with improved electrical properties, enhanced mechanical properties (e.g., high stretchability, toughness, and softness), and new desirable properties such as adhesion and self-healing (Table 2.2). Moreover, PEDOT-based film patch electrodes can be achieved with or without using soft substrates including PDMS, Ecoflex, PET, PEN, and SEBS.

Table 2.2 Summary of PEDOT:PSS based films for epidermal electronics.

Name	Components	Fabrication method	Electrical conductivity (S/cm)	Features	Thickness	Applications	Ref.
PEDOT:PSS Tattoo	PEDOT:PSS	Inkjet printing	~50 to 500 Ω sq^{-1} (sheet resistance)	Tattoo	150 nm	ECG and EMG	[48]
PEDOT:PSS Tattoo	PEDOT:PSS, DMSO, PVA	Printing	~160	Tattoo	< 30 μm	ECG monitoring	[49]
PWS films	PEDOT:PSS, WPU, D-sorbitol	Drop-cast	~70-550	Adhesive	20 μm	ECG, EMG, and EEG	[18]
PPT films	PEDOT:PSS, PVA, EG, TA	Drop-cast	~120	Adhesive	20-25 μm	ECG, EMG, and EEG	[50]
Adhesive/PEDOT-S film	PEDOT:S or PEDOT:PSS, acrylic ester copolymer	Spin coating	30-80 kΩ sq^{-1} (sheet resistance)	Adhesive	12 or 40 μm	EMG recording	[51]
PEDOT:PSS films	PEDOT:PSS	Drop-cast	~1-500	Water enabled healing	1 μm	OECTs	[43]
PEDOT:Tos films	PEDOT:Tos	Chemical polymerization of EDOT, Spin coating	~1600	Water enabled healing	~4–6 μm	--	[52]
PEDOT:OTf films	PEDOT:OTf	Chemical polymerization of EDOT, Spin coating	~2200	Water-enabled healing	~4–6 μm	--	[52]
SRT/PEDOT:PSS biocomposites	PEDOT:PSS, squid ring teeth (SRT) protein	Drop-cast	~120	Water-enabled healing	----	----	[53]
PEDOT:PSS-b-PPEGMEA films	PEDOT:PSS, poly(poly(ethylene glycol) methyl ether acrylate) (PPEGMEA)	Spin coating	~0.05	Water-enabled healing	~300 nm	----	[54]
PEDOT:PSS/PEG	PEDOT:PSS, PEG	Drop-cast	~100-400	Autonomic self-healing	15 μm	--	[55]
PEDOT:PSS/Triton X-100 composite films	PEDOT:PSS and Triton X-100	3D-printing, Drop-cast	~80-180	Autonomic self-healing	20 μm; 2 μm	Thermoelectric generator, OECTs	[56, 57]
Waterproof dry-type PEDOT:PSS	PEDOT:PSS, WPU, EG	Drop-cast	~1 Ω sq^{-1} (sheet resistance)	Long-term use (2 weeks), degradable	----	ECG and EMG monitoring	[58]

Thin PEDOT:PSS films have attracted interest in the field of epidermal electronic due to their improved contact interface [4, 7]. The thin patch electrodes could intimately attach to the skin even during movement, which is favorable to achieve a high signal-to-noise ratio (SNR) [59]. PEDOT:PSS-based nanoscale tattoo (150 nm thickness) skin patch electrodes obtained by ink-jet

printing PEDOT:PSS on the decal paper (Figure 2.12a) showed conformable contact to the skin (Figure 2.12b), and could supply high quality ECG and EMG bio-potentials (Figure 2.12 c and d) [48]. Although the thin films described above could achieve conformal interfaces with skin and excellent quality for bio-signal recordings, they are rather difficult to handle and not mechanically durable [4].

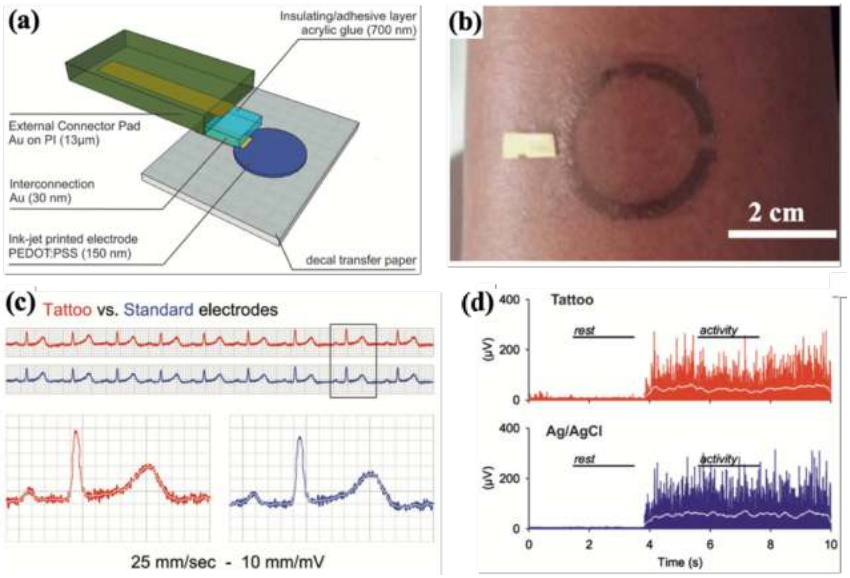

Figure 2.12 PEDOT:PSS-based ultrathin tattoo skin patch electrode for ECG and EMG recording. (a) Layers schematic 3D view of the tattoo electrodes; (b) Circular tattoo electrode on the arm; (c) Continuous ECG recording (top) and a single beat (bottom), achieved by tattoo (red) and standard (blue) electrodes; (d) Rectified EMG recording with using tattoo (red) and Ag/AgCl gel electrodes (blue). (a-d) are reproduced with permission [48].

Adhesive films are another attractive form for epidermal electronics, owing to their ability to adhere to the skin and achieve conformal contacts without the requirement for an adhesive tape. Additives such as dopamine, TA, and D-sorbitol are typically added to PEDOT:PSS suspension to achieve adhesive PEDOT:PSS composite films. Adhesive films (PWS films, thickness of ~20 μm) obtained from a blend of PEDOT:PSS suspension, waterborne polyurethane (WPU), and D-sorbitol (Figure 2.13 a and b) [18], showed high stretchability, good adhesion on dry (0.41 N/cm) and wet (0.56 N/cm) skin and could achieve high quality bio-potential (ECG, EMG, and EEG) recording (Figure 2.13c). Our group prepared adhesive films by blending PEDOT:PSS suspension, EG, and TA. The prepared PEDOT/EG/TA demonstrated high adhesion. The details are described in Chapter 5 of this thesis.

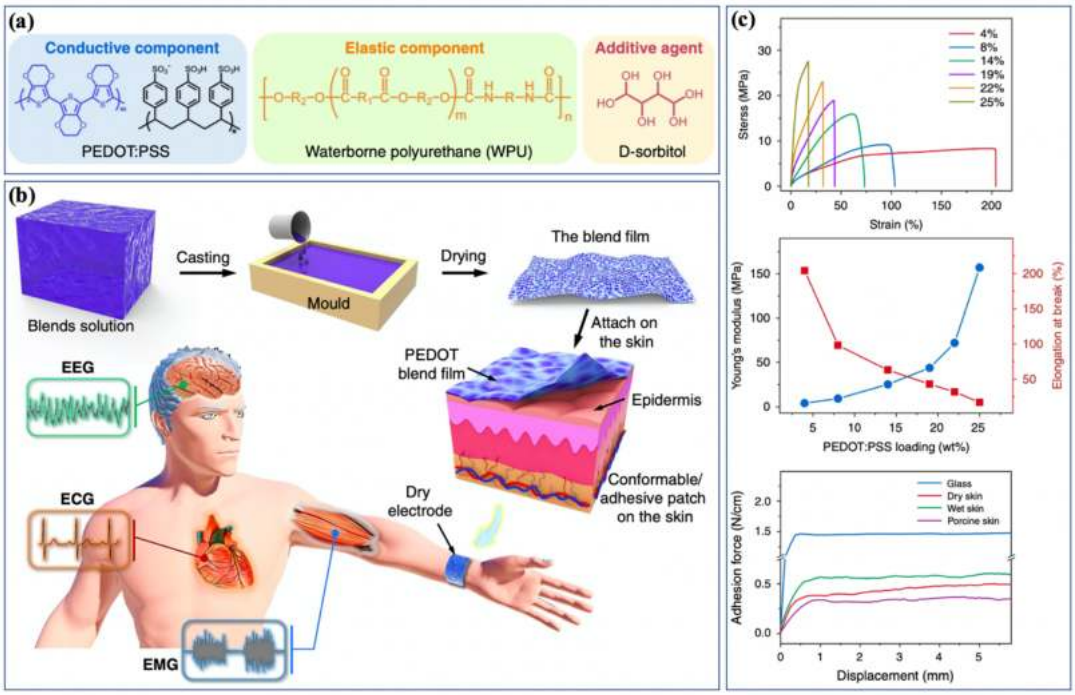

Figure 2.13 PWS adhesive films. (a) Chemical structures of PEDOT:PSS, WPU, and D-sorbitol. (b) Schematic illustration for the preparation of PWS films. (c) Characteristics of the films. Stress-strain plots (upper) with various PEDOT:PSS loadings, Young's modulus and elongation at break (middle), and Adhesion (bottom) of PWS films. (a-c) are reproduced with permission [18].

PEDOT:PSS composite films exhibiting self-healable behavior are highly desirable for bioelectronics, owing to the ability to recover their functionalities after enduring damage. Our group reported that PEDOT:PSS films can be electrically healed upon exposure to water after being cut [43]. The current almost returns to its initial value after several cut-healing cycles at different regions (Figure 2.14a). The SEM images show that the gap is "healed" after wetting (Figure 2.14b and c). The healing behavior was due to the water swelling of PSS chains in the film: the two separated parts of the film swelled after the addition of water to the damaged position, leading to the increase of their volume, thus enabling them to fill the gap. In addition, the wet PEDOT:PSS films demonstrated autonomic self-healing properties, which is likely attributed to their softness.

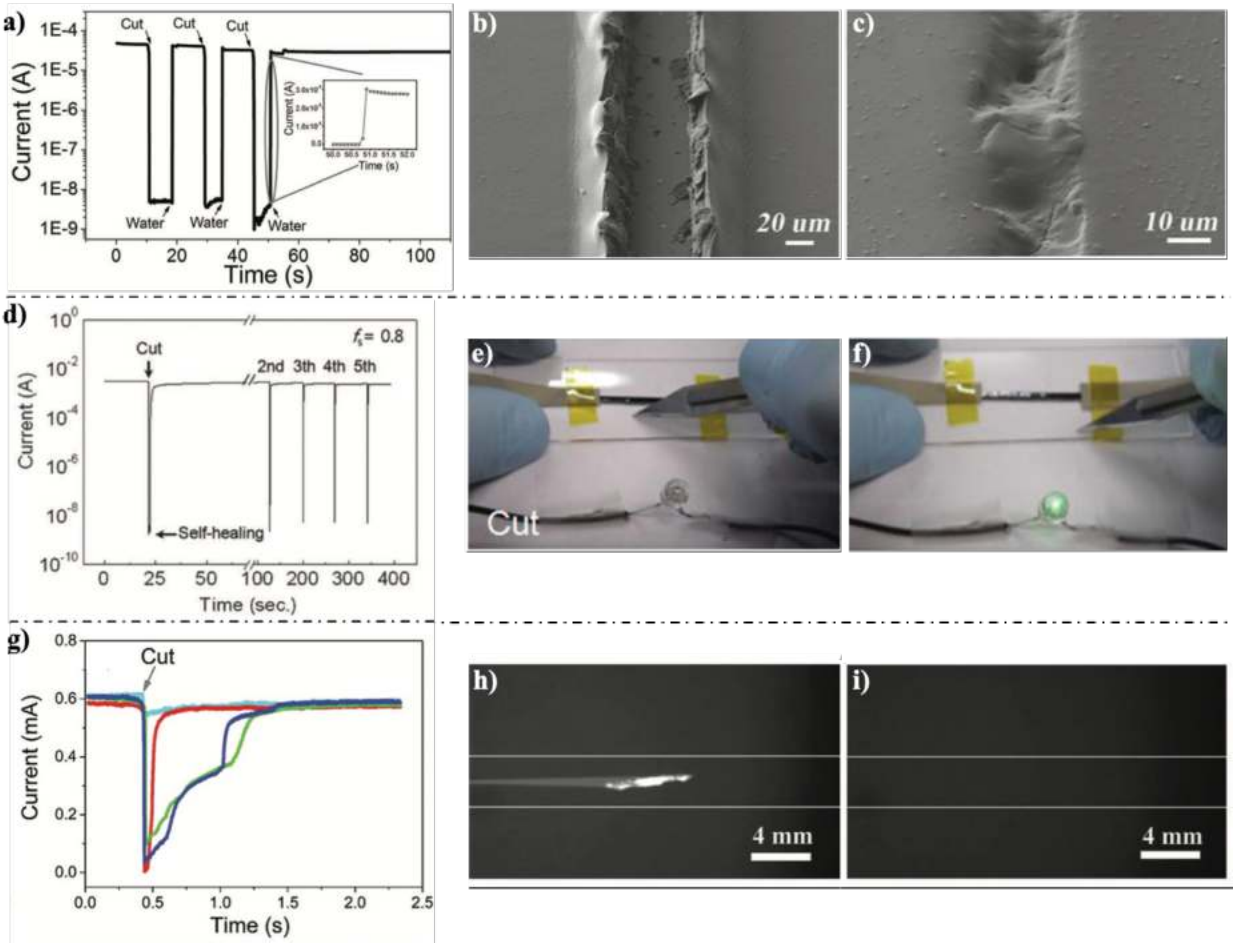

Figure 2.14 (a) current as a function of time for PEDOT:PSS film shows a cut-healing effect with a stainless-steel blade cut and a drop of water healing on the damaged area, 0.2 voltage was applied. SEM images display the damaged area of a PEDOT:PSS film before (b) and after (c) water healing. (a-c) are reproduced with permission [43]. (d) Time-lapse current plot for a PEDOT:PSS/Triton X-100 film during several "cut-heal" cycles. Digital photos of the self-healing process of a PEDOT:PSS/Triton X-100 film with a LED bulb lit off (cut, e) and lit on (healed, f). (d-f) are reproduced with permission [60]. (g) Current versus time measurements during the cut and healing process for four different films obtained from mixtures comprising PEDOT:PSS and 4% PEG-400. SEM images of the cut (h) and healed (i) area of a PEDOT:PSS/PEG film. (g-i) are reproduced with permission [55].

Several factors, such as additives, dopants' type, and processing methods, can influence the healing properties of PEDOT-based films [52, 61]. For instance, PEDOT:Tos (Tos: tosylate) and PEDOT:OTf (OTf: triflate) films synthesized via chemical polymerization exhibited fast healing ability enabled by water, while PEDOT:ClO_4 films obtained by electro-polymerization could not be healed by water [52]. The observed healing behavior is attributed to the high water swelling facilitated by the organic dopants, such as PSS, Tos, and OTf.

Autonomic self-healing behavior can be achieved by introducing additives (e. g., PEG and Triton X-100) into PEDOT:PSS suspension. Incorporating these additives into the films can decrease their crystallinity and increase their segmental mobility, resulting in altered mechanical properties such as decreased Young's modulus or increased viscoelasticity [62]. Films obtained from mixing PEDOT:PSS with Triton X-100 (a surfactant) demonstrated autonomic healing behavior upon repeated cut-healing cycles due to the high viscoelastic nanofibrillar network (Figure 2.14d-f) [60]. The two cut surfaces contact each other after removing the razor blade, and thus the current recovers its initial value.

In our group, self-healing films obtained from PEDOT:PSS and PEG exhibited an excellent autonomic healing ability, even after 100 cuts with an efficiency approaching 100% and a response time of less than 1 s (Figure 2.14g - i) [55]. The autonomic healing is due to the increased softness and viscoelasticity after the addition of PEG. The entanglement of PEG chains with PSS chains facilitates the flow of the separated parts of the film after the cut [55]. Recently, our group reported adhesive and self-healing films by mixing PEDOT:PSS with EG and TA. The PEDOT/EG/TA films showed two types of outstanding self-healing behavior: autonomic healing and cut-stick healing. The details are shown in chapter 5 of this thesis.

PEDOT:PSS-based epidermal electrodes can also be fabricated by mounting a PEDOT:PSS sensing layer onto various soft substrates, including PDMS, Ecoflex, PET, PEN, PI, parylene, cellulose, and SEBS [45, 65, 66 70]. Table 2.3 summarizes the preparation of PEDOT/PEDOT:PSS epidermal patches for healthcare with various substrates and methods such as spin-coating, drop-casting, inkjet printing, immersion coating, gravure-printing, and spray coating. Such soft substrates, which typically possess a low Young’s modulus (e. x. Ecoflex and silicone Rubber), not only provide a platform for the integration of sensors and circuits, but also could increase the mechanical properties of PEDOT:PSS [45, 63, 65]. Moreover, they can form conformal contacts to the skin due to their polymeric nature and mechanical similarity to human skin.

Table 2.3 Summary of PEDOT/PEDOT:PSS based skin patch on various substrates with different techniques.

Components	Substrates	Fabrication method	Active layer thickness	Feature	Applications	Ref.
PEDOT:PSS (PH1000) and STEC ionic additives	SEBS	Spin coating	--	High conductivity	Interconnects for LED and FET devices	[45]
PEDOT:PSS formulation	PEIE modified PDMS	Stencil printing	~9.9 μm	Multichannel concentric-ring electrodes	EMG, EEG, and ECG recording	[63]
PEDOT (Clevios)	Decal paper	Inkjet printing	200 μm (substrate)	Electrode arrays	Facial muscle EMG recording	[64]
PEDOT:PSS ink (768650)	Zonyl-modified Ecoflex® 00-30	Screen printing	--	Remarkable stretchability, large-scale fabrication	Stretchable electrochemical sensor	[65]
PEDOT:PSS	Polyimide foil	Inkjet printing	55 μm (substrate)	Multielectrode arrays	ECG and biceps muscle EMG recording	[66]
PEDOT:PSS	Ethylcellulose fiber paper (15 μm)	Immersion coating	30 μm	Self-wetting patch electrode	ECG, EOG, EEG recording	[67]
PEDOT:PSS	PET	Printing	--	Self-adhesive conductive	ECG recording	[5]
PEDOT:PSS (PH1000) formulation	PET film coated cellulose acetate, PDLLA coated PP film	Roll to roll gravure-printing	~110 nm	Ultra-conformable conducting polymer nanosheets and a high signal-to-noise ratio	Surface EMG recording	[68]
PEDOT:PSS ink (Clevios™ P Jet 700)	Polystyrene-polybutadiene–polystyrene nanosheet-PVA supported by PET	Gravure-printing, Inkjet printing	394 nm	Ultrathin film minimized the obstruction of the skin's natural deformations	Epidermal strain sensor	[15]
PEDOT:PSS (Clevios P Jet 700) based formulation	Transfer tattoo base paper (ethylcellulose)	Spin coating	80 nm	ultra-conformable conductive tattoo nanosheets	EMG recording of flexor carpi ulnaris muscle	[69]
PEDOT:PSS(Clevios PJet 700)	Transfer tattoo paper kit	Inkjet printing	~150 nm	Ultra-conformable Temporary Tattoo Electrodes	ECG and EMG recording on the face	[48]
PEDOT:PSS/Ag nanowire ink	PET	Screen printing	-- --	A transparent and conductive film	Transparent heaters	[70]
Ag electrode, PEDOT:PSS/GOPS/TX-100	PEN	Printing		Wireless Healthcare Monitoring	Temperature sensor	[71]
Silver nanowire, PEDOT:PSS	Natural rubber	Spin coating	up to ~80 nm (PEDOT:PSS)	High stretchability, transparent	Strain sensor	[72]
PEDOT:PSS	Hydroxyethyl cellulose	11-aminoundecanoic acid treatment, Spin coating		High stretchability, biocompatible	Strain sensor	[73]

The geometry of the sensing layer for epidermal electrodes is another factor affecting the mechanical properties and bio-signals recording quality. For instance, multichannel concentric-ring electrodes printed on ethoxylated polyethylenimine-modified PDMS substrate (Figure 2.15 a and b) showed improved adhesion and conformal contact to the skin (Figure 2.15c) [63]. By optimizing the PEDOT:PSS interface layer, the patch electrodes showed lower noise levels compared to commercial gel disc electrodes. The PEDOT:PSS-based dry electrodes presented excellent quality for electrophysiological recordings (e.g. EEG, ECG, and EMG, Figure 2.15d - f). FS geometry is another layout that is widely used in thin epidermal electronic systems (shown in Figure 2.7a). The FS pattern could endow the electrodes with enhanced stretchability, which is essential for wearable electronics.

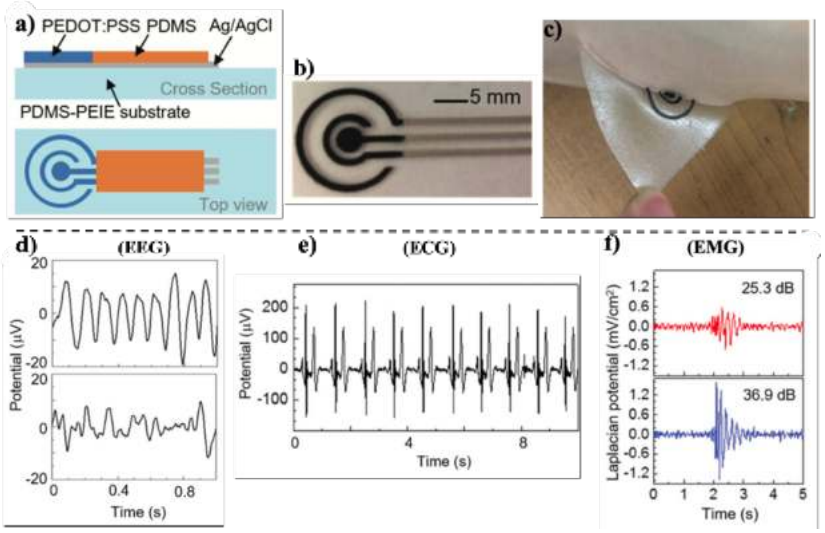

Figure 2.15 Schematic illustration (a) and optical image (b) of the concentric ring electrode; (c) Illustration of the adhesive electrode on the skin. The use of the electrode for EEG (d), ECG (e), and EMG (f) measurements. (a-f) are reproduced with permission [63].

2.6.2 PEDOT based textiles

PEDOT-based fabrics are promising electrodes for use in healthcare. Table 2.4 summarizes PEDOT:PSS-based textiles with different fabrication techniques. Among these techniques, immersion coating and printing are the main methods to introduce PEDOT:PSS onto textiles. For instance, a commercial PEDOT:PSS based fabric product (Hitoe^{TM}), obtained by coating PEDOT:PSS on PET nanofibers, is used for healthcare applications [74]. A cap integrated with Hitoe^{TM} textile electrodes was fabricated and utilized for EMG measurement [75]. The Hitoe^{TM}

electrode-integrated clothing can be used in long-term healthcare and medical support such as ECG monitoring [76]. Concentric-ring electrodes, prepared by screen-printing PEDOT:PSS ink on Mediatex® textiles, were integrated onto a belt and showed similar ECG-recording SNR when compared to Ag-deposited electrodes [77].

Although some processes have been developed for PEDOT:PSS fabrics, their stability, conformability, and bio-signal recording quality still remain a challenge.

Table 2.4 Summary of PEDOT:PSS based textile for health care.

Textile types	Materials	Fabrication method	Feature	Applications	Ref.
Mediatex® TT ACQ 120 µm bonded with an adjustable belt	PEDOT:PSS (C2100629D1)	Screen-printing	Concentric Ring Electrodes	ECG recording	[77]
Woven Fabrics	PEDOT:PSS (Clevios PH 500)	Immersion coating	Sandwiched structure with a foam as filler	ECG recording	[78]
100% interlock knit polyester fabric	PEDOT:PSS (Clevios™ PH1000)/IL gel	Stencil patterning	Using IL gel established low-impedance cutaneous contacts	ECG recording	[79]
100% cotton single jersey and cotton/Lycra single jersey	PEDOT:PSS (Clevios)	Screen-printing	Washable	ECG recording	[80]
Polyamide/Lycra textile fabric	Different Viscosity of PEDOT:PSS solutions	Immersion coating	Washable	ECG recording	[81]
A nonwoven polyethylene terephthalate T-shirt	PEDOT:PSS (Clevios PH 1000), formulation (DMSO and Triton X-100)	Screen-printing	Low sheet resistances	ECG recording	[82]
PET nonwoven fabric	PEDOT:PSS (Clevios PH1000)(with 5% DMSO)/graphite-graphene	Immersion coating	Low sheet resistance	ECG recording	[83]
Woven cotton and woven polyester	PEDOT:PSS (Clevios PH 500) with sorbitol, ethylene glycol or glycerol	Immersion coating	with a foam layer as filler	ECG recording	[84]
Polyamide, polyester, and cotton knitted fabrics	PEDOT:PSS (Clevios)	Dip-coating	Washable and reliable fabric electrodes sewn into bras	ECG recording	[85]
PET nanofibers	PEDOT:PSS	Immersion coating	Hitoe™ bioelectroedes integrated into a cap	EMG monitoring of masticatory muscle	[75]
Cotton/spandex blended fabric	EDOT, TsOH	In situ horseradish peroxidase catalyzed polymerization	Excellent heating durability and stability	Electrothermal heating and strain	[86]
Knitted cotton fabric	PEDOT:PSS, DMSO	Drop coated	No skin irritation	ECG recording	[87]

2.6.3 PEDOT or PEDOT:PSS based hydrogels

Owing to their biocompatibility, tunable electrical and mechanical properties, and high water content (70-99%) [13], conductive hydrogels are highly promising in the field of epidermal electronics [13, 88]. Generally, conductive hydrogels can be achieved either by pure conductive polymers (e .g., PEDOT, polypyrrole (PPy), or polyaniline (PANI)), or, in most cases, by incorporating conductive materials (e.g., conducting polymers, nanoparticles, silver nanowires, CNT, and graphene) into a matrix of insulating polymers (e. g., poly(acrylamide) (PAAM), poly(acrylic acid) (PAA), PVA, gelation, and agarose).Various methods have been reported for the preparation of conductive hydrogels, including physical mixing, in situ polymerization, ion chelation, and electrochemical syntheses. Here, we mainly review PEDOT or PEDOT:PSS-based conductive hydrogels.

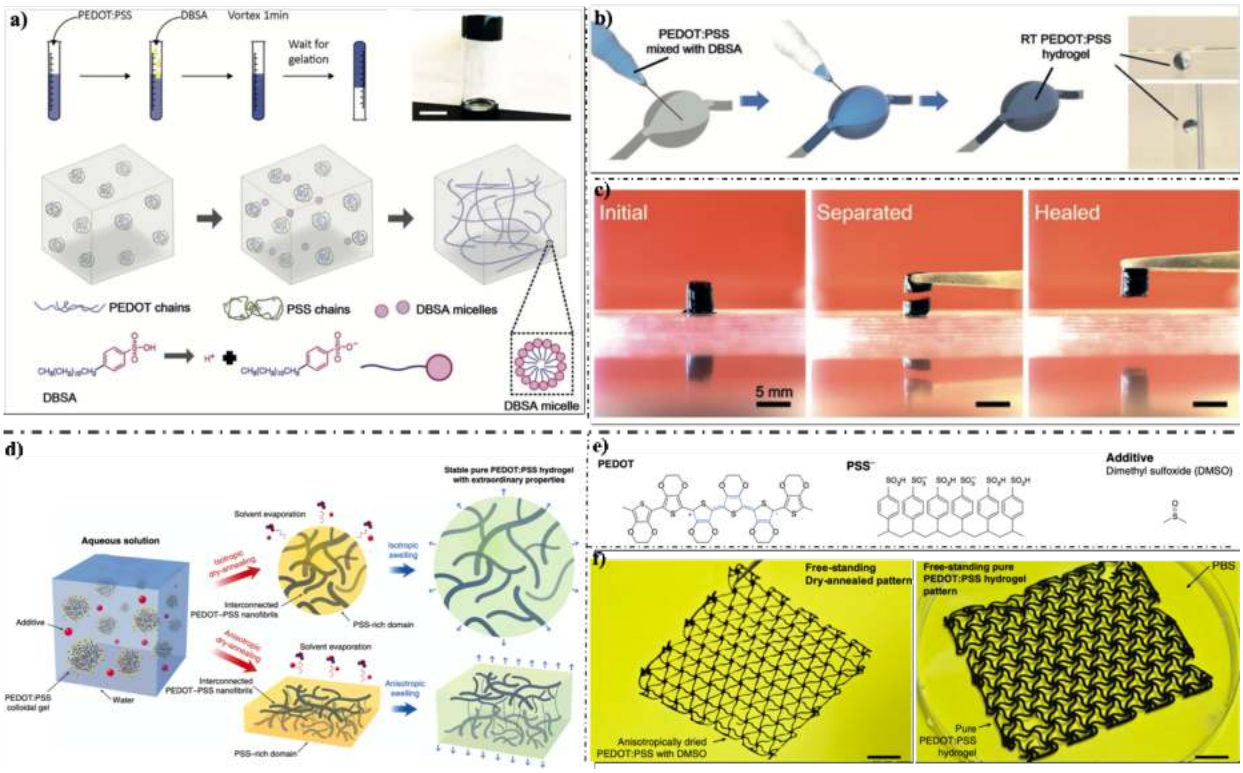

Figure 2.16 (a) Illustration of RT-PEDOT:PSS hydrogel preparation; (b) Injectable properties of RT-PEDOT:PSS hydrogels; (c) Illustration of self-healing of RT-PEDOT:PSS hydrogel by cut-stick process. (a-c) are reproduced with permission [89]. (d) Schematic illustration of pure PEDOT:PSS hydrogel preparation; (e) Chemical structures of PEDOT, PSS, and DMSO; (f) Free-standing pure PEDOT:PSS hydrogel pattern. (d-f) are reproduced with permission [90].

Pure PEDOT:PSS hydrogels can be obtained via directly cross-linking PEDOT chains to form a 3D network structure, enabled by acid treatments (e. g., H_2SO_4 and 4-dodecylbenzenesulfonic acid (DBSA)), dry-annealing and rehydration. For instance, pure PEDOT:PSS hydrogels prepared by mixing PEDOT:PSS aqueous solution with 0.1 mol/L H_2SO_4 and heating at 90 °C for 3 h, exhibited a conductivity of 0.5 S/cm, which increased to ~9 S/cm after the treatment of concentrated H_2SO_4 (18.4 mol/L). A supercapacitor, fabricated from the hydrogel, exhibited excellent electrochemical properties with a volumetric capacitance of 202 F/cm^3 at 0.54 A/cm^3. A similar hydrogel was prepared via blending PEDOT:PSS dispersion with DBSA (Figure 2.16a). The hydrogels showed room-temperature gelation behavior when the concentration of DBSA reached a critical threshold value of approximately 3 v/v% and exhibited a conductivity of 0.1 S/cm. In addition, the physically crosslinked hydrogels present injectable and self-healable properties because of the shear-thinning behavior of the mixture and high volumetric swelling ratios, respectively (Figure 2.16b-c).

By subsequently dry-annealing and rehydrating a mixture of PEDOT:PSS/DMSO, a physical cross-linked PEDOT:PSS hydrogel was achieved (Figure 2.16d-f). The prepared PEDOT:PSS hydrogels presented high electrical conductivity (20 S/cm in phosphate-buffered saline solution and 40 S/cm in deionized water) and high stretchability (~35%).

Despite conductive hydrogels obtained directly from cross-linked conductive polymers usually possess high conductivity, they tend to have poor mechanical properties. To enhance their mechanical properties, conductive polymers are usually mixed with insulating polymer materials to form 3D networks, such as PAA, PAAM, PVA, gelation, chitosan, and agarose. By adding different additives (borax, dopamine, TA, rGO, EG, glycerol, etc), such hydrogels could not only possess enhanced mechanical properties (e. g., stretchability, toughness, and viscoelasticity), but also show new functions including adhesion, self-healing, injectable ability, anti-freezing, and long-water retention (summarized in Table 2.5).

Table 2.5 Summary of PEDOT or PEDOT:PSS based hydrogels for healthcare.

Name	Components	Network	Methods	Conductivity (S/cm)	Features	Applications	Ref.
PEDOT:PSS hydrogels	PEDOT:PSS	Physical crosslinking between PEDOT chains	H_2SO_4 treatment	~9	High conductivity	Supercapacitor	[91]
PEDOT:PSS hydrogels	PEDOT:PSS	Physical crosslinking between PEDOT chains,	DBSA treatment	~0.1	Room-temperature gelation, self-healing and injectable	OECTs	[89]
PEDOT:PSS hydrogels	PEDOT:PSS	Physical crosslinking between PEDOT chains, and between PSS chains	DMSO treatment, dry-annealing and rehydration	~20 in PBS, ~40 in deionized water	High conductivity, high stretchability (35% strain)	----	[90]
PPy−PEDOT:PSS hybrid hydrogels	PEDOT:PSS, PPy	Physical crosslinking. electrostatic interaction between PPy and PSS	Chemical oxidative polymerization of the pyrrole	~9	Biocompatible, high conductivity	--	[92]
(f-BNNS)/PEDOT:PSS/PNIPAM hydrogel	PEDOT:PSS, PNIPAM, f-BNNS, clay	PNIPA cross-linked network and hydrogen bonding cross-linking	Polymerization of NIPAM	~0.0004	Stretchable (~2700% strain), self-healing	On-skin motion sensors ang on-skin joule heating patches	[93]
PAA-Al^{3+}/PEDOT:PSS/ZB	PEDOT:PSS, zwitterionic betaine (ZB), $AlCl_3$, PAA	PAA cross-linked network and coordination interaction between Al^{3+} and PAA	UV-induced polymerization of acrylic acid	----	Anti-freezing, high stretchable (~1460% strain)	Strain sensor	[94]
PVA/PAA-PEDOT:PSS-TA conductive hydrogel	PEDOT:PSS, PVA, polyacrylic acid, TA	PAA cross-linked network and physical PVA crosslinked network	Polymerization of acrylic acid and freeze-thaw	----	Stretchable (640 % strain) and adhesive (15 kPa)	Strain sensor and EMI	[95]
PEDOT/PVA/SA hydrogel	PEDOT, PVA, sulfosuccinic acid (SA)	Hydrogen bonding, crystallization, and electrostatic interaction	Polymerization of EDOT, freezing/thawing, SA soaking	~0.02	Self-healing, stretchable (600% strain)	Strain sensor	[96]
PSGO-PEDOT-PAM hydrogel	PEDOT, sulfonated GO, PAM	PAM chemical cross-linked network and physical crosslinks from PSGO-PEDOT nanosheets	Chemical polymerization of EDOT, dopamine, and AM	~1	High stretchability (~2000% strain), adhesive (20 kPa on porcine skin)	Strain sensor, ECG, EMG, and EEG recording	[97]
PAAM/PAA/GR/PEDOT:PSS hydrogel	PEDOT:PSS, polyacrylamide (PAAM), PAA, graphene	PAAM and PAA dual networks	Polymerization of PAAM and PAA	----	Adhesive, stretchable (500 % strain), self-healing	Strain sensor and capacitors	[98]
SV3/PVA hydrogels	PEDOT:PSS, PVA, borax, PG, DEG	Dynamic borate ester network, hydrogen bonds	Mixing	5.0×10^{-5}	Adhesive, highly stretchable, self-healing, low compressive Young's modulus	ECG and EMG recording	[99]
γ-PGA-GPTMS/PEDOT : PSS hydrogels	γ-polyglutamic acid (PGA), PEDOT:PSS, (3-glycidyloxypropyl) trimethoxysilane (GPTMS)	Interaction between PGA and GPTMS, Multiple hydrogen bonding	Mixing	0.13	Adhesive, self-healing, injectable	Strain sensor	[100]
PEDOT:heparin/HA-ALD/GC hydrogel	PEDOT:Hep, Aldehyde-modified hyaluronic acid (HA-ALD), glycol chitosan (GC)	Schiff base (imine) bond, electrostatic interaction between PEDOT:Hep and GC	Oxidation of hyaluronic acid, Polymerization of EDOT,	~0.03	Cytocompatible, injectable, adhesive	Strain sensor	[101]
CNT-PEDOT-PAM-PVA hydrogel	CNT, PEDOT:PSS, PVA, borax	hydrogen bonding, borate ester bonds, PAM cross-linked network	Polymerization of AM	--	Injectable, self-healing	Strain and Pressure Sensors	[102]
PHEA-PSS/PEDOT hydrogels	PHEA, PSS, PEDOT	PHEA, PSS, and PEDOT cross-linked networks.	Copolymerizing 2-Hydroxyethyl acrylate (HEA) with 4-Vinylbenzenesulfonic acid (SSS) and Polymerization of EDOT	~1	Self-healing, high conductivity	Pressure sensors	[103]

PEDOT:PSS/agarose nanocomposite hydrogel	PEDOT:PSS, Agarose	Multiple hydrogen bonding crosslinks between PEDOT:PSS and/or agarose	Microwave-heat and cooling	--	NIR irradiation assisted healing	Photothermal-based antibacterial composite	[104]
PDA-rGO/PEDOT:PSS/PAM organohydrogels	PEDOT:PSS, polyacrylamide, EG, polydopamine, rGO, Triton X-100, DMSO	PAAM networks, hydrogen bonds	Polymerization of PDA-rGO and PAM	~0.006 – 0.037	Stretchable (1350% strain), self-healable, anti-freezing, adhesive	Strain sensor	[105]
PEDOT:PSS/PVA/EG organohydrogel	PEDOT:PSS, PVA, EG	Hydrogen bonding, PVA crystallite network	Freezing/thawing	--	Anti-freezing, self-healing, stretchable (200-900% strain)	Strain sensors	[106]
PAM/PEDOT:PSS/MXene organohydrogel	Polyacrylamide (PAM), PEDOT:PSS, MXene, EG, LiCl	PAM cross-linked network, hydrogen bonds	Polymerization of acrylamide	----	Anti-freezing, long-water retention (90 days)	Strain sensor	[107]
PEDOT/PVA/EG organohydrogel	PEDOT, PVA, EG	Hydrogen bonding, PVA crystallite network	Chemical polymerization of EDOT and Freezing/thawing	~0.04	Anti-freezing, long-water retention (7 days), stretchable (400 % strain)	On skin sensor	[108]

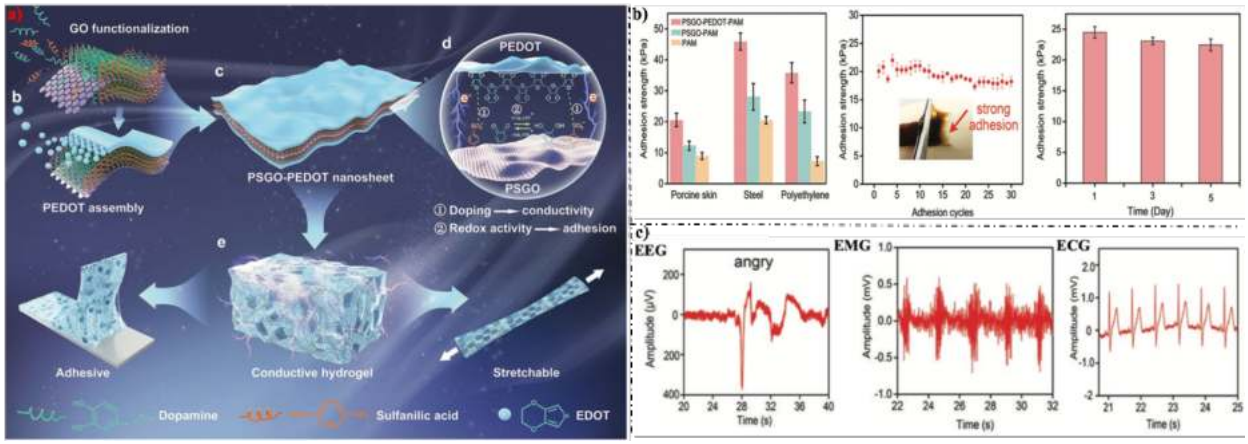

Figure 2.17 (a) Schematic diagram of PSGO-PEDOT nanosheet and its incorporation in hydrogel; (b) Adhesive properties of PSGO-PEDOT hydrogels; (c) EEG, EMG, and ECG recording. (a-c) are reproduced with permission [97].

Conductive hydrogels possessing high stretchability, adhesiveness, and self-healing abilities have widely attracted interest for their use in wearable electronics and bioelectronics due to their improved contact interface to the skin without the requirement for adhesives and the ability to restore their functionalities after enduring damage. A self-adhesive conductive hydrogel (called PSGO-PEDOT-PAM) was obtained via first assembling PEDOT on polydopamine-reduced and sulfonated graphene oxide (PSGO) and then introducing PSGO-PEDOT nanosheets on a PAM network (shown in Figure 2.7a) [97]. The prepared PSGO-PEDOT-PAM hydrogels demonstrated high stretchability (~2000% strain), high conductivity (1 S/cm), and excellent adhesion on porcine

skin (2.0 N, Figure 2.17 b). Skin patch electrodes fabricated from the hydrogels showed high quality for bio-signal recording (ECG, EEG, and EMG, Figure 2.17 c). Our group reported self-healable, highly stretchable and adhesive PEDOT:PSS-based hydrogels obtained from PVA, borax, and PEDOT:PSS ink. The details of this work are described in the thesis chapter 4.

Most conductive hydrogels reported so far might not be suitable for long-term usage in dry and cold environments, due to water evaporation or freezing occurring, which affects both mechanical and electrical properties. Therefore, moisturizing and anti-freezing organohydrogels have been developed via the incorporation of nontoxic anti-freezing agents such as EG [106, 109, 110] and glycerol [109, 111, 112] into the formulations. PEDOT:PSS/PVA/EG organohydrogels were prepared by freezing-thawing the mixture of PEDOT:PSS suspension, PVA, and EG (Figure 2.18a) [106]. The physically crosslinked organohydrogels not only exhibited anti-freezing abilities with a strain-sensitivity from ~ -55 to ~45 °C, but also showed high stretchability (200-900% strain) and self-healing behavior (Figure 2.18b-c). Similar PEDOT organohydrogels were obtained by the chemical polymerization of EDOT and repeatedly freezing/thawing the PEDOT/PVA/EG mixture [108]. The prepared organohydrogels exhibited a conductivity of 0.04 S/cm, high elongation at break (~400% strain), anti-freezing, as well as long-water retention (7 days). Our group recently reported PEDOT/EG/TA organohydrogels obtained from concentrated PEDOT:PSS suspension, EG, and TA. The details are shown in this thesis Chapter 6.

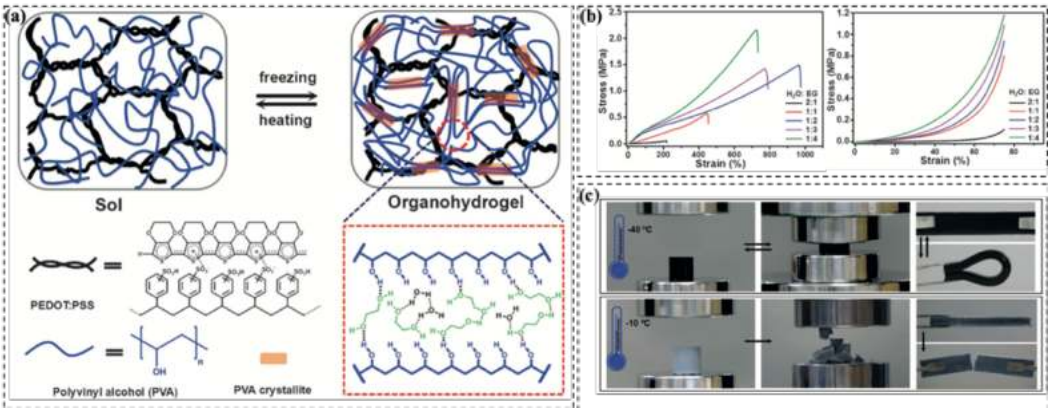

Figure 2.18 (a) Schematic illustration of the preparation PEDOT:PSS/PVA/EG organohydrogels; (b) Tensile (left) and compressive (right) stress–strain plot of the anti-freezing conductive organohydrogels with different mass ratios of H_2O and EG; (c) Digital photos of compressive and bending measurements at -40 °C for the anti-freezing organohydrogels (up) and at -10 °C for pure conductive hydrogel (without EG, down). (a-c) are reproduced with permission [106].

CHAPTER 3 METHODOLOGY

3.1 Preparation of PEDOT:PSS-based hydrogels, films, and organohydrogels

PEDOT:PSS screen printing paste (Clevios™ S V3, Heraeus, Germany), 10 wt% PVA solution, and borax are used to prepare SV3/PVA hydrogels. PEDOT:PSS (Clevios PH1000, Heraeus, Germany), EG, and TA are employed to fabricate PEDOT/EG/TA films. Concentrated PEDOT:PSS suspension (~3 wt% PEDOT:PSS content), EG, and TA are utilized to synthesize PEDOT/EG/TA organohydrogels. The preparation details are referred to in Chapters 4 (section 4.3.2), 5 (section 5.3.2), and 6 (section 6.3.2), respectively.

3.2 Fabrication of the SV3/PVA hydrogels, PEDOT/EG/TA films, and PEDOT/EG/TA organohydrogels epidermal patch electrodes

The SV3/PVA hydrogel patch electrodes were prepared by modifying Ambu® electrodes and by using copper tape and Parafilm. The details are referred to in Chapter 4 (section 4.3.4).

To fabricate PEDOT/EG/TA film patch electrodes, a stretchable silver ink was drop casted on a PET sheet. After drying at 100 °C for 5 min, the pre-prepared films were attached onto the substrate (Chapter 5, section 5.3.7).

Organohydrogel electrodes were prepared using Tegaderm tape, copper tape, a snap button, and a PET sheet (25 μm). The details are referred to in Chapter 6, section 6.3.3.

3.3 Electrical conductivity test

The electrical conductivity test is a measure of how easily electrons can flow through materials. A 2-probe method was used to measure the conductivity of SV3/PVA hydrogels. The hydrogel was placed into a plastic cylinder. Subsequently, both ends of the cylinder were sealed using conductive copper tapes, to which two tungsten probes were attached. The details are described in Chapter 4 section 4.3.7. The conductivities of PEDOT/EG/TA films and PEDOT/EG/TA gels were measured using a Biomomentum 4-point probe system connected to a source-measure unit (B2902A, Agilent). The details are presented in Chapter 5 (section 5.3.3) and Chapter 6 (section 6.3.4), respectively.

The conductivity (σ) of the gels and films was calculated using Equation 3.1:

$$\sigma = \frac{L}{R_A * S} \tag{3.1}$$

where R_A is the average resistance of the gels and films calculated, L and S are the length and section of the gels and films.

3.4 Mechanical characterization

Mechanical properties of materials (e. g., stretchability, compressive strength, and Young's modulus) are important for understanding how a material will behave under different loading conditions, and they can help design and optimize materials for the application of epidermal electronics.

3.4.1 Electromechanical tests

We performed tensile stress-strain measurements to assess the mechanical behaviors of PEDOT/EG/TA films. Some parameters acquired from stress-strain curves are the stretchability (defining the film's ability to stretch or elongate without breaking or undergoing permanent deformation), the elongation at break (referring to the maximum strain that the film can endure before break or fracture), and Young's modulus (extracted from the slope of the stress-strain curves in the range of 0-10% strain) of the films. The details are presented in Chapter 5 (section 5.3.4).

The electrical stability of PEDOT/EG/TA films during stretching refers to the ability of the conductive films to maintain their electrical properties while being subjected to stretching. It is an important consideration in many applications, such as in the design of flexible and stretchable electronics, sensors, and other devices that must maintain their electrical performance during mechanical deformation.

In this thesis, the electrical stability of PEDOT/EG/TA films during stretching is clarified by the resistance ratio (ε) change and was calculated as:

$$\varepsilon = \frac{R}{R_0} \tag{3.2}$$

Where R and R_0 are the resistances at stretching strain and 0% strain, respectively.

3.4.2 Compressive test

Compressive measurements, which used to determine the behavior of a material when subjected to a compressive load, are important for understanding the structural behavior and performance of materials. In this thesis, we performed compressive tests for SV3/PVA hydrogels and PEDOT/EG/TA organohydrogels, the details are presented in Chapter 4 (section 4.3.6) and 6 (section 6.3.5), respectively.

3.4.3 Creep-recover test

Creep-recovery measurements are a type of mechanical test used to evaluate the deformation of materials under sustained load. We carried out the measurement to assess the deformation of PEDOT/EG/TA films. The details are described in Chapter 5 (section 5.3.4).

3.5 Rheology measurements

Rheology is the study of the deformation and flow of matter under applied stresses. Rheological measurements can provide valuable insights into the physical properties of materials, including their viscosity, elasticity, and yield strength. We utilized a stress-controlled rheometer (MCR MultiDrive, Anton Paar, Austria) to measure the rheological properties of SV3/PVA hydrogels and PEDOT/EG/TA organohydrogels. The details are described in Chapter 4 (section 4.3.5) and Chapter 6 (section 6.4.2), respectively.

3.6 Adhesion strength measurements

An optimal design for epidermal electronics would involve a tight adherence to the skin to ensure reliable acquisition of high-quality signals, yet also allow for easy removal after use. We employed perpendicular adhesion (Figure 3.1a) and 90° peeling off (Figure 3.1b) measurements to assess the adhesion strength of SV3/PVA hydrogels and PEDOT/EG/TA films, respectively. Perpendicular adhesion testing is a type of adhesion test that measures the strength of the bond between two surfaces perpendicular to the plane of adhesion. A perpendicular force is then applied to the adhesive until it separates from the substrate. The force required to achieve separation is measured and used to determine the perpendicular adhesion strength of the adhesive. A 90°-peel test involves peeling a material away from a substrate at a 90-degree angle, forming a T-shape. The force required to peel the material is measured, and this can be used to determine the adhesion strength. The details are described in Chapters 4 (section 4.3.6) and 5 (section 5.3.4).

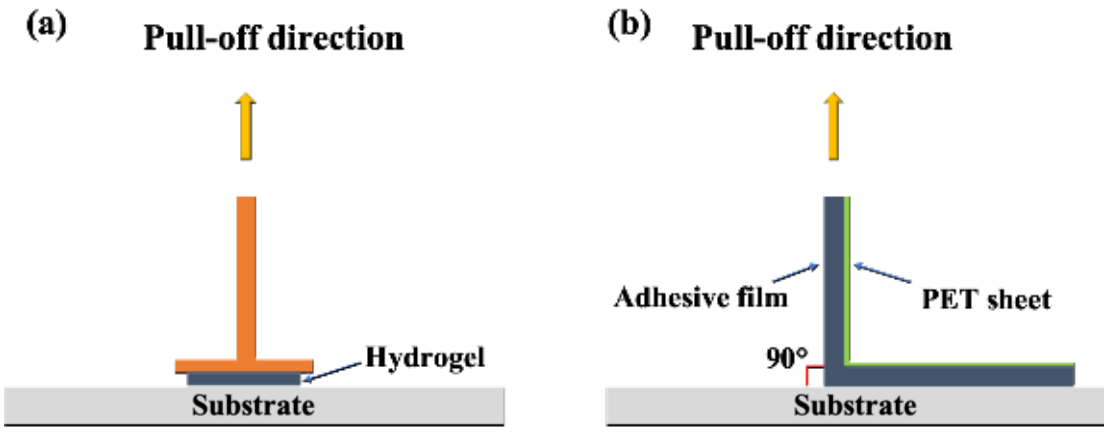

Figure 3.1 Adhesion tests schema. (a) Perpendicular adhesion strength and (b) 90° peel adhesion force measurements.

3.7 Self-healing test

Self-healing measurements are performed to evaluate the ability of materials to recover their electrical and mechanical properties after experiencing external damages. In this thesis, we applied continuous cycles of strain oscillatory shear to estimate the mechanical self-healing property of SV3/PVA hydrogels. We assessed the autonomic healing ability of PEDOT/EG/TA films by cutting the films at different regions. We used a circuit with a LED light and cut-stick procedures to illustrate the electrical self-healing of SV3/PVA hydrogels and PEDOT/EG/TA films. The electrical healing efficiency was calculated as:

$$\eta = \frac{I_{healed} - I_{damaged}}{I_{pristine} - I_{damaged}} \tag{3.3}$$

Where I is the current measured for the healed, damaged, and pristine films.

The details are presented in Chapter 4 section 4.3.8 and Chapter 5 section 5.4.3, respectively. In addition, an optical microscope was used to observe the in-situ healing process of the hydrogels and the films after being cutting by a scalpel or a stainless-steel blade.

3.8 Composition characterization

3.8.1 FTIR

Fourier-transform infrared (FTIR) spectroscopy is a type of vibrational spectroscopy used to analyze the infrared absorption or transmission of a material. In FTIR, a beam of infrared radiation is passed through a sample, and the amount of energy absorbed or transmitted by the sample is measured. FTIR is particularly useful for identifying and quantifying the functional groups present in a material, as each group has a characteristic absorption frequency in the infrared region. FTIR can be used to analyze a wide range of materials, including liquids, solids, and gases, and it is often used in the analysis of polymers, organic compounds, and biological materials. In the research project, we used FTIR to identify the chemicals in SV3/PVA hydrogels (e. g., PEDOT:PSS, PG, and DEG), PEDOT/EG/TA films (e. g., TA and EG), and PEDOT/EG/TA gels (e. g., PEDOT:PSS, EG, and TA) The FTIR tests are employed in absorption mode on a Perkin Elmer spectrum 65 spectrophotometer, with a scan range of 500 - 4000 cm^{-1}.

3.8.2 Zeta potential

Zeta potential is a technique to measure the electrostatic potential difference between the surface of a particle or a colloidal dispersion and the surrounding fluid. It is an important parameter that can provide information about the stability and behavior of colloidal systems. When particles are suspended in a liquid, they acquire an electrical charge due to the adsorption of ions from the surrounding medium. The magnitude and sign of this charge affect the behavior of the particles and their interactions with other particles. To elucidate the physical crosslinking network of PEDOT/EG/TA gels, we performed Zeta potential tests to investigate the effect of TA on the potential change of PEDOT:PSS suspension and the interaction between TA and PEDOT:PSS. The measurements were carried out on a Zetasizer Nano ZSP instrument (Malvern. Instruments Ltd., Worcestershire, UK). The details are described in Chapter 6 section 6.3.7.

3.9 Biocompatibility test

Biocompatibility testing, which is always required when materials or devices are intended to be used in contact with human tissue and little is known about their toxicity, assesses the compatibility of materials or medical devices with a biological system. Although PEDOT:PSS, PVA, borax, EG, and TA are reported to be biocompatible, we assessed the skin condition (damage or redness) after

wearing SV3/PVA hydrogel electrodes for 1h. In addition, we assessed the biocompatibility (cell viability) of PEDOT/EG/TA film by culturing C2C12 mammalian cells on the film-coated wells. The details are referred to in Chapters 5 section 5.3.9.

3.10 Characteristic of epidermal patch electrodes

The skin-electrode impedance, ECG, and EMG measurements were carried out to assess the performance of the hydrogel, film, and organohydrogels electrodes.

3.10.1 The skin-electrode impedance

The skin-electrode impedance is an important factor that indicates the quality of the electrodes and affects the performance of bio-signals monitoring. The impedance is significantly influenced by various factors including the subject object, skin conditions (e. g., hydration, temperature, and the presence of skin oils), electrodes, and testing time and location. Therefore, we performed the measurements on the same people, at the same location, and on the same day, with the hydrogel, film, and organohydrogel electrodes as working electrodes and two commercial Natus® Ag/AgCl gel electrodes as reference and counter electrodes.

3.10.2 ECG & EMG measurements

ECG and EMG, a representation of the electrical activities of the heart and muscle, are common diagnostic tools used in human healthcare, and their recording quality is vital for clinical diagnosis. We used a biosensing board (Cyton, OpenBCI, USA) set up with an amplifier gain of 24 to record ECG and EMG signals.

Bio-potentials are easily interfered by various noises including electromagnetic interference (caused by AC power, smartphones, smartwatches, and activity trackers) and movement from outside. In addition, the quality of ECG waveforms can be affected by different types of epidermal electrodes, monitoring instruments, and the placement of electrodes. To reduce the noise and for testing convenience, we used a three electrodes system for ECG recording with the ground and the positive electrodes placed on the left forearm and the negative electrode attached to the right forearm. For EMG, we recorded bio-potential caused by switching between relaxed and tense states of the flexor carpi muscle.

We performed ECG and EMG recordings under the following conditions:

i) The measurements were taken in a quiet environment.

i)The volunteer was in a resting state, without movement.

ii) The tests were away from AC power, smartphone, and wearable devices (e. g., smartwatches).

The ECG and EMG testing details and data analysis are described in Chapter 4 (section 4.3.10).

CHAPTER 4 ARTICLE 1 : SELF-HEALING, STRETCHABLE, AND HIGHLY ADHESIVE HYDROGELS FOR EPIDERMAL PATCH ELECTRODES

This article has been published in the journal "Acta Biomaterialia" on August 5th, 2021. The supporting information of this article is provided in Appendix A.

Xin Zhou[a], Ashna Rajeev[b], Arunprabaharan Subramanian[a], Yang Li[a], Nicolò Rossetti[a], Giovanniantonio Natale[b], Gregory A. Lodygensky[c, d], Fabio Cicoira[a*]

[a] Department of Chemical Engineering, Polytechnique Montréal, Montréal, Québec H3C 3A7, Canada

[b] Department of Chemical and Petroleum Engineering, Schulich School of Engineering, University of Calgary, 2500 University Dr. NW, T2N 1N4

[c] Department of Pediatrics, Sainte-Justine University Hospital Research Center, Montreal, QC, Canada

[d] Department of Pharmacology and Physiology, University of Montreal, Montreal, QC, Canada

* Corresponding author: fabio.cicoira@polymtl.ca

Keywords: Hydrogels, adhesion, self-healing, bioelectronics, PEDOT:PSS

4.1 Abstract

Flexible, self-healing and adhesive conductive materials with Young's modulus matching biological tissues are highly desired for applications in bioelectronics. Here, we report self-healing, stretchable, highly adhesive and conductive hydrogels obtained by mixing polyvinyl alcohol, sodium tetraborate and a screen printing paste containing the conducting polymer Poly (3,4-ethylenedioxythiophene) doped with polystyrene sulfonate (PEDOT:PSS) and diol additives. The as prepared hydrogels exhibited modelling ability, high adhesion on pig skin (1.96 N/cm^2), high plastic stretchability (>10000%), a moderate conductivity, a low compressive modulus (0.3-3.7

kPa), a good strain sensitivity (gauge factor = 3.88 at 500% strain), and remarkable self-healing properties. Epidermal patch electrodes prepared using one of our hydrogels demonstrated high-quality recording of electrocardiography (ECG) and electromyography (EMG) signal. Because of their straightforward fabrication, outstanding mechanical properties and possibility to combine the electrode components in a single material, hydrogels based on PVA, borax and PEDOT:PSS are highly promising for applications in bioelectronics and wearable electronics.

Keywords: Hydrogels, adhesion, self-healing, bioelectronics, PEDOT:PSS

4.2 Introduction

Epidermal patch electronics are widely explored for applications in human healthcare, such as monitoring of vital signs, body temperature and blood pressure, as well as for detection of analytes in bodily fluids [2-9]. Monitoring of vital signs, via techniques such as electrocardiography (ECG), electromyography (EMG), and electroencephalography (EEG), is of utmost importance for wearable electronics and point of care diagnostics. The acquisition of ECG, EMG, and EEG signals is typically achieved with metal electrodes, of ground strap, bar or cup type, or Ag/AgCl gel electrodes with adhesive pads [10, 11]. However, metal electrodes can lead to skin damage due to severe mechanical mismatch between skin and the electrode surface, while Ag/AgCl gel electrodes can result in skin irritation due to strong adhesion on the skin [4, 10, 12]. Moreover, these electrodes are based on rigid materials, which are unable to withstand bending and stretching. Therefore, there is a strong demand for soft conductive materials, able to mimic tissues (with a moduli of 0.5-500 kPa) [13] and adhere to irregular surfaces of human skin, from knuckle to knee joint, and achieve high-quality bio-potential recording without leading to skin irritation [4, 13].

Several soft materials have been used for epidermal patches, in form of thin films (e. g. nanosheets and tattoo electrodes) [7, 35, 36, 48, 68], bio-inspired adhesives [24-26], and conductive hydrogels [88, 113]. Conductive hydrogels are very promising candidates for epidermal patches, due to their tissue-friendly characteristics, high water content (70-99%, similar to tissues) [13], tunable electrical properties, flexibility, and biocompatibility [13, 88].

Polyvinyl alcohol (PVA)-borax hydrogels are widely studied for biomedical applications due to their biocompatibility, biodegradability, water solubility, easy processing and self-healing properties. To improve their mechanical, self-healing and electrical properties, PVA-borax hydrogels are often blended with other materials, including polydopamine (PDA) [113],

proanthocyanins/reduced graphene oxide (PC/rGO) [88], functionalized single-wall carbon nanotubes (FSWCNT) [114], graphene or silver nanowires [115], nanostructured cellulose nanofibers-polypyrrole complexes [116], agarose [117], and microfibrillated cellulose (MFC) [118]. For instance, PVA-borax hydrogels blended with polydopamine showed remarkable compliant, self-adhesive, and self-healing properties [113]. Incorporating PC/rGO into a PVA-borax hydrogel containing glycerol resulted into a material with excellent stretchability (> 5000%), compliance, and self-healing ability [88]. This hydrogel was used to fabricate strain sensors, which could detect skin epidermis movements including finger bending, facial expression changes and vocalization. In addition, electrodes based on this hydrogel were used to record ECG and EMG signals. Although many PVA-borax based hydrogels are reported, most of them are used as strain sensors and the development PVA-borax based hydrogels combining high self-healing, good mechanical properties, and adhesion ability is still challengeable, and the quality of recording vital signs still have room for improvement.

The conducting polymer Poly(3,4-ethylenedioxythiophene) doped with polystyrene sulfonate (PEDOT:PSS) has been incorporated in PVA hydrogels due to its biocompatibility, aqueous solubility, high conductivity and ability to modify mechanical properties, [13, 102, 119]. The commercial PEDOT:PSS screen printing paste (Clevios SV3) [64, 65], is a promising candidate for the fabrication of conductive hydrogels. This formulation contains high amounts of propylene glycol (PG, 60-80%) and diethylene glycol (DEG, 10-30%), which can form hydrogen bonds with PVA and borax resulting in improved compliance, self-healing properties, stretchability, and adhesion.

In this work we report self-healing, stretchable, highly adhesive and conductive hydrogels obtained by mixing PVA, borax and PEDOT:PSS screen printing paste. The hydrogels showed remarkable compliance on skin, outstanding plastic stretchability (10000% strain), fast self-healing, high interfacial adhesion, and low compressive Young's modulus. To demonstrate their high potential for bioelectronics applications, our hydrogels were used to fabricate electrophysiological epidermal patch electrodes, which showed performance similar to commercial Ag/AgCl gel electrodes for recording of ECG and EMG signals. Straightforward fabrication, outstanding mechanical properties and possibility to combine the electrode components in a single material, make our hydrogels highly promising for applications in bioelectronics and wearable electronics.

4.3 Materials and methods

The protocol for human experiments was approved by the ethical committee of Polytechnique Montréal (approval number CER- 2021-04-D).

4.3.1 Materials

Poly(vinyl alcohol) (PVA, 89,000-98,000 average molecular weight and 99+% hydrolyzed) and borax (sodium tetraborate decahydrate) were purchased from Millipore Sigma (St. Louis, Mo, USA). PEDOT:PSS screen printing paste (Clevios^{TM} S V3 STAB) was purchased from Heraeus (Germany). Copper tape (88.9 μm, mΩ/in. sq) was supplied from McMaster-Carr.

4.3.2 PEDOT:PSS/PVA hydrogel preparation

A 10 wt% PVA aqueous solution was prepared by dissolving PVA in ultrapure deionized (DI) water (18.2 MΩ cm at 25°C) in a water bath at about 90°C for 4 h. The PEDOT:PSS paste and the PVA solution were mixed in a 50 ml vial with a spatula for about 5 minutes. We used the following PEDOT:PSS/PVA ratios: 1:3 (3 g PE- DOT:PSS paste and 9 g PVA solution, henceforth named SV3/PVA- 1-3), 1:2 (3 g PEDOT:PSS paste and 6 g PVA solution, henceforth named SV3/PVA-1-2), 1:1 (3 g PEDOT:PSS paste and 3 g PVA solution, henceforth named SV3/PVA-1-1) and 2:1 (6 g PEDOT:PSS paste and 3 g PVA solution, henceforth named SV3/PVA-2-1). Successively, 1 ml of 0.262 M borax aqueous solution was added to the mixture in two steps: 0.5 ml were first added and the solution was stirred for several minutes, then the remaining 0.5 ml were added and the stirring was continued for 3 more minutes. The obtained hydrogels were left in the vial for 12 additional hours before use. For the SV3/PVA-1-3, the amount of borax solution was 1.3 ml. A PVA-borax hydrogel was prepared for comparison by mixing 3 g 10wt% PVA solution with 1 ml of 0.262 M borax solution.

4.3.3 SV3/PVA strain sensor fabrication and strain sensitivity

A stain sensor was prepared by using the acrylic tape (4910-VHB, 3M) and SV3-PVA-1-3 sample. Two pieces of copper tape were firstly fixed on the ends of a piece of VHB tape (40 × 19 × 1 mm). Successively, another VHB tape of the same size with a groove (20 × 9 × 1 mm) was attached on the VHB tape and filled with SV3/PVA-1-3 hydrogel. Finally, the strain sensor was completed by placing another piece of VHB tape (40 × 19 × 1 mm) on the top. In this way, the SV3/PVA hydrogel was encapsulated in a rectangular groove (Figure SA1).

The strain sensitivity of the SV3/PVA hydrogel was assessed by the gauge factor (GF, Eq. 4.1), which is defined as the ratio of the relative resistance change to the applied strain (ε).

$$GF = \left[\frac{R-R_0}{R_0}\right]/\mathcal{E} \qquad \text{Equation 4.1}$$

Where R_0 is the resistance at 0 % strain and R is the resistance at a given strain. An LCR meter (Keysight True RMS) was used to collect the electrical signal at a constant voltage of 3 V.

4.3.4 SV3/PVA electrodes preparation

The SV3/PVA hydrogel patch electrodes were prepared by modifying Ambu® electrodes. The SV3/PVA hydrogel was electrically connected via a copper tape on the backside and covered by a Parafilm with a diameter of 18 mm (Figure SA2). The SV3/PVA hydrogel was cast on the Parafilm. A Scotch® double-stick tape (3M) was used to attach the copper tape on the modified Ambu® electrode.

4.3.5 Characterization

FTIR spectroscopy

Fourier-transform infrared (FTIR) spectroscopy was performed in absorption mode with a scan range of 500 - 4000 cm^{-1} on a Perkin Elmer spectrum 65 spectrophotometer. The hydrogels were placed on the measuring area that covers the whole surface of the FTIR crystal.

Rheology

A stress-controlled rheometer (MCR 702 MultiDrive, Anton Paar, Austria) was employed to measure the rheological properties of the hydrogels using a parallel plate geometry (25 mm diameter) maintaining a gap of 1 mm. The linear viscoelastic regions (LVER) of the samples were estimated by conducting amplitude sweep measurements by varying the strain % in the range of 0.01 - 1000 at a constant frequency of 1 Hz. The frequency sweep measurements were conducted in the range of 0.5 - 500 rad/s angular frequencies at a constant value of strain %, well within the LVER. To estimate the mechanical self-healing property of the hydrogels we applied continuous cycles of low strain oscillatory shear, within the LVER (∼1 %), for a duration of 225 s and high strain, beyond the LVER, (∼100 % or ∼400 %) for a duration of 75 s at a constant angular frequency of 1 Hz. The samples were first loaded on to the stationary bottom plate and then the top plate was slowly moved down, automatically controlled by the Rheoplus software of the Anton

Paar MCR 702. The excess sample was trimmed off from the edges of the geometry. This ensured the complete filling of the sample between the plates before the measurement.

4.3.6 Mechanical characterization

Mechanical characterization (adhesion and compressive stress- strain tests) was carried out with a Mach-1 V500csst MA009 mechanical tester (Biomomentum Inc, Canada).

Adhesion measurements were performed between the hydrogels and pig skin samples (obtained from a local grocery store) in a perpendicular geometry. The pig skin was cut into 2 × 2 cm^2 pieces and cleaned with DI water. After drying with a paper tissue, the pig skin was fixed onto a glass slide using cyanoacrylate glue. The hydrogels (thickness: ~0.7 mm) were cast onto an indenter (with a diameter of 12 mm) which attached to the load cell, were brought into contact to the pig skin with a contact pressure of ~0.570 N/cm^2 for 8 seconds and successively pulled off with a speed of 18 mm/min. 6 samples of each hydrogel were attached and detached for 6 times and the adhesion force was calculated as the maximum force normalized to the area of skin covered by the hydrogel. The error corresponds to the standard deviation.

For compression tests, the hydrogels were cast into a cylindric mold with a height of ~4.5 mm and a diameter of ~12 mm, the cylindric hydrogels were compressed with a speed of 12 mm/min under a 70 N load cell in ambient condition. 3 samples for each type of hydrogel were tested. The reported values of the Young's modulus correspond to the average and the error to the standard deviation.

4.3.7 Electrical conductivity

A 2-probe method was used to measure the conductivity of the hydrogels. The hydrogel was placed into a plastic cylinder with a length of ~10 mm and an inner diameter of ~8 mm. Both sides of the cylinder were sealed with a conductive copper tape, to which two tungsten probes were connected. The current was recorded under a voltage sweep from -0.2 V to -0.1 V with an electrical probe station equipped with a National Instruments NI PXIe-1062Q source-measure unit controlled by Labview software. The conductivities (σ) of the hydrogels were calculated using the Ohm's law (Eq. 4.2).

$$\sigma = \frac{L}{R \times S} \qquad \text{Equation 4.2}$$

where R is the average resistance of the hydrogel calculated, L and S are the length and section of the hydrogel. The average resistance was calculated by each voltage sweep (-0.2 and -0.1V), and 3 samples for each hydrogel were tested.

4.3.8 Self-healing

An optical microscope (Carl Zeiss, Primovert, Germany) was employed to observe the self-healing process of SV3-PVA-1-3 hydrogel in-situ. A piece of hydrogel was placed on a glass slide and a scalpel was used to cut it.

Electrical self-healing experiments were carried out on SV3/PVA-1-3 hydrogel samples with dimensions of 40 mm × 5mm × 2 mm. Two conductive copper tapes were placed at the end bottom sides of the hydrogel (contacts length 5 mm) and an electrical contact was made via two tungsten probes on the copper tapes. The current was recorded with an electrical probe station equipped with a National Instruments NI PXIe-1062Q source-measure unit controlled by Labview software. A plastic Razor blade (GAYISIC) was used to cut and heal the hydrogels. The voltage applied during the healing experiment was 0.6 V. The electrical healing efficiency was calculated by the Eq. 4.3.

$$\eta = \frac{I_{healed} - I_{damaged}}{I_{pristine} - I_{damaged}}$$ Equation 4.3

Where I is the current measured for the healed, damaged, and pristine hydrogel.

4.3.9 Electrochemical impedance spectroscopy

An electrochemical workstation (VSP-300, BioLogic, France) was used to measure the skin-electrode impedance from 1 Hz to 100 kHz at 10 mV with a three-electrodes setup. SV3/PVA-1-3 hydro- gel was used as a working electrode and two commercial disposable Ag/AgCl adhesive disk electrodes (Natus®, MFI Medical, USA) were used as reference and counter electrodes, respectively. These electrodes were placed on the right lower forearm of a volunteer without skin preparation. The distance between two adjacent electrodes was 8 cm, and the diameter of these electrodes were calculated as 18 mm.

4.3.10 Electrophysiological signals recording

The electrophysiological signals (ECG and EMG) were recorded by a biosensing board (Cyton, OpenBCI, USA) set up with an amplifier gain of 24.

For recording of ECG signals, the SV3/PVA patch electrodes were attached to left (ground and positive electrodes) and right forearm (negative electrode) of a volunteer. The electrodes were connected into the biosensing monitor and the signals were recorded in real-time from the heart and the bandpass filter was set up 5-50 Hz, and a notch filter was used at 60 Hz during sampling ECG signals (250 Hz rate). The signals were analyzed offline using a second-order digital Butterworth filter at a cut-off frequency of 0.5 Hz to eliminate baseline drift.

Surface EMG (sEMG) recording was tested on the flexor carpi muscle of a volunteer with a bandpass filter of 15-50 Hz and a sample rate of 250 Hz. In detail, three electrodes were attached to the flexor carpi muscle of the right forearm of a voluntary with a spacing of 5 cm (center-center). EMG signals were recorded while clenching the fist for 1-2 s. The signals were analyzed offline using a second-order digital Butterworth filter with a cut-off frequency of 10 Hz to eliminate baseline drift and for the signal-to-noise ratio (SNR) computation. The baseline noise was obtained during relax phases where no muscle activity could be detected in the EMG signal (Figure SA3). A single value threshold of 15 μV on the absolute value of the signal was applied to separate signal from baseline noise. 3 samples for each type of electrodes were tested and the root mean square (RMS) signal values were calculated from 6 signal regions (1 - 2 s each) and RMS noise values were calculated from 7 noise regions (1 - 4 s each). EMG SNR was obtained from the Eq. 4.4.

$$SNR(dB) = 20log_{10}\frac{A_{sigal}}{A_{noise}} \quad \text{Equation 4.4}$$

Where A_{signal} and A_{noise} are the RMS amplitude value of signal and noise, respectively.

For both ECG and EMG 4 different brands commercial Ag/AgCl gel electrodes, including Natus® disposable adhesive disk electrodes (MFI Medical, USA), Skintact® F-301 (Leonhard Lang, Austria), Ambu® (R-00-S/25, USA), and 3M 2560 Red Dot™ electrodes (USA), were used for signal recording comparison.

4.3.11 Statistical analysis

The illustrations were draw by Microsoft PowerPoint version 16.22 and the graphs were plotted by Origin 2021. Data was expressed as means ± standard deviation. Statistical analysis was performed using Origin 2021.

4.4 Results and Discussion

4.4.1 Modelling and compliance properties of SV3/PVA hydrogels

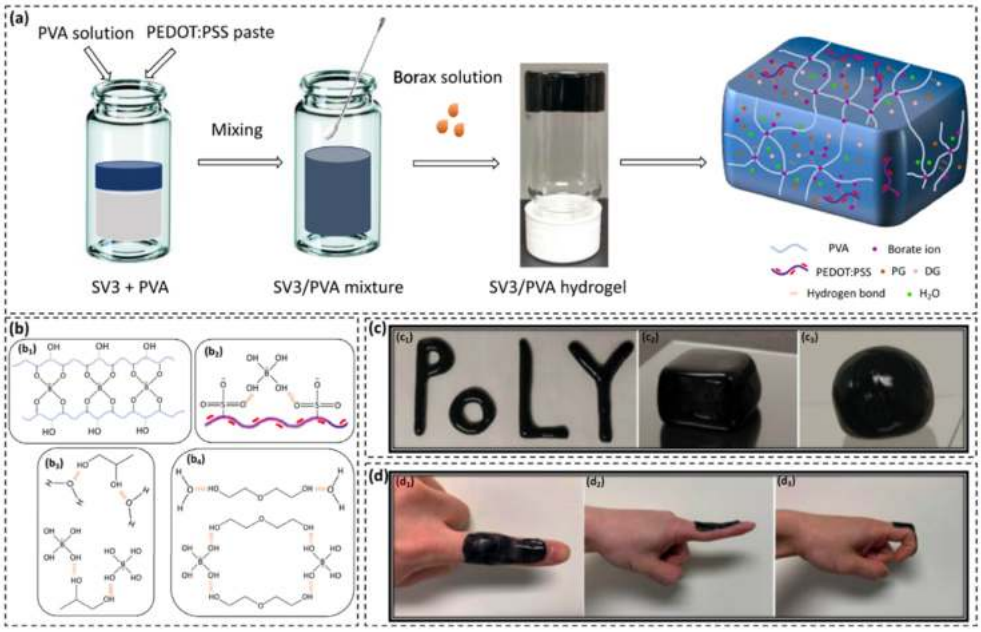

Figure 4.1 (a) Scheme of the processing of the hydrogels and 3D rendering of the hydrogel network. (b) Scheme of the chemical bonds which can be formed in the hydrogel: PVA-borax (b_1), PEDOT:PSS-borax (b_2), PG-water and borax-PG (b_3), DEG-water and borax-DEG (b_4). (c) Digital pictures of SV3/PVA-1-3 hydrogel modelled into various shapes: letters (c_1), cube (c_2) and sphere (c_3). (d) Digital pictures of SV3/PVA-1-3 hydrogel on the finger skin: top view (d_1), side view (d_2), side view during finger bending (d_3).

The SV3/PVA hydrogels were prepared by mixing the PVA aqueous solution, the PEDOT:PSS screen printing paste (Clevios SV3), and the borax aqueous solution (Figure 4.1a). The addition of the SV3 paste, rich in propylene glycol (PG) and diethylene glycol (DEG), to the PVA-borax system, led to hydrogels with improved mechanical properties. PVA-borax hydrogels are based on a network of dynamic borate ester bonds (Figure 4.1b_1), which provide self-healing and low modulus properties. However, these hydrogels show long healing times and a limited stretchability [21,26]. The addition of the SV3 paste brings significant changes to the network structure: the sulfonate groups of PEDOT:PSS and the -OH groups of PG and DEG might form hydrogen bonds with borate ions, to yield a borate-PEDOT:PSS network (Figure 4.1b_2), while PG and DEG might form hydrogen bonds with water and borate (Figure 4.1b_3-b_4). During gelation, the formation of

these hydrogen bonds is expected to decrease the amount of dynamic covalent bonds in the PVA-borax crosslinked network, facilitating the rearrangement of the PVA chains [21]. At the same time, the addition of PEDOT:PSS, PG, and DEG enhances the hydrogen bonding between -OH groups on PVA chains and -OH groups of PG and DEG and sulfonyl groups on PSS^- chains, which might enhance the softness of PVA-borax hydrogels. A similar effect has been found upon addition of glycerol to PVA-borax hydrogel [21,32].

The SV3/PVA hydrogels could be modelled into 3D objects of arbitrary shape, except SV3/PVA-2-1, which showed a liquid-like behavior. For instance, the SV3/PVA-1-3 hydrogel could be shaped into letters (Figure 4.1c_1), cubes (Figure 4.1c_2) and spheres (Figure 4.1c_3). It also fitted tightly on the irregular skin surface of fingers (Figure 4.1d_1-d_3) and could adapt to the finger movements (Movie SA1). Furthermore, it showed an outstanding plastic stretchability (Figure SA4 and Movie SA2) of more than 10000% its original length, i.e. from ∼2 cm to more than 2 m (inset of Figure SA4).

4.4.2 Rheological and Fourier-transform infrared (FTIR) spectroscopy properties

Measurements of the storage (G′) and loss moduli (G″) as a function of the angular frequency, were carried out to assess the rheological properties of the hydrogels (Figure 4.2a). The PVA hydrogel showed an elastic behavior, with the storage modulus exceeding the loss modulus over the entire frequency range. The presence of PEDOT:PSS, PG, and DEG in the PVA-borax network led to a decrease of G′ and G ″. This indicates a weakening of the mechanical strength and an enhanced softness of the samples, which explains the modelling properties of the hydrogels [21]. More importantly, the SV3/PVA hydrogels demonstrated different rheological characteristics with respect to PVA, with the exhibition of viscous behavior (G′ < G″) at lower frequency and elastic behavior (G′ > G″) at higher frequency. The crossover frequency (i.e., the intersection point of the G′ and G″ curves) shifted to higher frequency upon increasing the amount of SV3. It is worth noting that SV3/PVA-2-1 sample showed the lowest G′ and G″ values and an overlap of G′ and G″ over a wide range of frequencies, which indicates a very weak cross-linked network. This sample was therefore not be considered for electrode tests.

FTIR spectroscopy measurements (Figure 4.2b) were carried out to reveal the characteristic peaks of PVA hydrogel and SV3/PVA hydrogels containing various amounts of the PEDOT:PSS printing

paste, which also contains PG and DEG. The SV3/PVA hydrogels, unlike the PVA hydrogel, show characteristic peaks at around 2920 cm^{-1}, corresponding to -CH2 stretching, and around 1040 cm^{-1}, corresponding to -C-OH stretching [33], which confirm the presence of PG. The characteristic peak around 1085 cm^{-1}, corresponding the asymmetric C-O-C stretching of DEG [34], confirms the presence of DEG. The absorption peaks at around 830 and 980 cm^{-1}, corresponding to C-S bond stretching vibrations in the thiophene ring [35], and the peaks at around 1030 cm^{-1}, corresponding to the asymmetric stretching vibrations of benzene sulfonate [36], indicate the presence of PEDOT:PSS. The broad and intense peak at 3000-37000 cm^{-1} observed for all samples, is attributed to the symmetrical stretching vibration of -OH groups, which is sensitive to hydrogen bonding [23,37].

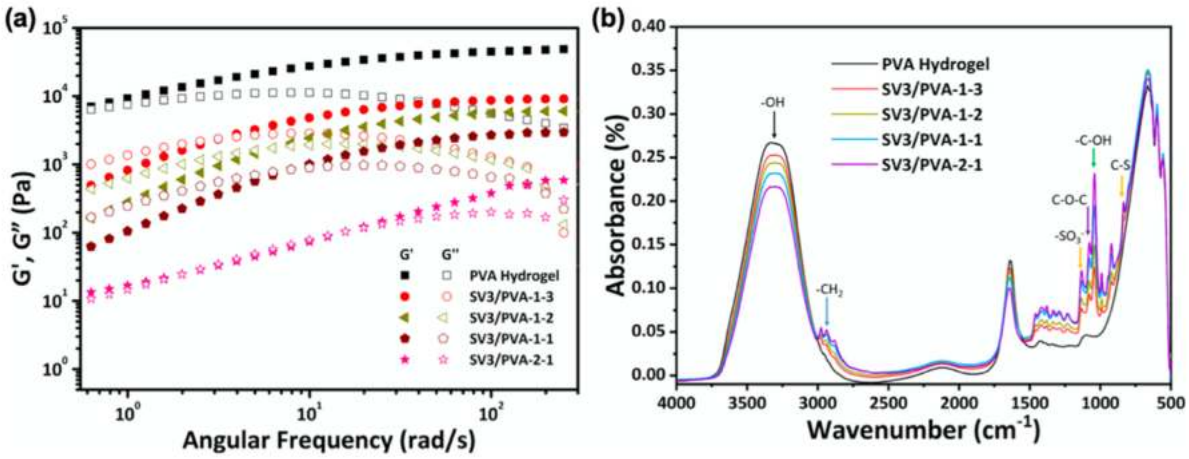

Figure 4.2 (a) Storage modulus (G′) and loss modulus (G″) as a function of angular frequency for PVA hydrogel and SV3/PVA hydrogels. (b) FTIR spectrum of SV3/PVA hydrogels and PVA hydrogel.

4.4.3 Adhesion and compressive mechanical properties

An ideal epidermal skin patch (e. g. ECG electrodes) should adhere to the skin tightly enough to ensure the acquisition of high-quality signals, while being easily removable after use. The interfacial adhesive properties of the hydrogels were investigated by perpendicular adhesion tests on pig skin (Figure 4.3a). The adhesion force of SV3/PVA-1-3, SV3/PVA-1-2, and PVA hydrogels drops rapidly after reaching the maximum value, while that of the SV3/PVA-1-1 hydrogel shows a gradual decrease. This behaviour indicates that the adhesion of SV3/PVA-1-1 on pig skin is

higher than its cohesion (Figure SA5). The extracted values of the adhesion force (Figure 4.3b and Table 4.1) reveal the higher adhesion of SV3/PVA hydrogels. The adhesion of SV3/PVA hydrogel moderately increased with increasing the SV3/PVA ratio. The SV3/PVA-1-3 hydrogel demonstrated outstanding adhesion on various materials, such as plastic, ceramic, glass, and stainless steel (Figure SA6). The high adhesion of SV3/PVA hydrogels on various substrates is likely due to the formation of hydrogen bonds originated by hydroxyl groups in PVA, DEG, and PG [27,38]. On the contrary, PVA-borax hydrogels show a low adhesion, which can be ascribed to PVA-borax crosslinking, leading to the decrease the number of hydroxyl groups available for hydrogen bonds [27]. On the other hand, the SV3/PVA-1-3 hydrogel was easily removed from the skin with a paper tissue, without leaving any residue (Figure SA7 and Movie SA3).

To further characterize the mechanical properties of SV3/PVA hydrogels, we conducted compression stress/strain measurements (Figure 4.3c). At low and moderate strains (up to ∼35%), all samples show a linear stress/strain relationship. At higher strain the relationship becomes nonlinear, likely due to irreversible deformation. The compressive Young moduli were extracted from the slope of the stress/strain relationship in the range 0-20% strain (Figure 4.3d and Table 4.1). The SV3/PVA hydrogels display a Young's modulus lower than the PVA hydrogel. This clearly indicates that the addition of the SV3 paste into the PVA-borax hydrogels leads to softer materials, likely due to the weakening of the interactions between PVA and borate ions (see Figure 4.1b). This result is in good agreement with the frequency sweep results, which show that G′ and G″ decreased upon addition of SV3 (Figure 4.2a). Overall, the low compressive modulus minimizes the mismatch with skin, making these materials ideal for on skin electrodes. It is worth to notice that biological tissues have moduli of 0.5-500 kPa, whereas the modulus of gold and silver is ∼80 GPa and that of stainless steel is ∼190 GPa.

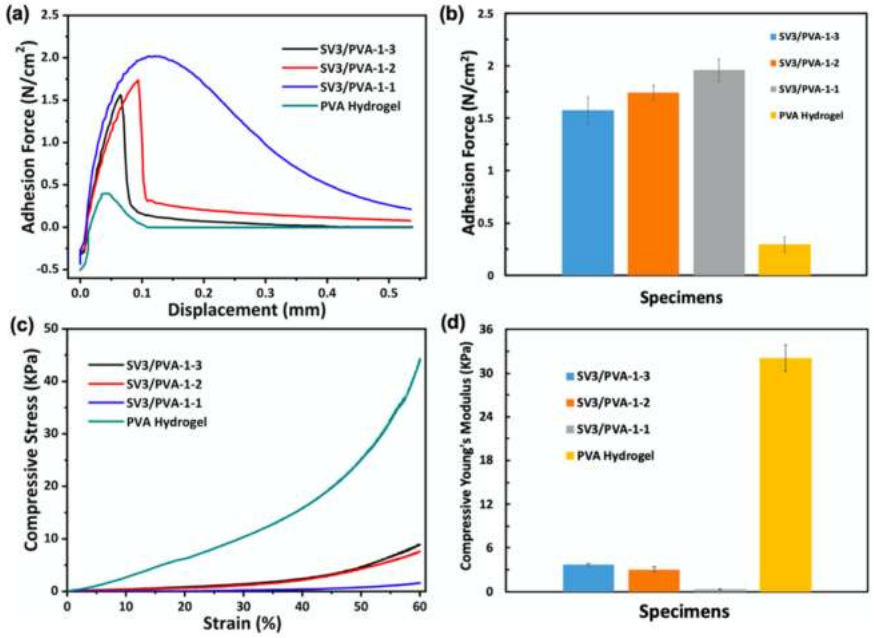

Figure 4.3 Adhesion and compressive stress-strain measurements of SV3/PVA-1-3, SV3/PVA-1-2, SV3/PVA-1-1, and PVA hydrogels. (a) Perpendicular adhesion force on pig skin versus displacement, (b) average perpendicular adhesion force on pig skin, (c) compressive stress versus strain, and (d) average compressive Young's modulus at 20% strain. Data for adhesion force (n = 6) and compressive Young's modulus (n = 3) are reported as mean ± standard deviation.

Table 4.1 Perpendicular adhesion on pig skin and compressive Young's modulus in the 0-20% strain range of SV3/PVA and PVA hydrogels. Data for adhesion force (n = 6) and compressive Young's modulus (n = 3) are reported as mean ± standard deviation.

Samples	Adhesion (N/cm^2)	Compressive Young's modulus (kPa)
SV3/PVA-1-3	1.57 ± 0.13	3.7 ± 0.2
SV3/PVA-1-2	1.74 ± 0.07	3.0 ± 0.4
SV3/PVA-1-1	1.96 ± 0.11	0.3 ± 0.05
PVA hydrogel	0.29 ± 0.07	32.0 ± 1.8

4.4.4 Mechanical and electrical self-healing properties

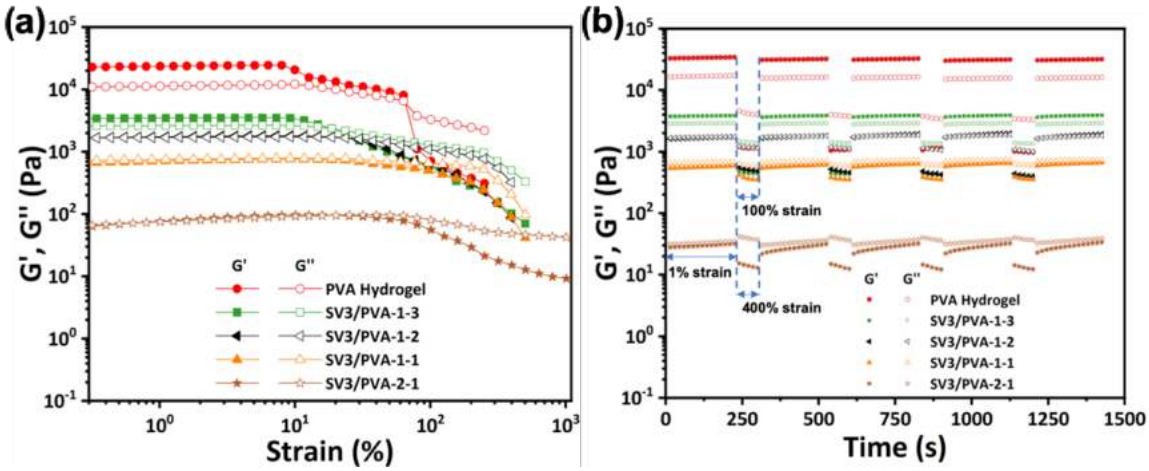

Figure 4.4 (a) Storage modulus (G′) and loss modulus (G″) versus strain% for PVA and SV3/PVA hydrogels (ω = 6.28 rad/s). (b) G′ and G″ versus time in continuous step strain sweep with an alternating small strain (1%, ω = 6.28 rad/s) and large strain (100% for PVA hydrogel, SV3/PVA-1-3, SV3/PVA-1-2, and SV3/PVA-1-1 and 400% for SV3/PVA-2-1, ω = 6.28 rad/s) oscillation force.

SV3/PVA hydrogels possess mechanical self-healing properties, as shown by rheology tests. Strain sweep measurements were carried out to first identify the linear viscoelastic region (LVER), i.e., the strain% range where G′ and G″ are almost constant, corresponding to a non-destructive shearing (Figure 4.4a). As the strain in- creases beyond the LVER, G′ and G″ systematically decrease with increasing strain%, indicating the destruction of the initial microstructure of the hydrogels. The LVER extends up to ∼10% strain for the PVA hydrogel and to higher values for the SV3/PVA hydrogels, with the critical strain% (i.e., the upper strain % limit of the LVER) moving to higher values with increasing SV3 content. The largest LVER is observed for the SV3/PVA-2-1 hydrogel (∼50%). Based on these results, cycles of low strain (1%) – high strain (100% or 400%) shearing were applied to assess the mechanical self- healing behavior of the samples, keeping the angular frequency constant at 1 Hz (Figure 4.4b). During the low strain interval, each sample was sheared at a constant strain% within its LVER, which ensured non-destructive shearing. This was followed by a high strain interval beyond the LVER. During this high strain interval, the microstructure of the samples underwent a complete breakdown. By applying several low strain-high strain cycles, allowed to assess if the structural deformation induced by the high strain was recovered when

returning to the low strain. The G′ and G″ of all samples decreased during the high strain interval and increased back to their original values during the low stain interval. This points to a structural deformation followed by a fast rheological recovery of the microstructure, which indicates mechanical self-healing. As an example, at 1% strain, the SV3/PVA-1-3 hydrogel displayed an elastic behavior, with a G′ of 3.80 kPa and a G″ of 2.86 kPa (loss factor: tan δ = G″/G′ ≈ 0.75). At 100% strain, G′ and G″ decreased to ∼0.45 kPa and 1.42 kPa respectively, resulting in a viscous-like behavior (tan δ = G″/G′ ≈ 3.2). When the strain amplitude was decreased back to 1%, the G′ and G″ returned to the initial values, indicating a rapid restoration of the hydrogel network (tan δ = 2.84 kPa/3.77 kPa ≈ 0.75). The above tests were performed at 25°C. To understand the influence of temperature we performed the amplitude sweep tests at both 25 and 37°C and presented in Figure SA8. This clearly shows that the linear viscoelastic region is not influenced by this temperature difference.

The mechanical self-heling properties of the hydrogels were further assessed by “cut and stick” experiments. Two separated pieces of the SV3/PVA-1-3 hydrogel remained stuck together as soon as they came into contact and the resulting piece could be stretched many times its original length (Movie SA4). The same experiment was not successful for the PVA hydrogel (Movie SA5). These results indicate the faster mechanical self-healing of the SV3/PVA-1-3 with respect to the PVA hydrogel.

Furthermore, an optical microscope was used to observe how the SV3/PVA-1-3 hydrogel heals after being cut by a scalpel (Figure SA9 and Movies SA6). A fracture was observed after cutting the hydrogel with the scalpel. However, the two separated parts rapidly came back into contact after removing the scalpel (healing time of ∼8 s at room temperature).

The self-healing mechanism PVA-borax hydrogels is typically explained by the formation of reversible boron ester bonds between the hydroxyl groups of PVA and sodium tetraborate [20]. However, the self-healing times for these materials are of a few minutes [32]. The enhancement of the self-healing properties upon addition of the SV3 paste may be due to the presence of PEDOT:PSS, PG and DEG, which can fill up the gap between the polymer chain and the cross-linking agent, providing more hydrogen bonds, thus facilitating the recombination of borax-diol and hydrogen bonding at the contact surface [32].

The SV3/PVA-1-3 hydrogel was selected for the electrical self- healing, skin-electrode impedance, ECG and EMG recording tests, due to its superior mechanical properties (highest compressive modulus and G′ and G″ values) with respect to the other SV3/PVA hydrogels.

The hydrogels here investigated show an electrical conductivity between ∼2.0×10^{-5} S/cm to ∼5.0×10^{-5} S/cm (Figure SA10), with SV3/PVA-1-3 being the most conductive. Electrical self-healing experiments were carried out with this material. For this purpose, we used a series circuit including two pieces of SV3/PVA-1-3 hydrogel, a light-emitting diode (LED), and a commercial 9 V battery. The LED lit up when the circuit was closed (Figure 4.5a_1) and it lit off when the circuit was opened by cutting the hydrogel with a plastic blade (Figure 4.5a_2). Subsequently, the LED lit up again (Figure 4.5a_3) when the two hydrogel pieces were brought into contact and remained stuck to each other (Movie SA7).

The current versus time plots show that the current recovers its initial value upon repeated cut-healing cycles (Figure 4.5b). To better visualize the time constant of the process, Figure 4.5c displays the current changes over time of the SV3/PVA-1-3 hydrogel during the first cut and heal process. Once the conductive hydrogel was completely cut off, the circuit opened, and the current dropped to the noise level. When the cut parts were brought together, the current reached a stable value within 2.0 s. It is worth noting that the cur- rent is higher than that of original value at the moment the two parts get back in contact, which might be due to transient ionic currents. The healing efficiency was calculated as about 100%.

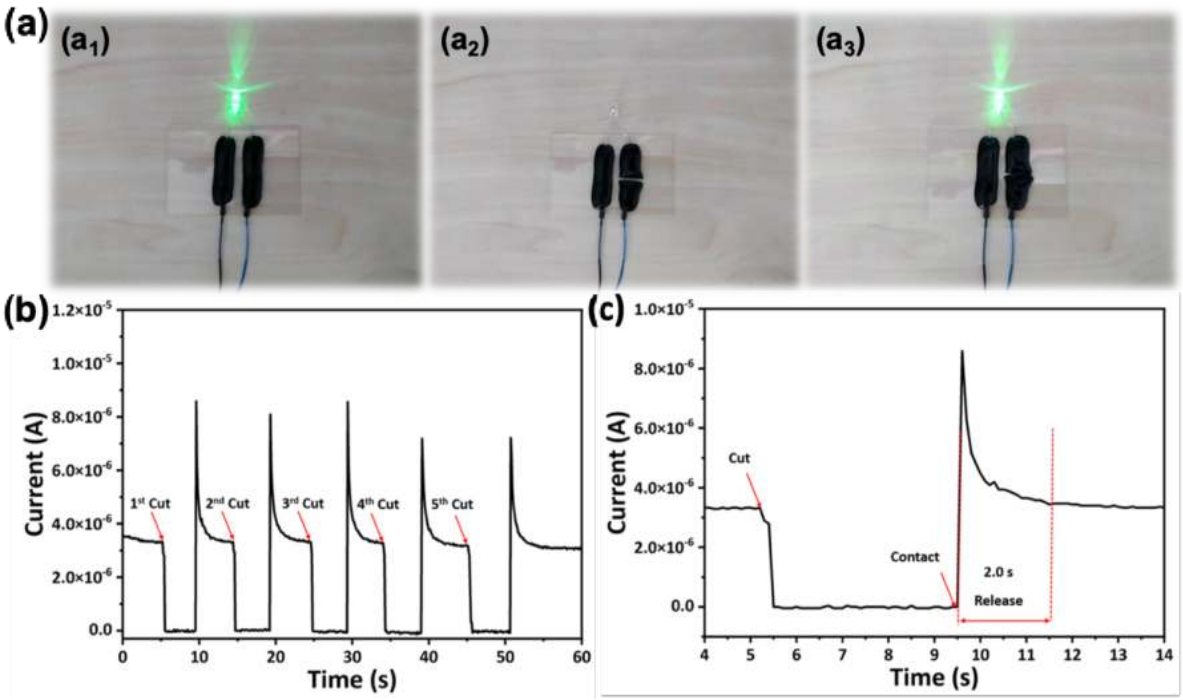

Figure 4.5 Electrical self-healing of SV3/PVA-1-3 hydrogel. (a) Circuit comprises the self-healing SV3/PVA-1-3 hydrogel in series with a battery and a LED indicator: (a_1) original (closed), (a_2) cut (open), and (a_3) healed (closed). (b) Current versus time measurements under a constant voltage of 0.6 V upon various cutting-healing cycles. (c) A magnification of b showing the time evolution of the electrical healing process after the first cut.

In summary, the SV3/PVA 1-3 hydrogel shows outstanding mechanical and electrical self-healing ability, which enable it to have great potential in applications of self-healing electronics including biosensors, electronic skin, and wearable electronics.

4.4.5 Strain sensitivity of SV3/PVA hydrogels

The strain sensitivity of SV3/PVA hydrogels was assessed by the gauge factor, which measures the change in electrical resistance upon strain (Figure SA11a). A strain sensor based on the SV3/PVA hydrogel showed a gauge factor of 2.38 ± 0.09 at 100% strain, which increased to 3.88 ± 0.46 at 500% strain (Figure SA11b).

4.4.6 Impedance properties on skin

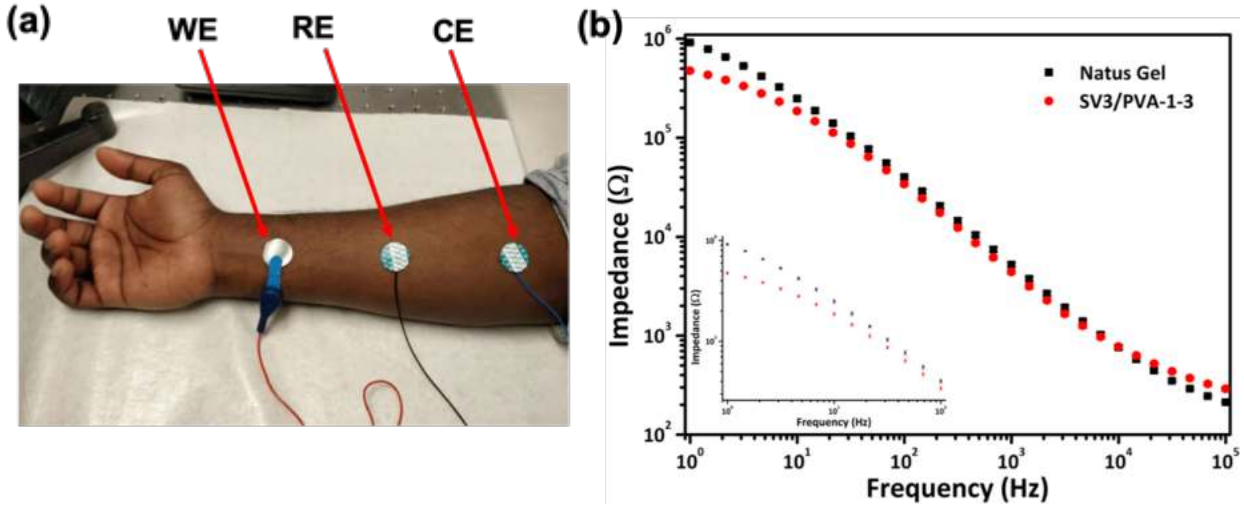

Figure 4.6 Characterization of the skin-electrode impedance without skin preparation and attachment pressure. (a) Impedance measurement configuration. (b) Skin-electrode impedance versus frequency for a SV3/PVA-1-3 hydrogel electrode and a commercial Natus® Ag/AgCl gel electrode. The diameter of the electrodes was 18 mm. The inset shows a magnification for measurements from 10 Hz to 100 Hz. Data for skin-electrode impedance are reported as mean ± standard deviation ($n = 3$). Note: WE: working electrodes, RE: reference electrodes, and CE: counter electrodes.

The skin-electrode impedance, an important factor that affects the quality of bio-signals recording, was studied for SV3/PVA-1-3 hydrogel electrodes on the skin of a volunteer (Figure 4.6a). The electrode under test acted as working electrode (WE), and commercial adhesive Ag/AgCl gel disk electrodes (Natus®) were used as reference (RE) and counter electrodes (CE). The working electrode placed on the skin was electrically connected with copper tape on the backside and covered by a Parafilm with a diameter of 18 mm. The impedance vs frequency plots (Figure 4.6b and inset) indicated that the SV3/PVA-1-3 hydrogel and the commercial adhesive Ag/AgCl gel disk electrodes performed overall similarly, with the SV3/PVA-1-3 electrode showing lower impedances at lower frequencies (e.g., ~185 kΩ versus ~250 kΩ for the Ag/AgCl gel disk electrodes at 10 Hz).

4.4.7 Epidermal electrodes for ECG and EMG recording

Ideal bioelectronics and wearable electronics (e. g. ECG electrodes) should integrate self-healing, good mechanical properties and high adhesion, to allow recording of high-quality bio-signals without using adhesives that might lead to skin irritation. The SV3/PVA hydrogels satisfy these requirements to a greater extent compared to similar hydrogels containing graphene [23], silver nanowires [23], MFC [26], FSWCNTs [22] (Table SA1).

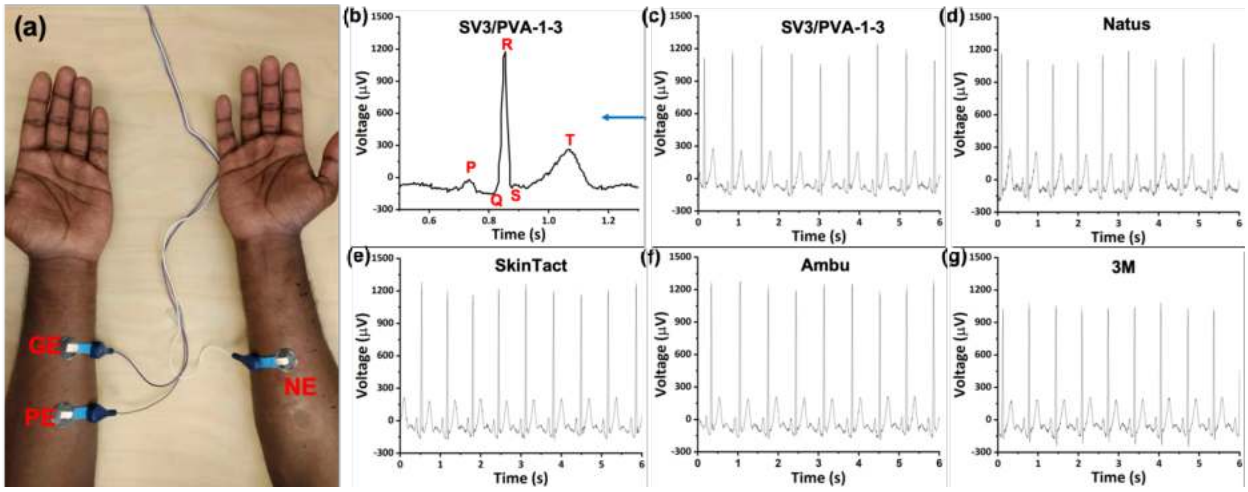

Figure 4.7 (a) ECG electrodes placed on the forearms of a volunteer. The ground (GE) and the positive (PE) electrodes are placed on the left forearm; the negative electrode (NE) is placed on the right forearm. ECG biopotentials (voltage versus time) recorded with SV3/PVA-1-3 hydrogel electrodes (b and c), commercial Natus®(d), SkinTact®(e), Ambu®(f), and 3M® (g) Ag/AgCl gel electrodes. The plot in (b) shows a magnification of the ECG signal between 0.5 - 1.3 s from the plot in (c).

Our conducting hydrogels are outstanding candidates for epidermal electrodes as they incorporate electroactive and adhesive properties and do not need additional components to be attached to the skin.

ECG is a common diagnostic tool used in human healthcare, and its recording quality is vital for clinical diagnosis. We recorded ECG bio-potentials with the ground and positive electrodes attached to left forearm and the negative electrode to the right forearm (Figure 4.7a). Among the ECG characteristic peaks (P, QRS, and T), the identification of P peaks is challenging due to the well-known weaker signal resulting from the fewer cardiac cells involved in atrial activation

compared to other ventricular activities [39]. The ECG signals between 0.5 s and 1.3 s recorded with SV3/PVA-1-3 hydrogel electrodes (Figure 4.7b) show well defined ECG characteristic peaks, even for the P wave, indicating the suitability of these electrodes for monitoring of bio-signals. The ECG signal recorded with of SV3/PVA hydrogel electrodes were compared with those recorded with 4 different types of commercial Ag/AgCl gel electrodes (Figure 4.7c-g). The results show that SV3/PVA electrodes exhibit recording quality similar to that of commercial Ag/AgCl gel electrodes.

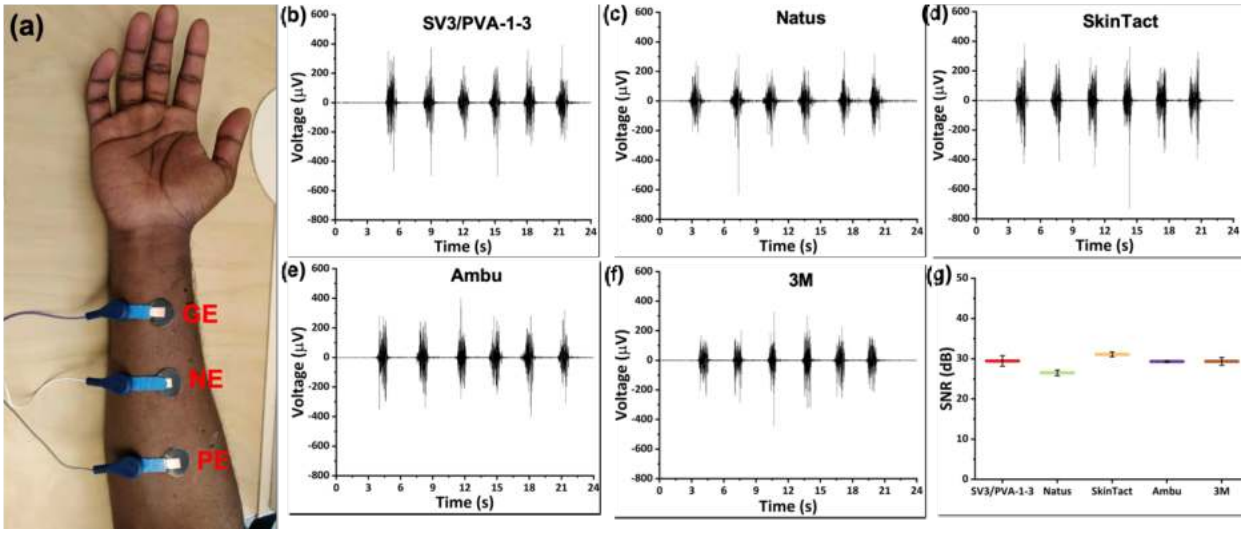

Figure 4.8 EMG signals recording for different electrode types. (a) EMG electrodes placed on the forearm of a volunteer. EMG biopotentials between the electrodes were recorded with ground electrode (GE), positive electrode (PE), and negative electrode (NE) on the right forearm. EMG monitoring with using (b) SV3/PVA-1-3 hydrogel electrodes, commercial (c) Natus®, (d) SkinTact®, (e) Ambu®, and (f) 3M® Ag/AgCl gel electrodes under relax and clenching phases. (g) Computed SNR values over the 24 s recording period for SV3/PVA-1-3 electrodes and 4 different commercial Ag/AgCl gel electrodes. SNR data are reported as mean ± standard deviation (n = 3).

Similar tests were performed to evaluate the EMG monitoring ability of SV3/PVA-1-3 hydrogel electrodes. For this purpose, the ground, positive and negative electrodes were attached to the right forearm of a volunteer (Figure 4.8a) and the change of bio-potential caused by switching between relaxed and tense states of the flexor carpi muscle was recorded. The EMG recording of SV3/PVA-1-3 hydrogel electrodes was compared to that achieved 4 different types of Ag/AgCl gel electrodes (Figure 4.8b-f). All the electrodes show similar potential change when switching the state of the

muscle. Notably, the SNR of EMG signals (Figure 4.8g) obtained by SV3/PVA electrodes (29.5 ± 1.3 dB) was similar to those obtained by the commercial Natus® (26.5 ± 0.7 dB), SkinTact® (31.1 ± 0.6 dB), Ambu® (29.3 ± 0.2 dB), and 3M® (29.4 ± 1.0 dB) Ag/AgCl gel electrodes, which indicates the suitability of SV3/PVA-1-3 hydrogel electrode for EMG recording. Furthermore, the SV3/PVA-1-3 hydrogel was easily removed from the skin without leaving any residue (Figure SA7 and Movie SA3). Moreover, compared to SkinTact®, 3M®, and Ambu® commercial Ag/AgCl gel electrodes, the as-prepared SV3/PVA-1-3 electrodes showed no skin damage or redness after 1 h wearing (Figure SA12).

4.5 Conclusions and perspectives

In summary, we fabricated self-healing, stretchable, highly adhesive and conductive hydrogels by mixing PVA, borax and a PEDOT:PSS screen printing paste. The addition of the PEDOT:PSS printing paste, rich in diols, to the PVA-borax network, results in materials with increased adhesion on skin, shorter self-healing times as well as enhanced softness and plastic stretchablility. One of our hydrogels was used to prepare epidermal patch electrodes, which demonstrated high quality ECG and EMG recording with a high SNR, similar to commercial devices. Furthermore, the electrodes made with our hydrogel were easy to remove from the skin without any skin damage or redness after 1 h wearing. Because of their straightforward fabrication and outstanding mechanical properties, hydrogels based on PVA, borax and PEDOT:PSS are highly promising for bioelectronics and wearable electronics. We believe that the most important challenges towards commercial applications are a fine tuning of the electronic and ionic conductivity of the materials and the integration of the hydrogel electrodes into flexible and stretchable printed circuits.

4.6 Acknowledgments

We thank Eric Quenneville (Biomomentum) for fruitful discussions. The Natural Science and Engineering Council Canada (NSERC) is acknowledged for Discovery Grants awarded to FC and GN that enabled this collaborative research. Equipment and infrastructure used for this research were acquired and maintained by the Canada Foundation for Innovation. XZ is grateful to China Scholarship Council for a PhD scholarship.

CHAPTER 5 ARTICLE 2 : STRETCHABLE, SOFT, HIGHLY ADHESIVE, AND SELF-HEALING CONDUCTIVE POLYMER FILMS FOR HEALTHCARE MONITORING

This article has been submitted in the journal "Nano-Micro Letters" on April 28th, 2023. The supporting information of this article is provided in Appendix B.

Xin Zhou[1], Pierre Kateb[1], Jinsil Kim[1], Gregory A. Lodygensky[2], Bénédicte Amilhon[3,4] Damiano Pasini[5], and Fabio Cicoira[1*]

[1] Department of Chemical Engineering, Polytechnique Montréal, Montréal, QC H3C 3A7, Canada

[2] Department of Pediatrics, Sainte-Justine University Hospital Research Center, Montréal, QC, Canada

[3] CHU Sainte-Justine Research Center, Montréal, QC H3T 1C5, Canada

[4] Département de Neurosciences, Université de Montréal, Montréal, QCH3T 1J4, Canada

[5] Department of Mechanical Engineering, McGill University, Montréal, QC H3A 0C3, Canada

*Corresponding author. E-mail: fabio.cicoira@polymtl.ca

5.1 Abstract

Conductive, soft, and stretchable electronic materials have become research hotspots for wearable and bioelectronic devices for healthcare monitoring. Herein, we report conductive, soft, stretchable, self-healing, highly adhesive, and biocompatible conductive polymer films obtained by mixing poly (3,4-ethylenedioxythiophene) doped with polystyrene sulfonate (PEDOT:PSS), ethylene glycol (EG), and tannic acid (TA). Our films demonstrated a moderate conductivity of ~15 S/cm, low Young's modulus of ~450 kPa, high stretchability (~90% strain), and high adhesion on several substrates. The films exhibited outstanding autonomous and *cut-stick* healing properties. Furthermore, the films did not exhibit cytotoxicity. Epidermal electrodes prepared using these materials exhibited low skin-electrode impedance at low frequency (1-100 Hz) compared to

commercial gel electrodes and high quality for electrocardiography (ECG) and electromyography (EMG) signal recordings compared to commercial Ag/AgCl gel electrodes.

Keywords: PEDOT:PSS; Self-healing; Adhesion; Bioelectronics; Epidermal electrodes; Conducting polymers

5.2 Introduction

Materials showing high electrical conductivity, softness, stretchability, adhesion, and self-healing are in high demand for applications in bioelectronics, wearable electronics and energy [2, 7, 26, 36, 47, 65, 120, 121]. In particular, such properties are highly desirable for epidermal electronics [62, 122], where materials need to achieve a delicate balance between several mechanical and electrical properties, such as i) low Young's modulus (e.g., 60-850 kPa for skin and muscles), to reduce the mismatch between the electrodes and bio-tissues that could lead to signal deterioration and skin damage; ii) high adhesion and conformal contact on the skin; iii) reasonable electrical conductivity; and iv) ability to retain mechanical and electrical performance over time. Several studies have shown that materials with such characteristics can be created by mixing conducting polymers, which typically exhibit poor mechanical properties, with other materials capable of imparting desired mechanical functionalities [120, 122].

The most widely used conducting polymer for such applications is poly (3,4-ethylenedioxythiophene) doped with polystyrene sulfonate (PEDOT:PSS) because of the high miscibility of its aqueous suspensions with a wide range of molecular, polymeric, and ionic materials. Flexible and stretchable conductors have been obtained by mixing PEDOT:PSS with polyols (e.g., xylitol, glycerol, and ethylene glycol), ionic liquids, or polymers (polyvinyl alcohol (PVA), poly(ethylene oxide) (PEO), polyethylene glycol (PEG), and Triton X-100). In addition, several PEDOT:PSS-based materials exhibit self-healing properties, which would also benefit the performance and sustainability of epidermal electrodes [43, 55, 62].

The adhesion strength, which is a critical characteristic of epidermal electronics, can also be tuned by mixing different materials. Adhesive films (thickness of 20 μm) made from a blend of PEDOT:PSS, waterborne polyurethane (WPU), and D-sorbitol [18], showed a Young's modulus of ~25 MPa, good adhesion on dry skin (~0.4 N/cm) and could achieve high quality bio-potential recording. Soft adhesive films prepared from a mixture of β-cyclodextrin, citric acid, PVA, glutaraldehyde, and PEDOT:PSS exhibited a low modulus of ~400 kPa, high stretchability (~700

strain), high interface adhesion (~1.2 MPa on a polyimide substrate), and a conductivity of ~37 S/cm. These films have been used as epidermal electrodes for electromyographic signal monitoring [120]. Tannic acid (TA), a natural polyphenol, has been widely investigated for improving the adhesion strength of PEDOT-based materials on a wide range of substrates, including human skin [123, 124]. Adhesive films obtained from PEDOT:PSS, PVA, EG, and TA [50] exhibited a stretchability of approximately 50% strain, a Young's modulus of ~18 MPa, good adhesion to porcine skin (~0.3 N/cm) and could be used as electrodes to record bio-signals. TA has also been used to prepare self-healing hydrogels in combination with poly(dimethyldiallylammonium chloride) (PDDA)) and FeIII [125], thioctic acid [126], silk fibroin [127], and PVA/PAAM [128]. Besides its effect on the mechanical properties, TA exhibits biocompatibility and antibacterial, antioxidative, and anti-inflammatory properties [123, 124, 129].

Herein, we report a conductive, stretchable, self-healing, adhesive material obtained from an aqueous mixture of PEDOT:PSS, ethylene glycol (EG), and tannic acid (TA). The films obtained from this material exhibited a low Young's modulus (~450 kPa), moderate electrical conductivity (~15 S/cm), high stretchability, high interfacial adhesion on glass and porcine skin, and outstanding electrical and mechanical self-healing properties. Soft epidermal film electrodes based on these materials showed performance comparable to that of commercial Ag/AgCl gel electrodes for ECG and EMG recordings. The cell viability assays showed no evidence of cell toxicity. The ease of processing, environmental sustainability, biocompatibility, and well-balanced electromechanical properties of this material make it ideal for applications in bioelectronics and wearable electronics.

5.3 Experimental Section

5.3.1 Materials

Tannic acid (TA), ethylene glycol (EG), isopropyl alcohol (IPA), and eutectic gallium-indium (EGaIn) were obtained from Millipore Sigma (St. Louis, Mo, USA). PEDOT:PSS (Clevios™ PH1000 aqueous suspension) was purchased from Heraeus Precious Metals (Germany). The PEDOT:PSS content in this formulation was between 1 and 1.3%, as declared by the supplier. Silver ink (Ag 520 EI) was donated by Chimet Sp.A (Italy). PET sheets (XF-122, 25 μm thick) were purchased from Polyonics (USA). Glass slides were obtained from Corning (USA). Teflon™ plates were purchased from McMaster Carr. Porcine skin samples were obtained from a local grocery store. Transparent (96-well plates) and black microplates (OptiPlate-96 well plates) were

supplied by Corning Life Sciences and PerkinElmer, respectively. Cell culture flasks (Nunc™ EasYFlask™), fetal bovine serum (FBS), and live/dead calcein AM/ethidium homodimer were obtained from Thermo Scientific. Trypsin, Dulbecco's modified Eagle's medium (DMEM), and C2C12 cells (mouse muscle cells) were supplied by American Type Culture Collection (ATCC, USA). Dulbecco's phosphate-buffered saline (DPBS; no calcium or magnesium) was obtained from Gibco™.

5.3.2 Film preparation

Clevios PH1000, EG, and TA (chemical structures in Figure 5.1a) were mixed, at the ratios listed in Table 5.1, in a planetary mixer (ARM-310, Thinky, USA) at 2000 rpm for 10 min. The samples were named according to the description in Table 5.1. The films were obtained by casting into glass or Teflon molds (for PEDOT/EG/TA-3 samples) with a thickness of ~1 mm and drying at 60 °C for 90 min. The film thickness was measured using a Mach-1 V500cst MA009 mechanical tester (Biomomentum Inc., Canada) with a spherical stainless-steel indenter with a diameter of 1 mm (values reported in Table 5.2). The TA concentration in the mixture was varied to optimize the mechanical properties of the films. PEDOT/EG/TA-3 films were used for creep deformation, self-healing, and fabrication of epidermal electrodes because of their high stretchability and adhesion properties.

Table 5.1 PEDOT/EG/TA film samples used in this study.

Samples	PEDOT:PSS suspension (wt%)	EG (wt%)	TA (wt%)
PEDOT/EG/TA-0	90.9	9.1	0
PEDOT/EG/TA-1	87.7	8.8	3.5
PEDOT/EG/TA-2	84.7	8.5	6.8
PEDOT/EG/TA-3	82.0	8.2	9.8

5.3.3 Conductivity Measurement

The conductivities of the samples were measured using a Biomomentum 4-point probe system (Figure SB1) connected to a source measure unit (B2902A, Agilent). The current voltage

characteristics were acquired with voltage steps of 0.1 V from 0.5 to 1 V. The conductivity (σ) of the films was calculated as follows:

$$\sigma = \frac{L}{R_A * S} \quad \text{Equation 5.1}$$

Where R_A is the average resistance and L and S are the length and section of the films, respectively. The reported conductivity values corresponded to the average of five measured samples, and the error corresponded to the standard deviation.

The conductivities of the films (reported in Table 5.2) ranged between ~90 S/cm (PEDOT/EG/TA-0) and ~17 S/cm (PEDOT/EG/TA-3) and decreased with increasing TA content.

5.3.4 Mechanical characterization

Electromechanical, creep-recovery, and adhesion measurements were performed using a Mach-1 V500cst MA009 mechanical tester (Biomomentum Inc., Canada).

For the electromechanical tests, the end sides of the films (10 mm × 40 mm) were connected to two electrical tensile grips with a gap of 10 mm. The films were stretched at a speed of 6 mm/min using a 70 N load cell. The resistance ratio was calculated as R/R_0, where R and R_0 are the resistances at a given strain and at 0% strain, respectively. The Young's modulus of the films was extracted from the slope of the stress-strain curves in the range of 0-10% strain. Three samples of each film type were tested.

Creep-recovery measurements were performed to evaluate the deformation and recovery behaviors of the films over time. A constant creep stress of 150 kPa was applied to the samples for 5 min, followed by a release for 10 min. The change in strain was measured over time, and the strain recovery was calculated as follows:

$$Strain\ recovery\ (\%) = \frac{L_0 - L}{L_0} \times 100 \quad \text{Equation 5.2}$$

where L and L_0 are the lengths of the film during recovery and upon immediate removal of constant stress, respectively.

Adhesion measurements were performed on glass and porcine skin in 90° peeling-off geometry (Figure SB2), according to ASTM D6862. The films were treated at 80 °C for 2 min before the test to remove surface moisture. Rectangular pieces of the films (10 × 60 mm) were attached to a PET

sheet for ease of handling and subsequently attached to the substrates (contact area of 10 × 40 mm^2). Adhesion force measurements were performed while detaching the films at a speed of 60 mm/min. Three samples of each film were measured, and the adhesion force was calculated as the average stable force normalized by the width of the film.

5.3.5 Fourier-transform infrared (FT-IR) spectroscopy

A Perkin Elmer Spectrum 65 spectrophotometer was used to record Fourier-transform infrared (FT-IR) spectra in absorption mode, with a scan range of 500~4000 cm^{-1} and 16 scans at a resolution of 4 cm^{-1}.

The spectra of the films (Figure SB3) showed the characteristic peaks of TA, EG, and PEDOT:PSS. The broad peak at 3000–3700 cm^{-1} observed for all samples is attributed to the stretching vibration of the -OH groups of EG and TA. The peaks at ~1620 cm^{-1} and ~1380 cm^{-1}, corresponding to the C=C and C-C bonds of the thiophene ring [130], and the band at ~1120 cm^{-1}, corresponding to the $-SO_3H$ group of PSS [130], indicate the presence of PEDOT:PSS. The peaks corresponding to C-H stretching (at ~2938 cm^{-1} and ~2875 cm^{-1}), C-O stretching (at 1084 cm^{-1}), and C-C-O symmetric stretching (882 cm^{-1}) [131] confirmed the presence of EG. The peak at ~1452 cm^{-1} corresponds to the stretching vibrations of the-C-$C_{aromatic}$ groups in TA [132].

5.3.6 Self-healing

The autonomous and cut-stick healing properties of the PEDOT/EG/TA-3 films were evaluated in two separate experiments.

Autonomous self-healing

Films (40 mm × 10 mm × 0.13 mm) were placed on a glass slide. The current flowing in the film upon application of a 0.2 V bias was measured with an electrical probe station (miBot, Imina Technologies, Switzerland) equipped with a Keysight source-measure unit (SMU B2902A). EGaIn traces were used to improve the electrical contact between the tungsten probes and films. A stainless-steel double-edge blade (Feather, Japan) was used to cut the film (the cut width was between 5 and 20 μm) while continuously monitoring the current. An inverted optical microscope (Carl Zeiss, Primovert, Germany) was used to visualize the self-healing process in real-time.

Cut-stick self-healing

For electrical healing, two pieces of conductive copper tape were placed at the extremities of the two films (contact length of approximately 5 mm), and a light-emitting diode (LED) was connected to the other side of the copper tape. The other extremities of the films were connected to an electrical probe station equipped with an Agilent source-measure unit using copper tape. To observe the electrical healing behavior, the films were cut with a stainless-steel knife blade (Craft Cutter) and successively manually stuck together. A voltage of 9 V was applied during the experiment. The electrical-healing efficiency was calculated as follows:

$$\eta = \frac{I_{healed} - I_{damaged}}{I_{pristine} - I_{damaged}} \qquad \text{Equation 5.3}$$

Where *I* is the current measured for the healed, damaged, and pristine films.

For mechanical cut-stick healing, the films (10 × 40 mm) were cut into two parts that were successively stuck together (overlap area:10 × 3 mm). Strain-stress tests were performed on these samples and the results were compared with those of the pristine samples. The films were stretched at a speed of 6 mm/min using a 70 N load cell.

5.3.7 Preparation of electrodes

The epidermal electrodes were prepared as follows: i) electrical contacts were made by casting stretchable silver ink onto a PET sheet and drying at 100 °C for 5 min; ii) PEDOT/EG/TA-3 disks were attached to the silver surface; and iii) a snap button was attached to the end of the PET sheet for connection to the electronics (Figure SB4).

5.3.8 Characterization of epidermal electrodes

Skin electrode impedance, ECG, and EMG measurements were performed as previously described [99]. For EMG recording, positive and negative electrodes were attached to the flexor carpi muscle of the right forearm and a ground electrode was placed on the elbow. Twelve signal regions and 13 noise regions were chosen for the root-mean-square (RMS) signal and RMS noise value calculations, respectively.

5.3.9 Biocompatibility essays

Cell culture was performed according to the standards of the American Type Culture Collection (ATCC). C2C12 cells were cultured in a flask in a culture medium containing DMEM with 10% FBS in an incubator (Sanyo MCO-17A, Japan) at a constant temperature of 37°C in a saturated humidity atmosphere (95% air / 5% CO_2). 10 µL sterilized PEDOT:PSS/EG/TA-3 mixture was coated onto the polystyrene (PS) wells, followed by drying at 60 °C overnight. Before cell plating, the coated wells were thoroughly rinsed with DPBS to remove excess acidic residues from the films. The cells were seeded onto PEDOT/EG/TA-3 film-coated PS wells. Uncoated PS wells sterilized with IPA were used as negative controls, whereas untreated wells were used as positive controls. For cell viability studies, 20000 cells per well were seeded and cultured for 24 h (day-1) and 72 h (day-3). Before the test, the samples were rinsed with DPBS (80 µL) after removing the culture medium on day-1 and day-3. A live/dead calcein AM/ethidium homodimer assay was used to stain the cells according to the manufacturer instruction on day-1 and day-3. Briefly, after rinsing the samples, 80 µL dye solution (4 µM EthD-1 and 2 µM calcein in DPBS) was added and incubated at 37°C for 30 min before the tests. The cells were observed under a microscope (EVOS M5000, Thermo Scientific, USA). For quantitative viability of cells, black microplates were used for spectrophotometric measurements on a microplate reader (Infinite 200 Pro, Tecan, Switzerland). The fluorescence of the solutions was measured spectrophotometrically at 494 nm excitation and 517 nm emission wavelengths. The cell viability (% live cell) was calculated as follows:

$$\%\ live\ cell = \frac{F(517)_{sam} - F(517)_{min}}{F(517)_{max} - F(517)_{min}} \qquad \text{Equation 5.4}$$

Where $F(517)_{sam}$, $F(517)_{max}$, and $F(517)_{min}$ are the average (three samples) fluorescence of PEDOT/EG/TA film-coated wells, positive control wells, and negative control wells, respectively. The reported values of cell viability corresponded to the calculated average value and the error of the standard deviation.

5.4 Results and Discussion

5.4.1 Mechanical and electrical tensile properties

The PEDOT/EG/TA film exhibited outstanding mechanical properties. They were easily folded (Figure 5.1b and Figure SB5a), exhibited excellent adhesion to the skin and the ability to adapt to finger movements (Figure 5.1c_1-c_3 and Movie SB1) and could adhere to various materials, such as

stainless steel (Figure SB5b), copper (Figure SB5c), glass (Figure SB5d), and PET (Figure SB5e) and withstood suspended weights up to 500 g (Figure SB5f, Movie SB2).

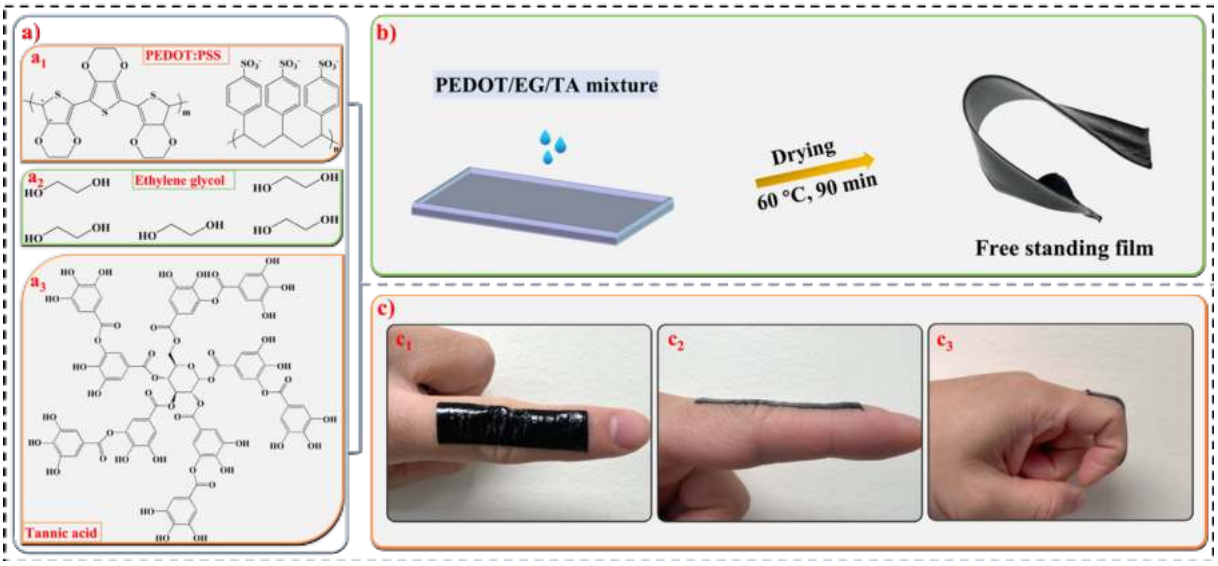

Figure 5.1 (a) Chemical structures of PEDOT:PSS (a_1), EG (a_2), and TA (a_3). Schematic of the film preparation (b). Digital pictures of free standing PEDOT/EG/TA-3 films on the finger skin: top view (c_1), side view (c_2), and side view during finger bending (c_3).

Stress-strain measurements (Figure 5.2a) showed that increasing the amount of tannic acid led to a decrease in the Young's modulus and an increase in the elongation at break (Figure 5.2b and Table 5.2), thus yielding more stretchable films. The resistance measurements acquired simultaneously revealed good electrical stability under strain (Figure 5.2c and Table SB1). For instance, at 30% strain, the typical human skin stretchability [18], PEDOT/EG/TA-3 films showed an increase of only ~2%, slightly lower than values reported in the literature [18, 50]. Remarkably, at 90% strain, the increase in the resistance was only ~20% of the initial value.

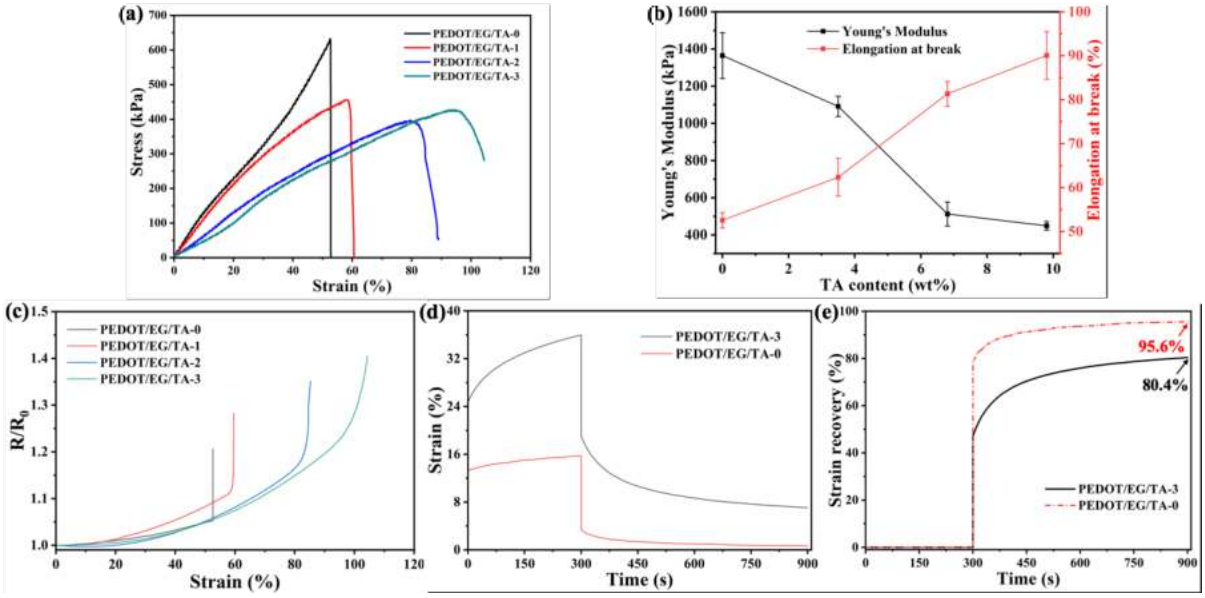

Figure 5.2 Mechanical and electrical tensile properties of PEDOT/EG/TA films. (a) Tensile stress versus strain. (b) Average tensile Young's modulus at 10% strain and elongation at break of films with different TA content. (c) Electrical resistance versus tensile strain of PEDOT/EG/TA films obtained during stress-strain measurements, as shown in Fig. 2a. (d) Creep deformation (strain vs time) and (e) strain recovery time plots of the PEDOT/EG/TA-0 and PEDOT/EG/TA-3 films. A constant creep stress of 150 kPa was applied for 5 min, and the strain was allowed to recover for 10 min after the stress removal. Tensile Young's modulus (n = 3) and elongation at break (n = 3) of films are reported as the mean ± standard deviation.

To study the effect of TA on the deformation and recovery behavior, we performed a comparative creep recovery test in the presence and absence of TA (PEDOT/EG/TA-3 and PEDOT/EG/TA-0 films, Figure 5.2d). Upon application of constant stress, both films exhibited instantaneous deformation, which steadily increased over time. After 5 min, the strain changes of ~10% for the PEDOT/EG/TA-3 films and ~2.5% were observed for PEDOT/EG/TA-3 and PEDOT/EG/TA-0 films, respectively. Ten minutes after the removal of the stress, the recovery was ~80% for the PEDOT/EG/TA-3 films and ~95% for the PEDOT/EG/TA-0 films (Figure 5.2e), indicating that the films containing TA had a greater tendency to deform.

The effect of TA on the mechanical properties of the films can be explained by the interactions between the PEDOT:PSS, EG, and TA. Hydrogen bonds can form between the hydroxyl groups of TA and EG and the sulfonate groups of PSS chains, while the hydrophobic benzene groups of TA and PEDOT can interact via π–π stacking [50]. We believe that both of these effects can weaken

the electrostatic interaction between PEDOT and PSS chains, thus increasing the polymer chain mobility, which in turn results in enhanced softness and deformation.

Table 5.2 Thickness, tensile Young's modulus in the 0 -10% strain range, elongation at break, 90° peeling-off adhesion on glass and porcine skin, and conductivity of the films. The thicknesses ranged between ~65 μm and ~130 μm, depending on the amount of TA. Data for the adhesion force (n = 3), tensile Young's modulus (n = 3), elongation at break (n = 3), and conductivity (n = 5) are reported as the mean ± standard deviation

Samples	Thickness (μm)	Young's modulus (kPa)	Elongation at break	Adhesion (N/cm)		Conductivity (S/cm)
			(%)	Glass	Porcine skin	
PEDOT/EG/TA-0	~ 65	136 ± 123	52.6 ± 1.8	~ 0.004	~ 0.004	91.7 ± 4.4
PEDOT/EG/TA-1	~ 85	1092 ± 54	62.3 ±4.3	0.01 ± 0	0.009 ± 0.002	39.2 ± 2.6
PEDOT/EG/TA-2	~ 110	513 ± 64	81.3 ± 2.8	4.3 ± 0.8	0.059 ± 0.007	22.0 ± 1.7
PEDOT/EG/TA-3	~ 130	449 ± 23	90.1 ± 5.4	5.9 ± 0.2	0.700 ±0.040	16.5 ± 0.7

5.4.2 Adhesion properties of PEDOT/EG/TA films

Measurements of the adhesion force on glass and porcine skin versus perpendicular displacement (Figure 5.3, data summarized in Table 5.2) clearly show that an increase in TA content leads to an increase in adhesion force. For instance, by increasing the TA content to ~10 wt% (PEDOT/EG/TA-3 film), the maximum adhesive force of the films approached 6 N/cm on glass and 0.7 N/cm on porcine skin. These values well compare with those of PEDOT:PSS/WPU/D-sorbitol films (e. g., 1.5 N/cm on the glass and ~0.3 N/cm on porcine skin) [18] and PEDOT:PSS/PVA/TA films (e. g., ~0.3 N/cm on the glass and ~0.3 N/cm on porcine skin) [50]. This high adhesion force is likely due to the catechol and pyrogallol aromatic ring structures present in TA [123, 124], which can form hydrogen bonds with the functional groups of the substrates.

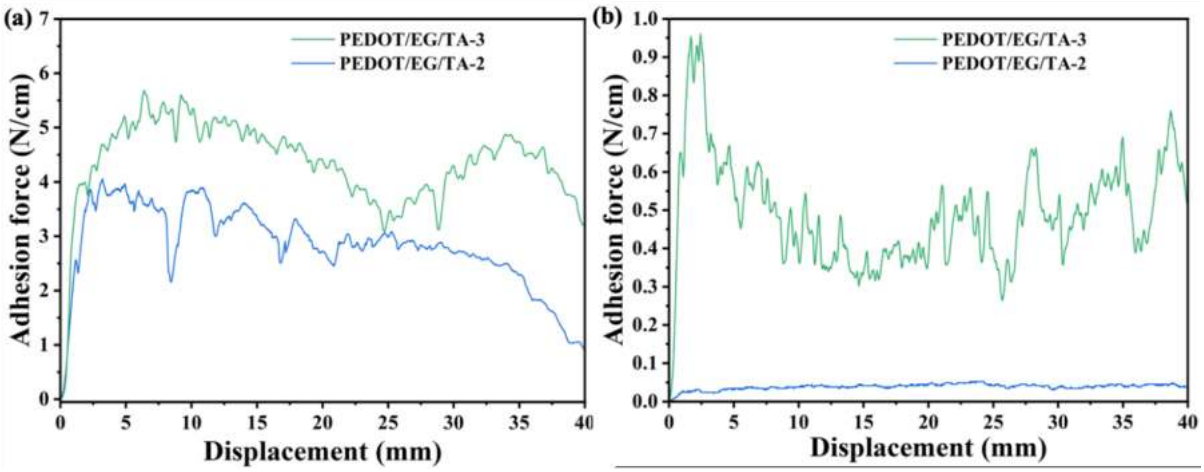

Figure 5.3 Adhesion force versus displacement for PEDOT/EG/TA-2 (~7% TA) and PEDOT/EG/TA-3 (~10% TA) films on glass (a) and porcine skin (b). A 90° peeling-off geometry is used. The fluctuations during the peeling process were likely caused by high adhesion on the glass, which led to damage during peeling (Figure SB6). The adhesion force dropped to noise level for TA contents below 3.5 wt% (Figure SB7).

5.4.3 Self-healing properties of films

The mechanical and adhesive properties of the PEDOT/EG/TA-3 films reported above led us to investigate autonomous and cut-stick healing (Figure 5.4).

Autonomous self-healing properties were studied by measuring the current flowing through the film while cutting it with a sharp blade. The current versus time plots (Figure 5.4a) show an autonomous recovery of the current to its initial value within approximately 30 s after the cut, even after repeated damage in different regions of the film. Optical microscope images taken during the process (Figure 5.4b, c, and d) show that the gap created by the cut healed completely after approximately 45 s. Real-time imaging of the process (Movie SB3) clearly reveals that healing started immediately after the cut and was completed after approximately 45 s. No healing effect was observed in the absence of TA (Figure SB8 and Movie SB4).

Cut-stick healing was demonstrated by measuring the current flowing into a series circuit including two pieces of PEDOT/EG/TA-3 films connected to a LED. The current was interrupted after the cut and recovered when the two extremities of the cut were stuck together. This process was repeated several times, with an electrical healing efficiency of approximately 100% (Figure 5.4e).

The healing effect was visualized using a similar circuit that included two PEDOT/EG/TA-3 films connected to an LED. The LED lit up when the circuit was closed (Figure 5.4f), and lit off when it was opened by cutting one of the films (Figure 5.4g). Subsequently, the LED lit up again when the two film pieces were stuck to each other (Figure 5.4h and Movie SB5).

To assess the mechanical healing of the films after cutting and stick-healing, we measured their tensile properties. The stress–strain curve of the healed films (Figure 5.4i) shows similar behavior to that of the intact ones. In addition, the healed films exhibited good cycling stability, as they could withstand loading–unloading for 100 cycles at a ramp strain of 30% (Figure SB9). Interestingly, the overlapping parts of the two reconnected films remained intact during the stretching process (Figure 5.4g, k, and Movie SB6), indicating high self-adhesive ability.

In the absence of TA, the films did not show autonomic or cut-stick healing. Although further investigation is necessary to clarify the healing mechanism, these remarkable healing properties can be attributed to the mechanical softness imparted by the presence of TA and the formation of hydrogen bonds between the species present in the films at the gap interfaces [55]. For cut-stick healing, an important role can be played by the large number of OH groups in the catechol and pyrogallol aromatic rings of TA. These OH groups can lead to high self-adhesion between the two via the formation of hydrogen bonds. As a result, the two separated films can adhere tightly and self-heal.

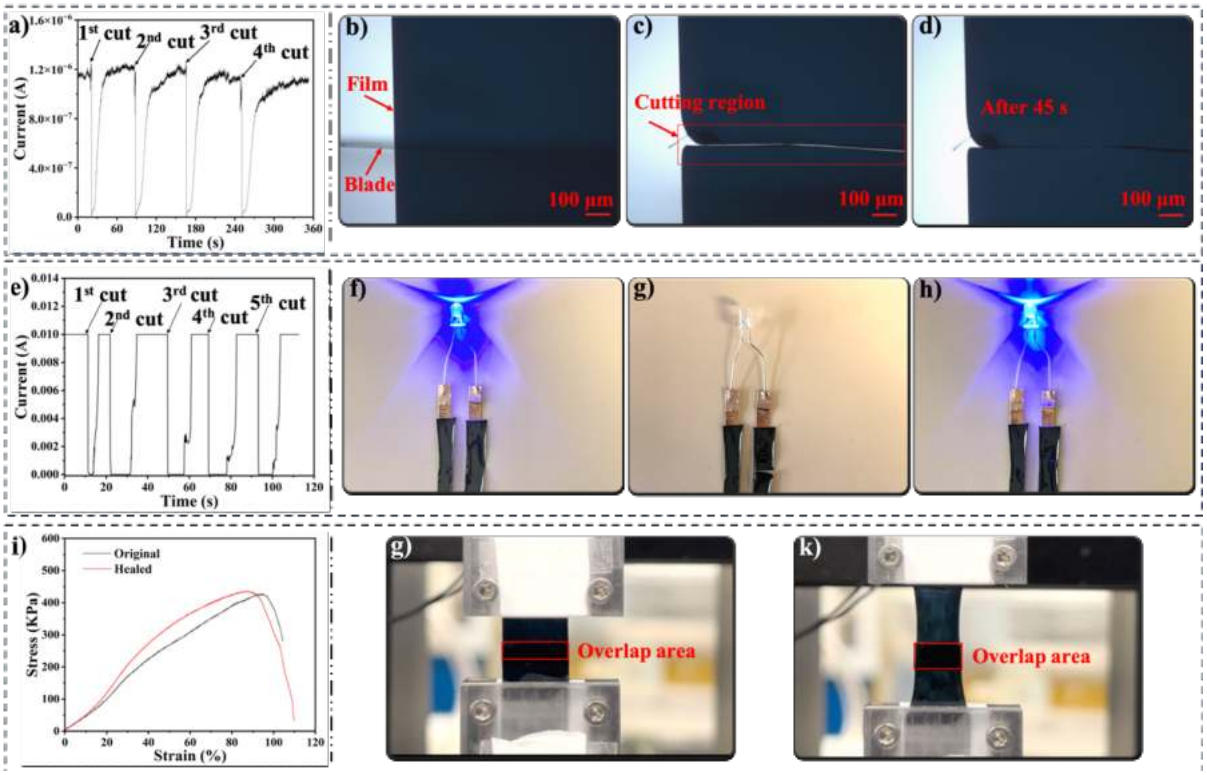

Figure 5.4 Electrical and mechanical autonomous (a-d) and cut-stick (e-k) healing properties of PEDOT/EG/TA-3 films. Autonomous healing process: a) Current versus time measurements under a constant voltage of 0.2 V upon various cutting-healing cycles, optical microscopy images of the self-healing process b) before cutting, c) after cutting, and d) after healing. Electrical cut-stick healing process: e) Current versus time measurements under a constant voltage of 9 V upon repeated cut-stick healing cycles; f-h) Visualization of the healing effect with an LED indicator: f) original (closed), g) cut (open), and h) healed (closed). Mechanical cut-stick healing process: i) tensile stress-strain plots of original and cut-stick healing films. Images of the film mounted on the tensile tester g) before stretching (the overlap area of film was 10 mm × 3 mm) and k) during stretching.

5.4.4 Skin-electrode impedance and ECG & EMG recording properties

The outstanding mechanical, electrical, adhesion, and self-healing properties of PEDOT/EG/TA-3 films make them suitable for soft epidermal electronics, which should ideally have a Young's modulus similar to that of the skin and adhere conformally to the skin to ensure the acquisition of high-quality signals.

To evaluate the PEDOT/EG/TA-3 film electrodes, skin electrode impedance versus frequency measurements were performed using a three-electrode setup (Figure SB10a). We performed the

measurements on the same volunteer, location, and during the same day, as the testing conditions (e.g., object, skin conditions, location, and time) can significantly affect the results. In the relevant frequency range up to 100 Hz (Figure SB10b and Table SB2), the film electrodes performed slightly better than the commercial adhesive Ag/AgCl gel disk electrodes (e.g., ~160 kΩ and ~220 kΩ for the film and gel disk electrodes at 10 Hz, respectively, Table SB2), while they performed similarly at high frequencies.

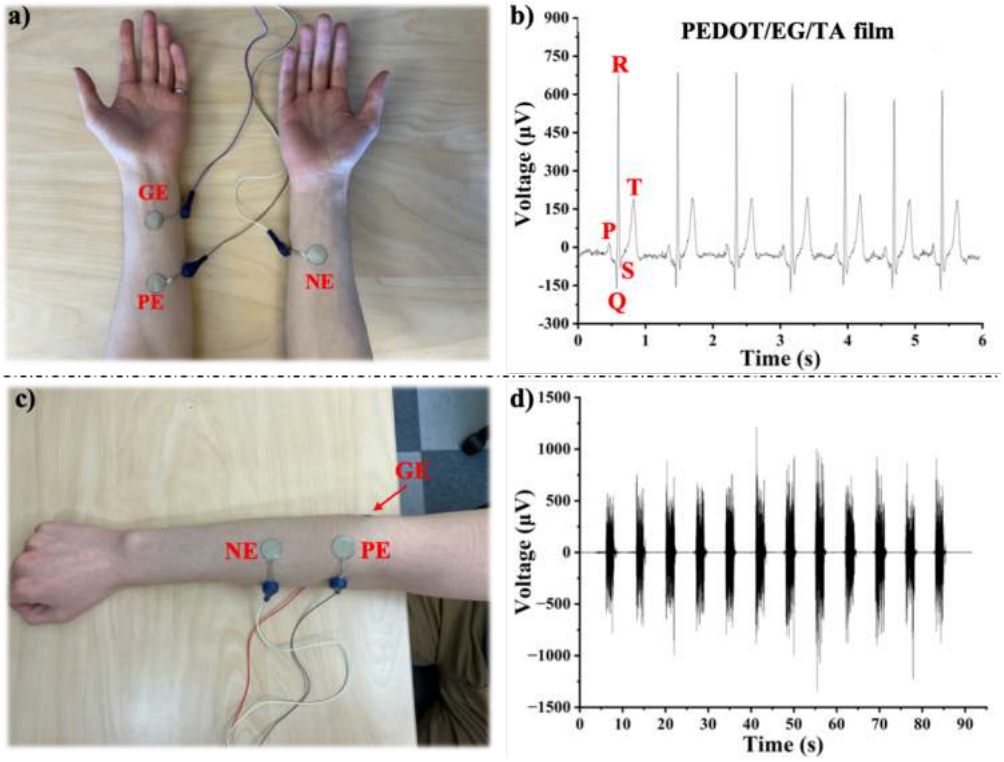

Figure 5.5 ECG and EMG signal recordings for the PEDOT/EG/TA film electrodes. a) Configuration of ECG measurements in a volunteer. Positive (PE) and ground (GE) electrodes were placed on the left forearm and the negative electrode (NE) was placed on the right forearm. b) ECG biopotentials (voltage versus time) recorded using PEDOT/EG/TA-3 film electrodes. c) Configuration of EMG measurements in a volunteer. EMG biopotentials between the electrodes were recorded with a PE and NE on the right forearm and a GE on the elbow. d) EMG monitoring with using PEDOT/EG/TA film electrodes.

Monitoring vital signs such as ECG and EMG is critical for point-of-care diagnostics. The ECG biopotentials were recorded by attaching the ground and positive electrodes to the left forearm and the negative electrode to the right forearm (Figure 5.5a). ECG voltage vs. time plots indicated that the PEDOT/EG/TA film electrodes exhibited well-defined ECG characteristic peaks, including the

P wave, QRS complex, and T wave (Figure 5.5b). Their performances were compared those with of three different types of commercial Ag/AgCl gel electrodes (Figure SB11a-c). The results revealed similar recording quality.

To assess the EMG monitoring ability of the PEDOT/EG/TA film electrodes, we attached the positive and negative electrodes to the right forearm and the ground electrode to the elbow of a volunteer (Figure 5.5c) and recorded the changes in biopotential resulting from switching between relaxed and tense states of the flexor carpi muscle for over 90 seconds. EMG voltage vs. time plots showed that the PEDOT/EG/TA film electrodes and three commercial Ag/AgCl gel electrodes showed similar potential changes when switching the state of the muscle (Figure 5d and Figure SB11d-f). Notably, the SNR of EMG signals recorded using the PEDOT/EG/TA film electrodes (37.0 ± 1.7 dB) was similar to that achieved using the commercial Natus® (34.1 ± 0.9 dB), 3M® (38.7 ± 0.8 dB), and Ambu® (36.2 ± 0.3 dB) Ag/AgCl gel electrodes (Figure SB11g).

The above results indicate that our film electrodes are suitable for bio-signal recording. In addition, our electrodes had several advantages. First, there is no requirement for the use of adhesive tape, owing to the high adhesion of the film electrodes. Second, our electrodes might benefit from the biocompatibility, antibacterial, antioxidative, and anti-inflammatory properties of TA [123, 124, 129].

5.4.5 Biocompatibility essay

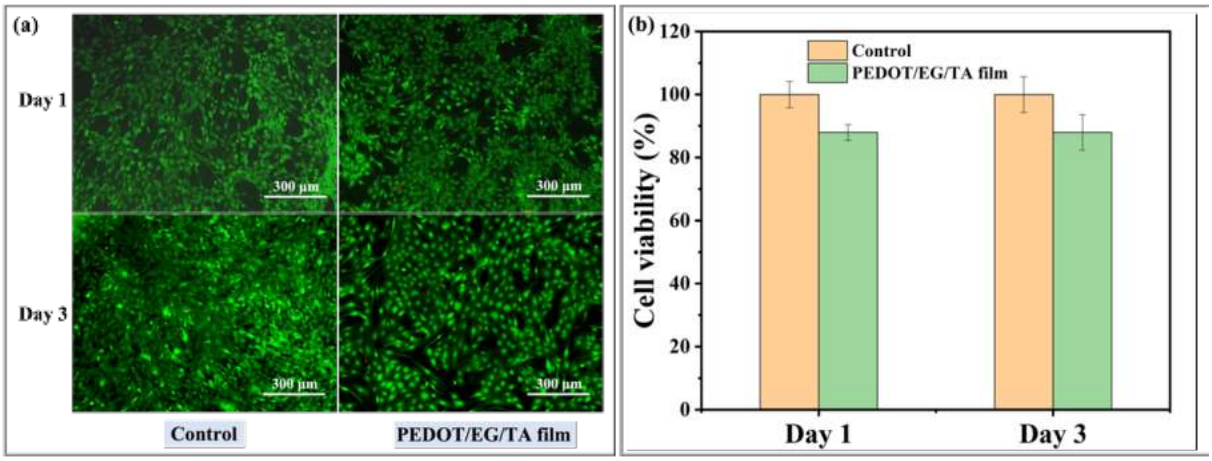

Figure 5.6 (a) Representative images of the live/dead assay of mouse muscle cells (C2C12) cultured on uncoated (positive control) and PEDOT/EG/TA-3 film-coated PS substrates for one and three days. (b) Quantitative analysis of cell viability. As a negative control, cell viability was approximately 0. Error bars represent standard deviation (n = 3).

Finally, we assessed the cytotoxicity of the PEDOT/EG/TA films by culturing C2C12 muscle cells on their surfaces. Figure 5.6a shows the staining results of the cells cultured on PEDOT/EG/TA film-coated and uncoated (positive control) wells with live cells (green) and dead cells (red). As confirmed by the predominance of green coloration (red coloration only visible at high magnification), the cells adhered to and proliferated on the PEDOT/EG/TA film-coated surfaces, with only a slight difference observed between the positive control and PEDOT/EG/TA film samples. Figure 5.6b shows that the relative cell viability, that is, the cell viability compared to the positive control group, on the PEDOT/EG/TA film was 88%, which was higher than the non-cytotoxicity criterion (70% of the control group) according to ISO 10993-5 [133]. In addition, the relative cell viability of the PEDOT/EG/TA film remained stable until day three. These results indicate that the PEDOT/EG/TA film provides a safe environment for cell growth, thereby ensuring its use in biological applications.

5.5 Conclusions and perspectives

In summary, we reported stretchable, soft, adhesive, and self-healing conducting polymer films obtained from an aqueous mixture of PEDOT:PSS/EG/TA. The addition of TA to PEDOT:PSS/EG results in materials with enhanced mechanical properties, high adhesion, and outstanding self-healing behavior. The films exhibited no cytotoxicity and provided a safe environment for cell proliferation. Using PEDOT/EG/TA-3 films, we fabricated epidermal patch electrodes exhibiting low skin-electrode impedance at low frequencies and high-quality ECG and EMG signal recording, similar to commercial Ag/AgCl gel electrodes. Our study provides a facile, straightforward, and effective method for developing stretchable, self-healing, and adhesive conductive materials for soft electronics and bio-applications. We believe that the most important challenges in future soft epidermal electronics are fine-tuning the mechanical properties, conductivity, and adhesion of materials, and the integration of the materials into soft patch electrodes.

Declaration of Competing Interest

The authors declare that they have no competing financial interests or personal relationships that could have influenced the work reported in this study.

5.6 Acknowledgments

The authors are grateful to Eric Quenneville (Biomomentum) for the fruitful discussions. This research was supported by the Natural Science and Engineering Council Canada (NSERC) through Discovery Grants awarded to the FC and DP and by a grant from the Transmedtech Institute (Canada First Research Excellence Fund) awarded to FC and GAL. The equipment and infrastructure used in this study were acquired and maintained by the Canada Foundation for Innovation. XZ is grateful to the China Scholarship Council for a Ph.D. scholarship. PK acknowledges the Pierre Arbour Foundation and NSERC for a Master's scholarship.

CHAPTER 6 ARTICLE 3 : SOFT, CONDUCTIVE AND ANTI-FREEZING CONDUCTING POLYMER ORGANOHYDROGELS

This article has been submitted in the journal "Advanced Sensor Research" on May 2nd, 2023. The supporting information of this article is provided in Appendix C.

Xin Zhou[a], Pierre Kateb[a], Floriane Miquet-Westphal[a], Gregory A. Lodygensky[b], Fabio Cicoira[a*]

[a] Department of Chemical Engineering, Polytechnique Montréal, Montréal, Québec H3C 3A7, Canada

[b] Department of Pediatrics, Sainte-Justine University Hospital Research Center, Montreal, QC, Canada

Corresponding author: Fabio Cicoira

Tel. +1-514-340-4711 x 2580; Fax: +1-514-340-2990

Email address: fabio.cicoira@polymtl.ca

Authors' email address: xin.zhou@polymtl.ca (Xin Zhou), pierre.kateb@polymtl.ca (Pierre Kateb), floriane.miquet-westphal@polymtl.ca (Floriane Miquet-Westphal), ga.lodygensky@umontreal.ca (Gregory A. Lodygensky)

6.1 Abstract:

Soft and conductive materials are highly desirable for wearable electronics. In particular, anti-freezing, long-water retention, and highly conductive gels with Young's modulus matching that of biological tissues show promise in bioelectronics. Herein, we report soft organohydrogels obtained by mixing poly (3,4-ethylenedioxythiophene) doped with polystyrene sulfonate (PEDOT:PSS), ethylene glycol (EG), and tannic acid (TA). The as-prepared PEDOT/EG/TA organohydrogel exhibited a low compressive Young's modulus of ~20 kPa, a conductivity of 15 S/cm, as well as anti-freezing and water retention properties. Epidermal patch electrodes prepared using the PEDOT/EG/TA gel exhibited low skin-electrode impedance at low frequency (1-100 Hz) and high-quality electrocardiography (ECG) and electromyography (EMG) signal recordings. Moreover, the PEDOT/EG/TA gel demonstrated long-term stability with high ECG recording quality after being placed under ambient conditions for seven days.

Keywords: PEDOT:PSS, organohydrogel, anti-freezing, high conductivity, long-water retention

6.2 Introduction

Soft and conductive materials with long-term stability have attracted interests in the field of epidermal bioelectronics due to their conformal contacts with skin and the ability to acquire bio-signals for long-term use. Applications include monitoring of vital signs (e.g., electrocardiography (ECG), electromyography (EMG), and electroencephalography (EEG)), measurement of body temperature and blood pressure and detection of analytes in bodily fluids [2, 4-7, 9]. ECG, EMG, and EEG are typically achieved with metal (ground strap, bar, or cup) or, in most cases, Ag/AgCl gel electrodes [10]. However, rigid metal electrodes are unable to withstand bending or stretching, which can result in skin damage or irritation and lead to high signals noise, whereas Ag/AgCl gel electrodes can lead to skin irritation due to strong adhesion on the skin and are prone to signal degradation in long-term use due to the drying of the gel [4, 10, 12, 18]. Therefore, there is a strong demand for soft conductive electronics that can form conformal interfaces with biological tissues for long-term use without leading to skin damage and irritation.

Various types of conductive soft materials have been used for on-skin electronics, in form of films [18, 36, 68, 69], bio-inspired adhesives [24-26], fabrics [76, 82, 134], and hydrogels [99, 102, 113, 114]. Conductive hydrogels are promising candidates for epidermal electronics because of their conformal contact with the skin, high water content (70-99%, similar to tissues) [13], ease of processing, tunable electrical and mechanical properties, and biocompatibility. Conductive hydrogels may be obtained from pure conductive polymers, e.g., poly (3,4-ethylenedioxythiophene) doped with polystyrene sulfonate (PEDOT:PSS), polypyrrole (PPy), or polyaniline (PANI)), or, in most of cases, by mixing conductive materials (e.g., conducting polymers, nanoparticles, nanowires, nanosheets, carbon nanotubes (CNTs), and graphene) with polymers, such as poly(vinyl alcohol) (PVA), poly(acrylic acid) (PAA), poly(acrylamide) (PAAM), or polyurethane (PU) [62, 135]. A hydrogel prepared by mixing a PEDOT:PSS aqueous suspension with 0.1 M H_2SO_4 exhibited a conductivity of ~9 S/cm after further concentrated sulfuric acid treatment [91]. Our group reported a hydrogel obtained by blending PEDOT:PSS into a PVA/borax system [99], which showed remarkable compliance on skin, outstanding plastic stretchability (10000% strain), self-healing, high adhesion on porcine skin (1.96 N/cm^2), and low compressive Young's modulus (~4 kPa). Electrodes based on this hydrogel have demonstrated high-quality recordings of ECG and EMG signals.

The conductive hydrogels reported so far might not be suitable for long-term use in dry and cold environments due to water evaporation or freezing, which affects both mechanical and electrical properties [110]. Moisturizing and anti-freezing organohydrogels have been developed by incorporating organic anti-freezing agents, such as ethylene glycol (EG) and glycerol into the formulations [106, 109-112]. However, these materials show rather low conductivity owing to the insulating matrix, typically made of PVA [111], PAAM [136], and PAA [112]. PVA/glycerol/polyaniline gels based on the glycerol–water binary mixture [111], exhibited anti-freezing properties and an electrical conductivity of ~0.003 S/cm. A glycerol–water hydrogel with polydopamine (PDA)-decorated CNTs conducting nanofillers and PAAM and PAA as the polymer matrix demonstrated anti-freezing and anti-drying properties, and a conductivity of ~0.08 S/cm [112]. As low conductivity limits applications in digital circuits, bioelectronics, electromagnetic interference shielding (EMI), thermoelectric, and energy storage [110, 137-139], the preparation of highly conductive hydrogels with anti-freezing, long-water retention properties, and Young's modulus matching that of biological tissues is in high demand.

TA, a natural polyphenol, has been widely used to prepare hydrogels from mixtures with PAAM/kaolin [140], silk fibroin [127], PVA/PAAM [141], and CNT/PVA/glycerol [142]. Moreover, TA exhibits biocompatibility and antibacterial, antioxidative, and anti-inflammatory properties [123, 124, 129], which can be exploited for medical applications, such as wound healing and infection treatments.

Herein, we report conductive organohydrogels obtained from aqueous mixtures of PEDOT:PSS, EG, and TA, which showed a low compressive Young's modulus of ~20 kPa, conductivity of 15 S/cm, as well as anti-freezing and water retention properties. Our gels were used to prepare epidermal electrodes for ECG and EMG recordings, which showed similar performance to that of commercial Ag/AgCl gel electrodes, even after storage in ambient air for 1 week. We also demonstrated the use of gel electrodes as human–machine interfaces to control the opening and closing of a robotic hand in real time. The simple fabrication, high conductivity, and mechanical properties make our gels highly promising for applications in bioelectronics electronics.

6.3 Materials and methods

The protocol for human experiments was approved by the ethical committee of Polytechnique Montréal (approval number CER-2021-04-D1). All the measurements (except for Zeta potential) in this study were conducted under ambient condition.

6.3.1 Materials

TA and EG were obtained from Millipore Sigma (St. Louis, Mo, USA). PEDOT:PSS (Clevios™ PH1000, PEDOT:PSS content ~1 wt% according to the supplier) was purchased from Heraeus Precious Metals (Germany). PET sheets (XF-122, with a thickness of 25 μm), used as substrates, were purchased from Polyonics (USA). Scotch® double-sided tapes and Tegaderm™ adhesive tapes were obtained from 3M. Copper tape (88.9 μm, 10 mΩ/in. sq) were supplied by McMaster Carr.

6.3.2 PEDOT/EG/TA organohydrogel preparation

A concentrated PEDOT:PSS suspension was obtained by evaporating approximately 2/3 of the weight of water in a Clevios PH1000 suspension. Specifically, 150 g of Clevios PH1000 were boiled on a hot plate until the weight of the suspension was reduced to ~50 g. To determine the weight percentage of PEDOT:PSS in the concentrated suspension we measured the mass of solid

films obtained by casting 2 g of the concentrated suspension and baking at 140 °C for 6 h. The weight percent of PEDOT:PSS ($W_{\%}$) was determined to be ~3, using the following equation:

$$W_{\%} = \frac{W_R}{W_o} \times 100 \qquad \text{Equation 6.1}$$

Where W_R is the mass of the films after baking, and W_o is the mass of the concentrated suspension.

PEDOT/EG/TA gels were prepared from a mixture of 10 g of concentrated PEDOT:PSS (62.5 wt%), 4 g of EG (25 wt%) , and 2 g of TA (12.5 wt%) (Table 6.1). After mixing the components at 2000 rpm for 10 min in a planetary mixer (ARM-310, Thinky Co.), the mixture was filtered (CHROMSPEC UV Syringe Filters, Nylon, 25 mm diameter, 5.0 μm pore size) and cast into a covered mold or vial. The gels were obtained by heating at 90 °C for 30 min. PEDOT/TA hydrogels (without EG) were obtained from a mixture of 10 g of concentrated PEDOT:PSS (83.3 wt%) and 2 g of TA (16.7 wt%) using the same procedure (Table 6.1).

Table 6.1 Summary of PEDOT/EG/TA gel samples used in this work.

Samples	Concentrated PEDOT:PSS (wt%)	EG (wt%)	TA (wt%)
PEDOT/EG/TA	62.5	25	12.5
PEDOT/TA	83.3	0	16.7

A concentrated PEDOT:PSS suspension was used to facilitate the gelation. Soft gels were obtained after heat treatment at moderate temperature (90 °C) for 30 min (Figure 6.1b). TA led to the gelation of concentrated PEDOT:PSS (Figure SC1, 3 wt% PEDOT/EG/TA and 3 wt% PEDOT/TA), whereas the pristine PEDOT:PSS suspension (PH1000) could not form a gel in the same conditions (Figure SC1).

6.3.3 Preparation of gel electrodes

Gel electrodes were prepared as follows (Figure SC2): a strip of copper tape was placed on a pre-cut PET sheet, and a snap button was attached at one end of the copper tape (Figure SC2a). A double- sided tape with a round hole (8 mm in diameter) at the center was placed on the copper/PET strip (Figure S2Cb). Tegaderm tape (with a central hole 8 mm in diameter, Figure SC2c) was

attached to the other side of the adhesive tape. A gel disc (diameter of 18 mm and thickness of ~1 mm, Figure SC2d) was placed on the center of a Tegaderm tape and connected to the copper tape (Figure SC2e).

6.3.4 Conductivity Measurement

The conductivities of the gel samples (rectangular geometry, ~40 mm × 7 mm × 0.55) were measured using a Biomomentum 4-point probe system (Figure SC3) connected to a source measurement unit (B2902A, Agilent). The voltage versus current with a voltage step of 0.1 V from 0.5 to 1 V were obtained and the conductivity (σ) of the gels was calculated using the Eq. 6.2.

$$\sigma = \frac{L}{R_A * S} \qquad \text{Equation 6.2}$$

Where R_A is the average resistance of the gels and L and S are the length and section of the gels, respectively. Five samples were measured for each gel. The reported conductivity values are the average of the five measured samples and the error corresponds to the standard deviation.

6.3.5 Mechanical characterization

Compressive stress-strain tests were performed using a Mach-1 V500cst MA009 mechanical tester (Biomomentum Inc., Canada). Cylindrical gels with a height of ~5 mm and a diameter of ~12 mm were compressed at a speed of 12 mm/min under a 70 N load cell. Three samples of each type of gel were tested. The reported compressive Young's modulus corresponds to the average of three measured samples, and the error corresponds to the standard deviation.

Rheological measurements were performed using a stress-controlled rheometer (MCR 502 MultiDrive from Anton Paar) and a parallel plate geometry (25 mm diameter). The rheological behavior of the PEDOT/EG/TA mixture and gels was studied at a shear rate of 0.1 - 10 s^{-1} to identify the change in viscosity. The frequency sweep measurements were conducted in the range of 0.1 - 100 rad/s angular frequencies at a constant strain of 0.25 %.

6.3.6 Fourier-transform infrared (FTIR) spectroscopy

Fourier-transform infrared (FT-IR) spectroscopy in absorption mode was performed using a Perkin Elmer Spectrum 65 spectrophotometer, with a scan range spanning from 500 to 4000 cm^{-1}.

FTIR spectroscopy (Figure SC4) was performed to characterize the surface functional groups of the gels. The gels made of TA, EG, and PEDOT:PSS showed the characteristic peaks of the functional groups of these species. The broad peak at 3000-3700 cm^{-1} observed for all samples is attributed to the stretching vibration of the -OH groups. The characteristic peaks at ~1620 cm^{-1} and ~1380 cm^{-1}, corresponding to the C=C and C-C bonds of the thiophene ring [130], and the band at ~1120 cm^{-1}, corresponding to the -SO_3H group of PSS [130], indicate the presence of PEDOT:PSS. The peaks at ~2938 cm^{-1} and ~2875 cm^{-1} correspond to C−H stretching, while those at 1084 cm^{-1} and 882 cm^{-1} correspond to C-O stretching and C-C-O symmetric stretching, respectively [131], confirming the presence of EG. A peak at approximately 1452 cm^{-1} was observed, corresponding to the stretching vibrations of the-C-$C_{aromatic}$ groups in TA [132], indicating the presence of TA.

6.3.7 Zeta potential measurements

Zeta potential was measured using a Zetasizer Nano ZSP instrument (Malvern. Instruments Ltd., Worcestershire, UK). 10 g Clevios PH1000 suspension were diluted for 10 times. 10 g the diluted suspension containing ~0.01 g PEDOT:PSS (corresponding to 1 mg/mL PEDOT:PSS aqueous solution) and 10 g the diluted suspension containing ~0.01 g PEDOT:PSS and ~0.06 g TA powder were used for the tests, and the measurements were performed at 25 °C. The amounts of PEDOT:PSS and TA for the tests were chosen taking into account the zeta potential testing conditions (maximum concentration of the particles is 10 mg/mL) and the actual amounts of PEDOT:PSS and TA used to prepare the gels (Table 6.1).

6.3.8 Water retention measurements

The water retention properties of the PEDOT/EG/TA and PEDOT/TA gels were evaluated by aging them under ambient conditions for seven days. The mass change (η) of the gels over time is determined as follows:

$$\eta = \frac{m}{m_0} \times 100\ \% \qquad \text{Equation 6.3}$$

where m and m_0 are the mass of the gel at a given time and initial mass of the gel, respectively.

6.3.9 Anti-freezing measurements

PEDOT/EG/TA and PEDOT/TA gels were stored at a temperature of -24 ℃ in a freezer for one day. The compressive stress-strain tests of the gels were carried out immediately after taking out

the gels from the freezer, and the time for the whole tests was ~30 s and ~50 s for the frozen PEDOT/TA gels and PEDOT/EG/TA gels, respectively.

6.3.10 Swelling properties

The swelling properties of the PEDOT/EG/TA gels were evaluated by measuring the changes in the height and diameter of the gel cylinder. The volumetric swelling ratio *J(c)* for was calculated using Equation 6.4:

$$J(c) = \frac{V}{V_i} \qquad \text{Equation 6.4}$$

Where V denotes the volume of the gel at a given soaking time and V_i is the volume of the gel after baking for 6 h.

6.3.11 Characterization of epidermal electrodes

Skin-electrode impedance, ECG, and EMG measurements were carried out following our prior research protocols [99]. To record EMG signals, positive (PE) and negative electrodes (NE) were placed on the flexor carpi muscle of the right arm, and a ground electrode (GE) was attached to the elbow. Twelve signal regions and 13 noise regions were selected to calculate the root-mean-square (RMS) signal and RMS noise values, respectively.

For the EMG-controlled robotic hand (Bionic Robot Hand, Robot shop Inc., Canada), the GE, PE, and NE were placed on the right forearm of the volunteer at an equal distance of 5 cm. The signals were collected using a biosensing board (Cyton, OpenBCI, USA) and transmitted to an Arduino UNO controlling the arm. The codes are available upon request to the corresponding authors.

6.4 Results and Discussion

6.4.1 Fabrication and characterization

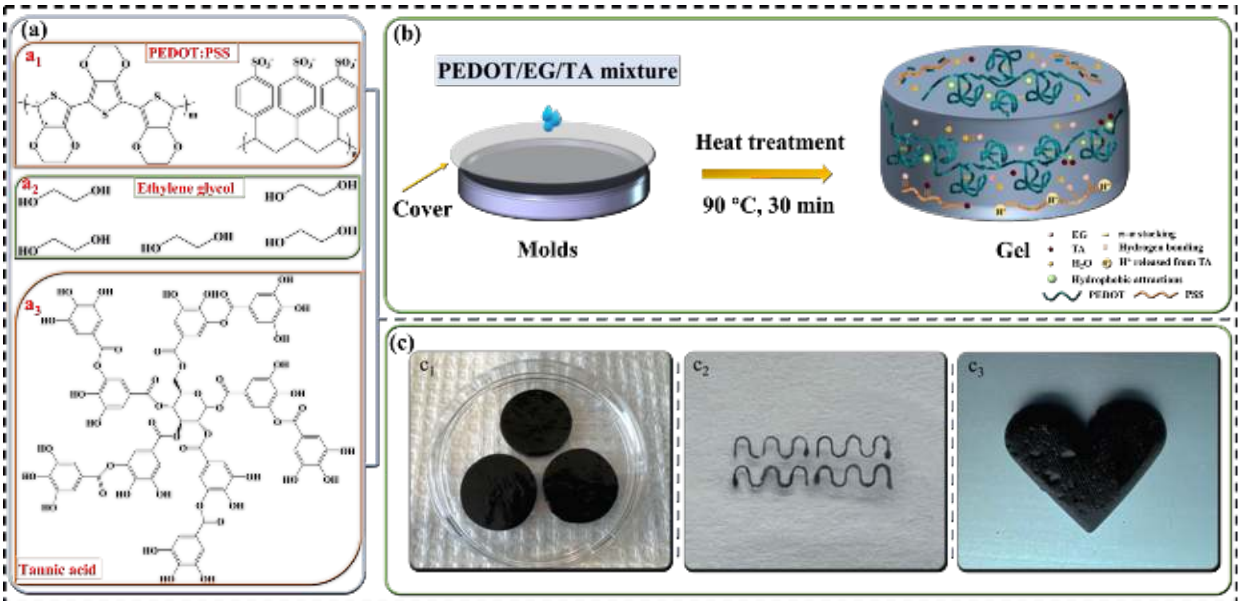

Figure 6.1 (a) Chemical structures of PEDOT:PSS (a_1), EG (a_2), and TA (a_3). (b) Schematic illustration of PEDOT/EG/TA gel preparation and 3D rendering of the gel network including PEDOT crosslink, hydrogen bonding, π–π stacking, and hydrophobic attractions. (c) PEDOT/EG/TA gel modelled into round disk (c_1), printed into curves, nozzle size:0.5 uL (c_2), and injected into a heart shape (c_3).

Soft gels were fabricated from mixtures of PEDOT:PSS, EG, and TA (chemical structures shown in Figure 6.1a). PEDOT:PSS is a conducting polymer widely used in bioelectronics because of its ease of processing from aqueous solutions, mixed electronic and ionic conductivity and biocompatibility [62]. EG, in addition to acting as a conductivity enhancer for PEDOT:PSS [143], is known to be a component of hydrogels with anti-freezing and moisturizing properties [106, 109, 144]. TA is expected to promote gel formation owing to its acidic and polyphenol properties, i.e. the ability to release H^+ in aqueous environment and form hydrogen bonds.

We observed that adding TA to the PEDOT:PSS suspension led to a decrease in the zeta potential from -32 mV to -9 mV (Figure SC5). In agreement with literature reports on PEDOT:PSS gelation induced by H_2SO_4 [91], this result may indicate a partial protonation of the PSS chains, which weakens the electrostatic attraction between PEDOT and PSS, thus exposing PEDOT chains to

each other and promoting their interchain interactions via π–π stacking and hydrophobic attractions, to form a connected 3D gel network.[89, 91] Because these processes are thermally activated, heating at moderate temperatures (for example, 90 °C) could accelerate the gel formation [91]. In addition to crosslinking, other possible interactions are hydrogen bonding between the OH groups of TA and EG and the sulfonate groups of PEDOT:PSS and π–π stacking and hydrophobic attractions between TA and PEDOT (Figure 6.1b).

According to the literature, physically crosslinked hydrogels are characterized by a decreases of viscosity upon increasing shear rate [91]. We therefore performed viscosity measurements to further confirm the presence of a crosslinked network. In agreement with the literature [89, 91], we observed that the viscosity of our gel decreases linearly with the shear rate (Figure SC6a). The storage modulus (G') was approximately 10 times the loss modulus (G") at angular frequencies of 0.1-100 rad s^{-1}, which implies that the elastic response is predominant (Figure SC6b).

It is interesting to note that the mixture of concentrated PEDOT:PSS, EG, and TA, used to prepare the gels, showed shear-thinning behavior (Figure SC7), that is, it became less viscous (i.e., flow more easily) under an applied shear stress. This property makes the mixture modellable, printable, and injectable. For instance, PEDOT/EG/TA gels with arbitrary shapes (e.g., round (Figure 6.1c_1) and ring (Figure SC8a) shapes) could be obtained by casting the PEDOT/EG/TA mixture into a mold. The mixture could also be printed into curves (Figure 6.1c_2) and letters (Figure SC8b) and injected into molds with a heart (Figure 6.1c_3 and Movie SC1) or strip (Figure SC8c) shape.

6.4.2 Mechanical properties

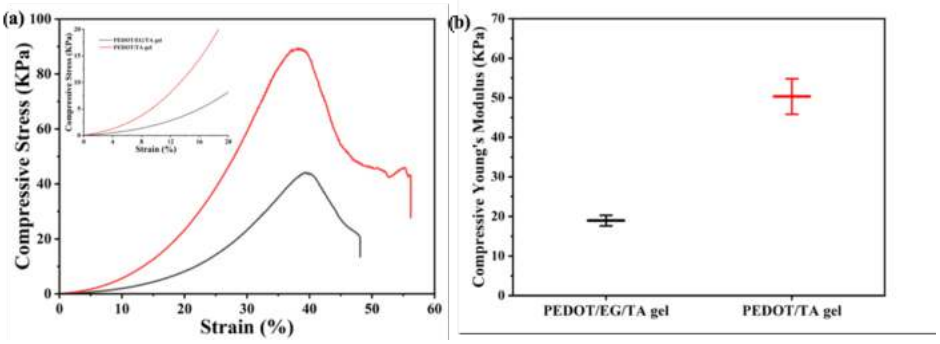

Figure 6.2 Compressive stress-strain and Young's modulus of gels. (a) Compressive stress versus strain (inset shows the magnification of compressive stress versus strain) and (b) average compressive Young's modulus at 10% strain of PEDOT/EG/TA and PEDOT/TA gels. Data for Young's modulus (n = 3) is reported as the mean ± standard deviation.

The compressive stress-strain curve of the gels (Figure 6.2a) shows a linear behaviour at low and moderate strains (Figure 6.2a inset). At higher strains, the relationship becomes nonlinear, likely owing to the deformation of the gel. The stress rapidly decreased at ~40%, likely due to the fracture of the gel. The gels without EG exhibited higher compressive stress. The compressive Young's moduli were extracted from the slope of the stress-strain relationship in the range of 0-10% strain (Figure 6.2b and Table 6.2). The PEDOT/EG/TA gel displayed a lower Young's modulus than PEDOT/TA gels. This clearly indicates that the addition of EG to PEDOT/TA results in softer materials, likely owing to the weakening of the interaction between the PEDOT and PSS chains.

Table 6.2 Compressive Young's moduli and gel conductivities in the 0-10% strain range. Data for the compressive Young's moduli (n = 3) and conductivities (n = 5) are reported as the mean ± standard deviation.

Samples	Young's modulus (kPa)	Conductivity (S/cm)
PEDOT/EG/TA	18.9 ± 1.3	15.2 ± 0.4
PEDOT/TA	50.3 ± 4.5	14.2 ± 1.9

6.4.3 Electrical characterization

Highly conductive hydrogels are important for a variety of application, such as the recording of human-machine interface, EMI, thermoelectric, and energy storage electrodes [110, 137-139]. The PEDOT/EG/TA gels achieved a conductivity of ~15 S/cm, which is higher than that of our PEDOT:PSS/PVA hydrogels (~5.0 x 10^{-5} S/cm)[99] and other PEDOT:PSS based hydrogels, such as concentrated H_2SO_4 treated PEDOT:PSS hydrogels (~9 S/cm) [91], PPy−PEDOT:PSS hybrid hydrogels (~8 S/cm) [92], and 4-dodecylbenzenesulfonic acid (DBSA) induced PEDOT:PSS hydrogel (~0.1 S/cm) [89].

6.4.4 Water retention and anti-freezing properties

Water retention ability is an important factor that affects the mechanical and electrical properties of gels. In the absence of EG, the gels showed fast shrinkage and deformation even after one day

(Figure 6.3a and SC9), whereas those containing EG maintained their shape even after seven days (Figure 6.3a and b). Mass change versus time plots (Figure 6.3c) showed that both gels experienced a substantial weight loss after one day, likely due to the evaporation of free water from the surface and the bulk. After this loss, their weight remained relatively stable, with PEDOT/TA gels experiencing an overall higher loss. The effect of EG on water retention is due to the formation of hydrogen bonds between water and EG, which help stabilize the gel network and prevent water evaporation.

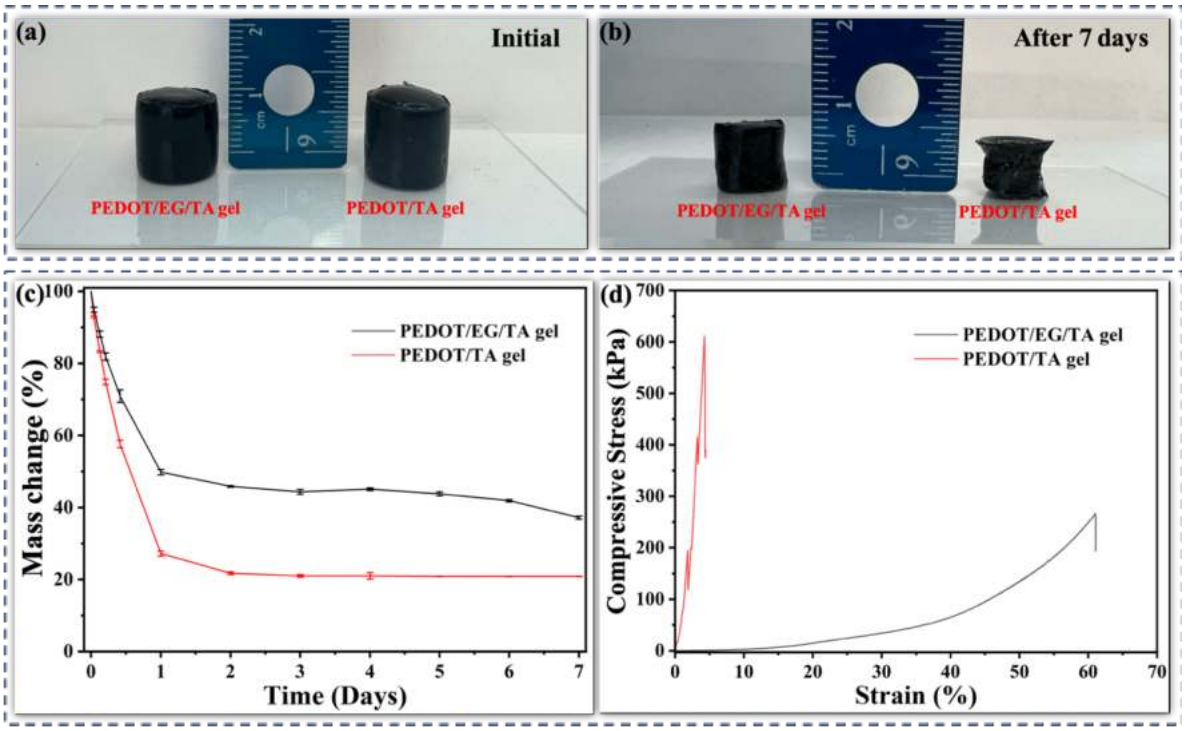

Figure 6.3 (a) Digital images of the fresh PEDOT/EG/TA and PEDOT/TA gels. (b) Digital images of PEDOT/EG/TA and PEDOT/TA gels stored at ambient temperature for seven days. (c) Mass change of PEDOT/EG/TA and PEDOT/TA gels over seven days. (d) Compressive stress versus strain of PEDOT/EG/TA and PEDOT/TA gels stored at ambient temperature for seven days. Data for mass change (n = 3) are reported as mean ± standard deviation.

The EG-containing gels also exhibited stable mechanical and electrical properties over time, which are important for their long-term use. Compressive strain measurements (Figure 6.3d and Figure SC10) indicate that the dehydrated PEDOT/EG/TA gel (with EG) exhibited a slow increase of

compressive stress with strain increasing and could withstand high strain (60%) without fracture, whereas the dehydrated PEDOT/TA gel (without EG) showed low compression resistance (~4% strain). A video taken to visualize the compressive mechanical properties (Movie SC2) shows that the dehydrated PEDOT/EG/TA gel remained soft and could be manually compressed without fracture. In contrast, the dehydrated PEDOT/TA gel became harder owing to water loss and resisted the compression without deformation. It is interesting to note that the pristine and dehydrated PEDOT/EG/TA gels showed different compressive behavior (Figure 6.2a and Figure 6.3d). The dehydrated PEDOT/EG/TA gels could withstand higher compressive strain (> 60% strain), which may be due to the strong interactions between EG, PEDOT:PSS, and TA.

The electrical conductivity of the PEDOT/EG/TA gels increased from ~15 S/cm on the first day to ~33 S/cm after seven days, likely due to the increased PEDOT:PSS concentration after the loss of water. It was not possible to measure the conductivity of the dehydrated PEDOT/TA gel using 4-point probe system, owing to its irregular shape resulting from water loss. However, using a digital multimeter, we determined that after 7 days the resistance of the PEDOT/TA gels increased by about 3 orders of magnitude, while that of PEDOT/EG/TA gels remained relatively stable.

Table 6.3 Comparison of the conductivities of PEDOT/EG/TA and PEDOT/TA gels before and after seven days. Data for the conductivities of the PEDOT/EG/TA gel (n = 5) and PEDOT/TA gel (n = 3) are reported as mean ± standard deviation.

Samples	Conductivity (S/cm)	
	initial day	after 7 days
PEDOT/EG/TA gel	15.2 ± 0.4	33.0 ± 2.3
PEDOT/TA gel	14.2 ± 1.9	Not measurable

Conductive gels with stable electrical and mechanical properties at low temperatures are desirable for applications in cold environments for biomedical and automotive industry to create a protective layer around the material and prevent ice formation and damage from freezing. Measurements of the gel resistance before and after freezing them at -24 °C for one day showed a change from 0.2 Ω to ~15 Ω for the PEDOT/EG/TA gel, and from 0.3 Ω to ~149 Ω (~500 times than its initial value)

for the PEDOT/TA gel (Figure SC11). This shows that the PEDOT/EG/TA gel maintained good electrical conductivity at low temperatures (< -20 °C). The change in resistance of PEDOT/TA hydrogels is due to the formation of ice crystals, which can cause the hydrogel to become more porous and less homogeneous. Ice crystals can create voids or gaps within the gel structure, which can cause the gel to have regions of higher or lower electrical conductivity. The incorporation of EG into PEDOT/TA hydrogels can help minimize the formation of ice crystals and preserve the connectivity between the conductive components of the gel, leading to less change in its electrical conductivity after freezing.

To better understand the effect of EG on the mechanical properties the gels at low temperature, we performed compressive measurements immediately after removing them from the freezer. The compressive strength-strain curves (Figure SC12) showed that the PEDOT/TA gel became hard because of the frozen water, resulting in increased compressive stress, whereas the PEDOT/EG/TA gel preserved its softness with low compressive stress and could be compressed by hand (Movie SC3). The formation of ice crystals can cause the hydrogel to become more brittle, leading to a decrease in its deformation resistance. This is because ice crystals can create voids or gaps within the gel structure, which weakens the overall mechanical strength of the gel. The anti-freezing properties of PEDOT/EG/TA gels can be attributed to EG, which can form a variety of molecular clusters with H_2O molecules, leading to a decrease in water vapor pressure. As a result, the gel does not readily crystallize and the freezing point is decreased [106].

6.4.5 Swelling ability of PEDOT/EG/TA gels

The swelling properties of the gels were investigated, as they significantly affect mechanical properties [145], nutrient transport, and drug delivery throughout the hydrogels [146]. Digital images show that the cylindrical gel shrunk and deformed after baking for 2 h, and then remained relatively stable (Figure 6.4a_{1-4}). Volumetric shrinkage ratio versus baking time plots (Figure 6.4b) reveal a large shrinkage after a baking for 2h, followed by a stability region. The shrinkage is of ~75 % after baking for 6 h. In contrast, the dehydrated gel retained its shape even after rehydration for 24 h (Figure 6.4c_{1-4}). Volumetric swelling ratio versus soaking time plots showed that the gel presented the largest volumetric swelling ratio after a rehydration for 8 h and then the change remained stable with a volumetric swelling ratio of ~135 % (with respect to the volume of the

dehydrated sample) after two days (Figure 6.4d); thus, it showed slow swelling ability and only partially recovered its volume.

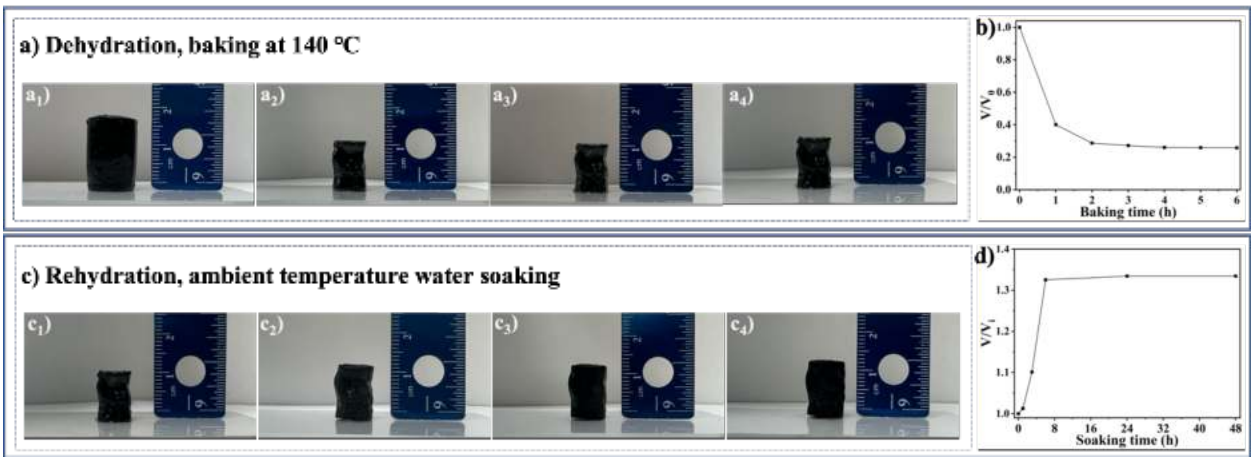

Figure 6.4 Swelling properties of PEDOT/EG/TA gels. (a) Digital images showing the volumetric shrinkage of the gel (cylindrical geometry) dehydrated at 140 °C for a_1) 0, a_2) 2, a_3) 4, and a_4) 6 h. (b) Volumetric shrinkage ratio versus time plots of PEDOT/EG/TA gel dehydrated at 140 °C for 6 h. (c) Digital images showing the volumetric swelling of the dried gel rehydrated at ambient temperature for c_1) 0, c_2) 3, c_3) 6, and c_4) 24 h. (d) Volumetric swelling ratio versus time plots of the dried gel rehydrated at ambient temperature for 48 h. V denotes the volume of the gel at a given baking or soaking time. V_0 is the initial volume of the gel before baking and V_i represents the volume of the gel after baking for 6 h (shown in Figure a_4).

6.4.6 Skin-electrode impedance, ECG & EMG measurements

The skin-electrode impedance was studied to assess the PEDOT/EG/TA gel electrodes in a three-electrode configuration (Figure SC13a). The impedance versus frequency plots (Figure SC13b) show that the PEDOT/EG/TA gel electrodes performed better than the commercial Ag/AgCl gel electrodes in the relevant frequency range up to 100 Hz (e.g., ~130 kΩ versus ~220 kΩ for the Ag/AgCl gel electrodes at 10 Hz, Table SC1), whereas both electrodes performed similarly overall at higher frequencies. The lower impedance at low frequencies might be due to the high conductivity and softness of the PEDOT/EG/TA gels.

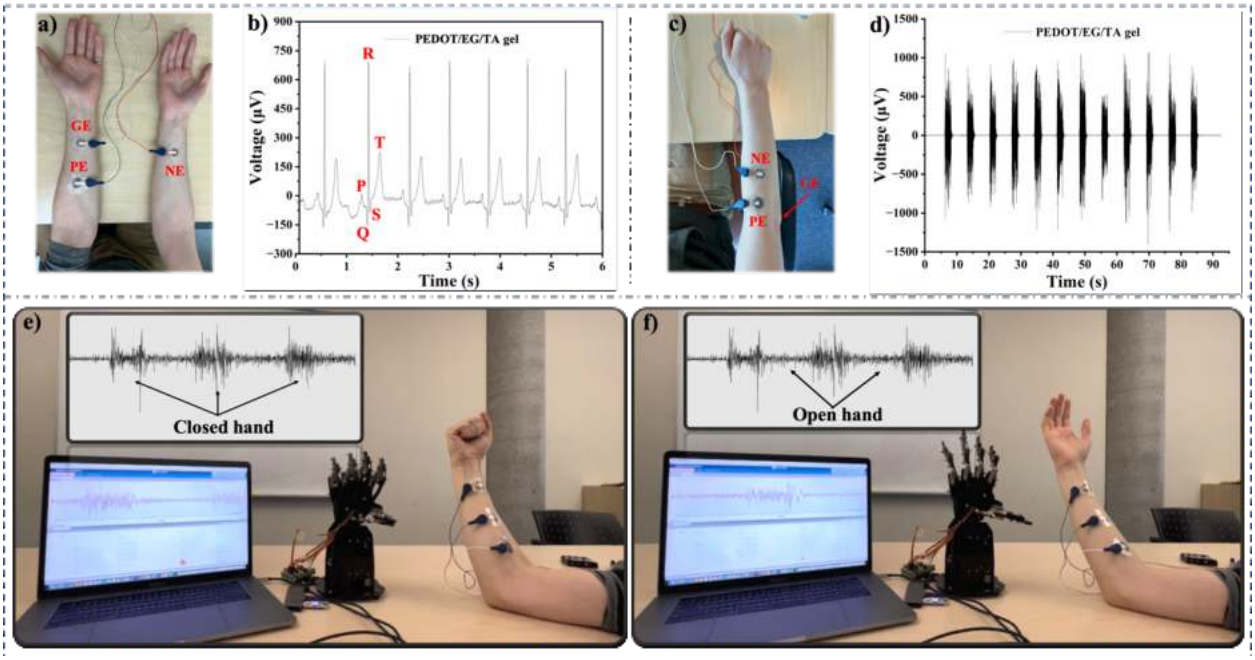

Figure 6.5 ECG and EMG signal recordings of PEDOT/EG/TA gel electrodes. (a) Configuration of ECG measurement in a volunteer. Positive (PE) and ground (GE) electrodes were attached to the left forearm, and a negative electrode (NE) was placed on the right forearm. ECG biopotentials (voltage versus time) were recorded using the PEDOT/EG/TA gel electrodes. (c) Configuration of EMG measurements on a volunteer. The EMG biopotentials between the electrodes were recorded using PE and NE on the right forearm and GE on the elbow. (d) EMG monitoring using PEDOT/EG/TA gel electrodes: EMG signals (PEDOT/EG/TA gel electrodes) were used to control the motion of the robotic hand, that is, closed (e) and open (f) hand.

ECG and EMG are diagnostic tools commonly used in human healthcare, and the quality of their recording is essential for accurate clinical diagnosis. To record ECG biopotentials, we attached ground (GE) and positive (PE) electrodes to the left forearm and negative electrode (NE) to the right forearm (Figure 6.5a). The voltage vs. time plots (Figure 6.5b) show that the PEDOT/EG/TA gel electrodes present well-defined ECG characteristic peaks, such as the P wave, QRS complex, and T wave, indicating the suitability of these electrodes for monitoring biosignals. We compared the ECG signals recorded using PEDOT/EG/TA electrodes with those recorded using three different types of commercial Ag/AgCl gel electrodes (Figure SC14a-c). The results indicate that the ECG recording quality of the PEDOT/EG/TA electrodes was comparable to that of commercial Ag/AgCl gel electrodes.

Similarly, to evaluate the EMG recording ability of the PEDOT/EG/TA gel electrodes, we performed EMG tests by placing PE and NE on the right forearm and GE on the elbow of a volunteer (Figure 6.5c), and recorded voltage changes produced by switching between relaxed and tense states of the flexor carpi muscle for over 90 s. The voltage vs. time plots (Figure 6.5d) indicate that the PEDOT/EG/TA gel electrodes and three different types of Ag/AgCl gel electrodes show similar potential changes when switching the state of the muscle (Figure SC14d-f). Notably, the PEDOT/EG/TA gel electrodes show a higher SNR of EMG signals (40.0 ± 2.2 dB) compared to those commercial Natus® (34.1 ± 0.9 dB), 3M® (38.7 ± 0.8 dB), and Ambu® (36.2 ± 0.3 dB) Ag/AgCl gel electrodes (Figure SC14g).

The detection of EMG signals for muscle motion can have essential applications in human–machine interfaces. For example, the PEDOT/EG/TA gel electrodes can capture EMG signals generated by opening and closing a hand, and transmit them to control an anthropomorphic robotic hand in real-time (Figure 6.5e and f and Movie SC4). Therefore, the gel electrodes can serve as a user interface, which may be due to the softness and high conductivity of the PEDOT/EG/TA gels electrodes. The EMG signal could also be used in combination with an EMG-controlled prosthetic device to enhance the strength of movements such as walking or lifting objects, or replace missing limbs, and therefore improve quality of life for patients with musculoskeletal impairments [147].

The long-term utilization of gels is important for continuous monitoring of vital signs, such as in the intensive care units and sleeping monitoring. Here, we evaluated the long-term stability of PEDOT/EG/TA gels by skin-electrode impedance measurement and ECG recording after aging the gels (without encapsulation) at ambient temperature for seven days. The impedance vs. frequency plots (Figure SC15a) indicate that the aged PEDOT/EG/TA gels and commercial Ag/AgCl electrodes performed similarly (values listed in Table SC2). The aged gel electrodes (Figure SC15b) show well-defined ECG characteristic peaks, indicating the suitability of the PEDOT/EG/TA gel electrodes for the long-term monitoring.

6.5 Conclusions and perspectives

In summary, we demonstrated a soft, conductive and anti-freezing conductive polymer organohydrogel obtained from PEDOT:PSS, EG, and TA. Physical crosslinking between the PEDOT polymer chains endowed the PEDOT/EG/TA gel with an electrical conductivity of 15 S/cm and a low compressive Young's modulus of ~20 kPa. The resulting PEDOT/EG/TA gel

exhibited anti-freezing properties as low as -20°C and long-water retention properties. Using the PEDOT/EG/TA gel, we demonstrated epidermal patch electrodes that show low skin-electrode impedance at low frequency (1-100 Hz) compared to commercial Ag/AgCl gel electrodes and high quality for ECG and EMG signal recording. The PEDOT/EG/TA gel electrodes show high potential for applications in human–machine interfaces. In addition, the PEDOT/EG/TA gels showed outstanding long-term usability for ECG recording after being placed under ambient conditions for seven days. Moreover, the PEDOT/EG/TA mixture exhibited good processability and could be printed or injected to prepare gels with the desired sizes and shapes for practical applications. This study provides an effective fabrication method for soft epidermal electronics. We believe that the challenges in gel-based soft electronics for long-term use include fine tuning of mechanical, conductivity, and water-retention ability and the integration of the gel into adhesive patch electrodes.

Declaration of Competing Interest

The authors have no conflicts of interest to declare.

6.6 Acknowledgments

This research was supported by the Natural Science and Engineering Council Canada (NSERC) through Discovery Grants awarded to the FC and by a grant from the Transmedtech Institute (Canada First Research Excellence Fund) awarded to FC and GAL. The equipment and infrastructure used in this study were acquired and maintained by the Canada Foundation for Innovation. XZ is grateful to the China Scholarship Council for a Ph.D. scholarship. PK acknowledges the Pierre Arbour Foundation and NSERC for a Master's scholarship.

CHAPTER 7 GENERAL DISSCUSSION

Soft, adhesive, and self-healable materials are promising candidates for epidermal electronics due to their improved contact to skin. To overcome the limitations of conventional epidermal patch electrodes, various soft materials (e. g., in the form of conductive gels, films, and fabrics) have been widely studied, however, the development and preparation of soft materials with suitable mechanical and adhesion properties, self-healing ability, and Young's modulus matching human skin still remains a challenge.

In Chapter 4, we prepared soft, stretchable, highly adhesive, and self-healable SV3/PVA hydrogels. We evaluated the effect of PEDOT:PSS screen-printing paste (rich in PG and DEG) on a PVA-borax hydrogel system. We found that incorporating the PEDOT:PSS paste into the hydrogel system can yield materials with enhanced plastic stretchability, softness, adhesion, and self-healing ability. These characteristics make them ideal for the fabrication of soft epidermal electrodes. We discovered that the SV3/PVA hydrogels exhibited different behaviors upon increasing the weight ratio of PEDOT:PSS paste to PVA solution to 2:1. For instance, the SV3/PVA-2-1 (PEDOT:PSS/PVA ratio = 2:1) samples presented a liquid-like behavior due to the weak dynamic borate ester bonds and they cannot be molded into arbitrary shapes. The SV3/PVA hydrogels demonstrated fast mechanical and electrical self-healing properties, which was confirmed by strain sweep and cut-stick measurements. At last, we fabricated the hydrogel based epidermal electrodes and assessed their ability for bio-signal recording. These electrodes showed low skin-electrode impedance, outstanding compliance to skin, as well as superior ECG and EMG recording capabilities, comparable to commercial Ag/AgCl gel electrodes.

In Chapter 5, we fabricated stretchable, adhesive, and self-healable films with Young's moduli like our skin. We investigated the stretchability, conductivity, and adhesion of the films with different amount of TA. There were several challenges regarding to the preparation of the adhesive films. Firstly, we found that the heating time and the concentration of TA has a huge influence on the adhesive film properties. For example, the adhesive films could not be peeled off from glass or Teflon substrates without damage if the heating time is longer than 100 min and the amount of TA is higher than 10 wt%. Thus, we set the heating time to 90 min, the temperature to 60 °C and the maximum amount of TA to ~10 wt%. Secondly, we found EG is a key component to prepare the adhesive films. EG is known to result in PEDOT:PSS composite with long-water retention

properties. We checked that the prepared adhesive films contains EG via FT-IR. Without added EG, the films become hard and brittle. In addition, the films also become hard and brittle after being stored in ambient environment for a few days (typically 3 days) or drying at high temperature (e. g. 120 °C for 3h). This hardening effect can be due to precipitation of TA upon loss of water and EG. In addition, films containing EG showed outstanding electrical stability during stretching. The resistance changed by 2% when being stretched to 30% strain, which is significantly lower than other PEDOT:PSS based adhesive films. In terms of self-healing, the films exhibited two different types of healing behavior: autonomous healing and cut-stick healing properties. This is a very important discovery for adhesive PEDOT:PSS based films.

Finally, in Chapter 6, we prepared soft and highly conductive organohydrogels with anti-freezing and long-water retention properties, which overcomes the existing limitations of conventional hydrogels functioning in a dry and cold environment for long-term use. The key parameters of gel synthesis are PEDOT:PSS concentration and heat temperature. We found that TA results in the gelation of concentrated PEDOT:PSS (3 wt% PEDOT/EG/TA or 3 wt% PEDOT/TA), while the non-concentrated PEDOT:PSS suspension (PH1000) cannot form a gel under the same conditions. In addition, heating at a moderate temperature (e.g. 90 °C) could accelerate the formation of gels. The gel formation can be due to the physical crosslinking between PEDOT polymer chains, which is confirmed by zeta potential and viscosity measurements. EG, besides acting as a softness enhancer, is known to yield hydrogels with anti-freezing and long-water retention properties. Compared to PEDOT/TA gels, the PEDOT/EG/TA gels exhibited a lower compressive Young's modulus and anti-freezing and long-water retention properties. Moreover, it is worth noting that our PEDOT/EG/TA gels showed high conductivity compared to other anti-freezing gels. The highly conductive gels could be used for a wide range of applications such as digital circuits, electromagnetic interference shielding, thermoelectrics, and energy storage. Furthermore, our gels showed insignificant volume swelling. At last, we designed epidermal electrodes with an off-set structure which is convenient for bio-signal recording.

This thesis contributes to scientific knowledge and wearable electronics and bioelectronics by:

1. Providing guidelines to prepare soft materials and epidermal patch electrodes.

The preparation of conductive, stretchable, self-healable, adhesive, soft, biocompatible materials for epidermal patch electrodes remain a challenge from a processing point of view and represents

an interesting opportunity for both fundamental and applied research fields. Our methods are effective for the preparation of conductive polymer based soft materials (in form of hydrogels, films, and organohydrogels) with Young's modulus matching biological tissues and the fabrication of soft epidermal patch electrodes that can achieve conformal contacts to skin and acquire high quality of ECG and EMG recording. These soft electrodes address the limitations of conventional epidermal electrodes, such as skin irritation and long-term use. We believe that our designs and methods will pave the way for the development of wearable electronics and epidermal bioelectronics. Although some limitations with the materials and the electrodes exist, as discussed in chapter 8, we believe that with further improvements, the requirements towards commercial applications can be met soon.

2. Providing insights and a deeper understanding of the self-healing behavior of PEDOT:PSS based adhesive films.

Despite many PEDOT:PSS based adhesive films being developed, there are no reports on the self-healing properties of these films. In this thesis, we prepared adhesive PEDOT/EG/TA films and they exhibited two types of self-healing behavior: autonomous healing, due to their mechanical softness enabled by the presence of TA, and cut-stick healing, due to the large number of OH groups of the catechol and pyrogallol aromatic rings present in TA. This discovery can facilitate the research in the field of self-healing adhesive films.

CHAPTER 8 CONCLUSION AND RECOMMANDATIONS

8.1 Conclusion

This thesis (Chapter 4 - 6) explored methods to prepare conductive soft materials, in the form of hydrogels, adhesive films, and organohydrogels, based on PEDOT:PSS, and to fabricate epidermal patch electrodes that can achieve conformal contact to skin. The performance of these electrodes was assessed by the skin-electrode impedance measurements and ECG and EMG recordings. These patch electrodes exhibited low skin-electrode impedance and high ECG and EMG recording quality, which is comparable to commercial Ag/AgCl gel electrodes. Many insights have been acquired regarding the adhesion, mechanical properties, and self-healing behavior. For instance, the addition of PEDOT:PSS ink into PVA-borax system resulted in SV3/PVA hydrogels with high adhesion and enhanced self-healing ability, which can be attributed to the large amount of hydrogen bonds resulted from PEDOT:PSS, PG, DEG, and PVA.

Soft materials are promising candidates for epidermal electronics due to their improved contact to skin. Our first goal is to design and prepare soft PEDOT:PSS-based materials with Young's modulus matching human tissues. Thus, we prepared SV3/PVA hydrogels with high stretchability, high adhesion, outstanding self-healing, and a low compressive Young's modulus (~ 4 kPa), which enables the materials to achieve conformal contact to skin. Secondly, we fabricated soft PEDOT/EG/TA films with a Young's modulus of 450 kPa, high stretchability, high interfacial adhesion, and excellent self-healing ability. The soft films could tightly adhere to skin. Lastly, to address the limitations of conventional hydrogels, we designed and prepared soft PEDOT/EG/TA organohydrogels with a low compressive Young's modulus (~19 kPa), anti-freezing, and long-water retention properties. Although the gels showed no adhesion, it can be attached to skin by a commercial tape and could be used for long-term.

Our second goal was to fabricate soft epidermal patch electrodes based on the soft PEDOT:PSS-based materials. To facilitate the connection between the electrodes and wires, we used snap buttons to make the electrodes. For the adhesive SV3/PVA hydrogel electrodes, we used Parafilm as support and copper tape to connect the hydrogels and the modified Ambu® electrodes. To electrically connect the PEDOT/EG/TA film electrodes, we employed a thin PET sheet with a silver ink deposited layer. Regarding PEDOT/EG/TA gel electrodes, we used Tegaderm tapes (a commercial painless tape) to attach the electrodes on the skin as the fresh PEDOT/EG/TA gels are

not adhesive. These three types of electrodes are soft and flexible and can form conformal contacts to skin.

Our third goal is to gain deeper knowledge about the self-healing behavior of these materials. For instance, we investigated mechanical self-healing behavior and electrical healing of SV3/PVA hydrogels by rheological measurements and cut-stick experiments, respectively. We explained the mechanism of self-healing of SV3/PVA hydrogels (due to the reversible boron ester bonds). For PEDOT/EG/TA films, we assessed and explained their autonomous and cut-stick healing. We used an optical microscope to observe the self-healing process of SV3-PVA hydrogels and PEDOT/EG/TA films.

8.2 Recommandations

In terms of soft and self-healable materials and epidermal patch electrode preparation, the following aspects are recommended for more exploration in future's work:

1) SV3/PVA hydrogels contain high water content, which may show poor stability with time because of water loss. In future, the hydrogel based epidermal electrodes need to be encapsulated for long-term usage.

2) PEDOT/EG/TA films will become hard and brittle after the loss of water and EG (normally 3 days in ambient environment). Therefore, a future prospect is to encapsulate the films and make epidermal electrodes for long-term use (> one week).

3) PEDOT/EG/TA gels showed moderate mechanical performance due to the physical crosslinked network between PEDOT chains. For instance, the gels are easily broken when stretched and they can only withstand ~ 40% compressive strain. Therefore, a future work is to improve their mechanical properties by introducing chemical or dynamic covalent bonds into the physical network.

4) PEDOT/EG/TA paste exhibited injectable and printable ability. Therefore, a future prospect is to design printable epidermal electronics (e. g., EEG electrode arrays and circuits).

5) For the fabrication of epidermal electrodes, the connection between soft materials and wires is important because the connection is expected to withstand increases in strain caused by movement while retaining stable electrical properties. The copper tape we used to prepare PEDOT/EG/TA organohydrogel patch electrodes is relatively hard and not suitable for long-term use as it can lead

to the deformation of the gel due to their mechanical mismatch. Therefore, a future improvement is needed by using soft metal films (e. g., Thin Ag films).

6) The geometry of epidermal electrodes can affect their mechanical properties and bio-signals recording quality. Therefore, a future prospect is to design new patterns for epidermal electrodes, such as filamentary serpentine meshes and concentric ring patterns, to improve their mechanical ability and bio-potential recording quality.

7) The PEDOT:PSS based epidermal electrodes we prepared are black, which might not be suitable for practical application in hospitals, especially for kids. Therefore, a future prospect is to design and prepare transparent electrodes. (e. g., thin PEDOT:PSS films can be transparent).

8) A 3-electrode system was applied to record ECG signals in this thesis. However, a 12-Lead ECG is a standard diagnostic tool in clinic scenarios by recording heart activities via 12 different perspectives. Therefore, a future prospect is to use a 12-Lead ECG system (10 electrodes) to evaluate the performance of the epidermal patch electrodes.

9) Self-healing materials show great potential in real applications. For example, self-healable display screen can resist the formation of scratches. Therefore, a future prospect is to use the gel and film as coating materials that can withstand more stress.

REFERENCES

[1] W. H. Organization. [Online]. Available: https://www.who.int/en/news-room/fact-sheets/detail/cardiovascular-diseases-(cvds).

[2] T. R. Ray *et al.*, "Bio-Integrated Wearable Systems: A Comprehensive Review," *Chem. Rev.,* vol. 119, no. 8, pp. 5461-5533, Apr 24, 2019, doi: 10.1021/acs.chemrev.8b00573.

[3] N. Lu, S. K. Ameri, T. Ha, L. Nicolini, A. Stier, and P. Wang, "Epidermal electronic systems for sensing and therapy," *Nanosensors, Biosensors, Info-Tech Sensors and 3D Systems 2017*, 2017, vol. 10167: International Society for Optics and Photonics, p. 101670J.

[4] I. Hwang *et al.*, "Multifunctional Smart Skin Adhesive Patches for Advanced Health Care," *Adv. Healthc. Mater.,* vol. 7, no. 15, p. e1800275, Aug 2018, doi: 10.1002/adhm.201800275.

[5] Y. Yamamoto *et al.*, "Efficient Skin Temperature Sensor and Stable Gel-Less Sticky ECG Sensor for a Wearable Flexible Healthcare Patch," *Adv. Healthc. Mater.,* vol. 6, no. 17, Sep 2017, doi: 10.1002/adhm.201700495.

[6] W. Gao *et al.*, "Fully integrated wearable sensor arrays for multiplexed in situ perspiration analysis," *Nature,* vol. 529, no. 7587, pp. 509-514, Jan 28 2016, doi: 10.1038/nature16521.

[7] J. W. Jeong *et al.*, "Materials and optimized designs for human-machine interfaces via epidermal electronics," *Adv. Mater.,* vol. 25, no. 47, pp. 6839-46, Dec 17 2013, doi: 10.1002/adma.201301921.

[8] H. U. Chung *et al.*, "Binodal, wireless epidermal electronic systems with in-sensor analytics for neonatal intensive care," *Science,* vol. 363, no. 6430, Mar 1 2019, doi: 10.1126/science.aau0780.

[9] H. U. Chung *et al.*, "Skin-interfaced biosensors for advanced wireless physiological monitoring in neonatal and pediatric intensive-care units," *Nat. Med.,* vol. 26, no. 3, pp. 418-429, Mar 2020, doi: 10.1038/s41591-020-0792-9.

[10] N. Meziane, J. G. Webster, M. Attari, and A. J. Nimunkar, "Dry electrodes for electrocardiography," *Physiol. Meas.,* vol. 34, no. 9, pp. R47-69, Sep 2013, doi: 10.1088/0967-3334/34/9/r47.

[11] J. X. J. Zhang and K. Hoshino, "Implantable and wearable sensors," in *Molecular Sensors and Nanodevices*, 2019, pp. 489-545.

[12] X. Xiao, G. Wu, H. Zhou, K. Qian, and J. Hu, "Preparation and Property Evaluation of Conductive Hydrogel Using Poly (Vinyl Alcohol)/Polyethylene Glycol/Graphene Oxide for Human Electrocardiogram Acquisition," *Polymers,* vol. 9, no. 7, Jun 30 2017, doi: 10.3390/polym9070259.

[13] V. R. Feig, H. Tran, M. Lee, and Z. Bao, "Mechanically tunable conductive interpenetrating network hydrogels that mimic the elastic moduli of biological tissue," *Nat. Commun.,* vol. 9, no. 1, p. 2740, Jul 16 2018, doi: 10.1038/s41467-018-05222-4.

[14] Y. Liu, M. Pharr, and G. A. Salvatore, "Lab-on-Skin: A Review of Flexible and Stretchable Electronics for Wearable Health Monitoring," *ACS Nano,* vol. 11, no. 10, pp. 9614-9635, Oct 24 2017, doi: 10.1021/acsnano.7b04898.

[15] Y. Tetsu *et al.*, "Ultrathin epidermal strain sensor based on an elastomer nanosheet with an inkjet-printed conductive polymer," *Appl. Phys. Express,* vol. 10, no. 8, 2017, doi: 10.7567/apex.10.087201.

[16] H. R. Lim, H. S. Kim, R. Qazi, Y. T. Kwon, J. W. Jeong, and W. H. Yeo, "Advanced Soft Materials, Sensor Integrations, and Applications of Wearable Flexible Hybrid Electronics in Healthcare, Energy, and Environment," *Adv. Mater.,* p. e1901924, Jul 8 2019, doi: 10.1002/adma.201901924.

[17] C. Dagdeviren *et al.*, "Conformal piezoelectric systems for clinical and experimental characterization of soft tissue biomechanics," *Nat. Mater.,* vol. 14, no. 7, pp. 728-36, Jul 2015, doi: 10.1038/nmat4289.

[18] L. Zhang *et al.*, "Fully organic compliant dry electrodes self-adhesive to skin for long-term motion-robust epidermal biopotential monitoring," *Nat. Commun.,* vol. 11, no. 1, p. 4683, Sep 17 2020, doi: 10.1038/s41467-020-18503-8.

[19] J. M. Karp and R. Langer, "Dry solution to a sticky problem," *Nature,* vol. 477, no. 7362, pp. 42-43, 2011.

[20] M. A. Smith, N. M. M. Jones, S. L. Page, and M. P. Dirda, "Pressure-Sensitive Tape and Techniques for its Removal from Paper," *J. Am. Inst. Conserv.,* vol. 23, no. 2, pp. 101-113, 2013, doi: 10.1179/019713684806028241.

[21] Z. Czech, K. Wilpiszewska, B. Tyliszczak, X. Jiang, Y. Bai, and L. Shao, "Biodegradable self-adhesive tapes with starch carrier," *Int. J. Adhes. Adhes.,* vol. 44, pp. 195-199, 2013, doi: 10.1016/j.ijadhadh.2013.03.002.

[22] Y. Shi, Y. Li, J. Wu, W. Wang, A. Dong, and J. Zhang, "A novel transdermal drug delivery system based on self-adhesive Janus nanofibrous film with high breathability and monodirectional water-penetration," *J. Biomater. Sci. Polym. Ed.,* vol. 25, no. 7, pp. 713-28, 2014, doi: 10.1080/09205063.2014.897596.

[23] M. K. Kwak, H. E. Jeong, and K. Y. Suh, "Rational design and enhanced biocompatibility of a dry adhesive medical skin patch," *Adv. Mater.,* vol. 23, no. 34, pp. 3949-53, Sep 8 2011, doi: 10.1002/adma.201101694.

[24] W. G. Bae, D. Kim, M. K. Kwak, L. Ha, S. M. Kang, and K. Y. Suh, "Enhanced skin adhesive patch with modulus-tunable composite micropillars," *Adv. Healthc. Mater.,* vol. 2, no. 1, pp. 109-13, Jan 2013, doi: 10.1002/adhm.201200098.

[25] D. M. Drotlef, M. Amjadi, M. Yunusa, and M. Sitti, "Bioinspired Composite Microfibers for Skin Adhesion and Signal Amplification of Wearable Sensors," *Adv. Mater.,* vol. 29, no. 28, Jul 2017, doi: 10.1002/adma.201701353.

[26] T. Kim, J. Park, J. Sohn, D. Cho, and S. Jeon, "Bioinspired, Highly Stretchable, and Conductive Dry Adhesives Based on 1D-2D Hybrid Carbon Nanocomposites for All-in-One ECG Electrodes," *ACS Nano,* vol. 10, no. 4, pp. 4770-8, Apr 26 2016, doi: 10.1021/acsnano.6b01355.

[27] F. Stauffer *et al.*, "Skin Conformal Polymer Electrodes for Clinical ECG and EEG Recordings," *Adv. Healthc. Mater.,* vol. 7, no. 7, p. e1700994, Apr 2018, doi: 10.1002/adhm.201700994.

[28] M. K. Choi *et al.*, "Cephalopod-Inspired Miniaturized Suction Cups for Smart Medical Skin," *Adv. Healthc. Mater.,* vol. 5, no. 1, pp. 80-7, Jan 7 2016, doi: 10.1002/adhm.201500285.

[29] S. Baik, D. W. Kim, Y. Park, T. J. Lee, S. Ho Bhang, and C. Pang, "A wet-tolerant adhesive patch inspired by protuberances in suction cups of octopi," *Nature,* vol. 546, no. 7658, pp. 396-400, Jun 14 2017, doi: 10.1038/nature22382.

[30] S. Baik, J. Kim, H. J. Lee, T. H. Lee, and C. Pang, "Highly Adaptable and Biocompatible Octopus-Like Adhesive Patches with Meniscus-Controlled Unfoldable 3D Microtips for Underwater Surface and Hairy Skin," *Adv. Sci.,* vol. 5, no. 8, p. 1800100, Aug 2018, doi: 10.1002/advs.201800100.

[31] D. W. Kim *et al.*, "Highly Permeable Skin Patch with Conductive Hierarchical Architectures Inspired by Amphibians and Octopi for Omnidirectionally Enhanced Wet Adhesion," *Adv. Funct. Mater.,* vol. 29, no. 13, 2019, doi: 10.1002/adfm.201807614.

[32] A. Mahdavi *et al.*, "A biodegradable and biocompatible gecko-inspired tissue adhesive," *Proc. Natl. Acad. Sci.,* vol. 105, no. 7, pp. 2307-12, Feb 19 2008, doi: 10.1073/pnas.0712117105.

[33] L. Xue *et al.*, "Hybrid Surface Patterns Mimicking the Design of the Adhesive Toe Pad of Tree Frog," *ACS Nano,* vol. 11, no. 10, pp. 9711-9719, Oct 24 2017, doi: 10.1021/acsnano.7b04994.

[34] M. Seong, J. Lee, I. Hwang, and H. E. Jeong, "Significant Adhesion Enhancement of Bioinspired Dry Adhesives by Simple Thermal Treatment," *Int. J. Pr. Eng. Manu-GT.,* vol. 6, no. 3, pp. 587-599, 2019, doi: 10.1007/s40684-019-00062-z.

[35] R. A. Nawrocki, H. Jin, S. Lee, T. Yokota, M. Sekino, and T. Someya, "Self-Adhesive and Ultra-Conformable, Sub-300 nm Dry Thin-Film Electrodes for Surface Monitoring of Biopotentials," *Adv. Funct. Mater.,* vol. 28, no. 36, 2018, doi: 10.1002/adfm.201803279.

[36] D. H. Kim *et al.*, "Epidermal electronics," *Science,* vol. 333, no. 6044, pp. 838-43, Aug 12 2011, doi: 10.1126/science.1206157.

[37] B. D. Paulsen, K. Tybrandt, E. Stavrinidou, and J. Rivnay, "Organic mixed ionic-electronic conductors," *Nat. Mater.,* vol. 19, no. 1, pp. 13-26, Jan 2020, doi: 10.1038/s41563-019-0435-z.

[38] M. J. Donahue *et al.*, "Tailoring PEDOT properties for applications in bioelectronics," *Mater. Sci. Eng. R Rep.,* vol. 140, 2020, doi: 10.1016/j.mser.2020.100546.

[39] S. Kee *et al.*, "Highly Deformable and See-Through Polymer Light-Emitting Diodes with All-Conducting-Polymer Electrodes," *Adv. Mater.,* vol. 30, no. 3, Jan 2018, doi: 10.1002/adma.201703437.

[40] L. Hu, J. Song, X. Yin, Z. Su, and Z. Li, "Research Progress on Polymer Solar Cells Based on PEDOT:PSS Electrodes," *Polymers,* vol. 12, no. 1, Jan 7 2020, doi: 10.3390/polym12010145.

[41] Z. Ma, D. Kong, L. Pan, and Z. Bao, "Skin-inspired electronics: emerging semiconductor devices and systems," *J. Semicond.,* vol. 41, pp. 000000-000000-14, 2020.

[42] Y. Li, R. Tanigawa, and H. Okuzaki, "Soft and flexible PEDOT/PSS films for applications to soft actuators," *Smart Mater. Struct.,* vol. 23, no. 7, 2014, doi: 10.1088/0964-1726/23/7/074010.

[43] S. Zhang and F. Cicoira, "Water-Enabled Healing of Conducting Polymer Films," *Adv. Mater.,* vol. 29, no. 40, Oct 2017, doi: 10.1002/adma.201703098.

[44] Y. Xia and J. Ouyang, "Significant different conductivities of the two grades of poly(3,4-ethylenedioxythiophene):poly(styrenesulfonate), Clevios P and Clevios PH1000, arising from different molecular weights," *ACS Appl. Mater. Interfaces,* vol. 4, no. 8, pp. 4131-40, Aug 2012, doi: 10.1021/am300881m.

[45] Y. Wang *et al.*, "A highly stretchable, transparent, and conductive polymer," *Sci. Adv.,* vol. 3, no. 3, p. e1602076, 2017.

[46] P. Li, K. Sun, and J. Ouyang, "Stretchable and Conductive Polymer Films Prepared by Solution Blending," *ACS Appl. Mater. Interfaces,* vol. 7, no. 33, pp. 18415-23, Aug 26 2015, doi: 10.1021/acsami.5b04492.

[47] L. V. Kayser and D. J. Lipomi, "Stretchable Conductive Polymers and Composites Based on PEDOT and PEDOT:PSS," *Adv. Mater.,* vol. 31, no. 10, p. e1806133, Mar 2019, doi: 10.1002/adma.201806133.

[48] L. M. Ferrari *et al.*, "Ultraconformable Temporary Tattoo Electrodes for Electrophysiology," *Adv. Sci.,* vol. 5, no. 3, p. 1700771, Mar 2018, doi: 10.1002/advs.201700771.

[49] Y. Chen, G. Zhou, X. Yuan, C. Li, L. Liu, and H. You, "Substrate-free, ultra-conformable PEDOT: PSS E-tattoo achieved by energy regulation on skin," *Biosens. Bioelectron.,* vol. 206, p. 114118, Jun 15 2022, doi: 10.1016/j.bios.2022.114118.

[50] J. Cao *et al.*, "Stretchable and Self-Adhesive PEDOT:PSS Blend with High Sweat Tolerance as Conformal Biopotential Dry Electrodes," *ACS Appl. Mater. Interfaces,* vol. 14, no. 34, pp. 39159-39171, Aug 31 2022, doi: 10.1021/acsami.2c11921.

[51] I. B. Dimov, A. Sautter, W. Lövenich, C. Neumann, and G. G. Malliaras, "Adhesive cutaneous conducting polymer electrodes," *Appl. Phys. Rev.,* vol. 9, no. 2, 2022, doi: 10.1063/5.0079616.

[52] Y. Li *et al.*, "Tailoring the Self-Healing Properties of Conducting Polymer Films," *Macromol. Biosci.,* vol. 20, no. 11, p. e2000146, Nov 2020, doi: 10.1002/mabi.202000146.

[53] Y. Kikuchi, A. Pena-Francesch, M. Vural, and M. C. Demirel, "Highly Conductive Self-Healing Biocomposites Based on Protein Mediated Self-Assembly of PEDOT:PSS Films," *ACS Appl. Bio. Mater.,* vol. 3, no. 4, pp. 2507-2515, Apr 20 2020, doi: 10.1021/acsabm.0c00207.

[54] L. V. Kayser *et al.*, "RAFT Polymerization of an Intrinsically Stretchable Water-Soluble Block Copolymer Scaffold for PEDOT," *Chem. Mater.,* vol. 30, no. 13, pp. 4459-4468, Jul 10 2018, doi: 10.1021/acs.chemmater.8b02040.

[55] Y. Li *et al.*, "Autonomic Self‐Healing of PEDOT:PSS Achieved Via Polyethylene Glycol Addition," *Adv. Funct. Mater.,* vol. 30, no. 30, 2020, doi: 10.1002/adfm.202002853.

[56] S. Kee, M. A. Haque, D. Corzo, H. N. Alshareef, and D. Baran, "Self‐Healing and Stretchable 3D‐Printed Organic Thermoelectrics," *Adv. Funct. Mater.,* vol. 29, no. 51, 2019, doi: 10.1002/adfm.201905426.

[57] J. Ko, X. Wu, A. Surendran, B. T. Muhammad, and W. L. Leong, "Self-Healable Organic Electrochemical Transistor with High Transconductance, Fast Response, and Long-Term Stability," *ACS Appl. Mater. Interfaces,* vol. 12, no. 30, pp. 33979-33988, Jul 29 2020, doi: 10.1021/acsami.0c07913.

[58] D. H. Lee, E. K. Lee, C. H. Kim, H. J. Yun, Y. J. Kim, and H. Yoo, "Blended Polymer Dry Electrodes for Reliable Electrocardiogram and Electromyogram Measurements and Their Eco-Friendly Disposal Led by Degradability in Hot Water," *Polymers,* vol. 14, no. 13, Jun 26 2022, doi: 10.3390/polym14132586.

[59] W. Dong, C. Zhu, W. Hu, L. Xiao, and Y. a. Huang, "Stretchable human-machine interface based on skin-conformal sEMG electrodes with self-similar geometry," *J. Semicond.,* vol. 39, no. 1, 2018, doi: 10.1088/1674-4926/39/1/014001.

[60] J. Y. Oh, S. Kim, H. K. Baik, and U. Jeong, "Conducting Polymer Dough for Deformable Electronics," *Adv. Mater.,* vol. 28, no. 22, pp. 4455-61, Jun 2016, doi: 10.1002/adma.201502947.

[61] M. Modarresi, A. Mehandzhiyski, M. Fahlman, K. Tybrandt, and I. Zozoulenko, "Microscopic Understanding of the Granular Structure and the Swelling of PEDOT:PSS," *Macromolecules,* vol. 53, no. 15, pp. 6267-6278, 2020, doi: 10.1021/acs.macromol.0c00877.

[62] Y. Li, X. Zhou, B. Sarkar, N. Gagnon-Lafrenais, and F. Cicoira, "Recent Progress on Self-Healable Conducting Polymers," *Adv. Mater.,* vol. 34, no. 24, p. e2108932, Jun 2022, doi: 10.1002/adma.202108932.

[63] K. Wang, U. Parekh, T. Pailla, H. Garudadri, V. Gilja, and T. N. Ng, "Stretchable Dry Electrodes with Concentric Ring Geometry for Enhancing Spatial Resolution in Electrophysiology," *Adv. Healthc. Mater.,* vol. 6, no. 19, Oct 2017, doi: 10.1002/adhm.201700552.

[64] L. Inzelberg *et al.*, "Printed facial skin electrodes as sensors of emotional affect," *Flex. Print. Electron.,* vol. 3, no. 4, 2018, doi: 10.1088/2058-8585/aae252.

[65] A. J. Bandodkar, R. Nunez-Flores, W. Jia, and J. Wang, "All-printed stretchable electrochemical devices," *Adv. Mater.,* vol. 27, no. 19, pp. 3060-5, May 20 2015, doi: 10.1002/adma.201500768.

[66] T. Roberts, J. B. De Graaf, C. Nicol, T. Herve, M. Fiocchi, and S. Sanaur, "Flexible Inkjet-Printed Multielectrode Arrays for Neuromuscular Cartography," *Adv. Healthc. Mater.,* vol. 5, no. 12, pp. 1462-70, Jun 2016, doi: 10.1002/adhm.201600108.

[67] X. Guo *et al.*, "A Self-Wetting Paper Electrode for Ubiquitous Bio-Potential Monitoring," *IEEE Sens. J.,* vol. 17, no. 9, pp. 2654-2661, 2017, doi: 10.1109/jsen.2017.2684825.

[68] A. Zucca, K. Yamagishi, T. Fujie, S. Takeoka, V. Mattoli, and F. Greco, "Roll to roll processing of ultraconformable conducting polymer nanosheets," *J. Mater. Chem. C,* vol. 3, no. 25, pp. 6539-6548, 2015, doi: 10.1039/c5tc00750j.

[69] A. Zucca *et al.*, "Tattoo conductive polymer nanosheets for skin-contact applications," *Adv. Healthc. Mater.,* vol. 4, no. 7, pp. 983-90, May 2015, doi: 10.1002/adhm.201400761.

[70] X. He *et al.*, "Screen-Printed Fabrication of PEDOT:PSS/Silver Nanowire Composite Films for Transparent Heaters," *Materials.,* vol. 10, no. 3, Feb 23 2017, doi: 10.3390/ma10030220.

[71] Y. F. Wang *et al.*, "Fully Printed PEDOT:PSS-based Temperature Sensor with High Humidity Stability for Wireless Healthcare Monitoring," *Sci. Rep.,* vol. 10, no. 1, p. 2467, Feb 12 2020, doi: 10.1038/s41598-020-59432-2.

[72] A. F. Wibowo *et al.*, "Highly stretchable and robust transparent conductive polymer composites for multifunctional healthcare monitoring," *Sci. Technol.,* vol. 23, no. 1, pp. 332-340, 2022, doi: 10.1080/14686996.2022.2070864.

[73] J. W. Han *et al.*, "Highly stretchable, robust, and conductive lab-synthesized PEDOT:PSS conductive polymer/hydroxyethyl cellulose films for on-skin health-monitoring devices," *Org. Electron.,* vol. 105, 2022, doi: 10.1016/j.orgel.2022.106499.

[74] I. TORAY INDUSTRIES. [Online]. Available: https://www.hitoe.toray/en/technology/index.html.

[75] A. Niijima, T. Isezaki, R. Aoki, T. Watanabe, and T. Yamada, "hitoeCap," presented at the Proceedings of the 2017 ACM International Symposium on Wearable Computers - ISWC '17, 2017.

[76] H. Nakashima and S. Tsukada, "Smart clothing with wearable bioelectrodes “hitoe”," in *Chemical, Gas, and Biosensors for Internet of Things and Related Applications*, 2019, pp. 163-176.

[77] J. V. Lidon-Roger, G. Prats-Boluda, Y. Ye-Lin, J. Garcia-Casado, and E. Garcia-Breijo, "Textile Concentric Ring Electrodes for ECG Recording Based on Screen-Printing Technology," *Sensors,* vol. 18, no. 1, Jan 21 2018, doi: 10.3390/s18010300.

[78] D. Pani *et al.*, "Evaluation of Novel Textile Electrodes for ECG Signals Monitoring Based on PEDOT:PSS-Treated Woven Fabrics," *2015 37th Annual International Conference of the Ieee Engineering in Medicine and Biology Society*, 2015, pp. 3197-3200.

[79] S. Takamatsu, T. Lonjaret, D. Crisp, J. M. Badier, G. G. Malliaras, and E. Ismailova, "Direct patterning of organic conductors on knitted textiles for long-term electrocardiography," *Sci. Rep.,* vol. 5, p. 15003, Oct 8 2015, doi: 10.1038/srep15003.

[80] A. Ankhili, X. Tao, C. Cochrane, V. Koncar, D. Coulon, and J. M. Tarlet, "Comparative Study on Conductive Knitted Fabric Electrodes for Long-Term Electrocardiography Monitoring: Silver-Plated and PEDOT:PSS Coated Fabrics," *Sensors,* vol. 18, no. 11, Nov 12 2018, doi: 10.3390/s18113890.

[81] A. Ankhili, X. Tao, C. Cochrane, V. Koncar, D. Coulon, and J. M. Tarlet, "Ambulatory Evaluation of ECG Signals Obtained Using Washable Textile-Based Electrodes Made with Chemically Modified PEDOT:PSS," *Sensors,* vol. 19, no. 2, Jan 21 2019, doi: 10.3390/s19020416.

[82] S. K. Sinha *et al.*, "Screen-Printed PEDOT:PSS Electrodes on Commercial Finished Textiles for Electrocardiography," *ACS Appl. Mater. Interfaces,* vol. 9, no. 43, pp. 37524-37528, Nov 1 2017, doi: 10.1021/acsami.7b09954.

[83] S. K. Sinha *et al.*, "Graphene and Poly(3,4-ethylene dioxythiophene):Poly(4-styrenesulfonate) on Nonwoven Fabric as a Room Temperature Metal and Its Application as Dry Electrodes for Electrocardiography," *ACS Appl. Mater. Interfaces,* vol. 11, no. 35, pp. 32339-32345, Sep 4 2019, doi: 10.1021/acsami.9b05379.

[84] D. Pani, A. Dessi, J. F. Saenz-Cogollo, G. Barabino, B. Fraboni, and A. Bonfiglio, "Fully Textile, PEDOT:PSS Based Electrodes for Wearable ECG Monitoring Systems," *IEEE Trans. Biomed. Eng,* vol. 63, no. 3, pp. 540-9, Mar 2016, doi: 10.1109/TBME.2015.2465936.

[85] A. Ankhili, X. Tao, C. Cochrane, D. Coulon, and V. Koncar, "Washable and Reliable Textile Electrodes Embedded into Underwear Fabric for Electrocardiography (ECG) Monitoring," *Materials,* vol. 11, no. 2, Feb 7 2018, doi: 10.3390/ma11020256.

[86] Y. Cui *et al.*, "Green preparation of PEDOT-based composites with outstanding electrothermal heating and durable rapid-response sensing performance for smart healthcare textiles," *Chem. Eng. J.,* vol. 446, 2022, doi: 10.1016/j.cej.2022.137189.

[87] Y. Maithani, A. Singh, B. R. Mehta, and J. P. Singh, "PEDOT: PSS treated cotton-based textile dry electrode for ECG sensing," *Mater. Today,* vol. 62, pp. 4052-4057, 2022, doi: 10.1016/j.matpr.2022.04.611.

[88] X. Pan *et al.*, "A bionic tactile plastic hydrogel-based electronic skin constructed by a nerve-like nanonetwork combining stretchable, compliant, and self-healing properties," *Chem. Eng. J.,* vol. 379, 2020, doi: 10.1016/j.cej.2019.122271.

[89] S. Zhang *et al.*, "Room-Temperature-Formed PEDOT:PSS Hydrogels Enable Injectable, Soft, and Healable Organic Bioelectronics," *Adv. Mater.,* vol. 32, no. 1, p. e1904752, Jan 2020, doi: 10.1002/adma.201904752.

[90] B. Lu *et al.*, "Pure PEDOT:PSS hydrogels," *Nat. Commun.,* vol. 10, no. 1, p. 1043, Mar 5 2019, doi: 10.1038/s41467-019-09003-5.

[91] B. Yao *et al.*, "Ultrahigh-Conductivity Polymer Hydrogels with Arbitrary Structures," *Adv. Mater.,* vol. 29, no. 28, Jul 2017, doi: 10.1002/adma.201700974.

[92] X. Ren *et al.*, "Highly Conductive PPy-PEDOT:PSS Hybrid Hydrogel with Superior Biocompatibility for Bioelectronics Application," *ACS Appl. Mater. Interfaces,* vol. 13, no. 21, pp. 25374-25382, Jun 2 2021, doi: 10.1021/acsami.1c04432.

[93] S. Cao, X. Tong, K. Dai, and Q. Xu, "A super-stretchable and tough functionalized boron nitride/PEDOT:PSS/poly(N-isopropylacrylamide) hydrogel with self-healing, adhesion, conductive and photothermal activity," *J. Mater. Chem. A,* vol. 7, no. 14, pp. 8204-8209, 2019, doi: 10.1039/c9ta00618d.

[94] E. Feng *et al.*, "A toughened, transparent, anti-freezing and solvent-resistant hydrogel towards environmentally tolerant strain sensor and soft connection," *Colloids Sur. A,* vol. 656, 2023, doi: 10.1016/j.colsurfa.2022.130390.

[95] Z. Zhou, W. Yuan, and X. Xie, "A stretchable and adhesive composite hydrogel containing PEDOT:PSS for wide-range and precise motion sensing and electromagnetic interference shielding and as a triboelectric nanogenerator," *Mater. Chem. Front.,* vol. 6, no. 22, pp. 3359-3368, 2022, doi: 10.1039/d2qm00690a.

[96] S. Wang, G. Guo, X. Lu, S. Ji, G. Tan, and L. Gao, "Facile Soaking Strategy Toward Simultaneously Enhanced Conductivity and Toughness of Self-Healing Composite Hydrogels Through Constructing Multiple Noncovalent Interactions," *ACS Appl. Mater. Interfaces,* vol. 10, no. 22, pp. 19133-19142, Jun 6 2018, doi: 10.1021/acsami.8b04999.

[97] D. Gan *et al.*, "Graphene Oxide‐Templated Conductive and Redox‐Active Nanosheets Incorporated Hydrogels for Adhesive Bioelectronics," *Adv. Funct. Mater.,* vol. 30, no. 5, 2019, doi: 10.1002/adfm.201907678.

[98] L. Dong, M. Wang, J. Wu, C. Zhu, J. Shi, and H. Morikawa, "Stretchable, Adhesive, Self-Healable, and Conductive Hydrogel-Based Deformable Triboelectric Nanogenerator for Energy Harvesting and Human Motion Sensing," *ACS Appl. Mater. Interfaces,* vol. 14, no. 7, pp. 9126-9137, Feb 23 2022, doi: 10.1021/acsami.1c23176.

[99] X. Zhou *et al.*, "Self-healing, stretchable, and highly adhesive hydrogels for epidermal patch electrodes," *Acta Biomater.,* vol. 139, pp. 296-306, Feb 2022, doi: 10.1016/j.actbio.2021.07.069.

[100] C. Zhang *et al.*, "Highly adhesive and self-healing γ-PGA/PEDOT:PSS conductive hydrogels enabled by multiple hydrogen bonding for wearable electronics," *Nano Energy,* vol. 95, 2022, doi: 10.1016/j.nanoen.2022.106991.

[101] Y. Xu *et al.*, "Cytocompatible, Injectable, and Electroconductive Soft Adhesives with Hybrid Covalent/Noncovalent Dynamic Network," *Adv. Sci.,* vol. 6, no. 15, p. 1802077, Aug 7 2019, doi: 10.1002/advs.201802077.

[102] F. Ye, M. Li, D. Ke, L. Wang, and Y. Lu, "Ultrafast Self‐Healing and Injectable Conductive Hydrogel for Strain and Pressure Sensors," *Adv. Mater. Technol.,* vol. 4, no. 9, 2019, doi: 10.1002/admt.201900346.

[103] X. Ding, R. Jia, Z. Gan, Y. Du, D. Wang, and X. Xu, "Tough and conductive polymer hydrogel based on double network for photo-curing 3D printing," *Mater. Res. Express,* vol. 7, no. 5, 2020, doi: 10.1088/2053-1591/ab8cfb.

[104] Y. Ko *et al.*, "Antibacterial poly (3,4-ethylenedioxythiophene):poly(styrene-sulfonate)/agarose nanocomposite hydrogels with thermo-processability and self-healing," *Carbohydr. Polym.,* vol. 203, pp. 26-34, Jan 1 2019, doi: 10.1016/j.carbpol.2018.09.026.

[105] Z. Xie *et al.*, "Ultrastretchable, self-healable and adhesive composite organohydrogels with a fast response for human–machine interface applications," *J. Mater. Chem. C,* vol. 10, no. 21, pp. 8266-8277, 2022, doi: 10.1039/d2tc00932c.

[106] Q. Rong, W. Lei, L. Chen, Y. Yin, J. Zhou, and M. Liu, "Anti-freezing, Conductive Self-healing Organohydrogels with Stable Strain-Sensitivity at Subzero Temperatures," *Angew. Chem. Int. Ed. Engl.,* vol. 56, no. 45, pp. 14159-14163, Nov 6 2017, doi: 10.1002/anie.201708614.

[107] S.-J. Wang *et al.*, "MXene reinforced organohydrogels with ultra-stability, high sensitivity and anti-freezing ability for flexible strain sensors," *J. Mater. Chem. C,* vol. 10, no. 33, pp. 11914-11923, 2022, doi: 10.1039/d2tc02148j.

[108] Y. Peng, B. Yan, Y. Li, J. Lan, L. Shi, and R. Ran, "Antifreeze and moisturizing high conductivity PEDOT/PVA hydrogels for wearable motion sensor," *J. Mater. Sci.,* vol. 55, no. 3, pp. 1280-1291, 2019, doi: 10.1007/s10853-019-04101-7.

[109] J. Wu *et al.*, "Ultrastretchable and Stable Strain Sensors Based on Antifreezing and Self-Healing Ionic Organohydrogels for Human Motion Monitoring," *ACS Appl. Mater. Interfaces,* vol. 11, no. 9, pp. 9405-9414, Mar 6 2019, doi: 10.1021/acsami.8b20267.

[110] D. Ma, X. Wu, Y. Wang, H. Liao, P. Wan, and L. Zhang, "Wearable, Antifreezing, and Healable Epidermal Sensor Assembled from Long-Lasting Moist Conductive Nanocomposite Organohydrogel," *ACS Appl. Mater. Interfaces,* vol. 11, no. 44, pp. 41701-41709, Nov 6 2019, doi: 10.1021/acsami.9b15412.

[111] C. Hu, Y. Zhang, X. Wang, L. Xing, L. Shi, and R. Ran, "Stable, Strain-Sensitive Conductive Hydrogel with Antifreezing Capability, Remoldability, and Reusability," *ACS Appl. Mater. Interfaces,* vol. 10, no. 50, pp. 44000-44010, Dec 19 2018, doi: 10.1021/acsami.8b15287.

[112] L. Han *et al.*, "Mussel-Inspired Adhesive and Conductive Hydrogel with Long-Lasting Moisture and Extreme Temperature Tolerance," *Adv. Funct. Mater.,* vol. 28, no. 3, 2018, doi: 10.1002/adfm.201704195.

[113] S. Liu *et al.*, "A compliant, self-adhesive and self-healing wearable hydrogel as epidermal strain sensor," *J. Mater. Chem. C,* vol. 6, no. 15, pp. 4183-4190, 2018, doi: 10.1039/c8tc00157j.

[114] M. Liao *et al.*, "Wearable, Healable, and Adhesive Epidermal Sensors Assembled from Mussel-Inspired Conductive Hybrid Hydrogel Framework," *Adv. Funct. Mater.,* vol. 27, no. 48, 2017, doi: 10.1002/adfm.201703852.

[115] G. Cai, J. Wang, K. Qian, J. Chen, S. Li, and P. S. Lee, "Extremely Stretchable Strain Sensors Based on Conductive Self-Healing Dynamic Cross-Links Hydrogels for Human-Motion Detection," *Adv. Sci.,* vol. 4, no. 2, p. 1600190, Feb 2017, doi: 10.1002/advs.201600190.

[116] Q. Ding *et al.*, "Nanocellulose-Mediated Electroconductive Self-Healing Hydrogels with High Strength, Plasticity, Viscoelasticity, Stretchability, and Biocompatibility toward Multifunctional Applications," *ACS Appl. Mater. Interfaces,* vol. 10, no. 33, pp. 27987-28002, Aug 22 2018, doi: 10.1021/acsami.8b09656.

[117] W. P. Chen, D. Z. Hao, W. J. Hao, X. L. Guo, and L. Jiang, "Hydrogel with Ultrafast Self-Healing Property Both in Air and Underwater," *ACS Appl. Mater. Interfaces,* vol. 10, no. 1, pp. 1258-1265, Jan 10 2018, doi: 10.1021/acsami.7b17118.

[118] B. Lu *et al.*, "One-Pot Assembly of Microfibrillated Cellulose Reinforced PVA–Borax Hydrogels with Self-Healing and pH-Responsive Properties," *ACS Sustain. Chem. Eng.,* vol. 5, no. 1, pp. 948-956, 2016, doi: 10.1021/acssuschemeng.6b02279.

[119] C.-C. Shih *et al.*, "A rapid and green method for the fabrication of conductive hydrogels and their applications in stretchable supercapacitors," *J. Power Sources,* vol. 426, pp. 205-215, 2019, doi: 10.1016/j.jpowsour.2019.04.030.

[120] P. Tan *et al.*, "Solution-processable, soft, self-adhesive, and conductive polymer composites for soft electronics," *Nat. Commun.,* vol. 13, no. 1, p. 358, Jan 18 2022, doi: 10.1038/s41467-022-28027-y.

[121] C. Xie, X. Wang, H. He, Y. Ding, and X. Lu, "Mussel‐Inspired Hydrogels for Self‐Adhesive Bioelectronics," *Adv. Funct. Mater.,* vol. 30, no. 25, 2020, doi: 10.1002/adfm.201909954.

[122] X. Su *et al.*, "A Highly Conducting Polymer for Self-Healable, Printable, and Stretchable Organic Electrochemical Transistor Arrays and Near Hysteresis-Free Soft Tactile Sensors," *Adv. Mater.,* vol. 34, no. 19, p. e2200682, May 2022, doi: 10.1002/adma.202200682.

[123] C. Chen, H. Yang, X. Yang, and Q. Ma, "Tannic acid: a crosslinker leading to versatile functional polymeric networks: a review," *RSC Adv.,* vol. 12, no. 13, pp. 7689-7711, Mar 8 2022, doi: 10.1039/d1ra07657d.

[124] Z. Guo *et al.*, "Tannic acid-based metal phenolic networks for bio-applications: a review," *J Mater. Chem. B,* vol. 9, no. 20, pp. 4098-4110, May 26 2021, doi: 10.1039/d1tb00383f.

[125] H. Fan, L. Wang, X. Feng, Y. Bu, D. Wu, and Z. Jin, "Supramolecular Hydrogel Formation Based on Tannic Acid," *Macromolecules,* vol. 50, no. 2, pp. 666-676, 2017, doi: 10.1021/acs.macromol.6b02106.

[126] C. Chen *et al.*, "Tannic acid–thioctic acid hydrogel: a novel injectable supramolecular adhesive gel for wound healing," *Green Chem.,* vol. 23, no. 4, pp. 1794-1804, 2021, doi: 10.1039/d0gc02909b.

[127] X. Gao, Q. Dai, L. Yao, H. Dong, Q. Li, and X. Cao, "A medical adhesive used in a wet environment by blending tannic acid and silk fibroin," *Biomater. Sci.,* vol. 8, no. 9, pp. 2694-2701, May 6 2020, doi: 10.1039/d0bm00322k.

[128] H. Fan, J. Wang, and Z. Jin, "Tough, Swelling-Resistant, Self-Healing, and Adhesive Dual-Cross-Linked Hydrogels Based on Polymer–Tannic Acid Multiple Hydrogen Bonds," *Macromolecules,* vol. 51, no. 5, pp. 1696-1705, 2018, doi: 10.1021/acs.macromol.7b02653.

[129] W. Shi *et al.*, "Tannic acid-inspired, self-healing, and dual stimuli responsive dynamic hydrogel with potent antibacterial and anti-oxidative properties," *J Mater. Chem. B,* vol. 9, no. 35, pp. 7182-7195, Sep 15 2021, doi: 10.1039/d1tb00156f.

[130] S. Khasim, A. Pasha, N. Badi, M. Lakshmi, and Y. K. Mishra, "High performance flexible supercapacitors based on secondary doped PEDOT-PSS-graphene nanocomposite films for large area solid state devices," *RSC Adv.,* vol. 10, no. 18, pp. 10526-10539, Mar 11 2020, doi: 10.1039/d0ra01116a.

[131] H. Çabuk, Y. Yılmaz, and E. Yıldız, "Vortex-Assisted Deep Eutectic Solvent-Based Liquid-Liquid Microextraction for the Analysis of Alkyl Gallates in Vegetable Oils," *Acta Chimica. Slovenica.,* vol. 66, no. 2, pp. 385-394, 2019, doi: 10.17344/acsi.2018.4877.

[132] M. A. Pantoja-Castro and H. González-Rodríguez, "Study by infrared spectroscopy and thermogravimetric analysis of tannins and tannic acid," *Rev. latinoam. quím.,* vol. 39, no. 3, pp. 107-112, 2011.

[133] Biological evaluation of medical devices – part 5: Tests for in vitro cytotoxicity. (2009).

[134] H. Liu *et al.*, "Stretchable Conductive Fabric Enabled By Surface Functionalization of Commercial Knitted Cloth," *ACS Appl. Mater. Interfaces,* vol. 13, no. 46, pp. 55656-55665, Nov 24 2021, doi: 10.1021/acsami.1c15268.

[135] T. Zhu *et al.*, "Recent advances in conductive hydrogels: classifications, properties, and applications," *Chem. Soc. Rev.,* 2023.

[136] X. Fan, W. Zhou, Y. Chen, L. Yan, Y. Fang, and H. Liu, "An Antifreezing/Antiheating Hydrogel Containing Catechol Derivative Urushiol for Strong Wet Adhesion to Various Substrates," *ACS Appl. Mater. Interfaces,* vol. 12, no. 28, pp. 32031-32040, Jul 15 2020, doi: 10.1021/acsami.0c09917.

[137] Q. Zhou *et al.*, "Mechanically Strong and Multifunctional Hybrid Hydrogels with Ultrahigh Electrical Conductivity," *Adv. Funct. Mater.,* vol. 31, no. 40, 2021, doi: 10.1002/adfm.202104536.

[138] J. Wang *et al.*, "Ultra-High Electrical Conductivity in Filler-Free Polymeric Hydrogels Toward Thermoelectrics and Electromagnetic Interference Shielding," *Adv. Mater.,* vol. 34, no. 12, p. e2109904, Mar 2022, doi: 10.1002/adma.202109904.

[139] D. Won *et al.*, "Digital selective transformation and patterning of highly conductive hydrogel bioelectronics by laser-induced phase separation," *Sci. Adv.,* vol. 8, no. 23, p. eabo3209, 2022.

[140] X. Fan *et al.*, "Tough polyacrylamide-tannic acid-kaolin adhesive hydrogels for quick hemostatic application," *Mater. Sci. Eng. C,* vol. 109, p. 110649, Apr 2020, doi: 10.1016/j.msec.2020.110649.

[141] MC10. [Online]. Available: https://www.mc10inc.com/mc10-pulse/wearable-technology-from-mc10-lor%C3%A9al-revolutionizes-skincare.

[142] P. He *et al.*, "Anti-freezing and moisturizing conductive hydrogels for strain sensing and moist-electric generation applications," *J. Mater. Chem. A,* vol. 8, no. 6, pp. 3109-3118, 2020, doi: 10.1039/c9ta12940e.

[143] M. A. Leaf and M. Muthukumar, "Electrostatic Effect on the Solution Structure and Dynamics of PEDOT:PSS," *Macromolecules,* vol. 49, no. 11, pp. 4286-4294, 2016, doi: 10.1021/acs.macromol.6b00740.

[144] R. M. Kumar, P. Baskar, K. Balamurugan, S. Das, and V. Subramanian, "On the perturbation of the H-bonding interaction in ethylene glycol clusters upon hydration," *J Phys .Chem. A,* vol. 116, no. 17, pp. 4239-47, May 3 2012, doi: 10.1021/jp300693r.

[145] F. Wu, Y. Pang, and J. Liu, "Swelling-strengthening hydrogels by embedding with deformable nanobarriers," *Nat. Commun.,* vol. 11, no. 1, p. 4502, Sep 9 2020, doi: 10.1038/s41467-020-18308-9.

[146] H. Park *et al.*, "Effect of swelling ratio of injectable hydrogel composites on chondrogenic differentiation of encapsulated rabbit marrow mesenchymal stem cells in vitro," *Biomacromolecules,* vol. 10, no. 3, pp. 541-546, 2009.

[147] D. Farina *et al.*, "The extraction of neural information from the surface EMG for the control of upper-limb prostheses: emerging avenues and challenges," *IEEE Trans. Neural. Syst. Rehabil. Eng.,* vol. 22, no. 4, pp. 797-809, Jul 2014, doi: 10.1109/TNSRE.2014.2305111.

[148] X. Su *et al.*, "A Solvent Co-cross-linked Organogel with Fast Self-Healing Capability and Reversible Adhesiveness at Extreme Temperatures," *ACS Appl. Mater. Interfaces,* vol. 12, no. 26, pp. 29757-29766, Jul 1 2020, doi: 10.1021/acsami.0c04933.

APPENDIX A SUPPLEMENTARY INFORMATION FOR ARTICLE 1 : SELF-HEALING, STRETCHABLE, AND HIGHLY ADHESIVE HYDROGELS FOR EPIDERMAL PATCH ELECTRODES

Xin Zhou[a], Ashna Rajeev[b], Arunprabaharan Subramanian[a], Yang Li[a], Nicolò Rossetti[a], Giovanniantonio Natale[b], Gregory A. Lodygensky[c, d], Fabio Cicoira[a*]

[a] Department of Chemical Engineering, Polytechnique Montréal, Montréal, Québec H3C 3A7, Canada

[b] Department of Chemical and Petroleum Engineering, Schulich School of Engineering, University of Calgary, 2500 University Dr. NW, T2N 1N4

[c] Department of Pediatrics, Sainte-Justine University Hospital Research Center, Montreal, QC, Canada

[d] Department of Pharmacology and Physiology, University of Montreal, Montreal, QC, Canada

[*] Corresponding author: fabio.cicoira@polymtl.ca

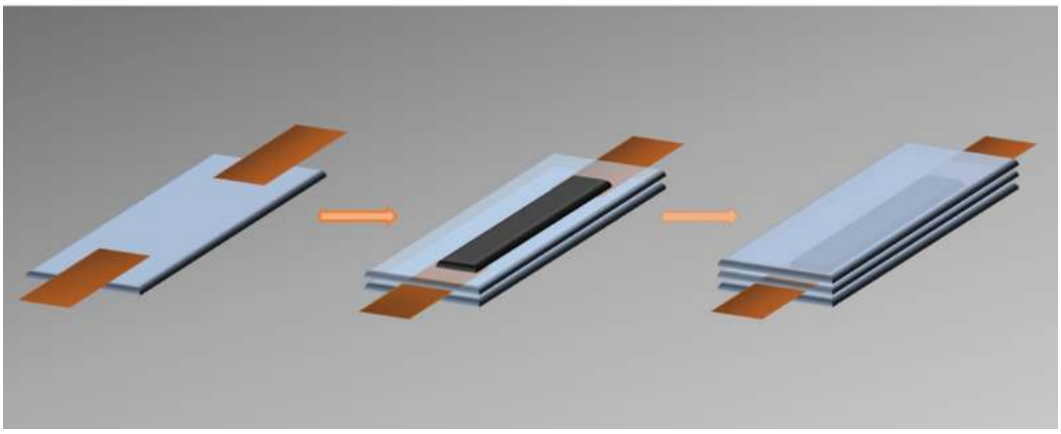

Figure SA1. Schematic illustration of SV3/PVA hydrogel based strain sensor preparation with using commercial VHB tape.

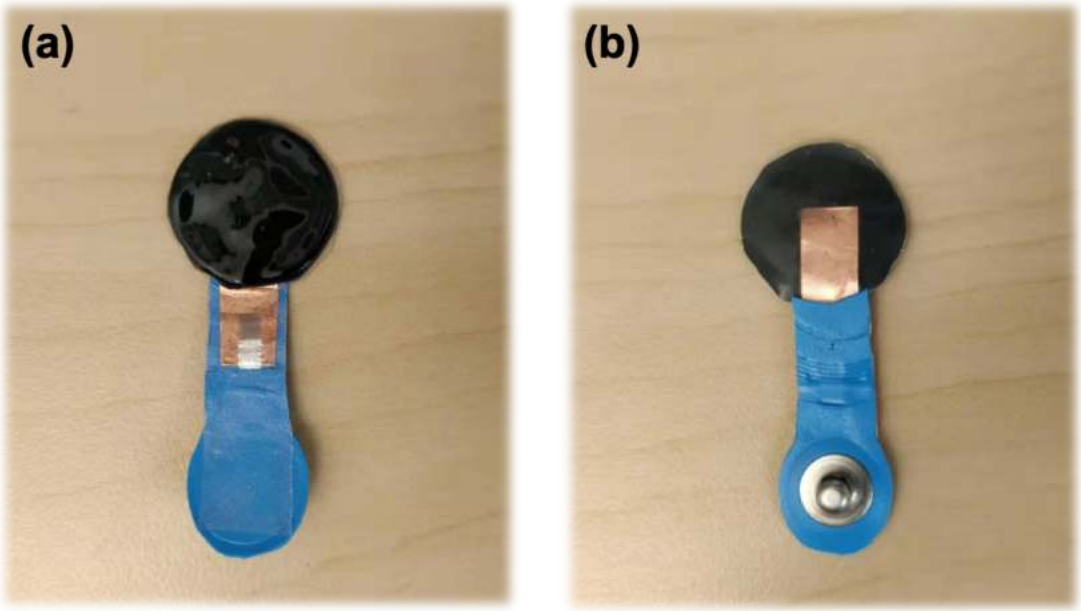

Figure SA2. Front (a) and back view (b) of SV3/PVA-1-3 hydrogel electrodes.

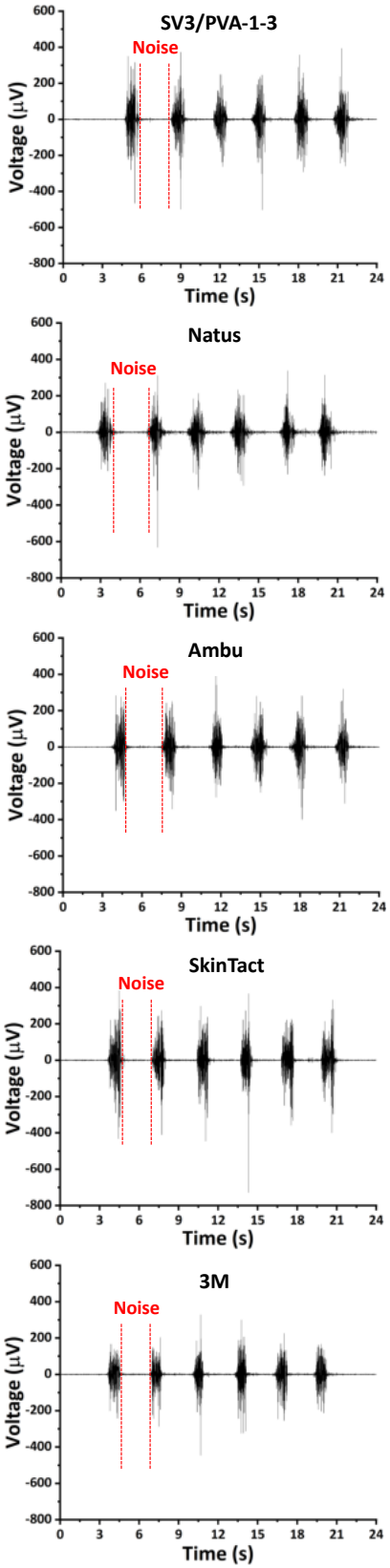

Figure SA3. Noise selection using the data from the EMG measurements.

Figure SA4. SV3/PVA-1-3 hydrogel manual stretching from an original length of 2 cm (insert) to a stretched length of more than 2 m. The weight of the stretched hydrogel was about 3 g.

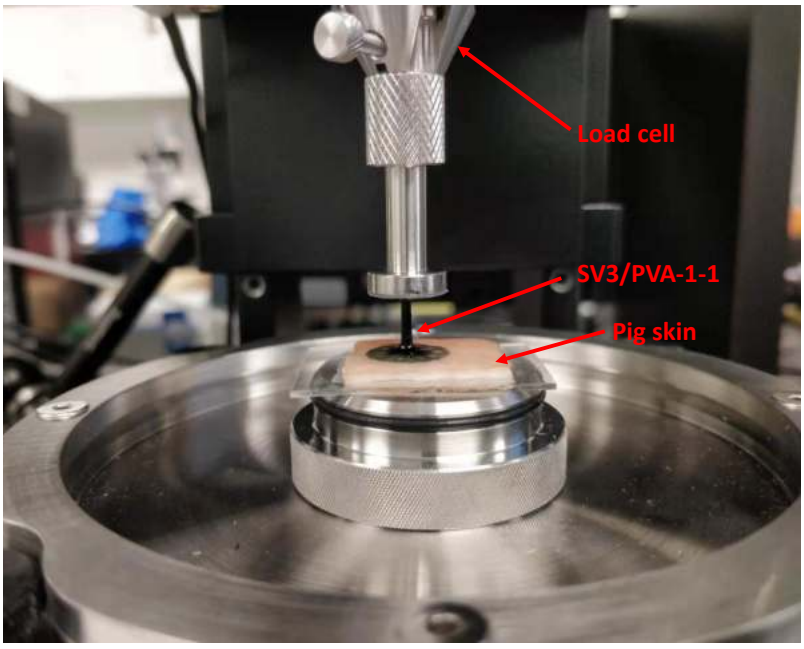

Figure SA5. The detachment process of SV3/PVA-1-1 hydrogel from pig skin.

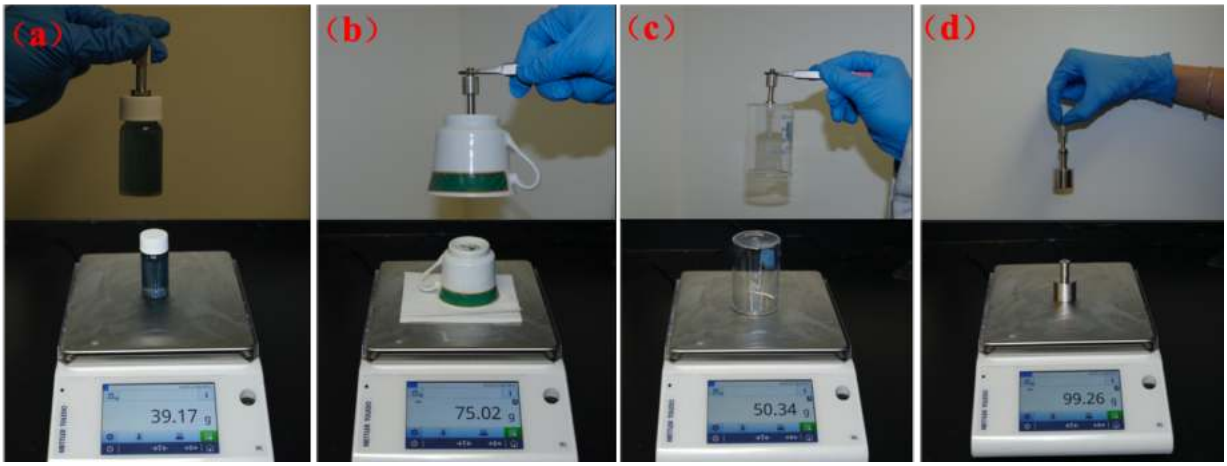

Figure SA6. Digital images of SV3/PVA-1-3 hydrogel adhesion to various materials: (a) plastic, (b) ceramic, (c) glass, and (d) stainless steel.

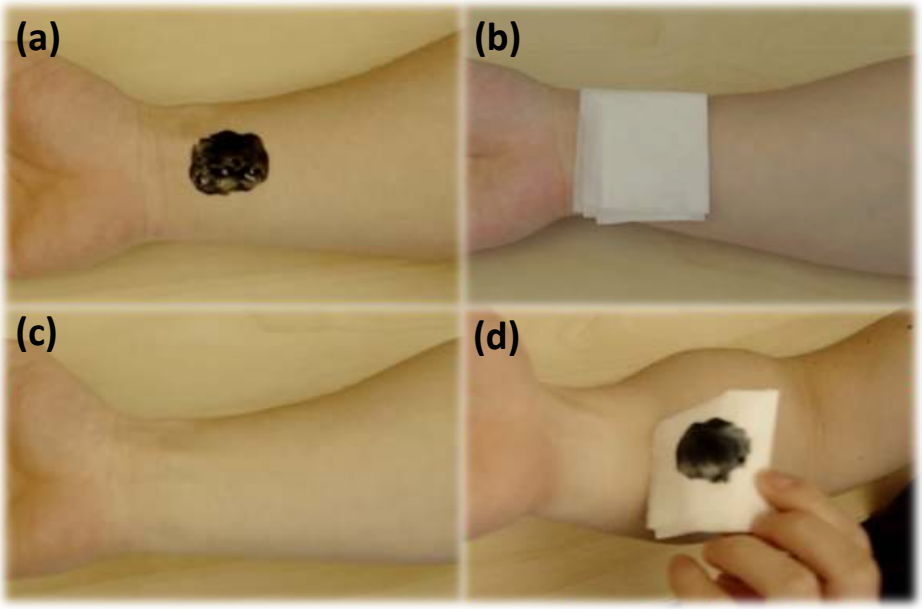

Figure SA7. Removal of SV3/PVA-1-3 hydrogel from skin with a paper. (a) Top view of the hydrogel on the wrist, (b) top view of a paper covering with the hydrogel, (c) top view of the wrist after the removal of the hydrogel, and (d) top view of the hydrogel on the paper.

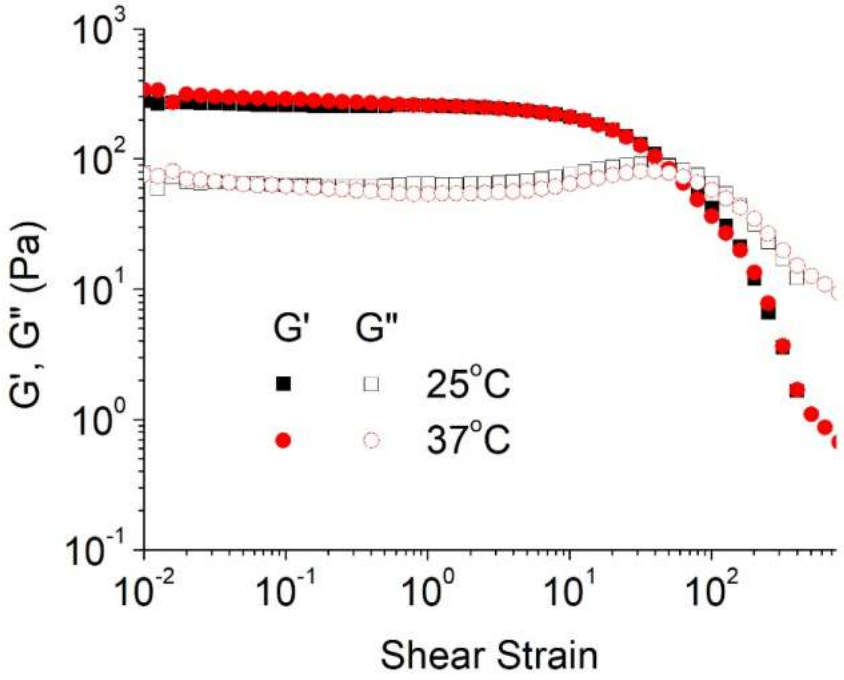

Figure SA8. Amplitude sweep of SV3/PVA-2-1 sample at 25 and 37℃.

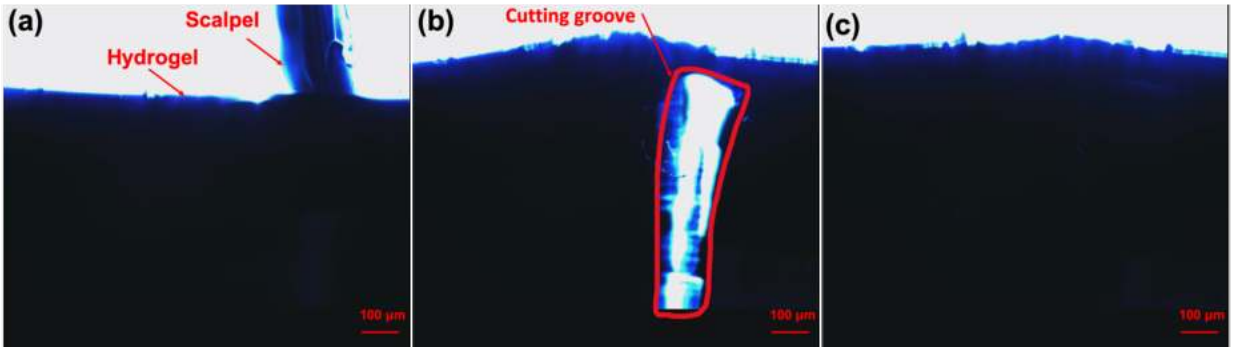

Figure SA9. In situ self-healing optical images of the SV3/PVA-1-3 hydrogel (a) before cutting, (b) after cutting, and (c) after healing.

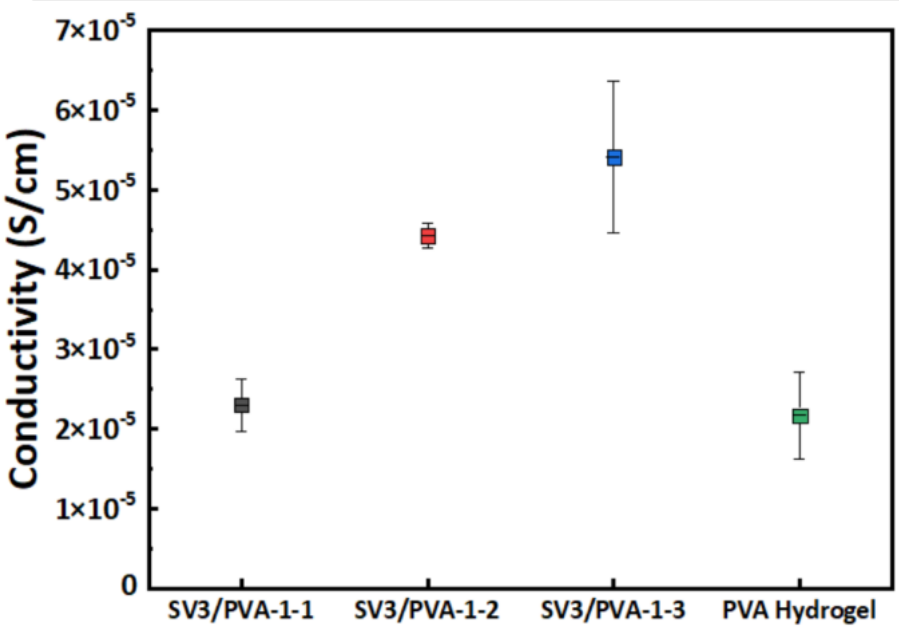

Figure SA10. Conductivity of SV3/PVA and PVA hydrogels. Data for the conductivity (n = 3) is reported as mean ± standard deviation.

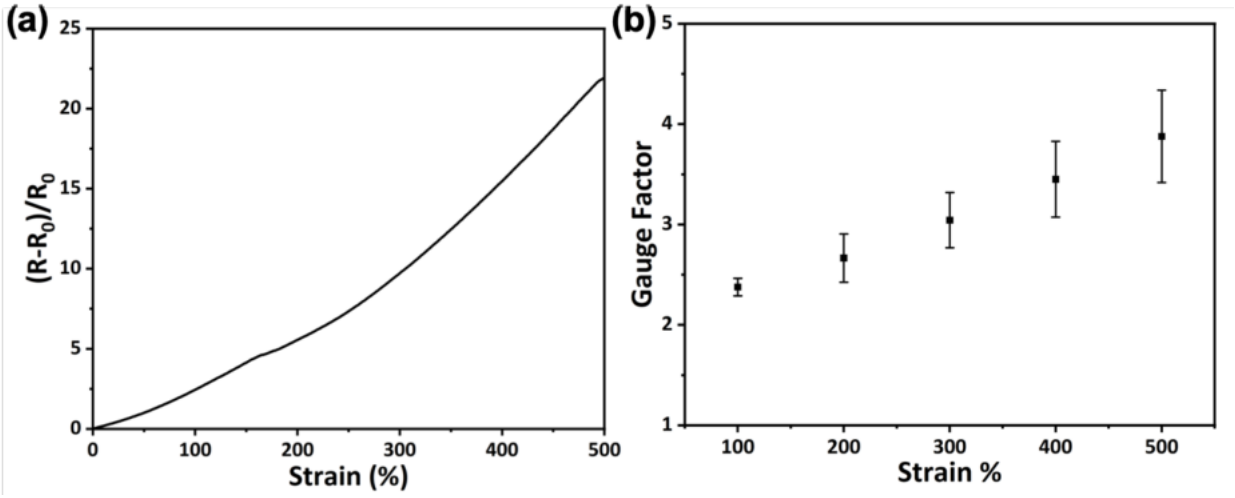

Figure SA11. Plot of (a) resistance change functioned with strain and (b) gauge factors at different strains for SV3/PVA-1-3 hydrogel based strain sensors. Data gauge factor are reported as mean ± standard deviation (n = 3).

Table SA1. Comparison between the SV3/PVA hydrogels and recently reported PVA-borax based hydrogels.

Hydrogel system	Conductive filler or other components	Young's modulus	Adhesion strength	Gauge factor	Healing efficiency and time	Applications	Ref.
PVA-borax	SWCNT, or graphene, or silver nanowire	--	--	1.51 (1000% strain)	98% within 3.2 s (electrical healing)	Strain sensor	[115]
PVA-borax	rGO, glycerol	--	~3 kPa (Pig skin, lap shear method)	14.14 (500% strain)	95.73% (a destructive shear test)	Strain sensor, ECG & EMG electrodes	[88]
PVA-borax	PDA	4.6 kPa (compression)	--	--	250 ms (electrical healing)	Strain sensor	[113]
PVA-borax	MFC	--	--	--	10 min (mechanical healing)	PH sensor	[118]
PVA-borax	PAA, EG	32.4 kPa (tensile strength)	31.6 kPa on glass and 27.1 on steel (perpendicular adhesion)	--	62.2% after 10.0 s (tensile strength)	Strain sensor	[148]
PVA-borax	FSWCNT, PDA	--	5.2 kPa (perpendicular adhesion on pig skin)	--	99% within 2.0 s (electrical healing)	Strain sensor	[114]
PVA-borax	PEDOT:PSS, PG, and DEG	3.7 kPa (compression)	19.6 kPa (perpendicular adhesion on pig skin)	3.88 (500%)	100 % within 3.2 s (electrical healing)	ECG & EMG electrodes	This work

Note: SWCNT: Single wall carbon nanotube, rGO: Reduced graphene oxide, PDA: Polydopamine, MFC: Microfibrillated cellulose, PAA: Polyacrylic acid, EG: Ethylene glycol, FSWCNT: Functionalized single-wall carbon nanotube, PG: propylene glycol, and DEG: diethylene glycol.

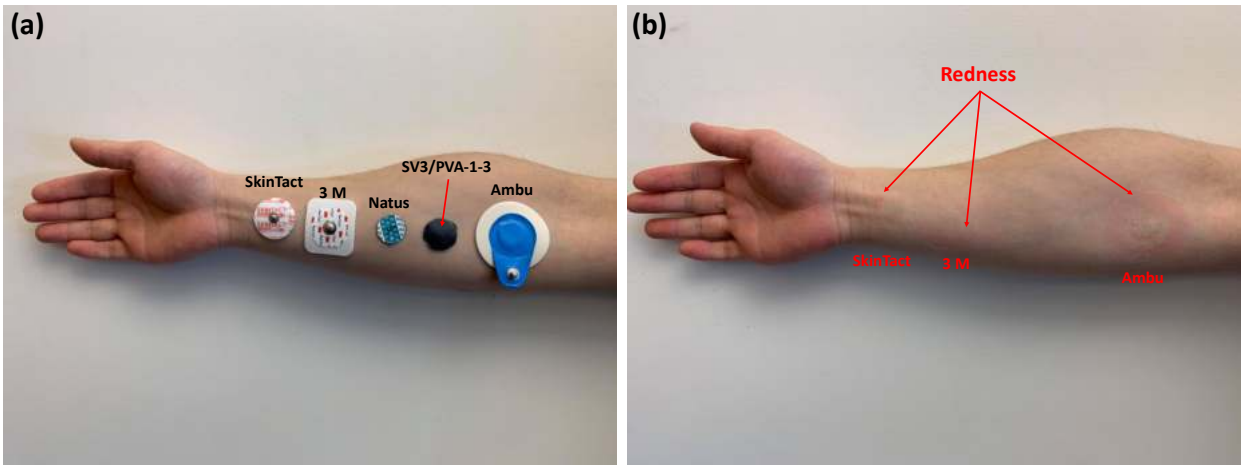

Figure SA12. (a) Different electrodes on the right forearm of a volunteer and (b) skin condition after 1 h wearing. SkinTact®, 3M®, and Ambu® commercial Ag/AgCl gel electrodes show skin redness after the removal from skin, while the SV3/PVA-1-3 hydrogel electrode and the Natus® commercial Ag/AgCl gel electrode show friendly properties to the skin without any skin redness.

APPENDIX B SUPPLEMENTARY INFORMATION FOR ARTICLE 2 : STRETCHABLE, SOFT, HIGHLY ADHESIVE, AND SELF-HEALING CONDUCTIVE POLYMER FILMS FOR HEALTHCARE MONITORING

Xin Zhou[1], Pierre Kateb[1], Jinsil Kim[1], Gregory A. Lodygensky[2], Bénédicte Amilhon[3,4] Damiano Pasini[5], and Fabio Cicoira[1*]

[1] Department of Chemical Engineering, Polytechnique Montréal, Montréal, QC H3C 3A7, Canada

[2] Department of Pediatrics, Sainte-Justine University Hospital Research Center, Montreal, QC, Canada

[3] CHU Sainte-Justine Research Center, Montréal, QC H3T 1C5, Canada

[4] Département de Neurosciences, Université de Montréal, Montréal, QCH3T 1J4, Canada

[5] Department of Mechanical Engineering, McGill University, Montreal, QC H3A 0C3, Canada

*Corresponding author. E-mail: fabio.cicoira@polymtl.ca

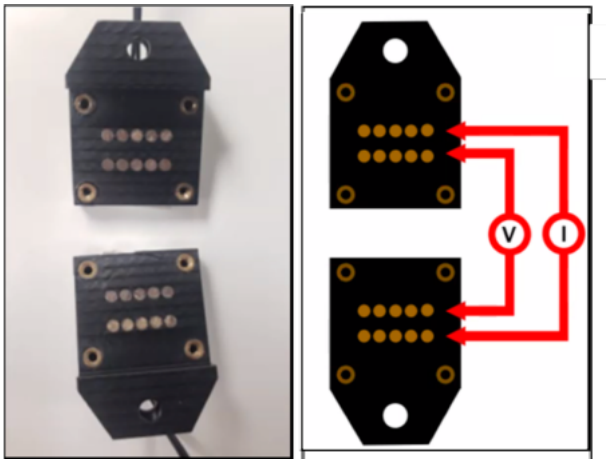

Figure SB1. The 4-points probe electrical tensile grips used in this study.

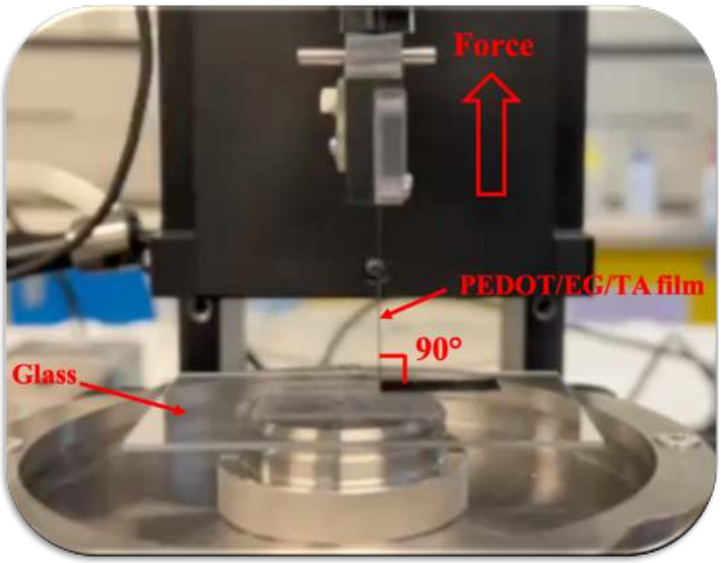

Figure SB2. 90° peeling off testing configuration.

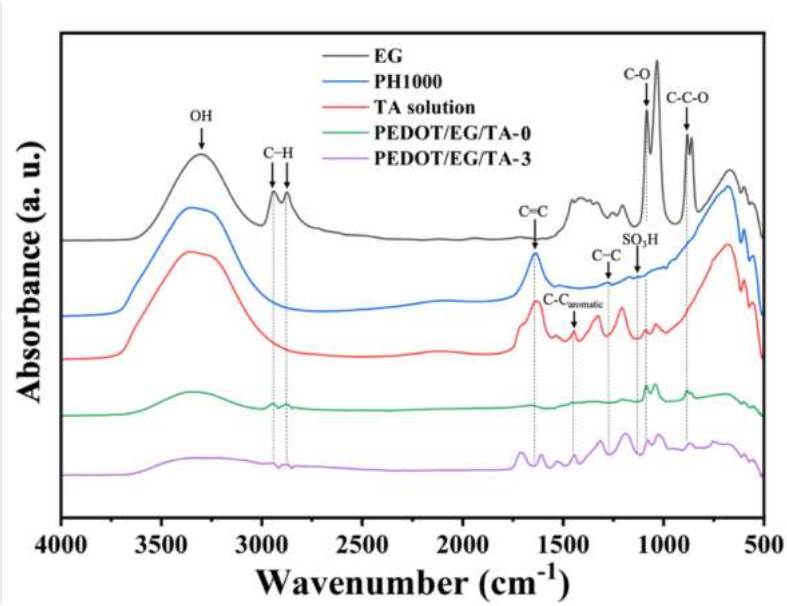

Figure SB3. FTIR spectrum of PEDOT/EG/TA films, EG, TA aqueous solution (0.12 g/mL), and PEDOT:PSS aqueous solution (PH1000)

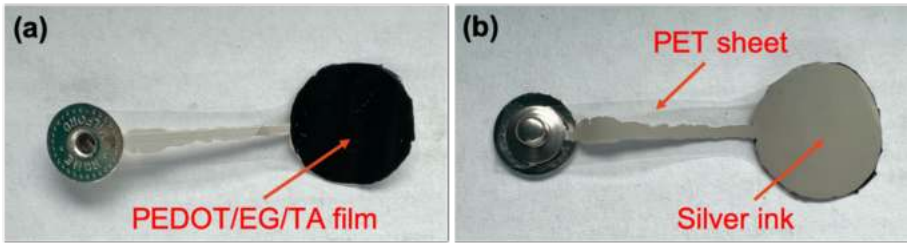

Figure SB4. PEDOT/EG/TA film electrodes. Front (a) and back view (b).

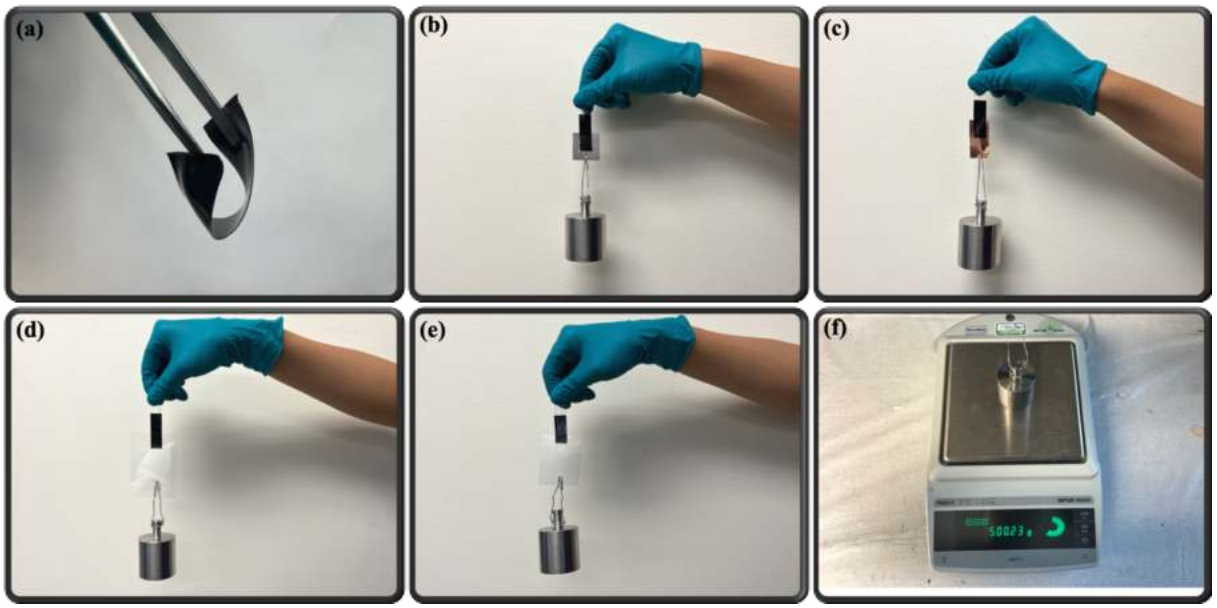

Figure SB5. Digital images. (a) Freestanding PEDOT/EG/TA-3 film adhering to tweezers. PEDOT/EG/TA-3 film adhering to various materials: (b) stainless steel, (c) copper, (d) glass, and (e) plastic PET sheet. (f) A weight of 500 g.

Table SB1. Electrical tensile resistance change (R/R_0) of PEDOT/EG/TA films at 30% strain and break. Data for R/R_0 (n=3) are reported as the mean ± standard deviation. R and R_0 are the resistance at a strain and initial strain (0%), respectively.

Samples	R/R_0	
	at 30% strain	at break
PEDOT/EG/TA-0	1.022 ± 0.004	1.060 ± 0.013
PEDOT/EG/TA-1	1.027 ± 0.004	1.123 ± 0.007
PEDOT/EG/TA-2	1.012 ± 0.002	1.161 ± 0.016
PEDOT/EG/TA-3	1.016 ± 0.003	1.235 ± 0.018

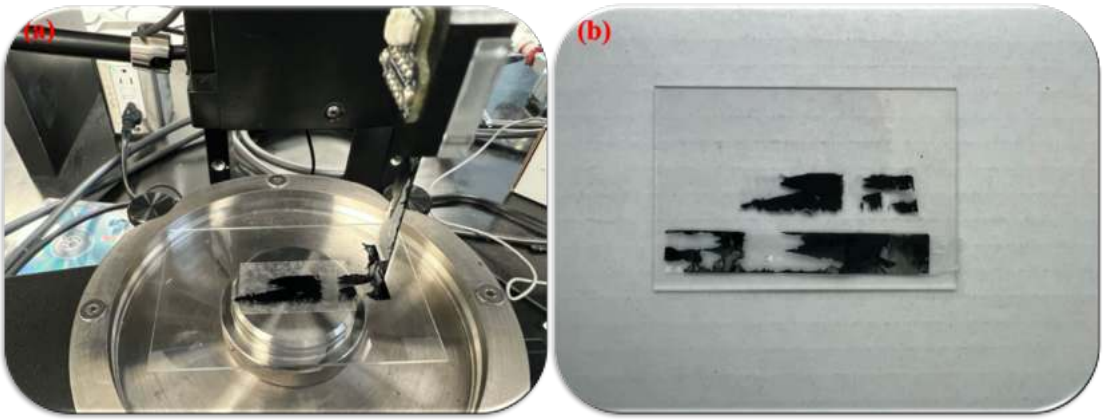

Figure SB6. PEDOT/EG/TA-3 film broke during 90° peeling off test. (a) 90° peeling off testing process and (b) the broken PEDOT/EG/TA-3 film on the glass.

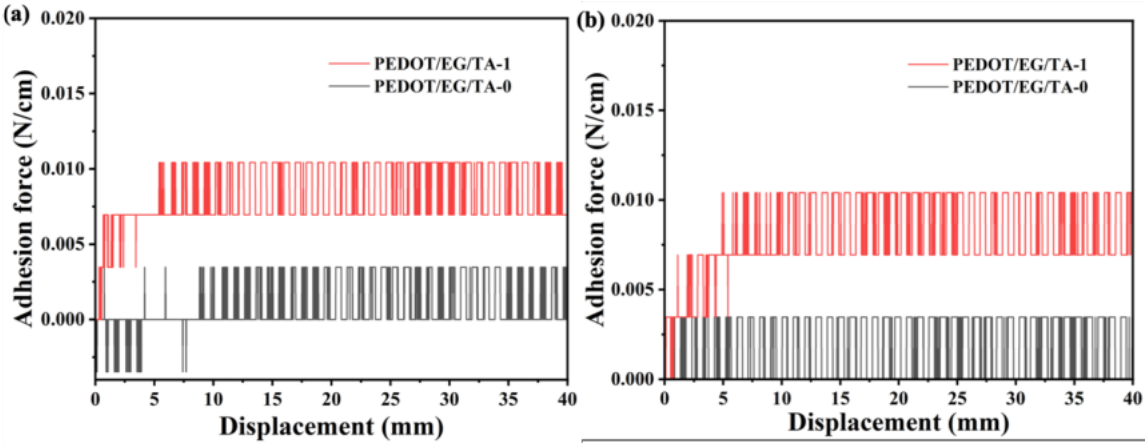

Figure SB7. 90° peeling-off measurements of PEDOT/EG/TA films. Force versus displacement of PEDOT/EG/TA-1 and PEDOT/EG/TA-0 films on the glass (a) and on the pigskin (b).

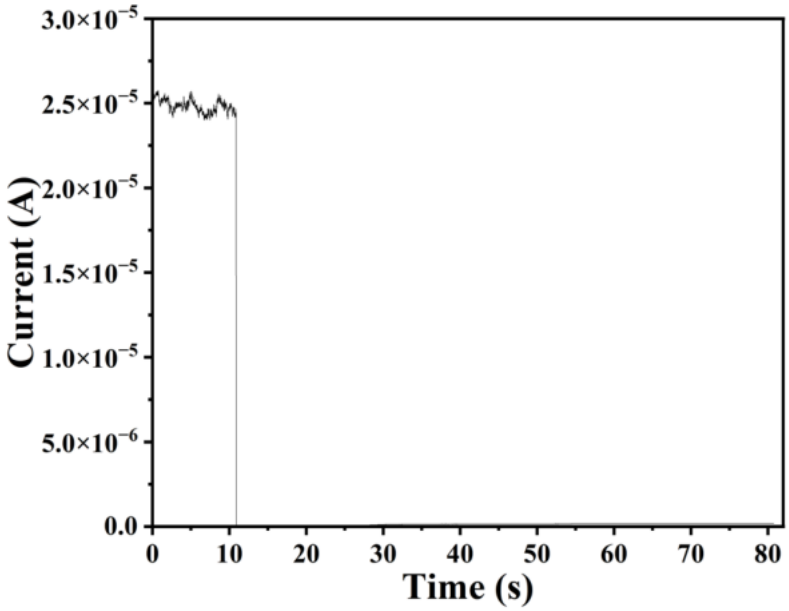

Figure SB8. Current versus time measurements of PEDOT/EG/TA-0 film under a constant voltage of 0.2 V upon the first cut.

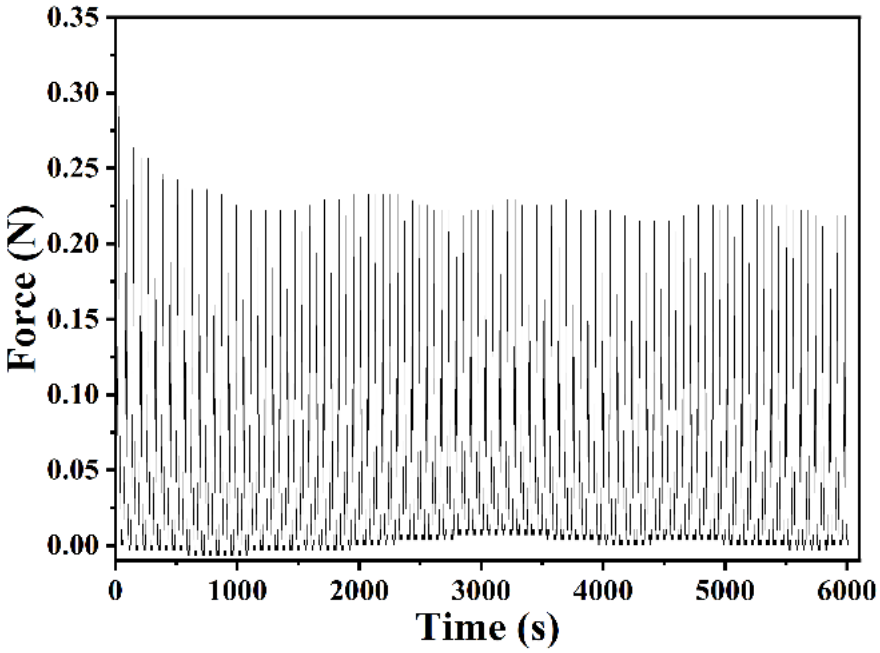

Figure SB9. Stretching stability of the healed PEDOT/EG/TA-3 film at a strain of 30%. Force versus time plots for 100 cycles.

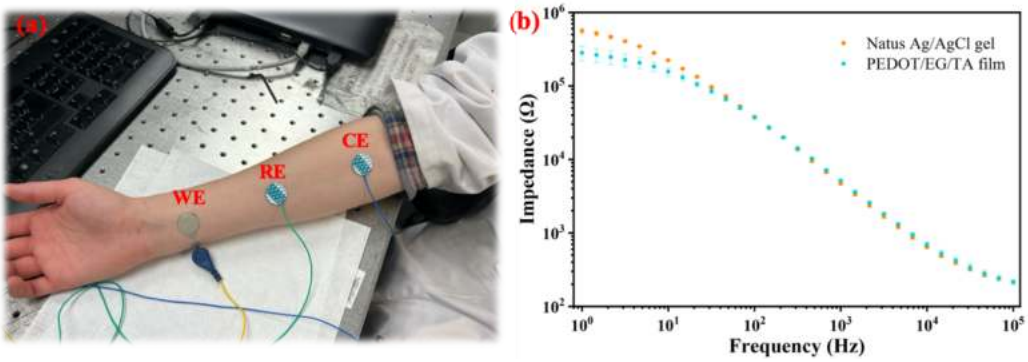

Figure SB10. Characterization of skin-electrode impedance. (a) Configuration of the skin-electrode impedance measurements of a volunteer. The electrode under test acted as the working electrode (WE), and commercial Ag/AgCl gel disk electrodes (Natus®) were used as the reference (RE) and counter (CE) electrodes. (b) Skin-electrode impedance versus frequency for PEDOT/EG/TA-3 film and commercial Natus® Ag/AgCl gel electrodes. Each electrode has a diameter of 18 mm. Measurements were performed on the same people, locations, and on the same day. Data for skin-electrode impedance are reported as mean ± standard deviation (n = 3).

Table SB2. Comparison of skin-electrode impedance of Natus and PEDOT/EG/TA-3 film electrodes. Data for the impedance (n = 3) are reported as the mean ± standard deviation.

Frequency	Impedance (KΩ)	
(Hz)	Natus	PEDOT/EG/TA-3 films
1	558 ± 51	282 ± 61
10	223 ± 5.2	157 ± 20
100	37.7 ± 1.7	37.3 ± 1.1

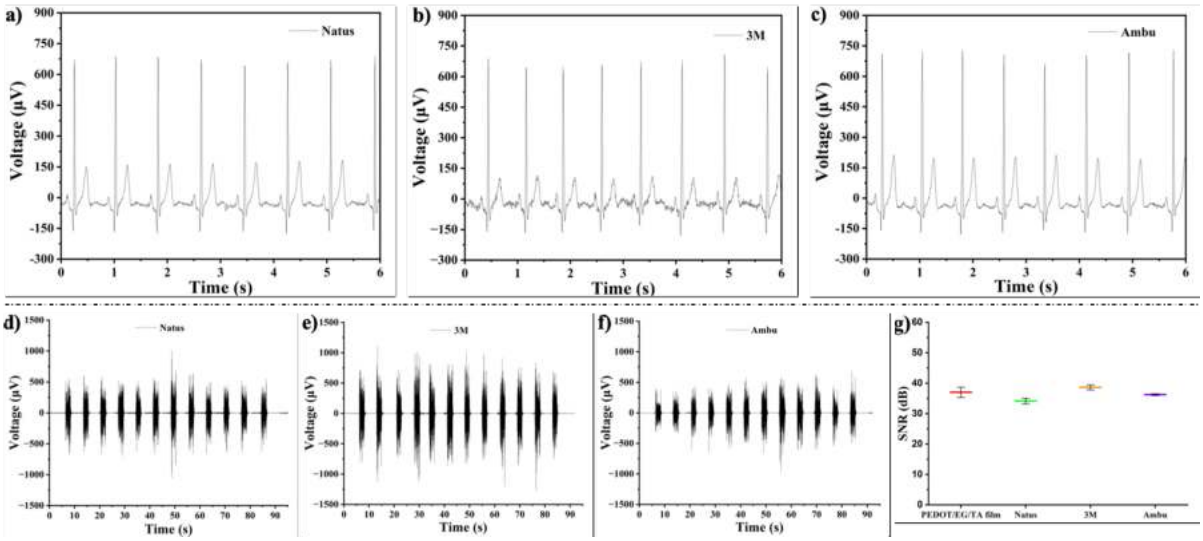

Figure SB11. ECG and EMG signal recordings for different commercial Ag/AgCl gel electrodes. ECG biopotentials (voltage versus time) were recorded using commercial Natus® (a), 3M® (b), and Ambu® (c) Ag/AgCl gel electrodes. EMG monitoring using commercial Natus® (d), 3M® (e), and Ambu® (f) Ag/AgCl gel electrodes during the relaxation and clenching phases. (g) Computed SNR values over the 90 s recording period for PEDOT/EG/TA film electrodes and three different commercial Ag/AgCl gel electrodes. SNR data are reported as mean ± standard deviation (n = 3).

APPENDIX C SUPPLEMENTARY INFORMATION FOR ARTICLE 3 : SOFT, CONDUCTIVE AND ANTI-FREEZING CONDUCTING POLYMER ORGANOHYDROGELS

Xin Zhou[a], Pierre Kateb[a], Floriane Miquet-Westphal[a], Gregory A. Lodygensky[b], Fabio Cicoira[a*]

[a] Department of Chemical Engineering, Polytechnique Montréal, Montréal, Québec H3C 3A7, Canada

[b] Department of Pediatrics, Sainte-Justine University Hospital Research Center, Montreal, QC, Canada

Corresponding author: Fabio Cicoira

Tel. +1-514-340-4711 x 2580; Fax: +1-514-340-2990

Email address: fabio.cicoira@polymtl.ca

Authors' email address: xin.zhou@polymtl.ca (Xin Zhou), pierre.kateb@polymtl.ca (Pierre Kateb), floriane.miquet-westphal@polymtl.ca (Floriane Miquet-Westphal), ga.lodygensky@umontreal.ca (Gregory A. Lodygensky)

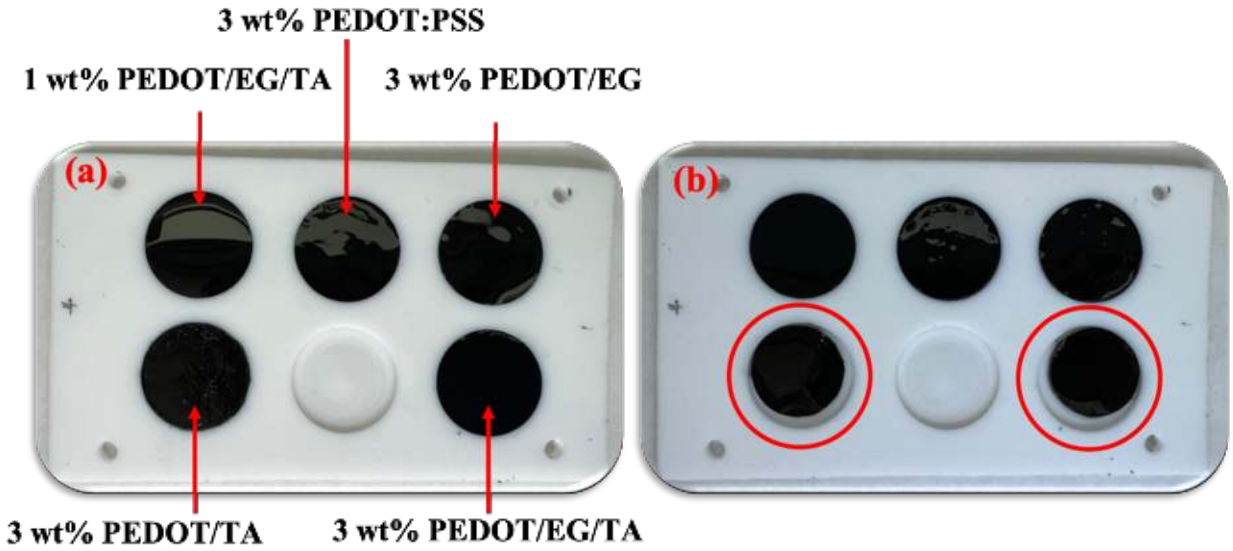

Figure SC1. PEDOT based mixtures before (a) and after (b) heat treatment at 90 °C for 30 min. The heat treatment induced a significant volume contraction of 3 wt% PEDOT/EG/TA and 3 wt% PEDOT/TA gels.

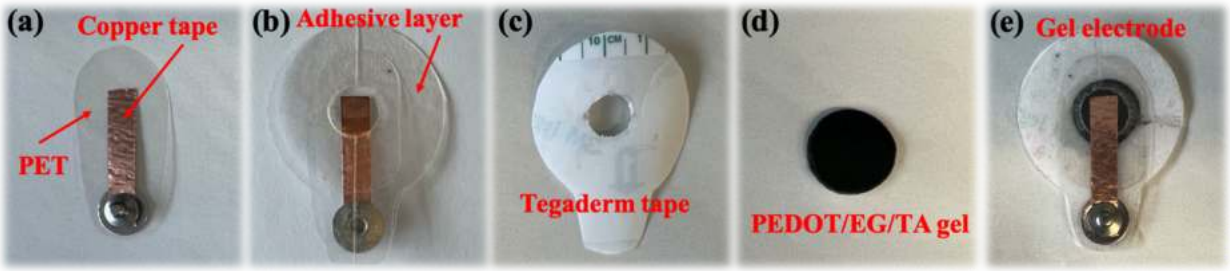

Figure SC2. The preparation of PEDOT/EG/TA gel electrodes. (a) A copper tape was attached on a pre-cut PET sheet, and a snap button was placed at one end of the copper tape, (b) front side view of a double- sided tape with a round hole (8 mm in diameter) at the center placed on the copper/PET strip, (c) an pre-cut Tegaderm tape, (d) disk of PEDOT/EG/TA gel with a diameter of 18 mm, and (e) back side view of the gel electrode.

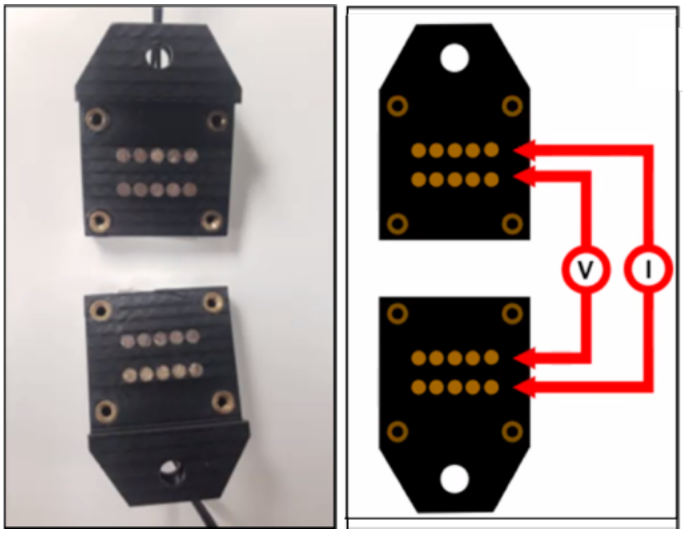

Figure SC3. A four-point probe electrical tensile grip made by Biomomentum Inc.

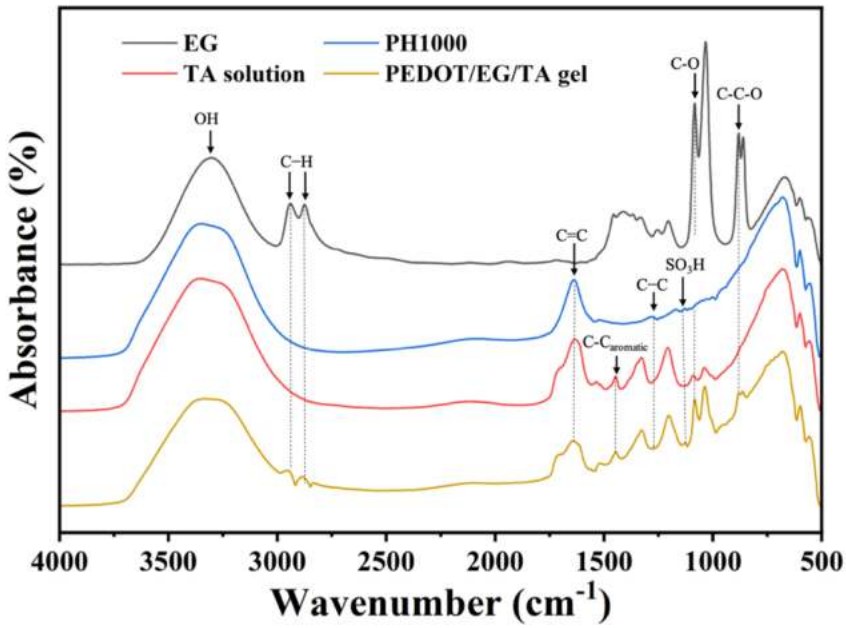

Figure SC4. FTIR spectrum of EG, PEDOT/EG/TA gel, TA solution, and PEDOT:PSS (PH1000).

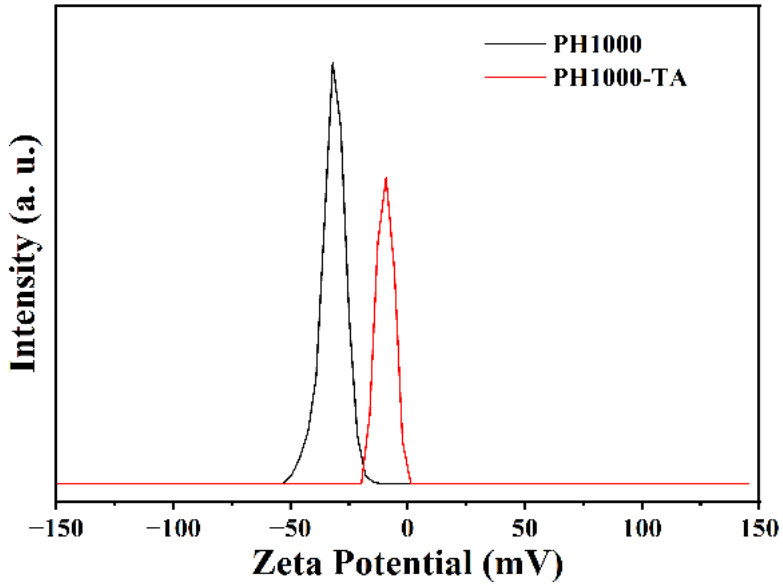

Figure SC5. Zeta potential distributions of diluted PEDOT:PSS (PH1000) and PEDOT:PSS/TA (PH1000-TA) suspensions. 10 g the diluted suspension containing ~0.01 g PEDOT:PSS (corresponding to 1 mg/mL PEDOT:PSS aqueous solution) and 10 g the diluted suspension containing ~0.01 g PEDOT:PSS and ~0.06 g TA powder were used for the tests, and the measurements were performed at 25 °C.

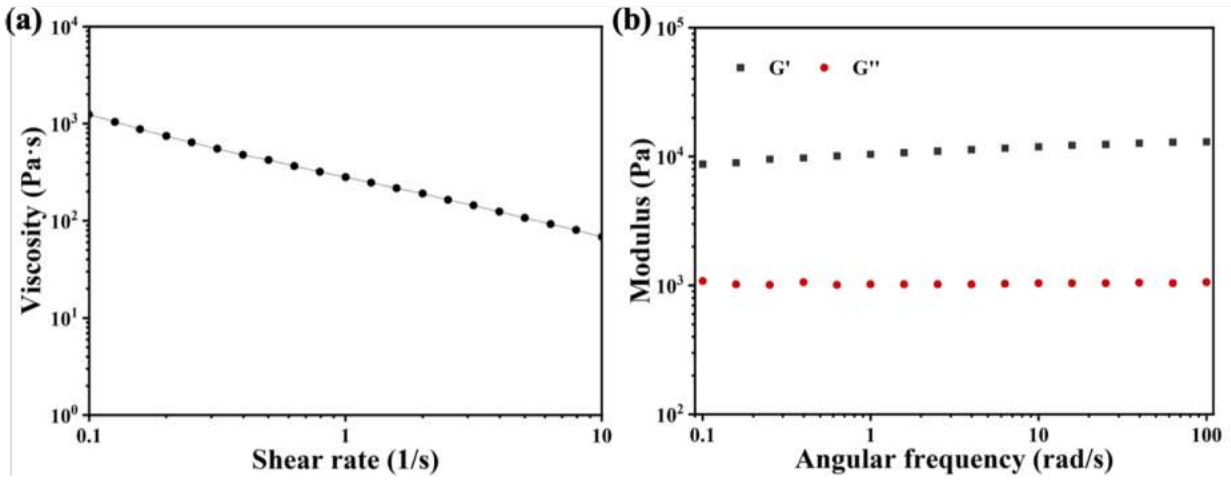

Figure SC6. (a) Viscosity of PEDOT/EG/TA gel as a function of shear frequency. (b) Dynamic rheological behavior of the gel.

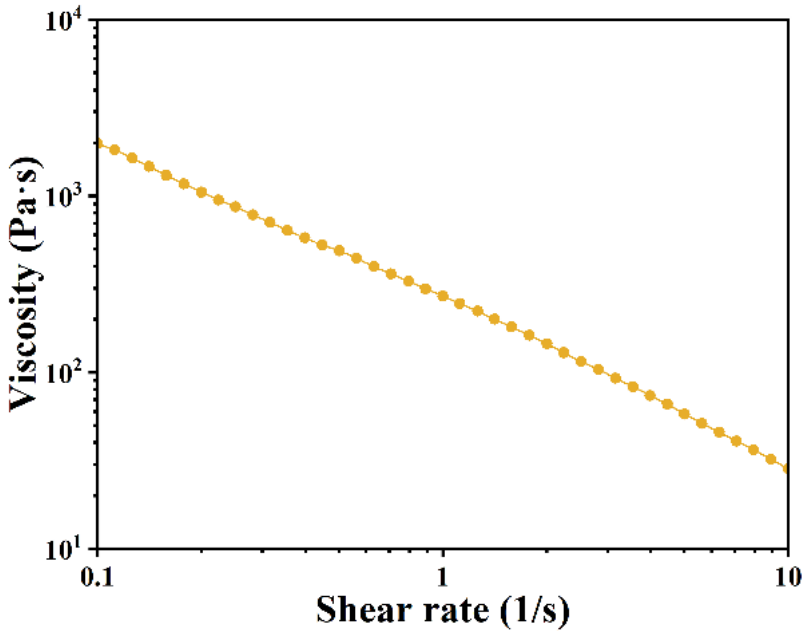

Figure SC7. Viscosity of PEDOT/EG/TA mixture as a function of shear frequency.

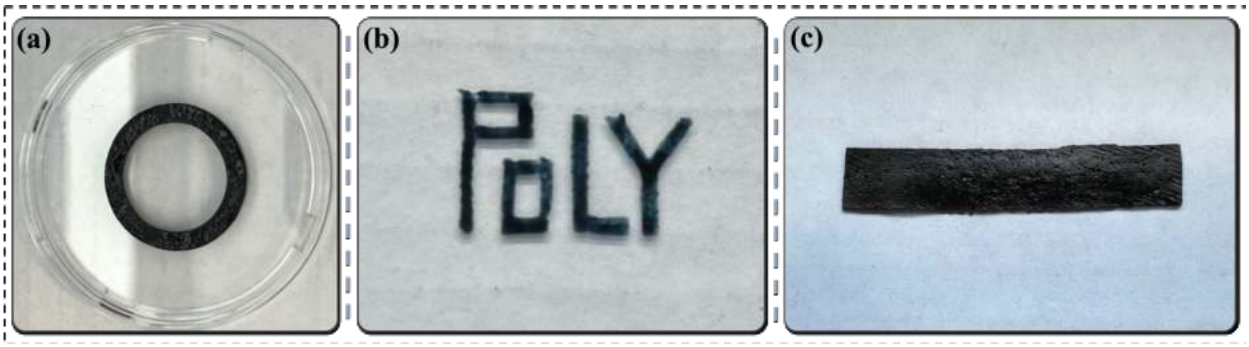

Figure SC8. PEDOT/EG/TA gel modelled into ring shape (a), printed into letters (b), and injected into a strip mold (c).

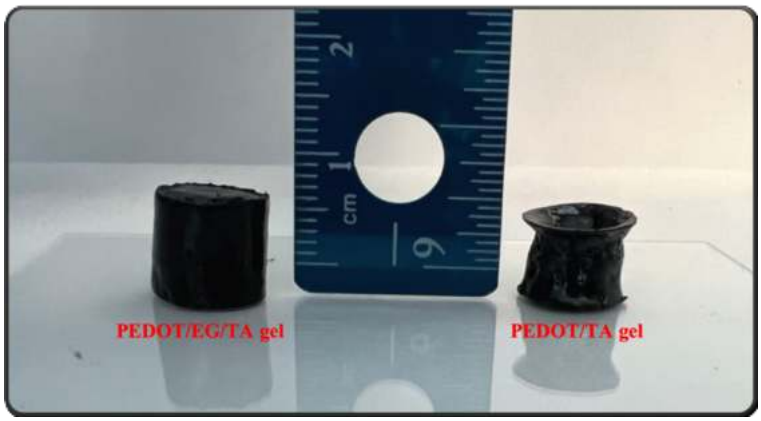

Figure SC9. Digital image of PEDOT/EG/TA and PEDOT/TA gels placed in ambient temperature after 1 day.

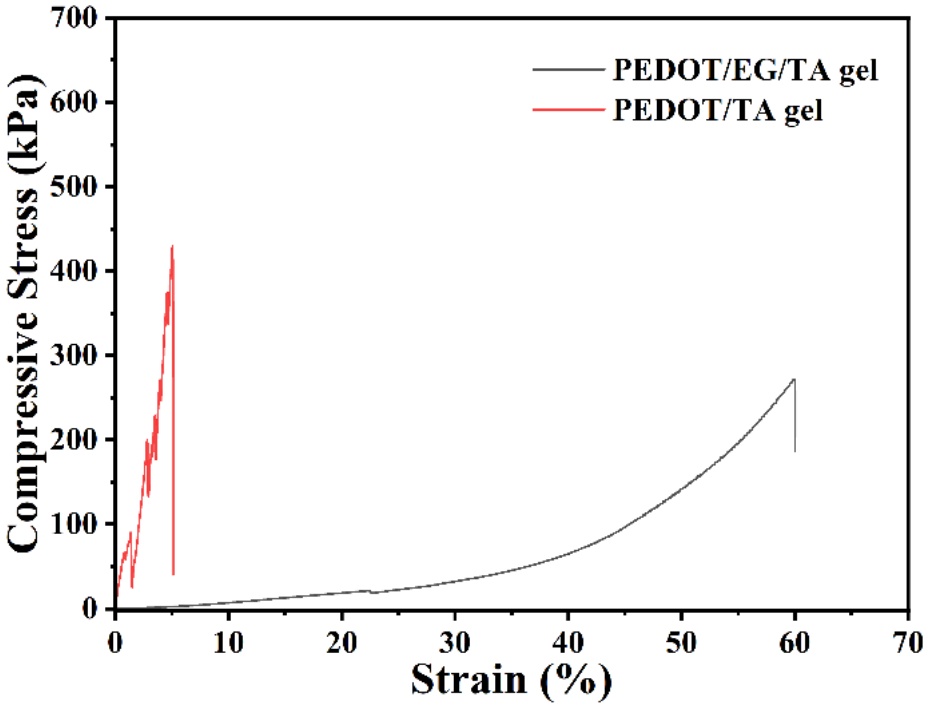

Figure SC10. Compressive stress versus strain of PEDOT/EG/TA and PEDOT/TA gels (sample 2) stored at ambient temperature for seven days.

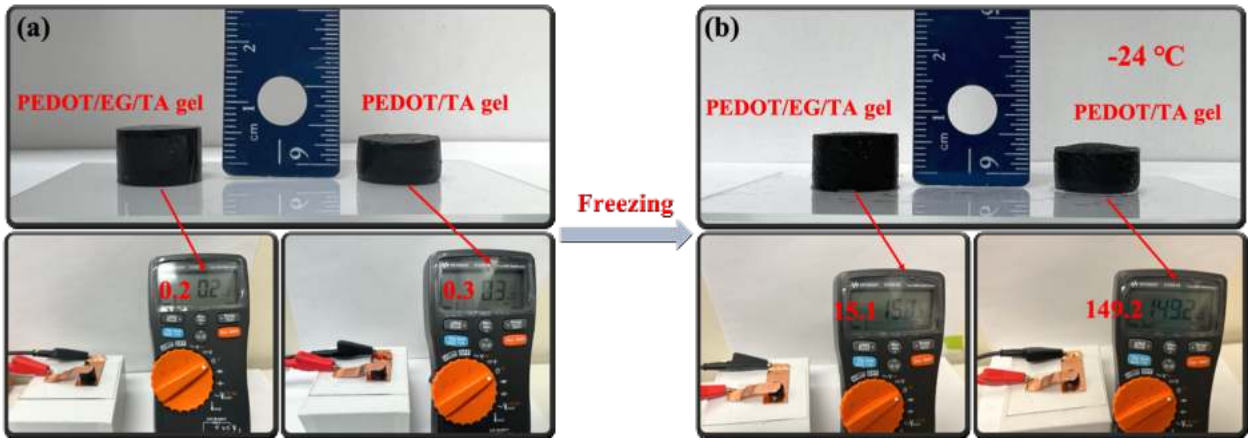

Figure SC11. Digital images of electrical properties of PEDOT/EG/TA and PEDOT/TA gels before (a) and after (b) freezing. The PEDOT/EG/TA gel is with a 13.8 mm diameter and 8.5 mm height and the PEDOT/TA gel is with 13.3 mm diameter and 6.6 mm height before the freezing. The resistance for the fresh gels was recorded when the data was stable (within 20 s) and the data for frozen gels was recorded immediately (~1 s) after starting the tests.

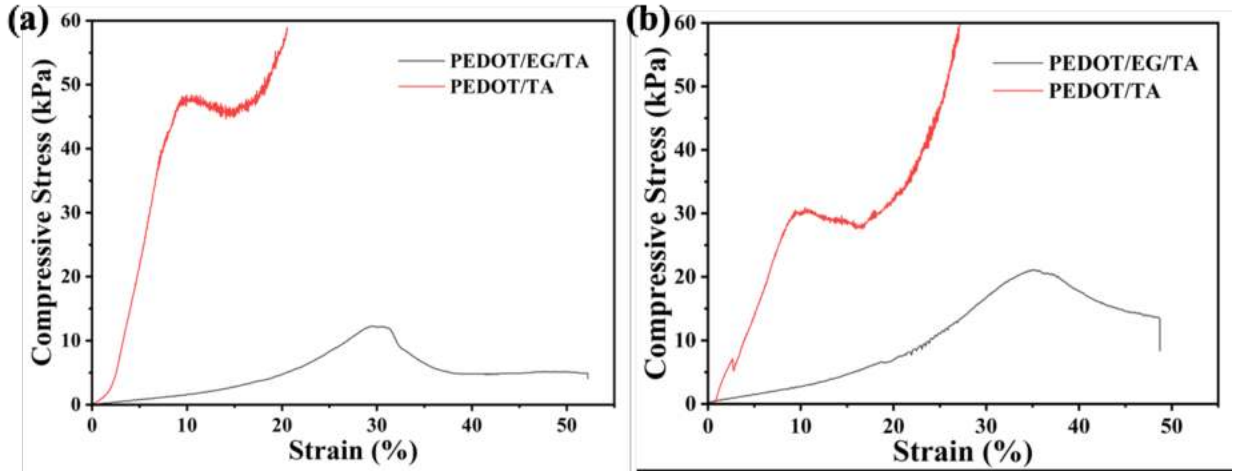

Figure SC12. Compressive stress versus strain of PEDOT/EG/TA and PEDOT/TA gels after freezing at -24 °C for 1 day. (a) Sample 1 and (b) sample 2. The measurements were carried out immediately after taking out the gels from the freezer.

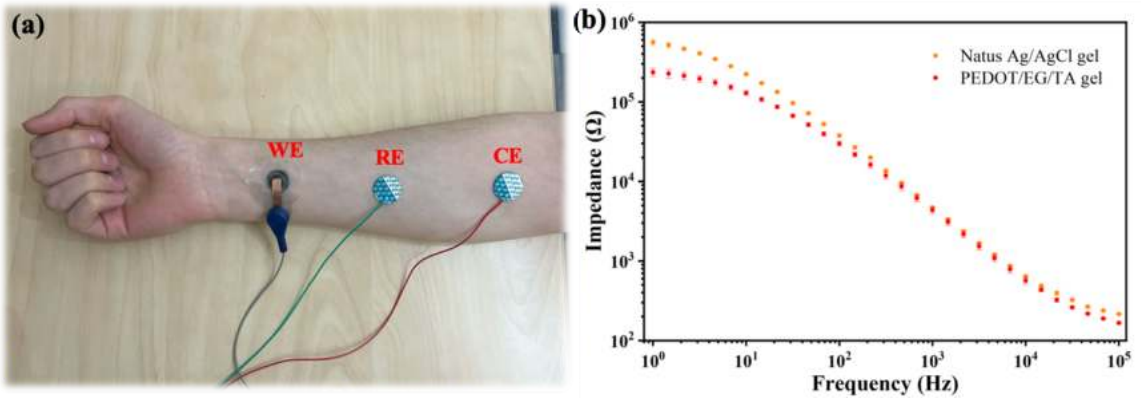

Figure SC13. Characterization of the skin-electrode impedance. (a) Configuration of the skin-electrode impedance measurement on a volunteer. The tested electrode acted as working electrode (WE), and commercial Ag/AgCl gel disk electrodes (Natus®) were used as reference (RE) and counter (CE) electrodes. (b) Skin-electrode impedance versus frequency plots for PEDOT/EG/TA gel and commercial Natus® Ag/AgCl gel electrodes. The diameter of the electrodes was calculated as 18 mm. The measurements were performed on the same person and the same day. Data for skin-electrode impedance are reported as mean ± standard deviation (n = 3).

Table SC1. Comparison of the skin-electrode impedance of Natus and PEDOT/EG/TA gel electrodes.

Frequency	Impedance (kΩ)	
(Hz)	Natus	PEDOT/EG/TA gel
1	558 ± 51	235 ± 28
10	223 ± 5	129 ± 9
100	37.7 ± 1.7	29.8 ± 2.0

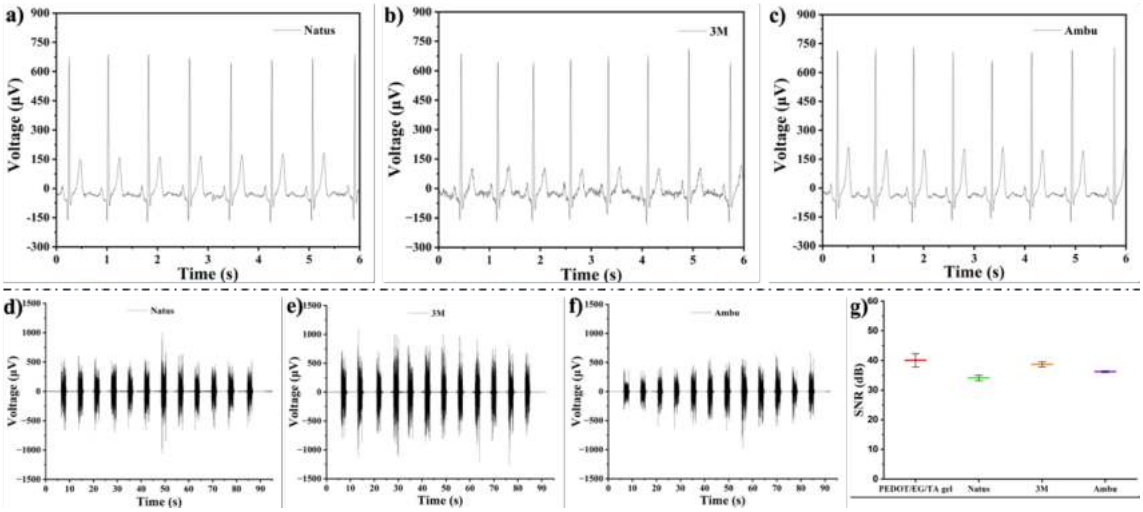

Figure SC14. ECG signals (voltage versus time) recorded with commercial Natus® (a), 3M® (b), and Ambu® (c) Ag/AgCl gel electrodes. EMG recording with using commercial Natus® (d), 3M® (e), and Ambu® (f) Ag/AgCl gel electrodes under relaxation and clenching phases. (g) Computed SNR values over the 90 s recording period for PEDOT/EG/TA gel electrodes and 3 different commercial Ag/AgCl gel electrodes. SNR data are reported as mean ± standard deviation (n = 3).

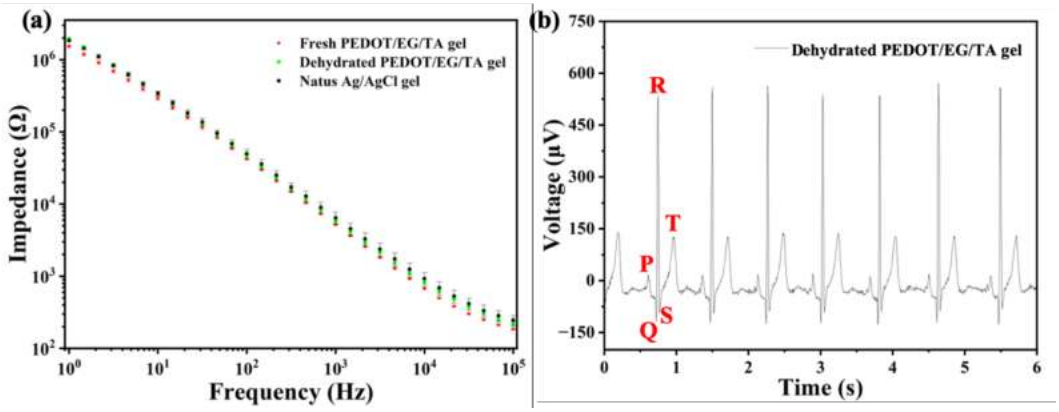

Figure SC15. The skin-electrode impedance and ECG recording with using PEDOT/EG/TA gels after placing in ambient temperature for 7 days. (a) Skin-electrode impedance versus frequency for fresh and dehydrated PEDOT/EG/TA gel electrodes and commercial Natus® Ag/AgCl gel electrodes. The diameter of the electrodes was calculated as 18 mm. The measurements were performed on the same people and the same day. Data for skin-electrode impedance are reported as mean ± standard deviation (n = 3). (b) ECG biopotentials (voltage versus time) recorded with dehydrated PEDOT/EG/TA gel electrodes.

Table SC2. Comparison of the skin-electrode impedance of Natus Ag/AgCl gel, fresh and dehydrated PEDOT/EG/TA gel electrodes.

Frequency	Impedance (kΩ)		
(Hz)	Natus	Fresh gel	Dehydrated gel
1	1840 ± 42	1530 ± 66	1950 ± 100
10	341 ± 23	291 ± 18	340 ± 27
100	50 ± 7	42 ± 1	47 ± 4

APPENDIX D LIST OF PUBLICATIONS AT POLYTECHNIQUE MONTREAL NOT INCLUDED IN THE THESIS

1. Y. Li, **X. Zhou**, B. Sarkar, N. Gagnon-Lafrenais, and F. Cicoira, "Recent Progress on Self-Healable Conducting Polymers," *Adv. Mater,* vol. 34, no. 24, p. e2108932, Jun 2022, doi: 10.1002/adma.202108932.
2. J. E. Hagler, J. Yeu, **X. Zhou**, G. Ducharme, B. Amilhon, and F. Cicoira, "Electrodeposited PEDOT:BF_4 Coatings Improve Impedance of Chronic Neural Stimulating Probes In Vivo," *Adv. Mater. Interfaces,* vol. 9, no. 35, 2022, doi: 10.1002/admi.202201066.

APPENDIX E PARTICIPATION TO CONFERENCES

1. **X. Zhou**, G. Lodygensky, and F. Cicoir. PEDOT:PSS based soft, healable, and highly adhesive hydrogels for monitoring human health. Poster presentation, MRS Fall Meeting, 2022, Boston.
2. **X. Zhou** and F. Cicoira. Soft, self-healing, and highly adhesive hydrogels for human healthcare. Poster presentation, MRS Fall Meeting, 2021, Montreal.
3. **X. Zhou** and F. Cicoira. PEDOT:PSS based hydrogel for human healthcare. Poster presentation, Canadian Chemical Engineering Conference, 2021, Montreal.
4. **X. Zhou** and F. Cicoira. PEDOT based flexible skin patch electrodes for monitoring human health. Poster presentation, IEEE NANO 2021, Montreal.